

DESIGN AND ENGINEERING OF VALUE-ADDED PRODUCTS FROM THE  
POLYLACTIDE (PLA) POLYMER

By

Preetam Kumar Giri

A DISSERTATION

Submitted to  
Michigan State University  
in partial fulfillment of the requirements  
for the degree of

Chemical Engineering – Doctor of Philosophy

2019

## **ABSTRACT**

### **DESIGN AND ENGINEERING OF VALUE-ADDED PRODUCTS FROM THE POLYLACTIDE (PLA) POLYMER**

By

Preetam Kumar Giri

The rate of adoption of the polylactide (PLA) polymer as a commodity plastic has been slow due to its inherently low toughness, low heat deflection temperature, slow rate of crystallization and poor melt strength. In the current work, we have focused on addressing these critical issues with PLA via four specific approaches, with the ultimate goal of expanding its portfolio of commercial applications. First, the incorporation of a novel Polylactide-Polydimethylsiloxane (PLA-PDMS) block copolymer for application as an impact modifier for injection molded PLA articles was studied. The PLA-PDMS copolymer was synthesized via a transesterification chemistry using reactive extrusion as a facile technique. The copolymer was added to neat PLA during the injection molding process at varying loading levels. Thermal annealing of the injection molded part was carried out to increase the percent crystallinity and subsequently the heat deflection temperature. The addition of the copolymer and the subsequent annealing was found to have an unprecedented synergistic effect on both the tensile and impact toughness of the PLA, which were improved by up to 200 and 500% respectively. A model was proposed to explain the unique behavior shown by the annealed PLA-PDMS system. Optimization of molding and annealing conditions were performed to ensure a cost-effective route towards commercialization.

Second, the use of a biobased mono-epoxy-functionalized cardanol molecule, derived from cashew nut shell liquid (CNSL), is explored as a “green” plasticizer. Reactive blends of the modifier with PLA, produced via twin-screw extrusion, was found to successfully reduce glass transition temperature of the PLA resulting in enhanced flexibility of the injection molded PLA specimens.

Thermal annealing of these specimens was found to improve heat deflection temperature by  $\sim 20^{\circ}\text{C}$  and the percent crystallinity by  $\sim 100\%$ . Mechanical properties of the annealed samples were observed to closely mimic the unique synergistic trend shown by the PLA-PDMS system. The model developed for the PLA-PDMS system was appropriately modified to take into account the behavior of the PLA-epoxy system.

Third, multifunctional epoxy-based chain extenders were reactively blended with PLA via twin-screw extrusion to improve its melt strength for applications in processing techniques such as blown films. A fossil-fuel based epoxy modifier and a biobased substitute derived from cardanol were used for the study. The effects of varying molar ratios and the type of processing used on the final rheological properties were first evaluated using model compounds to simulate PLA and then validated by reactions with PLA. Improvements in melt strength were characterized using dynamic oscillatory shear and uniaxial extensional viscosity measurements. The presence and type of chain extension evolved with each modifier was established.

The last section of the work involves the use of basalt and glass fibers to reinforce the PLA matrix for automotive interior applications. The PLA-based fiber composite materials were produced by adopting the Direct-Long Fiber Thermoplastic (D-LFT) approach, wherein continuous rovings of the fibers were directly fed into a twin-screw extruder. The D-LFT technique allows for a higher aspect ratio of the fiber in the matrix leading to improved load transfer at the fiber-matrix interface. Optimization of the process parameters, including screw configuration, was performed to ensure desired level of fiber breakage and dispersion, and to maximize the fiber content in the final composite material. PLA-based short fiber composites were prepared under similar processing conditions to demonstrate the efficacy of the D-LFT technique at preparing composite samples with a higher aspect ratio and improved mechanical performance over using short fiber.

Copyright by  
PREETAM KUMAR GIRI  
2019

Dedicated to the “pale blue dot” and all those who reside on it, especially my parents.

## ACKNOWLEDGMENTS

At the very outset, I would like to express my sincere gratitude to my adviser, Prof. Ramani Narayan, for his constant support and guidance throughout my journey in graduate school. I would especially like to thank him for giving me the freedom to explore the inspiring field of biobased materials on my own and providing me with necessary feedback as and when needed. This has truly enabled me in becoming an independent researcher and allowed me to constantly tinker around in the lab. His insistence on self-accountability is something I hope to strive for the rest of my career.

I would like to thank all the members of my dissertation committee, Dr. Jayaraman Krishnamurthy, Dr. Andre Lee, and Dr. James (Ned) Jackson, for their invaluable feedback during the course of my work. Their constructive comments have helped me gain deeper insights into my work and have also improved my technical writing and presentation skills.

I feel greatly indebted to Dr. Shilpa Manjure, Dr. Weipeng Liu, Matt Lundblad, Vineet Dalal, and the entire team at Natur-Tec for their constant feedback and frequent exchange of ideas. They have been instrumental in commercializing several biobased technologies and brainstorming with them gave a sense of what industrial expectations from academic research were. This has significantly affected my thought process when it comes to addressing an issue and I thank them for that.

I am also extremely grateful to our collaborators at the Ford Motor Company, Dr. Alper Kiziltas and Dr. Debbie Mielewski, for funding our work and their invaluable feedback during the progress of our work. I would like to thank Alper for introducing me to SPE conferences and activities which I have come to greatly enjoy. The group at Ford has set industry standards in incorporating biobased materials in automotive applications and also providing us with an opportunity to do the same.

I am thankful to our collaborators at the Cardolite Corporation, Dr. Chetan Tambe, Dr. Anbu Natesh and Timothy Stonis for giving me an opportunity to work with them and providing access to their products.

I express my heartfelt gratitude to all the members of the Composite Materials & Structures Center, especially Brian Rook, for always being there whenever I needed hands-on technical expertise or help with troubleshooting of processing equipment. I would also like to thank Aaron Walworth with the School of Packaging for his help and assistance in using their testing facilities. I would like to thank the members of the Center for Advanced Microscopy at MSU for their help. A word of thanks also goes to Dr. Dan Holmes at the Department of Chemistry for his help in understanding and using the NMR facilities.

A big cheer goes out to all the members of the Biobased Materials Research Group. Starting from the early days, I would like to thank Dr. Sudhanwa Dewasthale for being instrumental in having me join the group. I would also like to thank Dr. Jeff Schneider and Hugh MacDowell for showing me the ropes around the lab and helping me settle in. A huge thank you (and a big hug) to Dr. Chetan Tambe for everything, both personal and professional (the list is too long). I would also like to thank Sayli for her help and assistance whenever I needed them most. I would like to thank the undergraduate researchers who I worked with – Nathan Arnold, Clayton Threatt, Ian Scheper, Sara Kolar and Caleb Andrews – for their invaluable contribution to my graduate school work. A lot of it would simply not have been possible without their best efforts and I thank them for that. I would like to thank Manas for his help in the lab and keeping us entertained with his antics. Last but not least, I would like to thank and wish the very best to Apoorva and Moh for their future work at BMRG.

My Spartan life has not exactly been quite spartan, thanks largely to the following group of people

– Chetan (Chetanwaa), Oishi (Doc!), Aritra (Bhai), Saptarshi (Sap da), Sabyasachi (Baby Das), Sayli (Crazy Cat Lady), Kanchan (K.C.), Kirti (Chhota Don), Bhushan (Bhushan Da), Tridip (Tridip Da), Shreya (Shreya Di), Arkaprabha (Arka Da), Soumen (Soumen Da), Sunpreet, Dhritabrata (Piku Da) and a lot more!

Most importantly, I would like to thank my parents and family for their love and support all throughout my life, and their constant encouragement during my academic pursuits. I would also like to thank Barun (Aja), Sashwat (Kuku) and Anurag (Duky) for always being there for me.

# TABLE OF CONTENTS

|  |              |
|--|--------------|
| <b>LIST OF TABLES .....</b>  | <b>xi</b>    |
| <b>LIST OF FIGURES .....</b>   | <b>xii</b>   |
| <b>KEY TO ABBREVIATIONS .....</b>  | <b>xviii</b> |
| <b>1 INTRODUCTION .....</b>  | <b>1</b>     |
| <b>1.1 Motivation.....</b>   | <b>1</b>     |
| <b>1.2 Polylactide (PLA).....</b>  | <b>3</b>     |
| <b>1.3 Property Modification of PLA.....</b>   | <b>7</b>     |
| 1.3.1 Alteration of Stereochemistry and Processing.....  | 7            |
| 1.3.2 Copolymerization.....  | 8            |
| 1.3.3 Blending.....  | 9            |
| 1.3.4 Plasticization.....  | 9            |
| <b>1.4 Reactive Extrusion (REX).....</b>   | <b>10</b>    |
| <b>2 POLYLACTIDE-POLYDIMETHYLSILOXANE COPOLYMER FOR<br/>TOUGHENING APPLICATIONS .....</b>              | <b>14</b>    |
| <b>2.1 Introduction.....</b>   | <b>14</b>    |
| <b>2.2 Experimental .....</b>  | <b>15</b>    |
| 2.2.1 Synthesis and Characterization of Copolymer.....   | 16           |
| 2.2.1.1 Materials .....  | 16           |
| 2.2.1.2 Synthesis via REX .....  | 16           |
| 2.2.1.3 Characterization .....   | 17           |
| 2.2.2 Melt Blending and Injection Molding of Copolymer with Neat PLA .....                             | 19           |
| 2.2.2.1 Materials .....  | 19           |
| 2.2.2.2 Synthesis via REX and Injection Molding.....   | 19           |
| 2.2.2.3 Characterization .....   | 20           |
| <b>2.3 Results and Discussion.....</b>   | <b>22</b>    |
| 2.3.1 Synthesis and Characterization of Copolymer.....   | 22           |
| 2.3.2 Characterization of Blends of Copolymer with Neat PLA .....                                      | 29           |
| 2.3.2.1 Avrami Model Analysis.....   | 38           |
| 2.3.2.2 “Crystallization Induced Phase Segregation” Model.....   | 42           |
| 2.3.2.3 Single Step In-Mold Annealing .....  | 43           |
| <b>2.4 Conclusion and Future Work .....</b>  | <b>48</b>    |
| <b>3 REACTIVE BLENDING OF MONOFUNCTIONAL EPOXY MODIFIERS AS<br/>PLASTICIZERS FOR POLYLACTIDE .....</b> | <b>50</b>    |
| <b>3.1 Introduction.....</b>   | <b>51</b>    |
| <b>3.2 Experimental .....</b>  | <b>54</b>    |
| 3.2.1 Materials .....  | 54           |
| 3.2.2 Reactive Blending.....   | 55           |
| 3.2.3 Model Compound Study.....  | 56           |

|            |   |            |
|------------|---|------------|
| 3.2.4      | Characterization of Reactive Blends.....  | 56         |
| <b>3.3</b> | <b>Results and Discussion.....</b>  | <b>59</b>  |
| 3.3.1      | Model Compound Study.....   | 59         |
| 3.3.2      | Reactive Blending.....  | 60         |
| 3.3.3      | Characterization of Reactive Blends.....  | 63         |
| 3.3.4      | “Crystallization Induced Phase Segregation” Model.....  | 85         |
| <b>3.4</b> | <b>Conclusions and future work.....</b>   | <b>89</b>  |
| <b>4</b>   | <b>REACTIVE BLENDING OF MULTIFUNCTIONAL EPOXY MODIFIERS FOR RHEOLOGICAL ENHANCEMENT OF POLYLACTIDE .....</b>  | <b>92</b>  |
| <b>4.1</b> | <b>Introduction.....</b>  | <b>92</b>  |
| <b>4.2</b> | <b>Experimental .....</b>   | <b>94</b>  |
| 4.2.1      | Materials .....   | 94         |
| 4.2.2      | Model Compound Study.....   | 95         |
| 4.2.3      | Reactive Blending.....  | 95         |
| 4.2.4      | Characterization .....  | 96         |
| 4.2.5      | Rheological Characterization.....   | 98         |
| <b>4.3</b> | <b>Results and Discussion.....</b>  | <b>99</b>  |
| 4.3.1      | Model Compound Study.....   | 99         |
| 4.3.2      | Reactive Blending.....  | 104        |
| 4.3.3      | Characterization .....  | 108        |
| 4.3.4      | Rheological Characterization.....   | 115        |
| <b>4.4</b> | <b>Conclusions and Future Work.....</b>   | <b>129</b> |
| <b>5</b>   | <b>POLYLACTIDE BASED DIRECT-LONG FIBER THERMOPLASTICS (D-LFTs) FOR AUTOMOTIVE INTERIOR APPLICATIONS .....</b> | <b>132</b> |
| <b>5.1</b> | <b>Introduction.....</b>  | <b>132</b> |
| <b>5.2</b> | <b>Experimental .....</b>   | <b>135</b> |
| 5.2.1      | Materials .....   | 135        |
| 5.2.2      | D-LFT Extrusion Process .....   | 136        |
| 5.2.3      | Characterization .....  | 137        |
| <b>5.3</b> | <b>Results and Discussion.....</b>  | <b>139</b> |
| 5.3.1      | D-LFT Extrusion Process .....   | 139        |
| 5.3.2      | Characterization .....  | 143        |
| <b>5.4</b> | <b>Conclusions and Future Work.....</b>   | <b>157</b> |
| <b>6</b>   | <b>SUMMARY AND FUTURE WORK.....</b>   | <b>159</b> |
|            | <b>BIBLIOGRAPHY.....</b>  | <b>164</b> |

## LIST OF TABLES

|  |     |
|--|-----|
| Table 2-1: Tensile properties of the PLA-NHPDMS copolymers.....  | 28  |
| Table 2-2: Tensile properties of the annealed (A) and non-annealed blend formulations.....                               | 30  |
| Table 2-3: Crystallization half-time values and Avrami constants for the samples at different isotherms .....            | 40  |
| Table 2-4: Time taken for complete isothermal melt crystallization as simulated in the DSC ....                          | 47  |
| Table 3-1: Values for thermal transitions points and % crystallinity of the non-annealed and annealed (A) test bars..... | 71  |
| Table 4-1: Molecular weight distributions of neat and extruded PLA, and the blends of PLA with Joncryl and NC-547 .....  | 115 |
| Table 5-1: Comparison of properties of basalt fiber against glass and carbon fiber [260].....                            | 134 |
| Table 5-2: Fiber weight fractions as obtained from ash test. Fiber volume fractions as calculated using Equation 2 ..... | 144 |

## LIST OF FIGURES

|  |    |
|--|----|
| Figure 1-1: Increase in the production of plastics over the last 50 years (left), prediction of plastics waste for year the 2050 (right)[3] .....  | 2  |
| Figure 1-2: Closed-loop cycle showing the ideal path taken by biobased plastics (Image sourced from <a href="http://www.europeanbioplastics.org">www.europeanbioplastics.org</a> ).....            | 3  |
| Figure 1-3: Various routes for the synthesis of PLA[27] .....  | 4  |
| Figure 1-4: Stereoisomers of lactide [27] .....  | 5  |
| Figure 1-5: Schematic representation of a reactive extrusion system [47].....  | 11 |
| Figure 2-1: Schematic of transesterification reaction between PLA and the NHPDMS .....   | 23 |
| Figure 2-2: Screw configuration used on the extruder (feed to die - left to right).....  | 23 |
| Figure 2-3: Comparative FT-IR Spectra of neat PLA and the PLA-NHPDMS copolymer .....   | 25 |
| Figure 2-4: <sup>1</sup> H NMR spectra of purified PLA-NHPDMS copolymer .....  | 25 |
| Figure 2-5: DTG curve comparing neat PLA with the PLA-NHPDMS copolymer.....  | 26 |
| Figure 2-6: DSC curves of neat PLA and the copolymer .....   | 27 |
| Figure 2-7: TEM images of the copolymer obtained at X20,000 magnification.....   | 28 |
| Figure 2-8: Comparison of elongation at break values for the blend samples.....  | 30 |
| Figure 2-9: Stress-strain curves for the copolymer blended with neat PLA (A - annealed).....   | 31 |
| Figure 2-10: Comparison of the notched Izod impact strength for the blend samples.....   | 32 |
| Figure 2-11: DSC curves comparing annealed (A) and non-annealed formulations.....  | 33 |
| Figure 2-12: Comparison of FT-IR spectra of annealed PLA and copolymer samples.....  | 34 |
| Figure 2-13: DMA analysis of the blend samples showing storage modulus, loss modulus and tan delta.....  | 35 |
| Figure 2-14: SEM images of fracture surfaces of tensile tested samples - neat PLA, 10, 20 and 30% copolymer blended samples (from top to bottom), non-annealed on left and annealed on right ..... | 36 |

|  |    |
|--|----|
| Figure 2-15: SEM images of fracture surfaces of notched Izod impact tested samples - neat PLA, 10, 20 and 30% copolymer blended samples (from top to bottom), non-annealed on left and annealed on right, notch is at bottom of image..... | 37 |
| Figure 2-16: DSC isothermal melt crystallization times for different temperatures .....  | 39 |
| Figure 2-17: Variation of fractional crystallization with time for the samples at different isotherms .....  | 40 |
| Figure 2-18: Avrami double-log plots for the melt crystallization of the samples at different isotherms.....   | 41 |
| Figure 2-19: Schematic of model demonstrating the "Crystallization Induced Phase Segregation" behavior (PLA is shown in blue and PDMS is shown in red) .....   | 43 |
| Figure 2-20: Time taken for complete isothermal melt crystallization at 90°C .....   | 45 |
| Figure 2-21: Time taken for complete isothermal melt crystallization at 100°C .....  | 46 |
| Figure 2-22: Time taken for complete isothermal melt crystallization at 110°C .....  | 46 |
| Figure 3-1: Chemical structure of the Cardolite UL-513.....  | 53 |
| Figure 3-2: Chemical structure of the Cardolite NT-3000 (final product is a mixture of both compounds).....  | 54 |
| Figure 3-3: DSC scans showing the reaction behavior between the UL-513 with stearic acid (blue) and PEG (orange).....  | 59 |
| Figure 3-4: DSC scans showing the reaction behavior between the NT-3000 with stearic acid (blue) and PEG (orange).....   | 60 |
| Figure 3-5: Screw configuration used on the extruder (feed to die - left to right).....  | 61 |
| Figure 3-6: Schematic of the reaction between PLA and the UL-513.....  | 62 |
| Figure 3-7: Schematic of the reaction between PLA and the NT-3000.....   | 62 |
| Figure 3-8: FT-IR spectra of the UL-513 and the NT-3000 .....  | 64 |
| Figure 3-9: Comparative FT-IR Spectra of neat PLA and the purified blends of UL-513 and NT-3000 with PLA.....  | 65 |
| Figure 3-10: Comparative NMR Spectra of neat PLA and the purified blend of UL-513 .....  | 66 |
| Figure 3-11: Comparative NMR Spectra of neat PLA and the purified blend of NT-3000 .....   | 67 |
| Figure 3-12: DTG curve comparing thermal degradation behavior of neat PLA and UL-513 with their reacted blends .....   | 68 |

|   |     |
|---|-----|
| Figure 3-13: DTG curve comparing thermal degradation behavior of neat PLA and NT-3000 with their reacted blends .....   | 69  |
| Figure 3-14: DSC curves of neat PLA and the reactive blends with UL-513 and NT-3000 (pellets) .....   | 70  |
| Figure 3-15: DSC curves of neat PLA and the reactive blends with UL-513 and NT-3000 (test bars) - non-annealed and annealed (A) .....   | 72  |
| Figure 3-16: DMA analysis of the blends showing storage modulus for the samples (A – annealed) .....  | 73  |
| Figure 3-17: DMA analysis of the blends showing loss modulus for the samples (A – annealed) .....   | 74  |
| Figure 3-18: Comparison of strain at break values for the UL-513 blend samples .....  | 76  |
| Figure 3-19: Comparison of strain at break values for the NT-3000 blend samples .....   | 77  |
| Figure 3-20: Stress-strain curves for the UL-513 blends with neat PLA (A - annealed) .....  | 78  |
| Figure 3-21: Stress-strain curves for the NT-3000 blends with neat PLA (A - annealed) .....   | 79  |
| Figure 3-22: SEM images of fracture surfaces of tensile tested samples - neat PLA, 10-1, 10-2.5, 10-5, 10-7.5, and 5% UL-513 blend samples (from top to bottom), non-annealed on left and annealed on right.....  | 81  |
| Figure 3-23: SEM images of fracture surfaces of tensile tested samples - neat PLA, 10-1, 10-2.5, 10-5, 10-7.5, and 5% NT-3000 blend samples (from top to bottom), non-annealed on left and annealed on right..... | 82  |
| Figure 3-24: Comparison of the notched Izod impact strength for the UL-513 blend samples ...  | 83  |
| Figure 3-25: Comparison of the notched Izod impact strength for the NT-3000 blend samples .   | 84  |
| Figure 3-26: Schematic demonstrating the "Crystallization Induced Phase Segregation" phenomena in the PLA-epoxy blend samples.....  | 86  |
| Figure 4-1: Chemical structure of the BASF Joncryl-4368-C .....   | 93  |
| Figure 4-2: Chemical structure of the Cardolite NC-547 .....  | 93  |
| Figure 4-3: Model compound study showing the reaction between Joncryl and stearic acid using a DSC scan.....  | 102 |
| Figure 4-4: Model compound study showing the reaction between Joncryl and PEG using a DSC scan .....  | 103 |

|   |     |
|---|-----|
| Figure 4-5: Model compound study showing the reaction between NC-547 and stearic acid using a DSC scan.....   | 103 |
| Figure 4-6: Model compound study showing the reaction between NC-547 and PEG using a DSC scan .....   | 104 |
| Figure 4-7: Predicted structures formed due to the reaction between the PLA and Joncryl at less than 1 molar ratio of Joncryl to PLA (left), and at a greater than 1 molar ratio for Joncryl to PLA (right) ..... | 105 |
| Figure 4-8: Screw configuration used on the extruder (feed to die - left to right).....   | 106 |
| Figure 4-9: Schematic of reaction between PLA and Joncryl .....   | 107 |
| Figure 4-10: Schematic of reaction between PLA and NC-547 .....   | 107 |
| Figure 4-11: Comparative FT-IR Spectra of neat PLA and the blends with Joncryl and NC-547 .....   | 108 |
| Figure 4-12: Comparative <sup>1</sup> H NMR spectra of neat PLA and the reactive blend with Joncryl at 10 % by weight .....   | 109 |
| Figure 4-13: Comparative <sup>1</sup> H NMR Spectra of neat PLA and the reactive blend with NC-547 at 3.5 % by weight .....   | 110 |
| Figure 4-14: DTG curves comparing neat PLA and Joncryl with their blends .....  | 111 |
| Figure 4-15: DTG curves comparing neat PLA and NC-547 with their blends .....   | 112 |
| Figure 4-16: DSC curves of neat PLA and the blends with Joncryl and NC-547 .....  | 113 |
| Figure 4-17: Melt flow rates of the samples, tested at 190°C with a load of 2.16 kg .....   | 117 |
| Figure 4-18: Comparison of complex viscosity at varying shear rates for Joncryl blends (180°C) .....  | 120 |
| Figure 4-19: Comparison of complex viscosity at varying shear rates for Joncryl blends (200°C) .....  | 120 |
| Figure 4-20: Comparison of complex viscosity at varying shear rates for NC547 blends (180°C) .....  | 121 |
| Figure 4-21: Comparison of complex viscosity at varying shear rates for NC547 blends (200°C) .....  | 121 |
| Figure 4-22: Comparison of extensional viscosity at a strain rate of 0.5 s <sup>-1</sup> for Joncryl blends at 180°C .....  | 123 |

|  |     |
|--|-----|
| Figure 4-23: Comparison of extensional viscosity at a strain rate of 1.0 s <sup>-1</sup> for Joncryl blends at 180°C .....   | 123 |
| Figure 4-24: Comparison of extensional viscosity at a strain rate of 5.0 s <sup>-1</sup> for Joncryl blends at 180°C .....   | 124 |
| Figure 4-25: Comparison of extensional viscosity at a strain rate of 0.5 s <sup>-1</sup> for NC-547 blends at 180°C .....  | 125 |
| Figure 4-26: Comparison of extensional viscosity at a strain rate of 1.0 s <sup>-1</sup> for NC-547 blends at 180°C .....  | 125 |
| Figure 4-27: Comparison of extensional viscosity at a strain rate of 5.0 s <sup>-1</sup> for NC-547 blends at 180°C .....  | 126 |
| Figure 4-28: Extensional viscosity of each sample at 0.5, 1.0 and 5.0 s <sup>-1</sup> at 180°C .....   | 126 |
| Figure 5-1: Schematic showing the production of basalt fiber from basalt rock by melt spinning (Image sourced from <a href="http://www.basaltlft.com">www.basaltlft.com</a> ) .....        | 134 |
| Figure 5-2: Setup showing the fiber feeding mechanism for the D-LFT preparation .....  | 137 |
| Figure 5-3: Schematic showing the extrusion setup used for the D-LFT preparation. Fiber feed point at Zone 8 was used initially (top) and later optimized to feed at Zone 4 (bottom) ..... | 141 |
| Figure 5-4: Two kneading blocks as shown above were used to effectively melt PLA before fiber feed and break down fiber after fiber feed.....  | 142 |
| Figure 5-5: Ash testing of the samples to measure fiber loading content (before, during and after test).....   | 144 |
| Figure 5-6: Optical micrographs of fiber specimens used for measuring fiber length distribution (left) with the corresponding distribution (right) .....                                   | 145 |
| Figure 5-7: DSC scans of the composite samples showing thermal transitions .....   | 147 |
| Figure 5-8: Comparative stress-strain curves of the composite samples .....  | 148 |
| Figure 5-9: Strain at break values for the composite samples .....   | 149 |
| Figure 5-10: Tensile moduli of the composite samples .....   | 149 |
| Figure 5-11: Comparison of the experimental moduli data with the theoretical predictions using semi-empirical models available in existing literature .....                                | 151 |
| Figure 5-12: Impact strength of the composites samples as obtained from notched Izod test ...  | 152 |
| Figure 5-13: Storage moduli for the composite samples as a function of temperature .....   | 153 |

Figure 5-14: Tan Delta for the composite samples as a function of temperature..... 153

Figure 5-15: SEM images of fracture surfaces of tensile tested samples – (a) neat PLA, (b) SB, (c) LB, (d) LBx2, (e) SG and (f) LG. The images on the left are at a magnification of x70 and the ones on the right are at x200 ..... 155

Figure 5-16: SEM images of fracture surfaces of Izod impact tested (impact direction ←) samples – (a) neat PLA, (b) SB, (c) LB, (d) LBx2, (e) SG and (f) LG. The images on the left are at a magnification of x70 and the ones on the right are at x200..... 156

## KEY TO ABBREVIATIONS

|       |   |
|-------|---|
| PLA   | Polylactic acid, Polylactide              |
| PDMS  | Polydimethylsiloxane                      |
| PEG   | Polyethylene glycol                       |
| REX   | Reactive Extrusion                        |
| TGA   | Thermogravimetric Analysis                |
| DSC   | Differential Scanning Calorimetry         |
| DMA   | Dynamic Mechanical Analysis               |
| NMR   | Nuclear Magnetic Resonance                |
| FT-IR | Fourier Transform – Infrared Spectroscopy |
| DCM   | Dichloromethane, Methylene Dichloride     |
| SEM   | Scanning Electron Microscopy              |
| TEM   | Transmission Electron Microscopy          |

# 1 INTRODUCTION

Some excerpts are directly reproduced from *Giri, P., et al. (2018). Using Reactive Extrusion to Manufacture Greener Products: From Laboratory Fundamentals to Commercial Scale. American Chemical Society. 1304: 1-23*

## 1.1 Motivation

A recent technical report published by the World Economic Forum in collaboration with the Ellen MacArthur Foundation claims that by the year 2050, there will be more plastics in the ocean than fish [1]. Although this might not be the most accurate representation of the reality in 2050, it does paint a vivid picture of the plastics waste problem that we currently face (Figure 1-1). Over the past decade, the issue of plastics waste has been ubiquitous in both the scientific and non-scientific communities [2, 3]. Within the last 50 years, the production of plastics has gone up by almost 20 times, yet there exist very few viable end-of-life options to address the plastics waste generated (Figure 1-1). By current estimates, only 14% of the waste gets recycled, whereas 40% of it is diverted to landfills, 14% of it goes towards incineration or energy recovery, and a staggering 32% results in leakage to the environment [1]. The leakage of these plastics waste has recently led to the investigation into the formation of microplastics in both soil and marine environments and has been related to adverse health effects in all living creatures [4-8]. This dire situation has necessitated the immediate need for development of plastics with a viable end-of-life option.

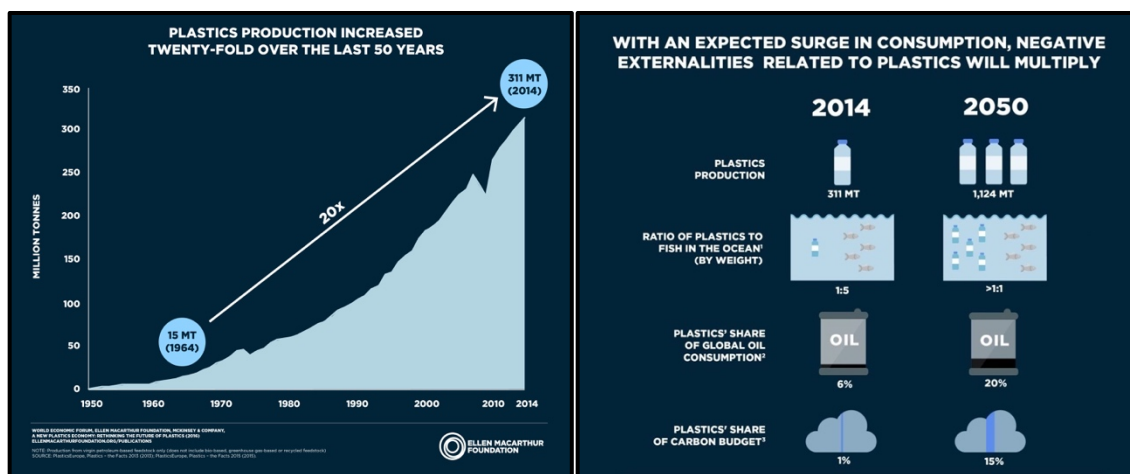


**Figure 1-1:** Increase in the production of plastics over the last 50 years (left), prediction of plastics waste for year the 2050 (right) [3]

Biobased plastics or materials have been defined by the IUPAC as being “*composed or derived in whole or in part of biological products issued from biomass (including plant, animal, and marine or forestry materials)*” [9]. Biobased plastics offer a significant value addition by reducing the amount of carbon footprint generated during their production [10]. Certain biobased plastics such as polylactic acid or PLA, also happen to be biodegradable under controlled conditions (for e.g. composting) thus offering the added benefit of having a viable end-of-life option [11]. Thus, materials such as PLA that are both biobased and biodegradable, hold the most promise when it comes to addressing the plastics waste problem by closing the loop around the production and use cycle (Figure 1-2). Despite a deluge of previously reported scientific literature on the synthesis and modification of PLA for various applications, only few cost-effective strategies exist, mostly due to these studies being academic in nature and often facing difficulty in scaling up [12-15]. Hence, going forward, the development of PLA-based materials with an optimum price to performance ratio forms the primary motivation of this thesis.

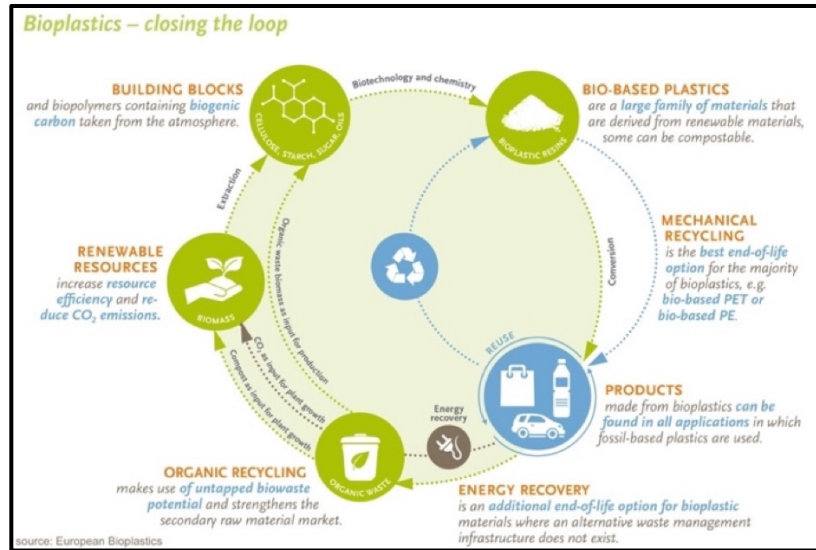


**Figure 1-2:** Closed-loop cycle showing the ideal path taken by biobased plastics (Image sourced from [www.europeanbioplastics.org](http://www.europeanbioplastics.org))

## 1.2 Polylactide (PLA)

The past few decades have seen an increasingly growing demand for biobased and biodegradable polymers to be commercially adopted as replacements for existing fossil-fuel based plastics. This need arises not only from the fact that the production of these plastics results in a significantly high carbon footprint, but also because of the lack of environmentally safe end-of-life options for the products made out of them [16-21]. This demand has also driven a significant amount of academic as well as industrial research into the production and property modification of biobased polymers, leading to the creation of a wide spectrum of these polymers, most notable of which is polylactide (PLA) [22]. PLA is a biodegradable aliphatic polyester derived from lactic acid which manifests itself in nature in several forms. Lactic acid or 2-hydroxypropionic acid, is a naturally occurring  $\alpha$ -carboxylic acid that can be artificially synthesized or obtained through bacterial fermentation [23]. Since lactic acid possesses an asymmetric carbon atom, it is optically active, and exists in the form of two enantiomers: the L(+) and the D(-). Most of the commercially manufactured lactic

acid is produced through the bacterial fermentation process since it provides better yields of the desired L-lactic acid and gives off reduced amount of by-products [13].

PLA was first synthesized by Wallace Carothers in 1932 at DuPont, by heating lactic acid under vacuum while removing the condensed water [24]. However, it was found that the resulting product was of low molecular weight and showed poor mechanical properties. PLA can also be synthesized from lactide, which is the cyclic di-ester of lactic acid. Currently, high molecular weight PLA is produced by either one of the following processes as shown in Figure 1-3 [12]: (a) ring-opening polymerization of the lactide monomer, or (b) polycondensation reaction of lactic acid followed by an azeotropic distillation process using a high-boiling solvent to drive the equilibrium reaction forward. The former process has been commercialized by Cargill Inc. [25], and the latter by Mitsui Toatsu Chemicals [26]. A third process involving the use of chain coupling agents to increase the molecular weight of the initial PLA formed has been explored but has not been adopted due to several factors such as added costs and presence of unreacted impurities in the final product [23].

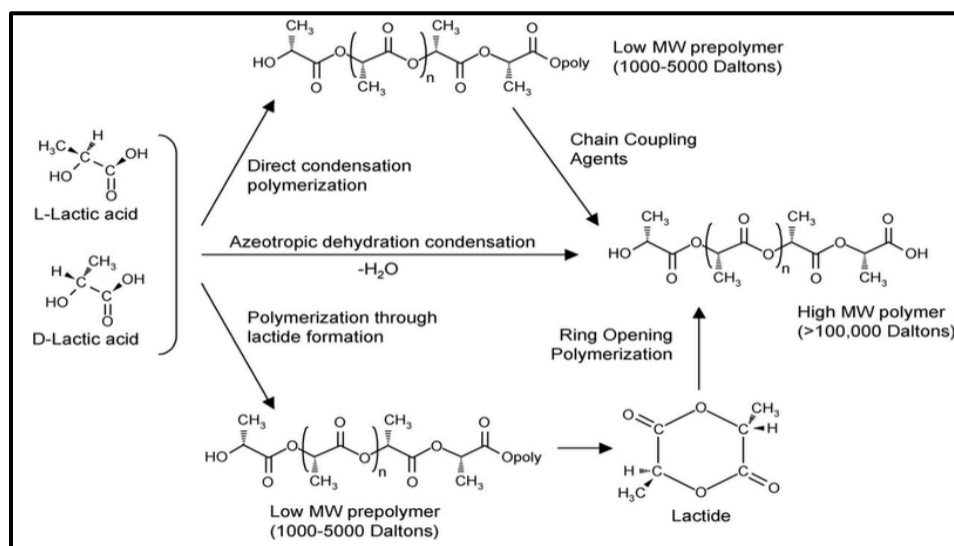


**Figure 1-3:** Various routes for the synthesis of PLA[27]

As shown in Figure 1-4, lactide exists in the form of three stereoisomers [8]: L-lactide, D-lactide and meso-lactide.

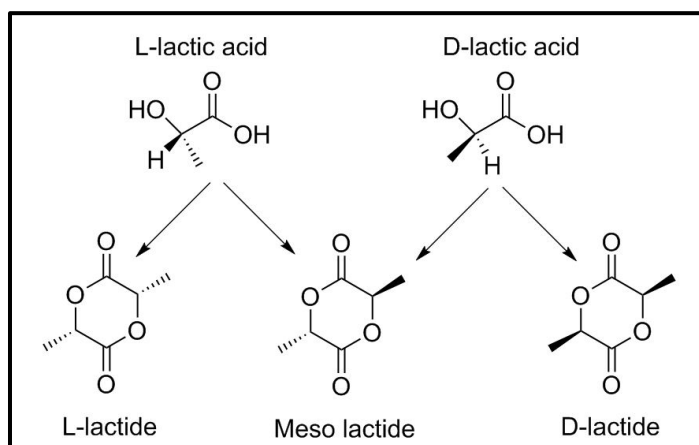


**Figure 1-4:** Stereoisomers of lactide [27]

The stereochemical composition of the PLA formed by the ring-opening polymerization of lactide is determined by the stereochemistry of the lactide monomers [12]. This is of considerable importance as several properties, including the melting point and the rate and extent of crystallization, are largely affected by the stereochemical makeup of the final PLA obtained as the product. Pure poly(L- or D- lactide) has a melting point of around 180°C, which reduces with an increase in content of a stereochemical impurity. This trend has also been observed for the rate and extent of crystallization. However, the glass transition temperature has been found to be independent of the stereochemical composition and lies in the range of 55 – 60°C. The thermal degradation of PLA sets in about 180 – 190°C, resulting in rapid loss of molecular weight, and is attributed to chain scission [23].

PLA exhibits excellent mechanical properties that are comparable to those of polystyrene (PS) [27]. The tensile strength, tensile modulus and flexural modulus of PLA have been found to be in the range of values for that of PS under similar testing conditions. Due to its similarity in properties

with PS, PLA is increasingly finding use as an environment-friendly substitute for PS. However, its toughness and elongation at break has been found to be considerably low and limits the use of PLA in certain applications.

The barrier properties of PLA have been well studied due to its importance as a packaging material [28]. It has been found that PLA performs better than PS when it comes to the permeability of oxygen, carbon dioxide and moisture. The migration of chemical species from bulk in PLA has been studied due to its extensive usage in the packaging of food and biomedical supplies. It was found that there was almost none to very little migration of lactic acid or its oligomers from the PLA into the packaged product, thus, granting PLA the status of “Generally Recognized as Safe” (GRAS) by the United States Food and Drug Administration [29].

Since it is a biobased plastic, the biodegradability of PLA has been thoroughly studied in order to further establish its standing as an environmentally friendly material [30]. It has been found that PLA is not readily susceptible to attack by microorganisms in soil and needs to break down to lower molecular weight oligomers before it starts degrading in a natural environment. However, there are a handful of known microbes that have been found to degrade PLA through the enzymatic route [30].

Due to its unique portfolio of properties, PLA has been used in a variety of applications, including packaging, manufacture of commodity items, and biomedical implants. Despite its versatility, PLA suffers from a few limitations, which restricts its processability and subsequently its potential applications. These include an inherently low toughness, low heat deflection temperature, slow rate of crystallization and poor melt strength. Extensive research has been carried out in order to resolve these issues [31], however, key issues still remain. Addressing these issues forms the primary focal point of this thesis.

## **1.3 Property Modification of PLA**

The properties of PLA can be tailored depending on the type of end-use application. Several strategies have been reported in literature in order to do achieve this [14, 32-34]. Since the key performance requirement that we have tried to address as a part of this thesis is the low toughness of PLA, we discuss previously reported strategies in order to develop an understanding of the processing techniques involved.

Toughness of a material can be defined as its ability to absorb energy and undergo plastic deformation before reaching its point of fracture [35]. Since the advent of inexpensive methods to produce PLA commercially, there has been significant attention placed on its commercial applications. However, the one major issue that has consistently plagued PLA has been its inherent brittleness or, otherwise stated, its low toughness [34]. This has severely restricted the commercial applications of PLA in several cases where higher impact strength is required. Several approaches, including plasticization, copolymerization and melt blending with tougher polymers, have been tried in order to improve its toughness. The major pitfall associated with each of these methods is that the increase in toughness is achieved at the expense of the tensile strength and modulus. Thus, developing a material with a desired balance of strength and toughness has become the subject of intensive research.

The following is a brief discussion of the various methods that have been implemented to improve the toughness of PLA in existing literature [14, 32, 33]:

### **1.3.1 Alteration of Stereochemistry and Processing**

It has been well established that the mechanical properties of PLA are strongly dependent on its stereochemical composition, its percentage of crystallinity and its orientation [36]. The mechanical properties including toughness were found to increase with an increase in percent crystallinity,

which in turn was found to be directly proportional to the stereochemical purity. Also, the toughness was found to increase with an increase in orientation. Since both stereochemical composition and orientation can be manipulated by altering processing conditions, toughness can be improved upon by utilizing this approach. However, it has been found that the increase in toughness due to these factors is marginal, and is lost during post-processing of the polymer, thus negating the use of this approach [33].

### **1.3.2 Copolymerization**

Copolymers of PLA with several other polymers have been synthesized in order to improve their overall mechanical properties. There are two major methods through which these PLA-based copolymers are produced: polycondensation reaction of lactic acid and the desired monomer, or the ring-opening polymerization of lactide with the monomer [33]. The most effective PLA copolymer systems that have resulted in an improvement in toughness include poly( $\epsilon$ -caprolactone) [37], PLA-poly(hydroxyalkanoate) [38], and PLA-poly(ethylene glycol) [39]. The toughness of these copolymers has been found to be dependent on the relative content of the polymers, the use of a catalyst during the copolymerization, and more importantly, the inherent miscibility between the two polymers [14]. The major complication associated with the studies conducted on PLA-copolymer systems is that there exists no uniform reporting of the measure of toughness, due to the use of different testing methods as well as the use of different sample types. This prevents a comprehensive comparative study of the efficacy of different copolymer systems in improving the toughness. Also, the repeatability of the properties obtained has been reported to be relatively low, and since they have been synthesized in small batch processes, few of them have been commercially viable [33].

### **1.3.3 Blending**

Blending of PLA with a tougher and more flexible polymer is another common route to increasing the toughness of neat PLA. There are several studies that have reported the blending of PLA with both biodegradable and non-biodegradable polymers in order to improve the toughness. Some of the notable PLA blends that have successfully resulted in improving toughness are: PLA/polycaprolactone [40], PLA/poly(hydroxyalkanoate) [41], and PLA/poly(butylene succinate) [42] among the biodegradable ones, and PLA/polyethylene [43], and PLA/Acrylonitrile-butadiene-styrene [32] among the non-biodegradable ones. The improvement in toughness has been generally found to be dependent upon the content of the modifier added, and the miscibility between PLA and the modifier [33]. The advantage of blending lies in the fact that it is less expensive compared to copolymerization. However, its major disadvantage in most cases is that the immiscibility between PLA and the modifier leads to phase-separation. This occurs usually with physical aging as well as during processing, leading to loss of the improvement obtained initially. In order to enhance the miscibility, numerous compatibilizers have been tried and tested. Yet, this still remains a major setback to the blending approach [33].

### **1.3.4 Plasticization**

The addition of various plasticizers to PLA to make it tougher has been attempted with varying degrees of success [32]. Plasticizers are quite commonly used to increase the flexibility of a polymer by increasing its free volume, subsequently reducing its glass transition temperature. The increase in free volume increases the mobility of the polymer chains leading to better ductility and toughness. The most effective plasticizers that have been used to improve the toughness of PLA include: lactide monomer, citrate esters, glycerin triacetate, poly(ethylene glycol) and poly(ethylene oxide) [14]. The improvement in toughness has been found to increase with the

plasticizer content up to a certain point, beyond which the toughening effect is reversed due to leaching out of the plasticizer at higher concentrations [33]. Plasticization offers the benefit of ease of processing and being inexpensive. However, the major drawback with plasticization lies in the fact that a significant plasticizer content is required to obtain the desired toughness, and also, there is considerable leaching of the plasticizer with time [14].

The methods outlined above are the major routes to improving the toughness of PLA, however, as highlighted, each has its own merits and demerits. Also, one major downside that is observed across all methods is that the increase in toughness obtained is almost always accompanied by a simultaneous reduction in tensile strength. Thus, designing a PLA-based system with the ideal balance of both is critical. In the current work, we will explore several techniques to improve the toughness of PLA and compare them with properties observed in prior studies.

#### **1.4 Reactive Extrusion (REX)**

All of the work that will eventually be discussed as a part of this thesis was performed using extrusion-based processes, more specifically, reactive extrusion (REX). This necessitates the development of an understanding of this processing technique.

Extrusion-based systems offer a continuous and inexpensive route for the processing of polymers. Specifically, reactive extrusion (REX) is an extremely versatile method that can be well-adapted for a wide-range of applications, including polymerization reactions [44], chemical modifications of polymers through grafting, branching and functionalization reactions, and also physical modifications such as reactive blending and compatibilization [45, 46].

Figure 1-5 the schematic of a basic REX process. Solid and liquid reactants are fed through a feeder and an injection pump, respectively. The barrel which consists of individually heated blocks, also houses the screw elements, where the mixing and conveying occurs. The final product

exits the extruder through a die at the end of the barrel. The motor at the front of the assembly powers the screws by providing the necessary torque. Extruders are usually of two major types: single-screw or twin-screw, and in the case of twin-screw, they are available in two major configurations, i.e. co-rotating and counter-rotating. As evident, in the co-rotating twin-screw extruder, the two screws rotate in the same direction, whereas, in the counter-rotating configuration, the rotation of the screws are in opposite directions to each other [47].

The different components of an extruder give rise to several controllable process parameters including the screw configuration, the screw speed, the feed rate and the temperature profile. Through the manipulation of these parameters, we can create a range of unique operating conditions. The screw configuration is composed of a combination of conveying elements that carry the reaction mixture forward, and the kneading elements, which apply a shear force on the reaction mixture thereby providing the thorough mixing needed.

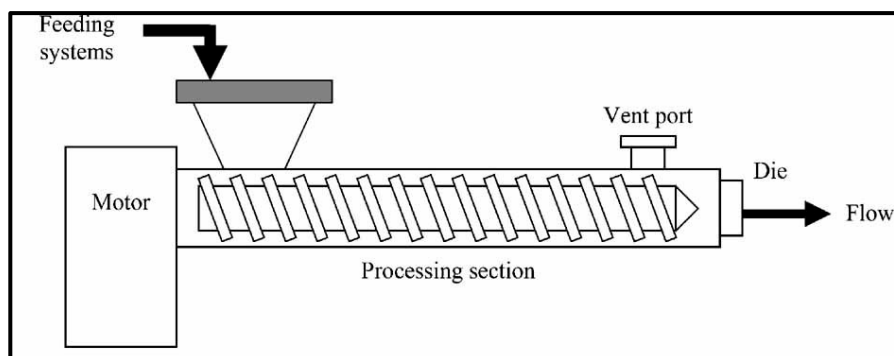


**Figure 1-5:** Schematic representation of a reactive extrusion system [47]

Reactive extrusion offers several advantages over conventional polymer processing, such as [48]:

- a. Continuous process with significantly low reaction time compared to batch processing. This prevents prolonged exposure to elevated operating temperatures that could easily lead to the undesired thermal degradation of the polymer being processed.

- b. Being a solvent-free process, it eliminates the added costs of having solvent inlet and recycling streams, and also avoids the usage of potentially harmful solvents, thus ensuring a safer approach.
- c. The shear forces produced by the screw elements spread out the reaction mixture and create thin layers of the material in the area between the screws. This exposes a high surface area that is available for the reaction to occur. Furthermore, this minimizes the temperature gradients developed due to drastic increase in viscosity during polymerization reactions; thus, ensuring efficient heat and mass transfer within the system.
- d. It offers efficient downstream devolatilization of the reaction mixture to remove gaseous byproducts, which drives the reaction forward, thus resulting in a higher efficiency.
- e. Its modular buildup allows for control over several processing parameters. This along with the fact that multiple input streams can be incorporated into the system makes the REX ideal for a diverse range of applications.

REX has been extensively used for the polymerization and property modifications of several biobased and biodegradable plastics and will be the processing technique-of-choice used for the entirety of this work [49, 50].

Having taken an in-depth look into the current status of research in PLA, and having developed an understanding of reactive extrusion, further studies into the property modification of PLA will be carried out. The first chapter will focus on the synthesis of a novel copolymer for impact modification of the PLA. The second chapter deals with the use of a biobased plasticizer to improve the flexibility of PLA. In the third chapter, we explore the use of a biobased chain extender to improve the melt strength of PLA. Lastly, the fourth chapter focuses on the production of PLA-

based direct long fiber thermoplastics for automotive interior applications.

The work done in the first three chapters was carried out in collaboration with Natur-Tec (a division of Northern Technologies International Corporation), MN, USA. The work in chapters 2 and 3 were also performed in collaboration with the Cardolite Corporation, PA, USA. For the last chapter dealing with the PLA composite materials, all the work done was in collaboration with the Ford Motor Company, MI, USA.

## 2 POLYLACTIDE-POLYDIMETHYLSILOXANE COPOLYMER FOR TOUGHENING APPLICATIONS

### 2.1 Introduction

Due to its unique portfolio of properties, polylactide (PLA) makes for an excellent candidate for injection-molded disposable articles. Being both biobased and biodegradable, it ensures a lower carbon footprint while providing for viable end-of-life options. Also, the mechanical properties including tensile strength and modulus are within the range of polystyrene (PS), thus making it a suitable option as a potential replacement for PS. However, PLA still faces performance issues that limit its usage in injection-molded commodity items. These include poor tensile and impact toughness arising due to a high glass transition temperature, a low heat deflection temperature preventing its use at elevated temperatures, and last but not the least, a slow rate of crystallization that further negatively impacts its mechanical performance [15].

Some of the common approaches adopted to increase the toughness of PLA include manipulation of the stereochemical makeup of the PLA during either the manufacturing or the processing step, blending of the PLA with an impact modifier, rubber toughening agent or a plasticizer, or using PLA based copolymers as modifiers to ensure better compatibility thus leading to improved mechanical properties. There exists a plethora of literature describing means and methods to successfully improve upon the ductility of PLA, however, only a select few have been found to be both effective as well as economically viable [14, 32-34, 36, 51, 52].

The objective of this study was to use the copolymerization route to develop a silicone-based PLA copolymer to act as an impact modifier in a neat PLA matrix. The rationale behind choosing silicone was to exploit its inherent flexibility to toughen the base PLA resin. PDMS has an extremely flexible -Si-O-Si- backbone arising due to the fact that the rotational energy around a

(CH<sub>3</sub>)<sub>2</sub>Si-O- bond is only 3.3 kJ/mol whereas in comparison it is 13.8 kJ/mol around a CH<sub>2</sub>-CH<sub>2</sub> bond in polyethylene [53]. This is also evidenced by the fact that the glass-transition temperature of PDMS is around -120°C, and further supports the hypothesis that the incorporation of a PDMS phase in PLA would make it more ductile [54]. However, PLA and PDMS are both highly incompatible with each other owing to their difference in solubility parameters, (Hildebrand solubility parameter  $\delta$ ,  $\delta_{\text{PLA}} = 19.8 \text{ MPa}^{1/2}$  and  $\delta_{\text{PDMS}} = 15.1 \text{ MPa}^{1/2}$ ), which hinders their miscibility [55]. This justifies the requirement for a PLA-PDMS copolymer which would instead have a  $\delta$  value that would be closer to the average of  $\delta_{\text{PLA}}$  and  $\delta_{\text{PDMS}}$ , (considering the formation of a diblock copolymer), thus resulting in improved compatibility with a PLA matrix as opposed to direct blending of PLA and PDMS. Based on these theoretical assumptions, the current study focuses on first synthesizing a PLA-PDMS block copolymer, followed by blending of the copolymer with neat PLA in order to achieve the desired improvement in properties.

Reactive extrusion (REX) was chosen as the preferred technique for carrying out the transesterification reaction leading to the formation of the block copolymer. REX provides an expeditious, solvent-free, and cost-efficient method, that also offers enhanced mass and heat transfer during the reaction as opposed to a batch process [44, 56]. Since the residence time during the REX process is in the order of 2~3 minutes, the use of amine-terminated PDMS was proposed due to the higher reactivity of primary amines, as opposed to the unreactive methyl end groups in regular PDMS. Thermal annealing was used as a post processing method for introducing higher crystallinity into the PLA matrix, since the injection molding process does not allow for sufficient time for the PLA to fully crystallize, thus leading to poor mechanical properties [57].

## 2.2 Experimental

The experimental work on this project was carried out under two distinct sections: the first part

involved the synthesis of a range of copolymers by reacting a particular grade of PLA with varying molecular weights of the NHPDMS, followed by their characterization. The second part involved the selection of the copolymer with the optimal mechanical performance and melt blending it with a specific injection-molding grade of PLA to obtain the desired improvements in mechanical performance.

## **2.2.1 Synthesis and Characterization of Copolymer**

### **2.2.1.1 Materials**

The 3051D commercial grade of PLA was used for this section and was sourced from NatureWorks LLC (Minnesota, USA). This grade has a weight-average molecular weight of  $\sim 130,000$  g/mol and a meso-lactide content of  $\sim 8\%$  [58]. Aminopropyl-terminated polydimethylsiloxane (NHPDMS) of three different molecular weights, 1000, 5000 and 30,000 g/mol, were purchased from Gelest Inc. (Pennsylvania, USA). The transesterification catalyst, tin(II)-ethylhexanoate or  $\text{Sn}(\text{Oct})_2$ , was purchased from Sigma-Aldrich (Wisconsin, USA), along with the other required reagents including dichloromethane and methanol. Deuterated chloroform ( $\text{CDCl}_3$ ) which was used as the solvent for NMR analysis, was purchased from Cambridge Isotope Laboratories (Massachusetts, USA).

### **2.2.1.2 Synthesis via REX**

The copolymer was synthesized via a transesterification reaction between the PLA and the NHPDMS using reactive extrusion as a facile technique to carry out the reaction. Since PLA is easily susceptible to hydrolytic degradation, especially in the presence of elevated temperatures and shear forces in an extruder, the PLA pellets were dried at  $60^\circ\text{C}$  in an oven for 24 hours prior to being extruded. The NHPDMS and  $\text{Sn}(\text{Oct})_2$  were mixed along with the PLA pellets before being fed into the hopper. A Century ZSK-30 (Michigan, USA) co-rotating twin screw extruder

with a screw diameter of 30mm and a L/D ratio of 42 was used for the process. The temperature profile used on the extruder going from the feed section to the die was as follows: 140/150/160/160/160/170/170/170/160°C. The screw speed and throughput were 125 rpm and 150 gm/min respectively. The extrudate in the form of a strand was quenched by passing it through a cold-water bath and then pelletized. The pellets were then dried in an oven at 60°C for 24 hours before being characterized.

In order to remove any unreacted NHPDMS from the extrudate, a precipitation method was adopted for the purification of the sample [59]. The extrudate was first dissolved in dichloromethane, which dissolves the neat PLA, the copolymer and the unreacted NHPDMS. This was followed by the addition of an excess quantity of methanol which precipitates out the PLA and the copolymer leaving the unreacted NHPDMS in solution. This process was repeated for at least three times to ensure complete purification. The purified sample was then used for Fourier Transform Infrared Spectroscopy (FT-IR) and NMR studies. It should be noted that the purification step was not used for the copolymer while preparing injection molded samples.

### **2.2.1.3 Characterization**

FT-IR spectra of neat PLA and the purified product were recorded using the ATR mode of a Shimadzu IRAffinity-1 spectrometer (Shimadzu Co., Japan) equipped with a single reflection MIRacle ATR attachment (PIKE Technologies, USA). The spectra were obtained in the absorption mode within the spectral range of 4000-600  $\text{cm}^{-1}$ .

$^1\text{H}$  NMR analysis of the samples were performed by first dissolving the purified extrudate in a deuterated chloroform ( $\text{CDCl}_3$ ) solvent. The spectra were recorded on a 500 MHz Varian Unity Plus NMR spectrometer (Varian Associates Inc., USA) at room temperature. Spectra of the purified extrudate were compared with that of neat PLA to observe for peak shifts post-reaction.

The thermal degradation properties were evaluated using a thermogravimetric analyzer, TGA Q50 (TA Instruments, USA), by heating the sample from room temperature to 550°C at a rate of 10°C/min under a nitrogen atmosphere. Also, the thermal transitions of the samples were obtained by using a differential scanning calorimeter, DSC Q20 (TA Instruments, USA). The samples were heated up to 200°C starting at room temperature at a rate of 10°C/min under a nitrogen atmosphere. Injection molded tensile test bars were prepared using a table-top DSM micro-injection molding machine. The neat copolymer pellets, as well as the mixture of neat PLA and copolymer pellets in the required weight ratio, were mixed and fed into the co-rotating twin-screw DSM Micro 15cc compounder (DSM Research B.V., The Netherlands) at a temperature of 190°C and a screw speed of 100 rpm. After attaining a constant level of torque which ensures thorough mixing, the polymer melt is transferred to a DACA Micro injector (DACA Instruments, USA) with a barrel temperature of 190°C. The melt is then injected into the appropriate mold, which is maintained at a temperature of 50°C, at an injection pressure of ~10 bar, and then held for ~15 seconds inside the mold to cool down before being removed.

The tensile testing was carried out on an Instron model 5565-P6021 (Instron, USA) mechanical testing fixture setup with a 5 kN load cell. The testing was carried out in accordance with the ASTM D882-12 standard test method for tensile properties of thin plastic sheeting[13]. The rate of grip separation was set at 12.5 mm/min which was as per the ASTM D882 specifications. A minimum of six replicates were used to ensure repeatability of the test data.

Transmission electron microscopy (TEM) was used to study the dispersion of the NHPDMS within the PLA phase in the copolymer samples. An ultra-high resolution JEOL 2200FS (JEOL Ltd., USA) transmission electron microscope was used to perform the imaging on the samples at an accelerating voltage of 200 kV. The images were collected using a Gatan Multiscan camera (Gatan

Inc., USA). Ultrathin sections (~100 nm) of the copolymer samples were cut from the injection molded tensile test bars using a Leica CM1850 Cryostat cryo-ultramicrotome (Leica Biosystems Inc., USA).

## **2.2.2 Melt Blending and Injection Molding of Copolymer with Neat PLA**

### **2.2.2.1 Materials**

The 3001D injection-molding grade of PLA, supplied by NatureWorks LLC (Minnesota, USA) was used for this section of the study. The 3001D grade has a similar molecular weight to that of the 3051D grade, however, its meso-lactide content is around 1~2% as opposed to the 8% in the 3051D, thus making the 3001D much more thermally stable [58]. This is clearly demonstrated by the fact that the melting point ( $T_m$ ) of the 3051D grade is ~150°C, whereas that of the 3001D grade is ~170°C. For this section of the study, only the 30,000 g/mol grade of the NHPDMS from Gelest, Inc. was used. The other reagents used were the same as those used in the previous section. Three different nucleating agents were used for the in-mold annealing experiments. A talc masterbatch was procured from Natur-Tec (Minnesota, USA). The masterbatch was composed of PLA with a talc loading level of 10% by weight. A high purity grade of poly(D-lactide), PDLA – D070, was obtained from Total-Corbion PLA (The Netherlands). Licomont Nav101, a commercially available proprietary nucleating agent was obtained from Clariant AG (Switzerland). The PDLA-D070 and the Licomont Nav101 were used as is, and also in the form of a masterbatch during the molding process. The masterbatch for each of the nucleating agents with PLA was prepared via twin-screw extrusion at our lab.

### **2.2.2.2 Synthesis via REX and Injection Molding**

The PLA-NHPDMS copolymer was synthesized using the same reactive extrusion procedure as described earlier. However, for this section, a LabTEch LTE-26 (LabTEch, Thailand) co-rotating

twin screw extruder with a screw diameter of 26mm and a L/D ratio of 44 was used. The temperature profile used on the extruder going from the feed section to the die was as follows: 170/175/180/180/180/185/185/185/185°C. The screw speed and throughput were 100 rpm and 150 gm/min respectively. The appropriate composition, i.e. 95% by weight of dried PLA pellets along with 5% by weight of the 30,000 g/mol NHPDMS were premixed along with 0.1% of the catalyst, Sn(Oct)<sub>2</sub>, before being fed into the hopper. The synthesized copolymer was used as-obtained for melt blending and injection molding with the neat PLA 3001D without any additional purification steps.

A thermal annealing step was introduced in this section of the study to increase the amount of crystallinity in the samples. This was achieved by placing the injection molded article, either the tensile test bar or the notched Izod test specimen, in a vacuum oven (no vacuum was applied during the process), while laying them out on a flat tray. The temperature of the oven was uniformly maintained at 95°C for the entire duration of the annealing process which lasted for 1 hour. At the end of 1 hour, the tray holding the samples was carefully removed from the oven and the samples were allowed to cool down slowly to room temperature. The samples were allowed to equilibrate for at least a day before any testing was performed on them.

### **2.2.2.3 Characterization**

The tensile test specimens needed to study the mechanical behavior of the blends were prepared using a DSM micro-injection molding machine by following the same methodology and equipment as used in the earlier section. Also, injection molded test bars required for the notched Izod impact testing were prepared using an 82-ton Toshiba EC85SX (Toshiba Machine Co., USA) injection molding machine. The barrel and the mold temperatures were set at 190°C and 24°C respectively. The injection pressure used was 330 psi and the holding time was set at around ~30s.

The tensile testing was performed using an Instron test setup in accordance with the ASTM D882 standards as described earlier.

The notched Izod impact properties were studied using a Tinius Olsen Model IT504 (Tinius Olsen, USA) pendulum impact tester equipped with a Tinius Olsen Model Impact 104 test controller. The testing was carried out in accordance with the ASTM D256 standard test method for determining the Izod pendulum impact resistance of plastics [60]. The samples were notched using a Tinius Olsen Model 899 Specimen Notcher. The test specimens had dimensions of 0.5 X 0.125 inches and the notch marked was 0.1 inch deep. A minimum of six replicates were used to ensure repeatability of the test data.

A JEOL 6610LV scanning electron microscope (SEM) was employed to obtain the surface morphology images for the fracture surfaces of the tensile and impact test specimens. The fractured surfaces were mounted vertically, and a carbon coating was applied for conductivity.

Dynamic mechanical analysis (DMA) was carried out on the samples using an RSA-G2 Solids Analyzer (TA Instruments, USA) to evaluate the storage modulus, loss modulus and the loss factor ( $\tan \delta$ ) as a function of temperature. The gage section of the tensile test specimens was used as the test sample. Testing was carried out using the three-point bending mode, going from 25 - 160°C at a constant heating rate of 3°C/min and frequency of 1 Hz.

Gel swell analysis was performed on the samples in order to observe if there was any development of cross-linking following the annealing process. The analysis was performed in accordance with the ASTM D2765 standard test method for determination of gel content and swell ratio [61]. Samples measuring 0.5 X 0.5 inches were cut from injection molded test bars and were secured by pouches made using a fine wire mesh. Each of the pouches was then placed inside a jar containing

dichloromethane for 24 hours, after which they were removed and completely dried. The dry sample weights were measured before and after placing them in the solvent.

The crystallization kinetics of the samples were evaluated using a differential scanning calorimeter (DSC Q20, TA Instruments, USA). The isothermal melt crystallization behavior was studied using the following procedure: the samples (~10 mg) were heated from room temperature up to 200°C at 10°C/min, where they were isothermally held for 10 minutes to eliminate any previous thermal and stress history. The samples were then cooled down to one of five different isothermal temperatures (90, 95, 100, 105 and 110°C) at a rate of 20°C/min where they were set to equilibrate and were held for a sufficient amount of time to allow for the crystallization process to reach completion. The simulated in-mold annealing using the DSC also followed a similar route.

## **2.3 Results and Discussion**

### **2.3.1 Synthesis and Characterization of Copolymer**

Reactive extrusion (REX) was used to achieve the transesterification reaction between the PLA and the NHPDMS resulting in an amide linkage between the two blocks. The Sn(Oct)<sub>2</sub>, a commonly used transesterification catalyst for PLA was used to aid the reaction through chain scission of the PLA. Figure 2-1 shows a schematic description of the reaction resulting potentially in a diblock or triblock structure.



directly proportional effect on the molecular weight of the resultant copolymer and the ~2-minute residence time corresponding to a torque value of 35% was found to be optimal. Consequently, 0.1% by weight of catalyst and a ~2-minute residence time was adopted for the rest of the study. Also, the reaction of the PLA with the catalyst showed a drastic decrease in molecular weight due to the chain scission of the PLA by the Sn(Oct)<sub>2</sub>. However, upon the introduction of the NHPDMS, along with the PLA and catalyst, the molecular weights were found to be significantly higher, thus providing the first confirmation of the reaction between the PLA and the NHPDMS [62].

FT-IR spectroscopy was used to provide further validation for the transesterification reaction. The FT-IR analysis was carried out on the purified copolymer sample in order to prevent any unreacted NHPDMS from interfering with the results. Figure 2-3 shows a comparative FT-IR spectra of neat PLA (3051D) and the PLA-NHPDMS copolymer. The peak at 800 cm<sup>-1</sup> and 1750 cm<sup>-1</sup> corresponding to the -Si-C- bond on the NHPDMS and the C=O bond on the PLA clearly demonstrates the presence of both the blocks in the purified copolymer sample [63]. This provides conclusive evidence of the reaction between the PLA and the NHPDMS blocks, thus establishing that it is not simply a direct blend of the two components.

<sup>1</sup>H NMR spectroscopy was used to further validate the occurrence of reaction between the PLA and the NHPDMS. As shown in Figure 2-4, three distinct peaks corresponding to the two blocks of PLA and PDMS were observed with a sample of the purified extrudate. The characteristic peaks of PLA at 1.6 ppm and 5.2 ppm corresponding to the methyl and methylene protons respectively were observed. Also, a peak at ~0.1 ppm corresponding to the methyl protons on the -Si-O-Si- backbone were observed [64]. The presence of these peaks corresponding to the individual blocks in a purified sample was used as a secondary confirmation for the reaction between them.

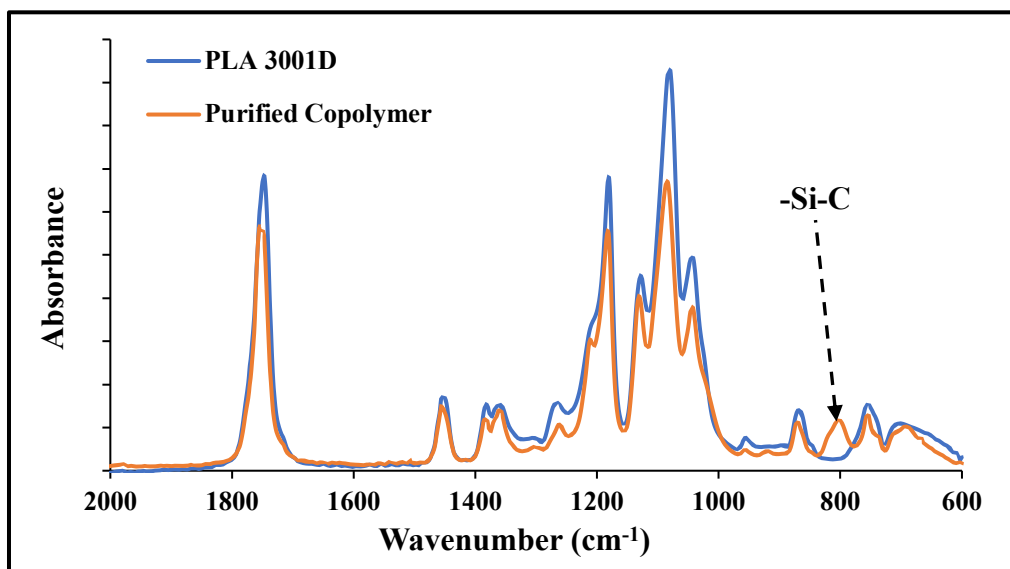


Figure 2-3: Comparative FT-IR Spectra of neat PLA and the PLA-NHPDMS copolymer

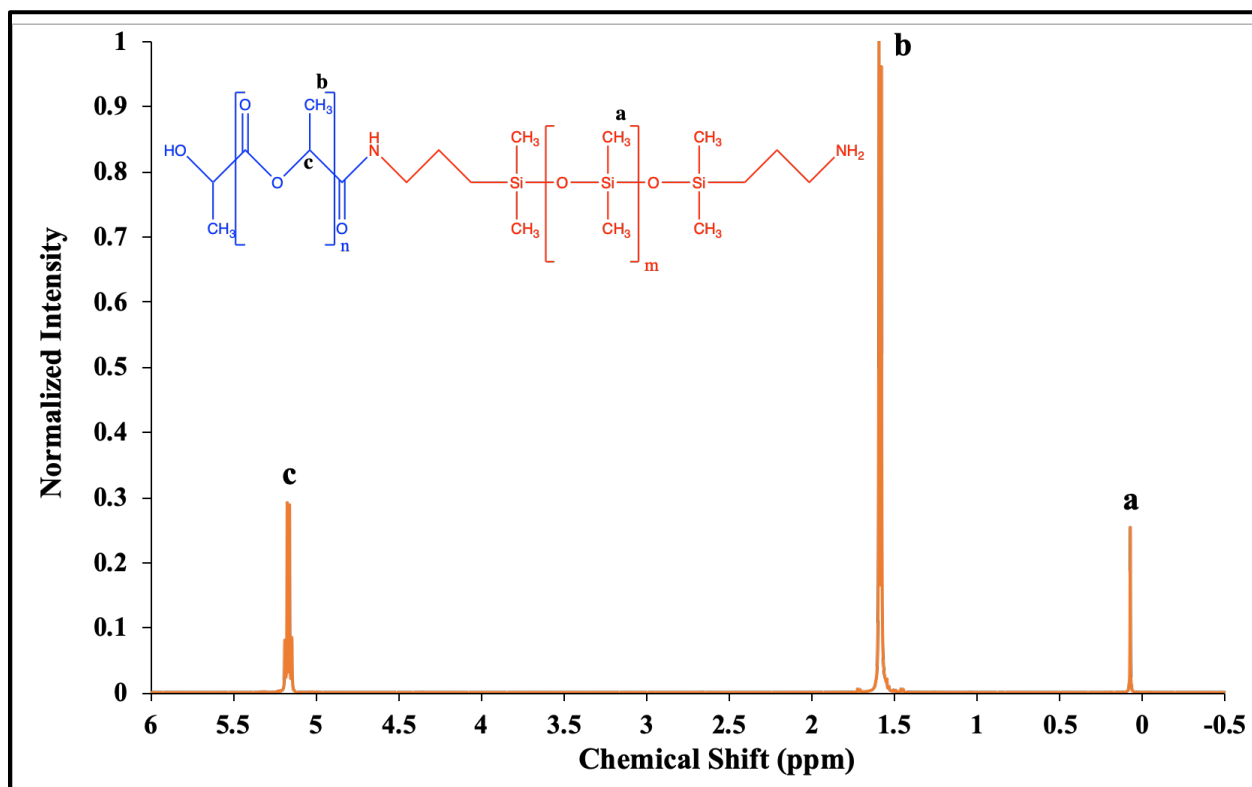
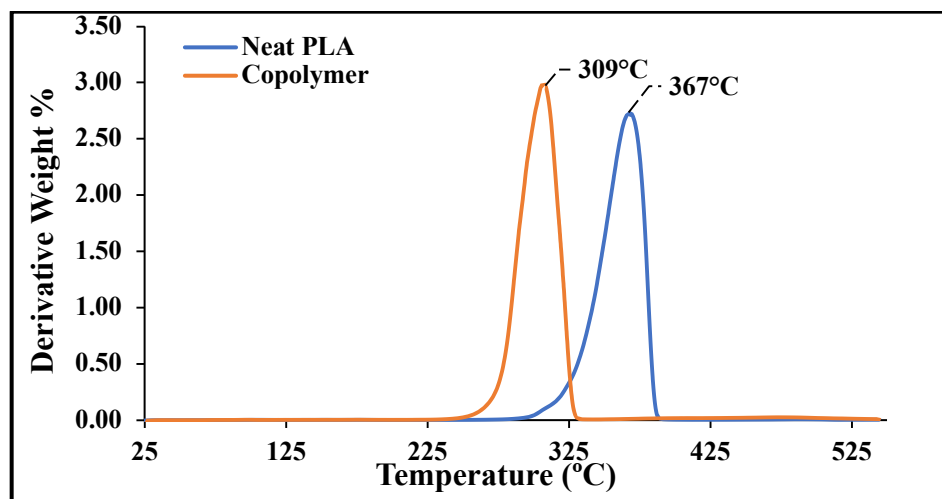


Figure 2-4:  $^1\text{H}$  NMR spectra of purified PLA-NHPDMS copolymer

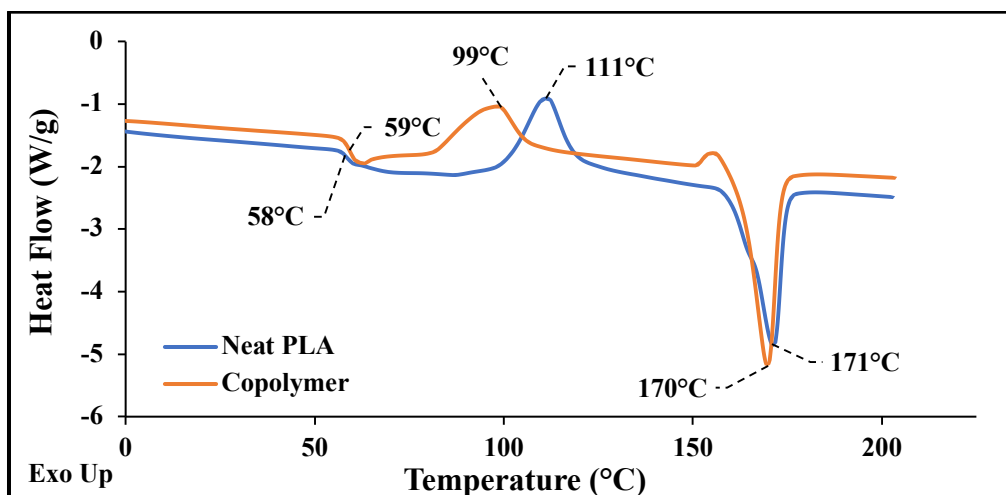
Thermogravimetric analysis was used as a simple yet effective tool in order to identify the characteristic peak thermal degradation temperature of the neat PLA as well as the copolymer.

Figure 2-5 shows the derivative thermal gravimetric (DTG) curve of the both. The peak thermal degradation of the neat PLA was found to be at approximately 367°C whereas that of the PLA-NHPDMS copolymer was at around 309°C. The loss of thermal stability can be attributed to the loss in molecular weight of the PLA after reaction with the NHPDMS.



**Figure 2-5:** DTG curve comparing neat PLA with the PLA-NHPDMS copolymer

The thermal properties of neat PLA and the copolymer were measured by performing a standard heating scan using a DSC. Figure 2-6 shows the DSC curves obtained from the first heating scan carried out at 10°C /min. It can be observed that the glass transition temperature ( $T_g$ ) and the melting temperature ( $T_m$ ) of the neat PLA remain unchanged at around ~58°C and ~170°C respectively after the reaction with the NHPDMS, however the cold crystallization temperature ( $T_{cc}$ ), was found to reduce from ~111°C to ~99°C. This behavior can be attributed to the fact that the NHPDMS induces a certain degree of branching in the PLA matrix which could potentially behave as nucleation sites, thus resulting in the onset of cold crystallization at a lower temperature [65].



**Figure 2-6:** DSC curves of neat PLA and the copolymer

TEM images of the copolymer samples were obtained in order to observe the dispersion of the NHPDMS phase in the PLA matrix. Figure 2-7 shows the TEM images of the copolymer samples. The NHPDMS phase can be observed as the dark spheres in the image. This is because of the heavier Si atoms in the NHPDMS which can scatter the electrons more efficiently thus providing a difference in contrast. Since the molecular weights of the individual blocks are high, a spherical morphology of the NHPDMS blocks can be observed. This is found to be consistent with existing literature on PLA-PDMS block copolymers, and is attributed to reduced chain mobility, thereby preventing the formation of long-range ordered structures [55].

The tensile properties of the copolymer samples were studied by testing the injection molded specimens of the same. Table 2-1 gives an overview of the properties obtained as a result of the tensile testing [62]. As would be expected, the incorporation of the flexible NHPDMS component into the brittle PLA matrix improves the elongation at break values of the samples, thus resulting in an improved ductility of the PLA.

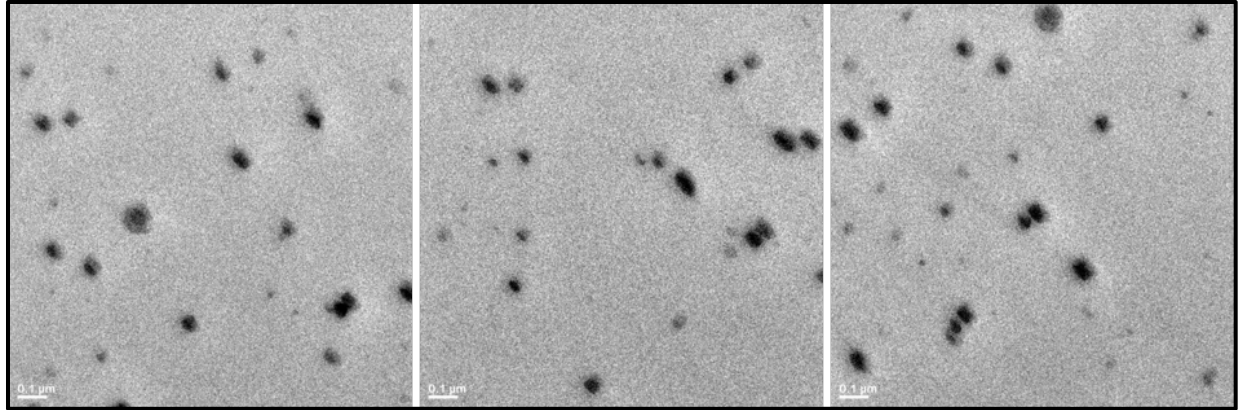


**Figure 2-7:** TEM images of the copolymer obtained at X20,000 magnification

Although the improvement in the strain at break values were achieved at a slight loss of modulus and yield stress, the overall toughness of the copolymer samples was found to be higher as compared to neat PLA. Considering the data from Table 2-1, it was hypothesized that the copolymer containing 5% of the 30,000 g/mol NHPDMS would give the maximum improvement in toughness upon addition to the neat PLA, since it had resulted in the greatest improvement in strain at break. Thus, this was the grade of copolymer chosen for the next section of the study.

**Table 2-1:** Tensile properties of the PLA-NHPDMS copolymers

| <b>NH-PDMS<br/>MW [g/mol]</b> | <b>NH-<br/>PDMS<br/>[%]</b> | <b>Modulus<br/>[GPa]</b> | <b>Yield<br/>Stress<br/>[MPa]</b> | <b>Strain at<br/>Break [%]</b> | <b>% Strain<br/>Improvement</b> |
|-------------------------------|-----------------------------|--------------------------|-----------------------------------|--------------------------------|---------------------------------|
| PLA 3051D                     | 0                           | 1.57                     | 66.9                              | 8.76                           | -                               |
| 1000                          | 3                           | 1.43                     | 61.7                              | 10.10                          | 15.19                           |
| 1000                          | 5                           | 1.39                     | 55.4                              | 10.82                          | 23.47                           |
| 5000                          | 3                           | 1.56                     | 63.8                              | 11.39                          | 29.96                           |
| 5000                          | 5                           | 1.47                     | 59.4                              | 12.89                          | 47.06                           |
| 30000                         | 3                           | 1.46                     | 59.4                              | 13.13                          | 49.86                           |
| <b>30000</b>                  | <b>5</b>                    | <b>1.38</b>              | <b>57.6</b>                       | <b>14.27</b>                   | <b>62.86</b>                    |
| 30000                         | 7                           | 1.37                     | 52.5                              | 12.86                          | 46.69                           |

### **2.3.2 Characterization of Blends of Copolymer with Neat PLA**

This section of the report focuses on the evaluation of the properties of the blends of neat PLA with the copolymer. For this part, the PLA used was the 3001D grade as mentioned earlier. The copolymer formulation used was the grade having 5% by weight of the 30,000 g/mol NHPDMS. Hereafter, they are referred to as “neat PLA” and “copolymer” respectively. All the requisite samples for the melt blended neat PLA and copolymer compositions were prepared by injection molding, where the neat PLA and copolymer pellets were manually pre-mixed in the appropriate ratio and then fed. Thermal annealing of the injection molded blend samples were carried out in order to eliminate any cold crystallization present, thereby increasing the final percent crystallinity of the samples.

Thermal annealing of the samples was found to be a pivotal point in the study of the blend formulations due to the unique properties that were observed post the annealing process. In order to evaluate the phenomenon causing this change in properties, all further analyses involved the characterization of the annealed blend samples as well.

Tensile properties of the samples were evaluated and are presented in Table 2-2. As is clearly evidenced by the data, the annealing process brings about a considerable improvement in the elongation at break values over the neat PLA. The improvement in the elongation at break is realized at a minimal loss of modulus and yield stress, and as a matter of fact, the annealing process results in values of modulus and yield stress for the blend samples that are slightly higher than that of neat PLA. Also, the addition of the copolymer by itself causes only a marginal improvement in the properties, however, in combination with annealing, a synergistic effect of the two phenomena are observed resulting in a significant enhancement in the overall toughness of the material.

**Table 2-2:** Tensile properties of the annealed (A) and non-annealed blend formulations

| Sample                         | Modulus [GPa] | Yield Stress [MPa]  | Elongation at Break [%] | % Improvement in Strain |
|--------------------------------|---------------|---------------------|-------------------------|-------------------------|
| Neat PLA – 3001 D              | 1.75          | 83.84 ± 1.93        | 7.56 ± 0.19             | —                       |
| Neat PLA - A                   | 1.89          | 88.17 ± 5.35        | 7.98 ± 0.66             | 5.55                    |
| PLA + 10% Copolymer            | 1.65          | 80.71 ± 1.22        | 8.88 ± 0.42             | 17.46                   |
| <b>PLA + 10% Copolymer - A</b> | <b>1.89</b>   | <b>84.11 ± 3.58</b> | <b>14.11 ± 2.41</b>     | <b>86.64</b>            |
| PLA + 20% Copolymer            | 1.6           | 78.99 ± 0.44        | 9.20 ± 0.77             | 21.69                   |
| <b>PLA + 20% Copolymer - A</b> | <b>1.94</b>   | <b>82.51 ± 1.78</b> | <b>21.59 ± 3.11</b>     | <b>185.58</b>           |
| PLA + 30% Copolymer            | 1.64          | 80.37 ± 0.92        | 8.64 ± 0.73             | 14.29                   |
| <b>PLA + 30% Copolymer - A</b> | <b>1.87</b>   | <b>80.21 ± 1.88</b> | <b>24.71 ± 4.87</b>     | <b>226.85</b>           |

Figure 2-8 shows the elongation at break values for the blend samples, and Figure 2-9 shows the stress-strain curves obtained for the same. It is evident from the data that neither the addition of the copolymer nor the annealing process by themselves are responsible for the improvement in the toughness. However, the combined effect of both processes results in almost up to a 200% increase in the elongation at break value (at 30% by weight of copolymer loading). Also, the values were found to increase uniformly with an increase in the copolymer content in the samples.

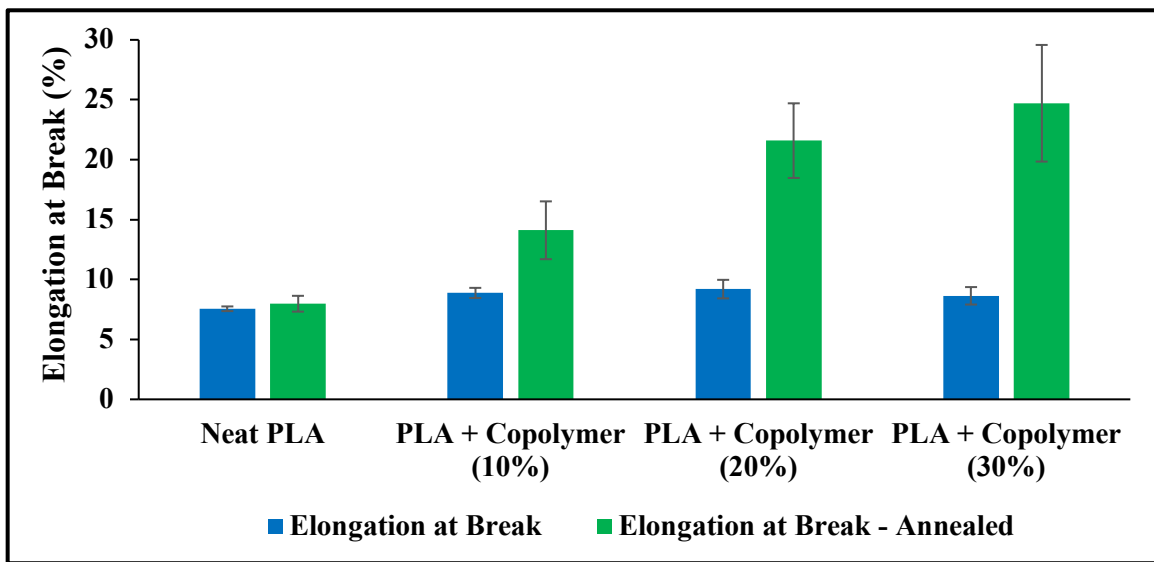


**Figure 2-8:** Comparison of elongation at break values for the blend samples

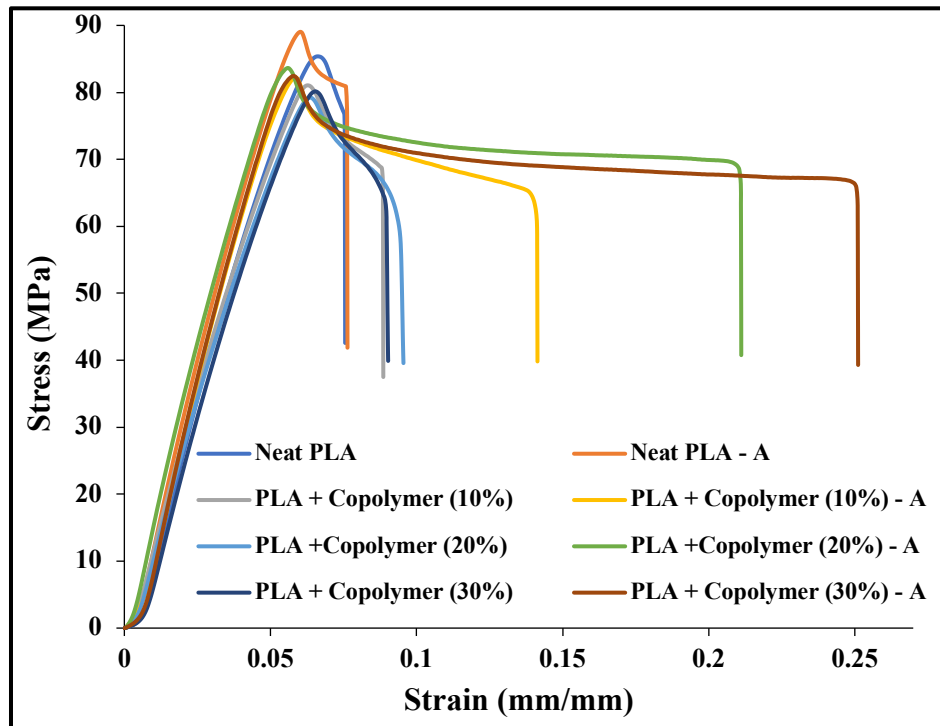


**Figure 2-9:** Stress-strain curves for the copolymer blended with neat PLA (A - annealed)

Figure 2-10 shows the notched Izod impact strength for the blend samples. Again, a trend similar to that observed with the elongation at break values was seen with the impact strength values as well. The impact strength values were found to increase with an increase in the amount of copolymer introduced into the system. The synergistic effect of the addition of the copolymer followed by the annealing process, was also observed with the impact testing results. The addition of the copolymer by itself was actually found to have decreased the impact strength marginally. However, upon annealing, a substantial improvement was observed (almost a 500% increase over neat PLA at 30% by weight loading of the copolymer). Annealing of the neat PLA by itself showed only a slight increase in its impact strength, but the addition of the copolymer followed by annealing resulted in a significant improvement, thus clearly demonstrating the interdependence of the two phenomena in obtaining the desired mechanical properties.

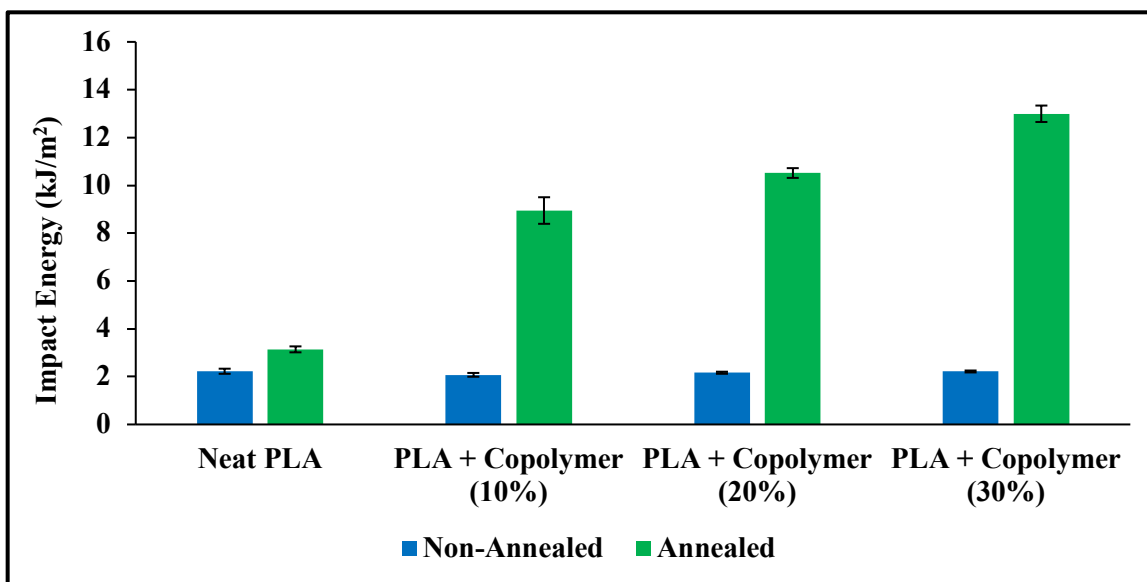


**Figure 2-10:** Comparison of the notched Izod impact strength for the blend samples

Although there exist several reports individually relating to either the addition of an impact modifier to neat PLA [32, 33], or the use of thermal annealing to obtain a toughened PLA product [66-69], there have only been a few studies that have considered adopting a two-step approach by incorporating both the processes in order to toughen PLA [70-73]. Even amongst these, only four report having achieved an improvement in impact strength [74-77], however, after a thorough review of existing literature, no studies were found where both tensile as well as impact toughness of PLA were found to be greatly improved with the adoption of this two-step approach. Thus, this makes the PLA/PLA-NHPDMS blend a unique system to investigate. All further characterization was performed in order to find a suitable rationale to explain for the changes in behavior observed. Since the major changes in mechanical behavior were observed post-annealing, a closer look was taken at the physical changes that could possibly occur in the PLA/PLA-NHPDMS system during the annealing process.

Thermal annealing essentially allows sufficient time for slow-crystallizing polymers to attain maximum extent of crystallinity. Since PLA happens to have slow crystallization kinetics, the

injection molding process does not allow for complete crystallization to occur, thus giving rise to cold crystallization in the as-molded product. The annealing process at temperatures above the  $T_g$  of the PLA allows the chains to attain the required thermal energy to slowly rearrange themselves thus removing any cold crystallization developed during the molding process. This is shown in the DSC curves of the annealed samples which are presented in Figure 2-11 clearly showing the absence of a cold crystallization peak at around 100~110°C.

FT-IR spectroscopy has been used as a quick and effective means to identify modifications in the crystal structure of PLA brought about by thermal annealing. Figure 2-12 shows the peak at 921  $\text{cm}^{-1}$  observed in only the PLA and copolymer samples that have been annealed. This peak has been attributed to the presence of the more stable  $\alpha$ -form of PLA crystal structure thus, suggesting that the PLA chains in the matrix have achieved a long-range order through the annealing process [78]. This could further imply that the more ordered PLA chains would cause crystallization induced phase separation between the PLA and NHPDMS phases.

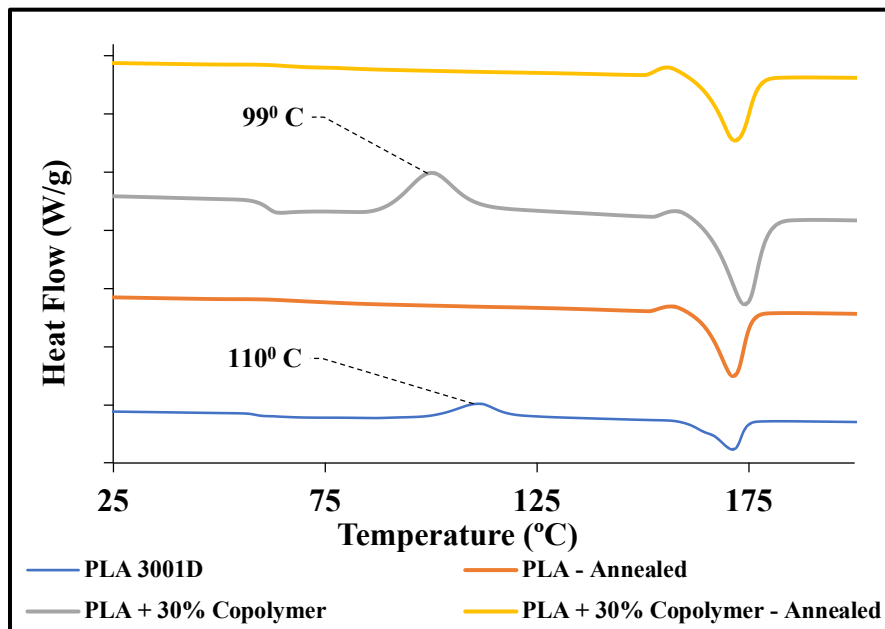


**Figure 2-11:** DSC curves comparing annealed (A) and non-annealed formulations

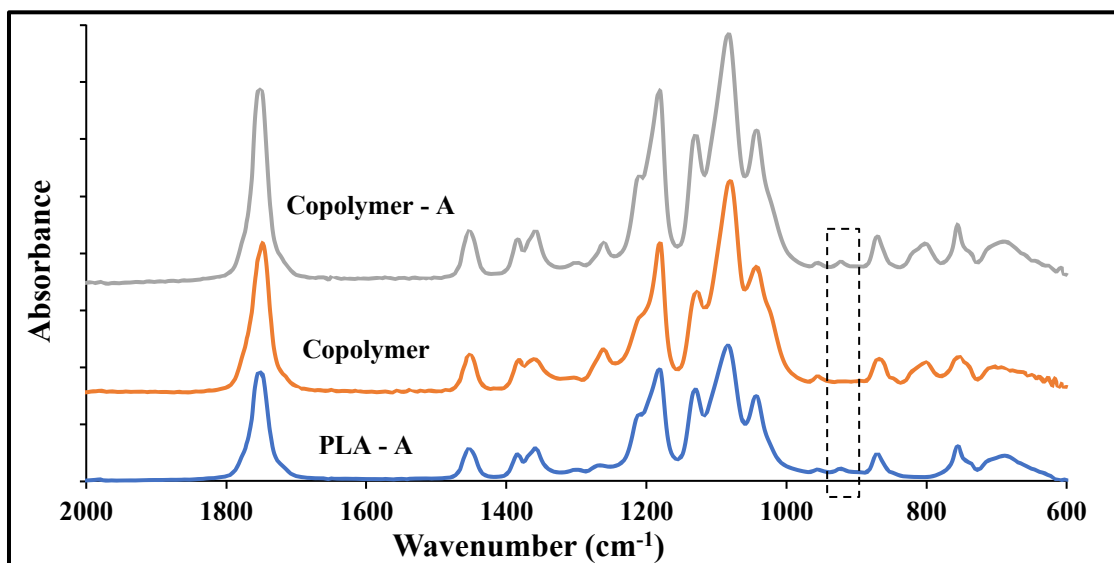


**Figure 2-12:** Comparison of FT-IR spectra of annealed PLA and copolymer samples

Dynamic mechanical analyses of the blend samples were performed in order to correlate the thermal transitions observed in the sample with the physical structure. Figure 2-13 shows the storage and loss modulus curves, along with the  $\tan \delta$  (damping factor) as a function of temperature. For the storage modulus ( $E'$ ), it is observed that the annealed samples displayed higher moduli values at elevated temperatures as opposed to the non-annealed ones. This is as expected since the thermal stability of PLA has been found to increase with an increase in the crystallinity of the samples [68]. The loss modulus ( $E''$ ) and  $\tan \delta$  showed predictable behavior as well in terms of exhibiting a distinct peak at the  $T_g$  of PLA. The  $E''$  peak for the annealed samples was found to shift to a higher temperature and also broaden, suggesting improved thermal stability and the improved ability for energy absorption respectively [79]. This corroborates the fact that the annealed samples had higher impact strength as compared to non-annealed ones. The  $\tan \delta$  curve for the annealed sample displayed a reduction in height as well as the broadening of the peak. This is commonly attributed to a more densely packed structure which could arise due to the PLA chains being packed more closely post-annealing (much higher extent of crystallinity) [60].

An anomaly was however noticed with the  $E''$  and  $\tan \delta$  curves. A shoulder was observed in the  $E''$  peaks for the non-annealed samples at around  $\sim 65^\circ\text{C}$  which corresponded to the major  $E''$  peak position for the annealed samples. A similar shoulder was observed in the  $\tan \delta$  peaks for the non-annealed samples at around  $\sim 57^\circ\text{C}$  which corresponded to the major peak position of the non-annealed samples in the  $E''$  curve. This could be attributed to the crystalline and amorphous regions in the sample behaving differently under the applied load. The fact that the small shoulder in the  $E''$  curves for non-annealed samples transitions to the major peak for the annealed samples would validate this observation (due to the shift to a higher crystallinity system).

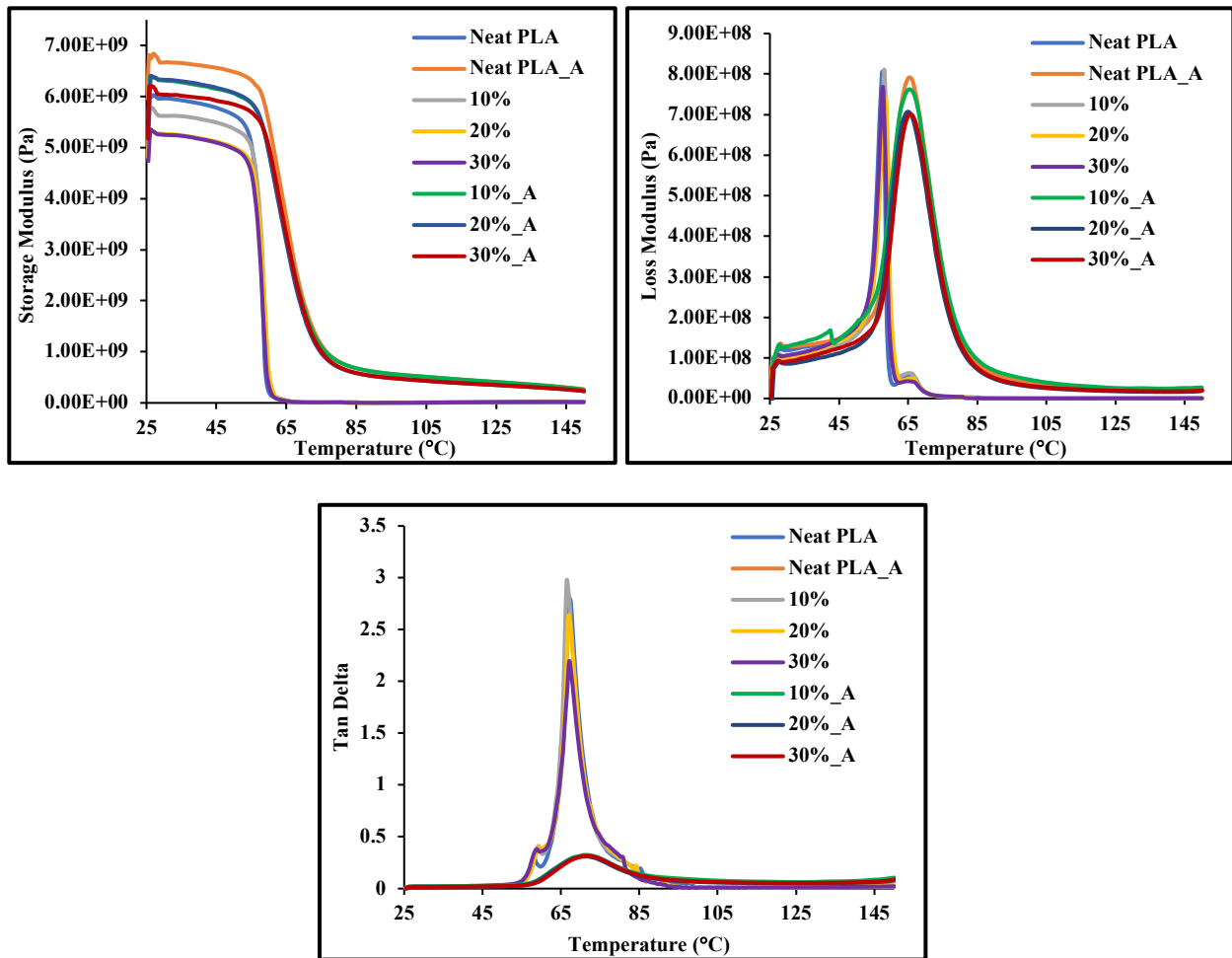


**Figure 2-13:** DMA analysis of the blend samples showing storage modulus, loss modulus and tan delta

SEM images of the fracture surfaces of the tensile and notched Izod impact tested samples are shown in Figure 2-14 and Figure 2-15 respectively. Looking at the fracture surfaces of the tensile tested samples, it can be observed that for both the annealed and non-annealed samples, the morphology became increasingly “rough” with the increase in the amount of copolymer added to the blends, thus suggesting a gradual transition towards a more plastic deformation and ductile fracture [80, 81]. Also, for each composition, the non-annealed sample displayed a more uniform and smoother surface, indicating a more brittle fracture and thus low toughness as compared to its annealed equivalent. Thus, the fracture morphology of the samples was found to be consistent with the results obtained from the tensile testing.

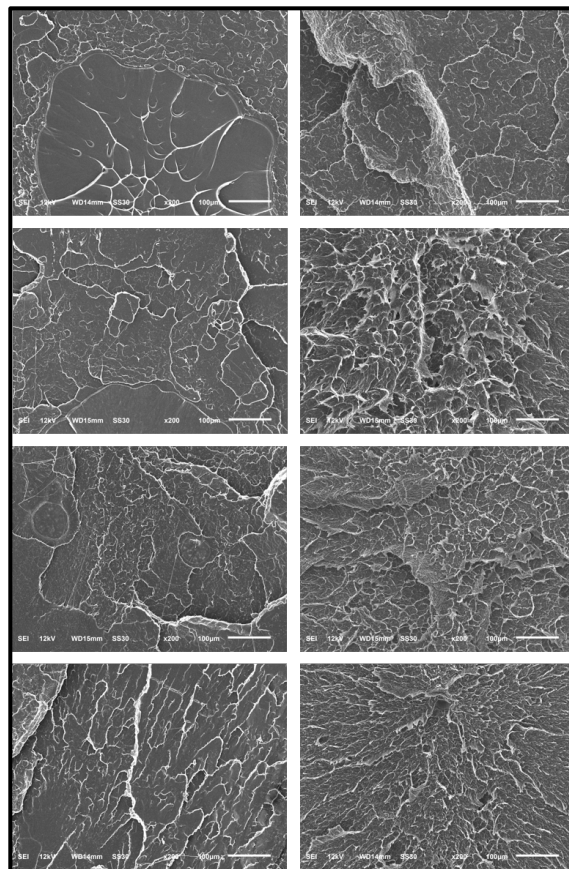


**Figure 2-14:** SEM images of fracture surfaces of tensile tested samples - neat PLA, 10, 20 and 30% copolymer blended samples (from top to bottom), non-annealed on left and annealed on right

The SEM images of the fractured surface of the notched Izod impact tested samples, as shown in Figure 2-15, followed a similar trend. The formation of fibrils was observed along the direction of the crack propagation. The density and fineness of the fibrils was found to increase in samples with higher impact strength, thus enabling them to absorb and dissipate energy more effectively. As can be observed from the images, the fibrils become finer and denser with the annealed samples which follows the trend from the impact test data. This is in agreement with existing literature that shows similar fracture morphology [80, 82, 83].

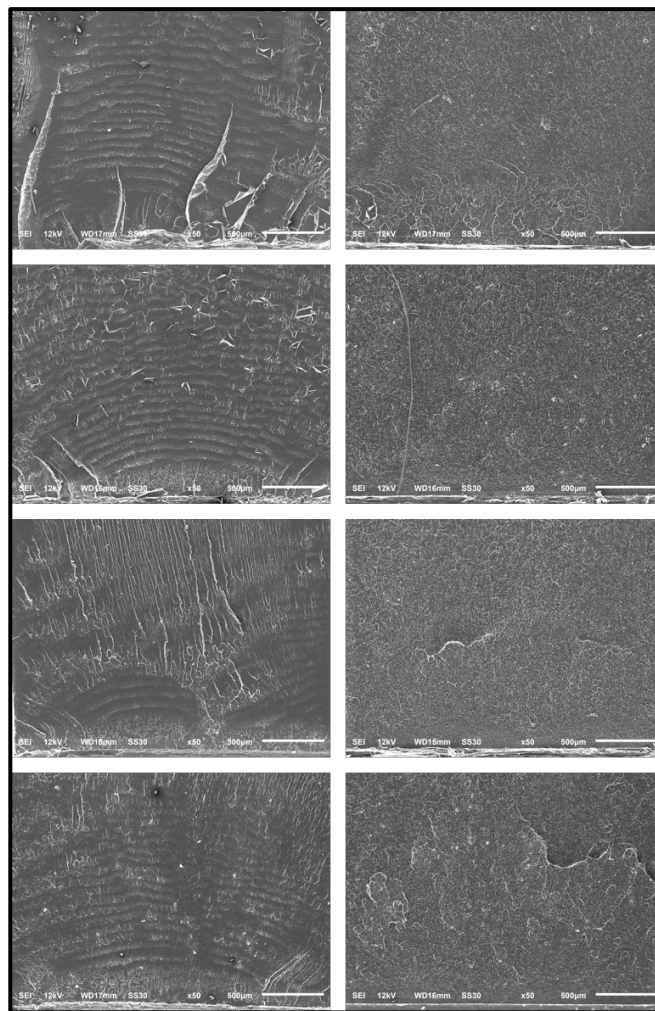


**Figure 2-15:** SEM images of fracture surfaces of notched Izod impact tested samples - neat PLA, 10, 20 and 30% copolymer blended samples (from top to bottom), non-annealed on left and annealed on right, notch is at bottom of image

After evaluating all the mechanical and thermal characterization data, it can be clearly observed that the thermal annealing step almost exclusively results in a significant improvement in the toughness of the PLA. This necessitated a closer look at the physical changes brought about by the annealing process in order to account for the changes in properties observed. Since annealing involved a heat treatment process, two hypotheses were tested to justify for the behavior of the samples. First, the assumption that the heat treatment was introducing a certain crosslinking mechanism through the -Si-O-Si- backbone, which in turn could result in the improvement in properties, was proposed. Second, the theory that the copolymer particles dispersed through the PLA matrix were acting as nucleating sites to promote rapid crystallization was studied.

The possibility of formation of a crosslinked network was negligible owing to the fact that there was no active silicone functionality to initiate it. The assumption was tested out regardless to completely ensure that no crosslinking was present. This was done through the gel swell analysis method by soaking the samples in dichloromethane (DCM). All of the samples, regardless of whether they were annealed or not, were found to completely dissolve in the DCM solvent, thus proving that no crosslinked network was developing.

#### **2.3.2.1 Avrami Model Analysis**

The second hypothesis proposing that the copolymer particles were acting as nucleating sites was based on the assumption that they would result in a much faster rate of crystallization and would potentially cause the growth of spherulites (3-dimensional growth of crystals). These spherulites would then act as stress concentrators in the PLA matrix and could thus account for the improved absorption and dissipation of energy in the bulk material. This theory was tested by monitoring the isothermal melt crystallization kinetics of the neat PLA and the blend formulation having 30% of the copolymer in it, through an Avrami-style kinetics approach. An Avrami exponent ( $n$ ) value of

~3 would typically imply a spherulitic growth [84, 85]. The isothermal melt crystallization kinetics were studied at five different isothermal temperatures (90, 95, 100, 105 and 110°C), and the data was modeled in accordance with the Avrami equation [65]:

$$X(t) = 1 - \exp(-kt^n)$$

$$\ln[-\ln(1 - X(t))] = n \ln t + \ln k$$

where, X(t) is the fractional crystallinity at a given time t during the crystallization from melt process, n is the Avrami exponent indicating the mechanism of nucleation and growth of the crystals, and k is the crystallization kinetic constant for nucleation and growth rate. The X(t) and t data was collected using the results from the DSC experiments. The  $\ln[-\ln(1-X(t))]$  vs.  $\ln t$  values were then plotted and the values for  $\ln k$  and n were derived by linear fitting of the experimental data. The results of the analyses are shown in Figure 2-16, Figure 2-17, and Figure 2-18, and the half-time values for the melt crystallization process of the samples, and the Avrami constants are reported in Table 2-3.

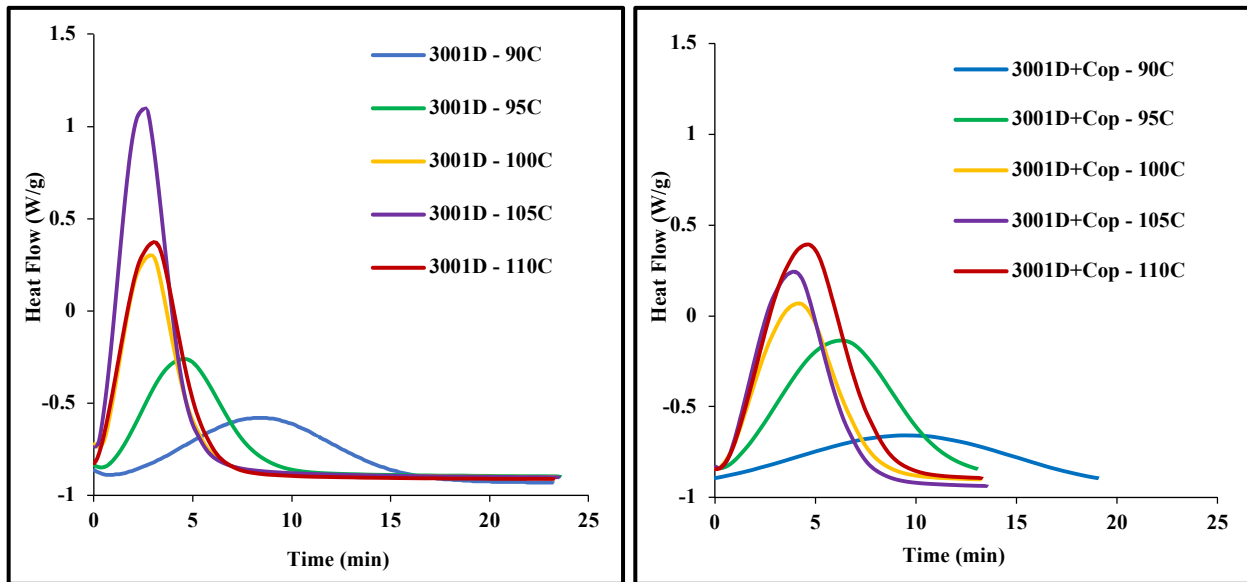


**Figure 2-16:** DSC isothermal melt crystallization times for different temperatures

From the Avrami analysis, two deductions become evident: first, the melt crystallization kinetics for the blend samples were definitely slower as compared to neat PLA, and second, the addition of the copolymer does not affect the growth mechanism of the crystals.

**Table 2-3:** Crystallization half-time values and Avrami constants for the samples at different isotherms

| Sample            | $t_{1/2}$ (min.) | n      | ln k    | k        |
|-------------------|------------------|--------|---------|----------|
| 3001D – 90°C      | 6.68             | 2.3856 | -4.8973 | 7.47E-03 |
| 3001D – 95°C      | 3.17             | 2.075  | -2.7632 | 6.31E-02 |
| 3001D – 100°C     | 2.07             | 2.1168 | -1.9067 | 1.49E-01 |
| 3001D – 105°C     | 1.87             | 2.0448 | -1.6431 | 1.93E-01 |
| 3001D – 110°C     | 2.54             | 2.155  | -2.3773 | 9.28E-02 |
| 3001D+Cop – 90°C  | 8.20             | 2.1487 | -4.889  | 7.53E-03 |
| 3001D+Cop – 95°C  | 4.80             | 2.1773 | -3.7813 | 2.28E-02 |
| 3001D+Cop – 100°C | 3.39             | 2.2229 | -3.0797 | 4.60E-02 |
| 3001D+Cop – 105°C | 2.84             | 2.106  | -2.565  | 7.69E-02 |
| 3001D+Cop – 110°C | 3.72             | 2.308  | -3.3958 | 3.35E-02 |

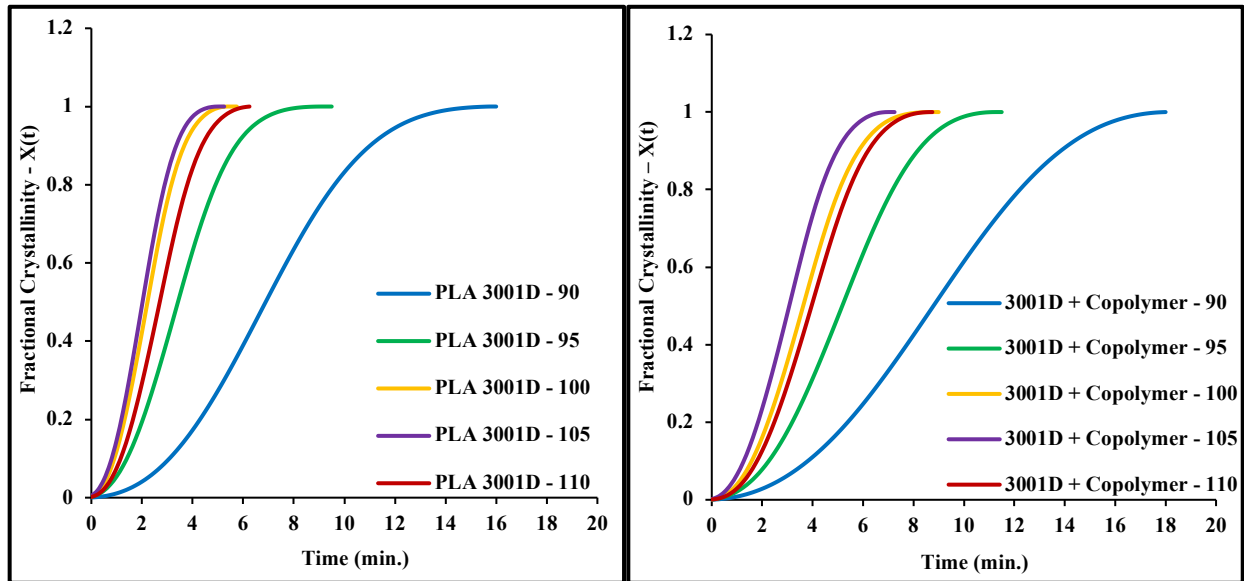


**Figure 2-17:** Variation of fractional crystallization with time for the samples at different isotherms

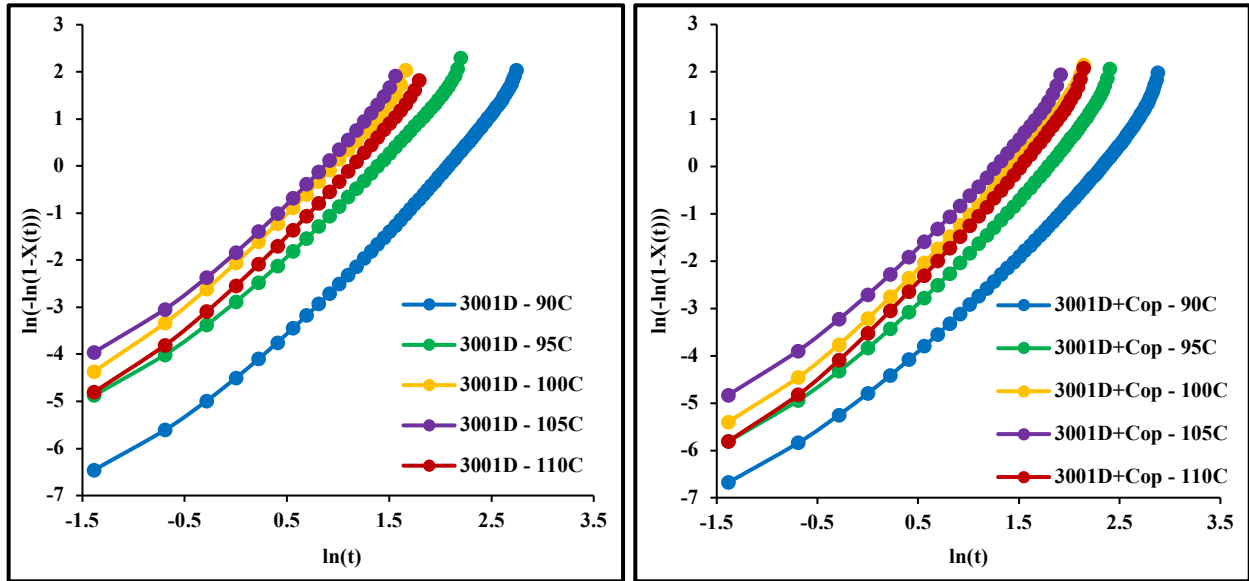


**Figure 2-18:** Avrami double-log plots for the melt crystallization of the samples at different isotherms

The first conclusion can be inferred from the fact that at all the isothermal temperatures, the half-time needed to attain crystallization was found to be uniformly higher for the blend samples as opposed to the neat PLA. This could be attributed to the fact that the copolymer domains in the PLA matrix were in fact preventing the PLA from crystallizing faster, thus defeating our notion that they would act as nucleation sites which could promote faster crystallization kinetics. Also, the second conclusion can be deduced by looking at the Avrami constant,  $n$ , values for all the formulations at the different isotherms. Since all of the values lie within the  $2 < n < 3$  range, the crystal growth can be assumed to be 2-dimensional in nature [86]. This clearly shows that the addition of the copolymer was not affecting the shape or growth of the crystals formed, and thus, was most likely not contributing to any sort of toughening mechanism involving spherulites as the load bearing components in the matrix. The data obtained from the isothermal melt crystallization studies however were fundamental to understanding the relation between time and temperature conditions for optimizing the annealing process. Since annealing requires a significant input of

thermal energy, the optimization of the process in terms of time required is a critical requirement for commercial scale-up. As is evident from the study, a higher annealing temperature would require a reduced time period for complete crystallization. However, since PLA might suffer from degradation at elevated temperatures of above 100°C, the recommended ceiling temperature for annealing should be at 100°C.

### **2.3.2.2 “Crystallization Induced Phase Segregation” Model**

Considering all of the characterization and analyses done thus far, a satisfactory explanation for the significant improvement in properties required further study of the system. Since there have been no prior reports of similarly behaving PLA-based systems so far, the study was extended to look at other polymeric based systems exhibiting similar properties. It was found that a relatively similar synergistic effect had been reported in a few polymeric systems and was referred to as the “crystallization-induced phase segregation” effect [87-90]. The phenomenon was reported in binary polymeric blends where during the annealing process, one of the components of the blend would crystallize to form well-ordered domains thereby causing the other component to coalesce and form a greater particle size. The conclusions from these studies were adapted to the PLA-PDMS system, and a representative schematic of the model can be seen in Figure 2-19. The blue chains and the red dots represent the PLA chains and the dispersed PDMS domains respectively. Since the PLA phase is a semi-crystalline material, the annealing process initiates the formation of ordered structures of the PLA chains leading to the coalescence of the PDMS domains. This leads to an increase in the particle size of the PDMS which would account for the improvement in the overall toughness of the material. It has been widely reported that a primary criterion for rubber toughening is that the particle size of the dispersed rubber phase must lie within a particular range in order for the toughening behavior to take effect [91-93]. It is likely that the coalescing of the

PDMS domains results in a particle size that is within range of this critical value for the PLA-PDMS system. Also, the retention of the tensile modulus could be attributed to the presence of the well-ordered PLA crystallites that would impart stiffness. This hypothesis very accurately accounts for the behavior observed in this system; however, this still needs experimental validation through appropriate imaging techniques such as TEM.

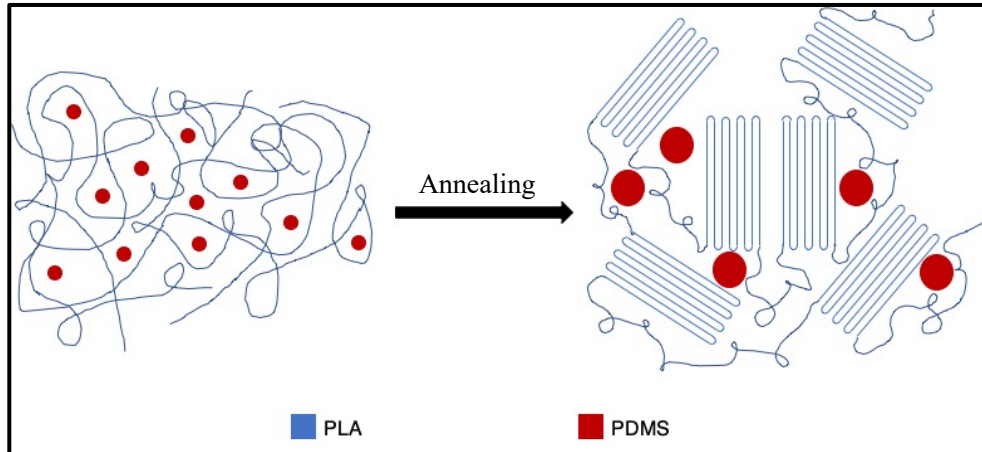


**Figure 2-19:** Schematic of model demonstrating the "Crystallization Induced Phase Segregation" behavior (PLA is shown in blue and PDMS is shown in red)

### 2.3.2.3 Single Step In-Mold Annealing

The study so far has looked at effectively improving the properties of neat PLA by incorporating a PLA-PDMS impact modifier followed by thermal annealing. The next step for this study was to convert this two-step process where the annealing was done post-processing to a single-step approach where the annealing could be done in-mold. This would reduce overall processing costs as well as prevent the need for a separate oven or heating apparatus to anneal the samples. However, in order to achieve this, the molded part would ideally have to completely crystallize before being ejected from the mold. This is a major issue with PLA since it is a slow-crystallizing polymer and would thus prevent processing via the single-step in-mold annealing route. Thus, in order to successfully adopt the in-mold annealing method, the effect of the use of nucleating agents

was investigated. The nucleating agents would enhance the rate of crystallization thus enabling the in-mold annealing approach. The effect of using three different nucleating agents were investigated for the study, namely, talc, poly(d-lactide) (PDLA), and Licomont Nav101 from Clariant. The talc was added in the form of a masterbatch during the molding process to an effective loading level of 2% by weight. The PDLA was used as received in the form of pellets during molding, as well as in the form of a masterbatch, both at an effective loading level of 5% by weight. The Clariant Licomont Nav101 was also used as received, as well as in the form of a masterbatch, both at an effective loading level of 0.5% by weight, as per manufacturer's specifications. All of the formulations, apart from the neat PLA, were molded with a 30% addition of the PLA-PDMS copolymer during molding along with the required amount of the nucleating agent and the balance being neat PLA.

Initially, the molding of the samples was carried out using a mold heated to 90, 100 and 110°C. It was found that despite the proper ejection of the part itself from the mold at 90 and 100°C, the sprue would still remain at a high temperature, thus preventing the complete separation of the part from the mold. This was observed with holding and cooling times as much as 50% more than that needed for molding at room temperature. It should be noted that with an appropriate molding setup with cooling lines attached to the sprue, it should be possible to mold at temperatures up to 100°C. At 110°C, it was observed that the part would not eject even after increasing holding times and would remain stuck to the mold.

Since it was not feasible to prepare test specimens using the hot mold, the samples with nucleating agents were prepared with the mold at room temperature first. Next, they were tested under simulated annealing conditions using the DSC. For this study, the room-temperature molded samples were first heated up to 200°C to erase any associated thermal history. They were then

rapidly cooled down to a fixed isothermal annealing temperature of 90, 100 and 110°C, and held there till complete crystallization occurred. The time taken for the complete crystallization to occur was recorded for each sample. The data obtained is as follows.

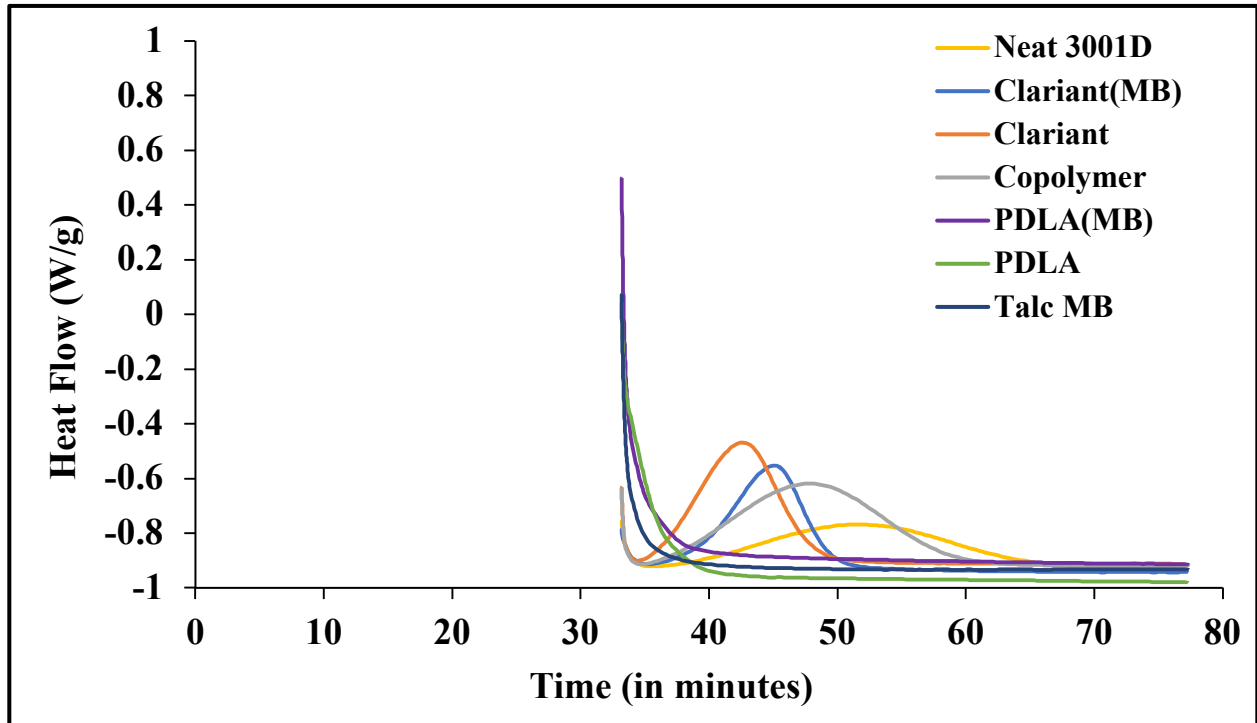


**Figure 2-20:** Time taken for complete isothermal melt crystallization at 90°C

Figure 2-20, Figure 2-21 and Figure 2-22 show the relative time taken for crystallization at the three different temperatures. Table 2-4 lists these times as a comparison.

It can be clearly observed for all samples that with an increase in temperature from 90°C to 100°C, the time taken for crystallization was significantly reduced, however, the time slightly increased with a rise of temperature to 110°C.

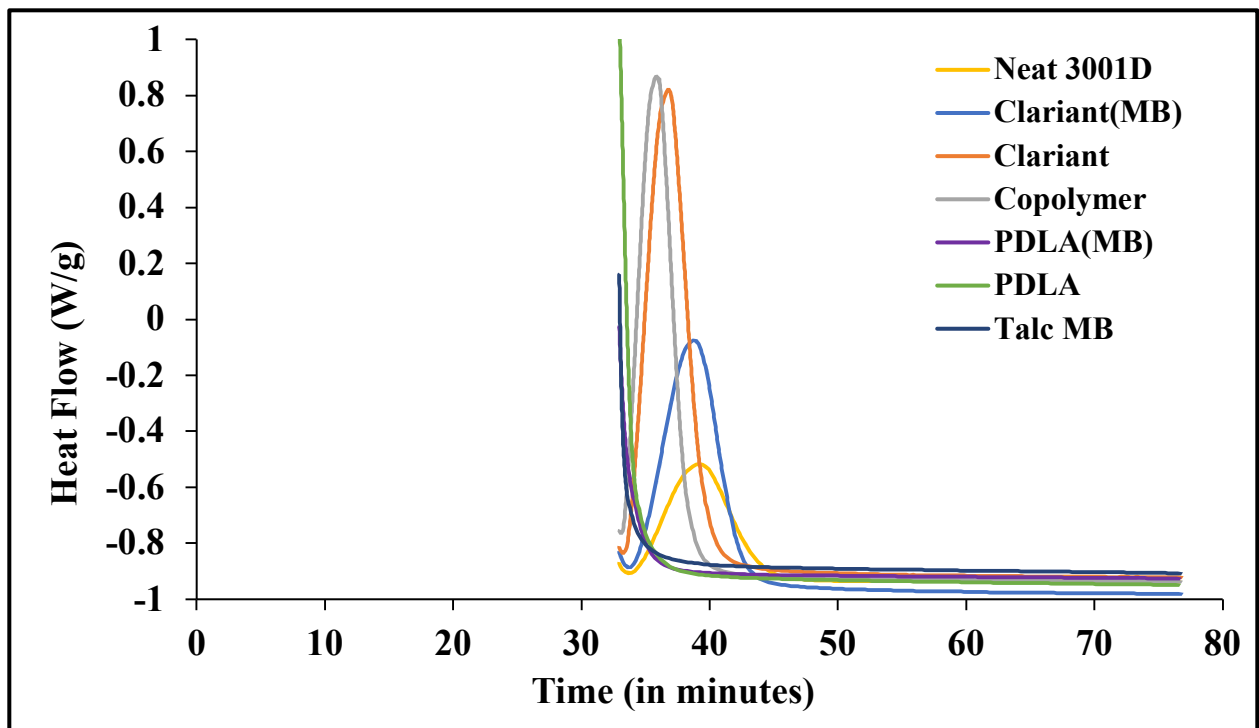


Figure 2-21: Time taken for complete isothermal melt crystallization at 100°C

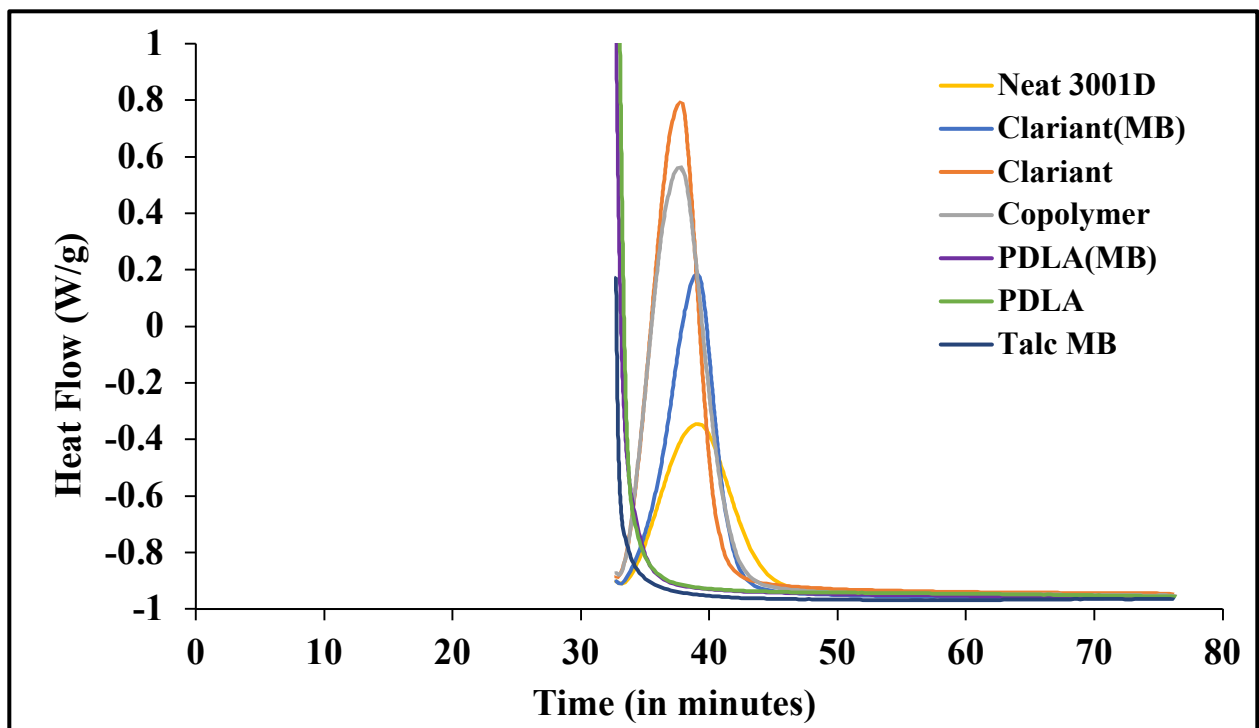


Figure 2-22: Time taken for complete isothermal melt crystallization at 110°C

Also, the samples with the talc masterbatch, the PDLA, and the PDLA masterbatch, were found to crystallize faster than could be detected by the DSC, thus indicating their efficacy at nucleating the PLA + Copolymer formulation. Thus, in order to successfully incorporate the one-step in-mold annealing process, it is recommended to use either of these three formulations. The Licomont Nav101 was found to be moderately effective at reducing the crystallization time, however, unlike the PDLA and talc, it did not completely eliminate the detected crystallization peak.

**Table 2-4:** Time taken for complete isothermal melt crystallization as simulated in the DSC

| <b>Sample Components</b>                    | <b>Isothermal Annealing Temperature (°C)</b> | <b>Simulated Annealing Time (min)</b> |
|---|--|---------------------------------------|
| Neat PLA                                    | 90   | 24.6                                  |
|   | 100  | 9.2                                   |
|   | 110  | 10.0                                  |
| PLA + Copolymer (30%)                       | 90   | 17.8                                  |
|   | 100  | 5.0                                   |
|   | 110  | 8.0                                   |
| PLA + Copolymer + Talc                      | 90   | /                                     |
|   | 100  | /                                     |
|   | 110  | /                                     |
| PLA + Copolymer + PDLA                      | 90   | /                                     |
|   | 100  | /                                     |
|   | 110  | /                                     |
| PLA + Copolymer + PDLA (MB)                 | 90   | /                                     |
|   | 100  | /                                     |
|   | 110  | /                                     |
| PLA + Copolymer + Clariant Licomont Nav 101 | 90   | 12.8                                  |
|   | 100  | 6.0                                   |
|   | 110  | 8.0                                   |
| PLA + Copolymer + Clariant (MB)             | 90   | 13.6                                  |
|   | 100  | 10.1                                  |
|   | 110  | 9.2                                   |

Despite the advantages of the in-mold annealing route, there are certain disadvantages associated with it. First, due to the longer cycle times during the molding process, the PLA would degrade further and lose molecular weight thereby leading to poor mechanical properties. Second, the nucleating agent could interfere with the formation of the “crystallization-induced phase segregated” structure that was observed with the PLA-PDMS system, thus resulting in insignificant improvements in mechanical properties over that of neat PLA. Initial mechanical characterization confirms these arguments by demonstrating poor properties resulting from the one-step in-mold annealing process. Further optimization of the process conditions is critical for the adoption of the one-step process and forms the basis for the future study of the work.

## **2.4 Conclusion and Future Work**

In conclusion, a PLA-NHPDMS copolymer was synthesized via a transesterification reaction involving PLA and amine-terminated PDMS, following a reactive extrusion route. A class of copolymers were synthesized by varying the molecular weight and amount of NHPDMS used. The purified copolymer was then characterized to confirm the occurrence of reaction by utilizing FT-IR spectroscopy. The thermal properties of the copolymer were measured using TGA and DSC techniques. The presence and morphology of the NHPDMS phase in the PLA matrix was confirmed using TEM imaging. Lastly, the mechanical properties of the copolymers were studied using tensile testing to determine the composition of copolymer that would result in the maximum improvement in toughness.

In the second part of the study, the copolymer synthesized using 5% by weight of the 30,000 g/mol NHPDMS, which was found to have the highest value of toughness, was melt blended with neat PLA and then injection molded into test bars for further characterization. Thermal annealing of the injection molded specimens was then carried out to maximize the percent crystallinity and remove

traces of cold-crystallization formed during the molding process. DSC studies were employed to measure the thermal properties of the blends, and also to monitor the crystallization kinetics of the samples. FT-IR spectroscopy was used as a simple tool to identify the changes in the crystal structure brought about by annealing. The tensile and notched Izod impact testing of the samples revealed an unprecedented improvement in the tensile and impact toughness caused due to a synergistic effect of the addition of the copolymer and the annealing process. DMA studies confirmed that the annealing process resulted in higher crystallinity and improved heat stability. Gel swell analysis, and the study of isothermal melt crystallization kinetics using the Avrami model, done in order to find a suitable rationale behind the improvement in mechanical properties were inconclusive.

A model describing the behavior shown by the PLA-PDMS system was proposed. The “crystallization-induced phase segregation” model was presented to account for the unique behavior demonstrated by the two-step approach of first incorporating the modifier followed by thermal annealing that resulted in a significant improvement in tensile and impact toughness.

The future work related to this study would involve using TEM as an imaging technique to observe the “crystallization induced phase segregation” effect by comparing particle sizes of the PDMS phases before and after the annealing process. This would provide conclusive evidence that this effect was being observed in this system and thereby experimentally prove the proposed hypothetical model. Also, possible techniques to be explored would be XRD analysis of the specimens to determine more precisely the changes in the crystal structure of the PLA caused by the annealing process.

Optimization of process conditions for the adoption of the one-step in-mold annealing method also needs to be performed. The amount of nucleating agent, temperature setting for the mold and

holding/cooling times need to be optimized to provide the optimum amount of mechanical performance.

### **3 REACTIVE BLENDING OF MONOFUNCTIONAL EPOXY MODIFIERS AS PLASTICIZERS FOR POLYLACTIDE**

#### **3.1 Introduction**

Poly lactide (PLA) is currently the most commercially successful biobased plastic in production. There has been a significant investment in terms of capital and research in order to expand the portfolio of commercial applications for PLA. Despite having similar mechanical properties as that of polystyrene and PET and having a lucrative price point of ~\$1/lb., PLA suffers from key disadvantages that restrict its commercial adoption for certain applications [52, 94-96]. PLA has a high glass-transition temperature of ~60°C and thus exists as a brittle polymer at room temperature. This prevents its applications in areas where toughness is desired as a material characteristic. Also, PLA has a low elongation to break when subject to a tensile load and thus this restricts its applications where a high structural strength is required. There are several strategies that have been aimed at improving the toughness and ductility of PLA for high strength and flexibility applications [32-34, 97-99]. These approaches have mostly focused on either one of the following: (i) addition of a plasticizer to reduce  $T_g$  and thus improve flexibility, (ii) blending with a more ductile polymer, or (iii) manipulation of stereochemistry and processing. Each of these methods has shown a varying degree of success at achieving the desired toughness, however, not necessarily in a cost-effective manner. The current study focuses on improving the flexibility of PLA through the addition of a plasticizer.

Plasticizers are ubiquitously used within the polymers and plastics industry to impart flexibility. They usually tend to be low molecular weight compounds that are directly blended with the polymer via extrusion-based processes. The improvement in flexibility through the incorporation of a plasticizer is brought about by the fact that these small plasticizer molecules disperse

themselves within the polymeric matrix creating additional free volume which becomes available for the polymer chains to move around more freely. This increase in chain mobility is reflected as an improvement in flexibility or ductility of the polymer and a reduction in the  $T_g$  of the polymer [100-102].

Several studies have focused on incorporating plasticizers in PLA in order to improve its flexibility and its overall mechanical performance. The plasticizers used have included both biobased as well as fossil-fuel based compounds. Also, the plasticizers used were either monomers or oligomeric molecules. In terms of biobased plasticizers, the most common ones that have been used include esters derived from biobased sources such as citrate esters[103-109]. The most commonly used fossil-fuel based plasticizers is poly(ethylene glycol), which has been used at its various molecular weights as an effective plasticizer [110-113]. Despite the numerous studies that have been done to incorporate plasticizers into PLA, there has been little success through this approach. This is primarily due to the fact that the plasticizers being small molecules tend to leach out of the polymeric matrix over time and thus negate the improvements achieved through their addition. Leaching out of the plasticizer results not only in loss of mechanical properties but it also affects the surface of the plastic part, becoming tacky to the touch due to the migration of the plasticizer to the surface. This is observed to proceed further with aging of the sample [114, 115]. The leaching out of the plasticizer can be significantly reduced if the plasticizer molecules are covalently bonded to the PLA chain. Few studies have focused on achieving this via reactive blending of the plasticizers with the PLA [116-118].

The current study aims to adopt a similar approach wherein the plasticizer is reacted with PLA using reactive extrusion as a facile technique. Two different epoxy-based plasticizers will be used for this study. First, a biobased epoxy derivative of cardanol, UL-513, will be used as a potential

plasticizer. Cardanol, which has been extensively explored as a biobased platform for performance chemicals, is derived from cashew nut shell liquid (CNSL) which is a by-product of the cashew nut industry [119]. Thus, the UL-513 can be considered a more sustainable choice of plasticizer. Cardanol and its derivatives have previously been looked into as potential plasticizers for PLA with promising results [120-124]. However, their reactive blends with PLA has not been studied so far and warrants further investigation. Figure 3-1 shows the chemical structure for the UL-513 molecule. It is hypothesized that the presence of elevated temperatures and shear within the extruder would cause the epoxy ring to open and react with the carboxylic end group of a PLA chain.

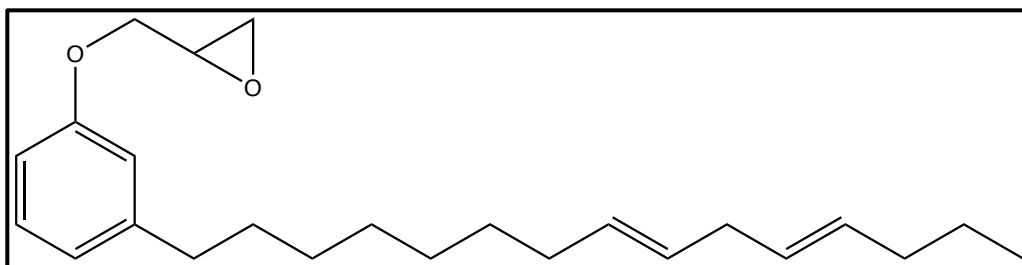


**Figure 3-1:** Chemical structure of the Cardolite UL-513

Another epoxy-based plasticizer, NT-3000, in this case non-biobased, will be used to improve the flexibility of the PLA. The NT-3000 is an aliphatic monoglycidyl ether containing alkyl chains of length C12 to C14. Both the UL-513 and NT-3000 are produced by Cardolite Corporation and are typically used for applications in the coatings and adhesives industry. Figure 3-2 shows the chemical structure of the NT-3000.

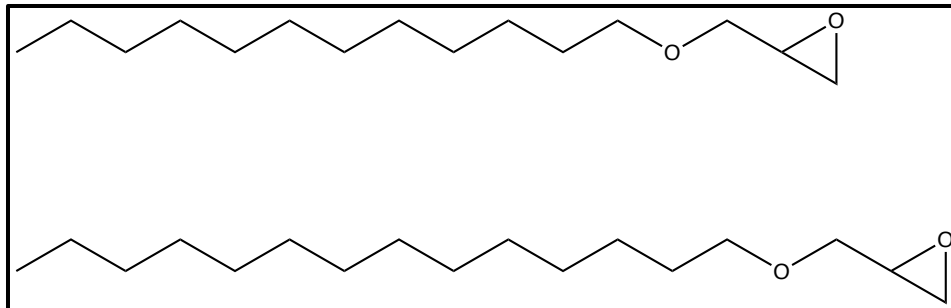


**Figure 3-2:** Chemical structure of the Cardolite NT-3000 (final product is a mixture of both compounds)

Apart from the source from which they are derived, a fundamental difference between the UL-513 and the NT-3000 is that the UL-513 is an aromatic compound whereas the NT-3000 is an aliphatic compound. The current study would also serve as a comparison between the plasticizing effects of the two types. An additional aspect that would be considered of interest would be to see if the end-capping of the carboxylic groups in the PLA would result in an improvement in the hydrolytic stability of the PLA since the hydrolysis of PLA has been known to be self-catalyzed by its carboxylic end groups [125].

## 3.2 Experimental

### 3.2.1 Materials

A commercially available semi-crystalline grade of PLA, 3001D, was used for this study. The PLA was sourced from NatureWorks LLC (Minnesota, USA). The 3001D grade of PLA has a weight average molecular weight of ~150,000 g/mol and a meso-lactide content of around ~2%. Two different monofunctional epoxy compounds, Ultra LITE 513 and NT-3000, were kindly provided by Cardolite Corporation (Pennsylvania, USA). The UL-513 is a low-viscosity monofunctional epoxy reactive diluent used for coatings and adhesives applications. It has a viscosity of 20-35 cPs at 25°C, and an epoxy equivalent weight (EEW) of 350-425. It has a density of 0.95-0.98 kg/m<sup>3</sup> at room temperature. The NT-3000 is an aliphatic monoglycidyl ether containing C12-C14 alkyl

chains. It has an even lower viscosity of 5-10 cPs at 25°C and an EEW of 275-300. Other reagents and NMR solvents used were purchased from Sigma-Aldrich (Wisconsin, USA) and Cambridge Isotope Laboratories (Massachusetts, USA) respectively.

### **3.2.2 Reactive Blending**

The reactive blends of the PLA with the two monofunctional epoxy compounds were carried out using reactive extrusion. Identical processing conditions were used for both the epoxy modifiers to maintain uniformity during comparison of properties. The PLA pellets were dried overnight in a convection oven at 60°C prior to the extrusion process. This was done in order to remove residual moisture in the PLA which might accelerate its degradation under shear in the extruder. The epoxy compounds in the form of low-viscosity fluids were premixed with the PLA pellets before being fed into the hopper. A Century ZSK-30 co-rotating twin-screw extruder with a screw diameter of 30 mm and a L/D ratio of 42 was used for the reactive blending. The temperature profile used for this process was as follows: 140/150/160/170/180/185/185/185/180/175°C. The screw speed was set at 100 rpm, and the throughput for the UL-513 and NT-3000 were set at 200 and 160 gm/min respectively. A higher throughput was used for the UL-513 to enable faster pelletization. The extrudate in the form of a strand was quenched by passing through an ice-cooled water bath and subsequently pelletized. The pellets were then dried overnight in a convection oven at 50°C to remove excess moisture prior to characterization.

Two different sample purification methods were used to remove the unreacted epoxy compounds from the extrudate. First, a Soxhlet extractor was used with toluene as the solvent. Approximately 2.5 gm of the extrudate was placed inside a cellulosic thimble, which was then introduced into the extractor setup. The toluene was heated to its boiling point and an attached condenser was used to condense the toluene vapors back into the extractor. The extraction was carried out over a period

of 24 hours. In this manner, the extrudate sample passed through several solvent washing cycles to remove traces of the unreacted epoxy compound. In the second technique, a certain amount of the extrudate was dissolved in DCM, which would dissolve the PLA, the unreacted epoxy, and the reacted PLA-epoxy blend. Once the sample was completely dissolved, an excess of n-hexane was added to the solution which would leave behind the unreacted epoxy in solution and would precipitate out the PLA and the PLA-epoxy reacted blend. This purification process was repeated for at least three times to remove all traces of the unreacted epoxy. The purified and solvent washed extrudate was then used for FT-IR and  $^1\text{H}$  NMR analysis.

### **3.2.3 Model Compound Study**

A model compound study was performed to evaluate the reactivity of the epoxy compounds with the end-groups of the PLA chain. For the study, stearic acid with two terminal carboxylic acid groups was used to evaluate reactivity of the -COOH termination of the PLA with the epoxy, whereas, polyethylene glycol (PEG-400) with two terminal hydroxyl groups was used to evaluate reactivity of the -OH termination of the PLA with the epoxy. The stearic acid, PEG-400 and the epoxy compounds were thoroughly mixed in appropriate ratios using a mortar and pestle. A small sample (~10-15 mg) of the reaction mixture was then placed in a DSC hermetic pan and then sealed. The pan was then introduced into the DSC oven. The oven was equilibrated to 10°C before placing the pan inside. The sample was then heated to 250°C at 10°C/min and the heat flow vs. temperature data was recorded. A DSC Q20 (TA Instruments, USA) setup was used to carry out the experiments.

### **3.2.4 Characterization of Reactive Blends**

FT-IR spectra of neat PLA and the purified extrudate in the form of a film were recorded using the ATR mode of a Shimadzu IRAffinity-1 spectrometer (Shimadzu Co., Japan) equipped with a

single reflection MIRacle ATR attachment (PIKE Technologies, USA). The spectra were obtained in the absorption mode within the spectral range of 4000-600  $\text{cm}^{-1}$ . The film samples were prepared by the solvent-casting method, wherein the samples were dissolved in DCM and were cast on to petri dishes. The solvent was then allowed to evaporate at 40°C in a convection oven.

$^1\text{H}$  NMR analysis of the sample was performed by first dissolving the purified extrudate in a deuterated chloroform ( $\text{CDCl}_3$ ) solvent. The spectra were recorded on a 500 MHz Varian Unity Plus NMR spectrometer (Varian Associates Inc., USA) at room temperature. Spectra of the purified extrudate were compared with that of neat PLA to observe for peak shifts post-reaction.

The thermal degradation properties were evaluated using a thermogravimetric analyzer, TGA Q50 (TA Instruments, USA), by heating the sample from room temperature to 550°C at a rate of 10°C/min under a nitrogen atmosphere. The thermal transitions of the samples were obtained by using a differential scanning calorimeter, DSC Q20 (TA Instruments, USA). The samples were first heated up to 200°C starting at room temperature at a rate of 10°C/min under a nitrogen atmosphere to erase any thermal history associated with processing. They were then heated back up to 200°C at 10°C/min. The heat flow vs. temperature data was then recorded and plotted.

The tensile test specimens for the reactive blends were prepared using an 85-ton Cincinnati Milacron (Ohio, USA) injection molding machine. The barrel and nozzle temperatures were set at 380/350/350°F and 375°F respectively. The mold was held at room temperature. The screw speed was set to 100 rpm and the injection pressure used was 800 psi. The total cycle time was set at around ~90s. Thermal annealing of the injection molded test specimens was performed using a regular lab-scale convection oven. The oven was heated to 95°C before introducing the samples, which were placed in an aluminum tray. Samples were placed in a manner to minimize warpage during the annealing process.

The tensile testing was carried out on an Instron model 5565-P6021 (Massachusetts, USA) mechanical testing fixture setup with a 5 kN load cell. The testing was carried out in accordance with the ASTM D638-14 (Type I sample size) standard test method for tensile properties of plastics [126]. The rate of grip separation was set at 5 mm/min which was as per the ASTM D638 specifications. A minimum of six replicates were used to ensure repeatability of the test data.

A JEOL 6610LV scanning electron microscope (SEM) was used to obtain the surface morphology images for the fracture surfaces of the tensile test specimens. The fractured surfaces were mounted vertically using a two-part epoxy, and a carbon coating was applied for conductivity. The mounted samples were then imaged under a high vacuum.

The notched Izod impact properties were studied using a Ray-Ran RR-IMT (Warwickshire, UK) pendulum impact tester equipped with a Techni-Test test software. The testing was carried out in accordance with the ASTM D256 standard test method for determining the Izod pendulum impact resistance of plastics [32]. The samples were notched using a Tinius Olsen Model 22-05-03 Motorized Specimen Notcher (Pennsylvania, USA). The test specimens had dimensions of 63.5 mm X 12.7 mm and the notch marked was 2.54 mm deep. A minimum of six replicates were used to ensure repeatability of the test data.

Dynamic mechanical analysis (DMA) was performed on the samples using a RSA-G2 Solids Analyzer (TA Instruments, USA) to evaluate the storage and loss modulus, as well as the tan delta phase lag factor as a function of temperature. The gage section of the tensile test specimens was cut out into segments of length 50 mm using a bandsaw for the testing. The tests were carried out using the three-point bending mode, within a range of 30°C – 150°C at a heating rate of 3°C/min and a frequency of 1 Hz.

### 3.3 Results and Discussion

#### 3.3.1 Model Compound Study

A model compound study was performed in order to demonstrate reactivity of the epoxy group with the carboxylic and hydroxyl end groups of the PLA, using stearic acid and PEG-400 to simulate the respective end groups, following a procedure as described earlier. The results of the DSC scans are as shown in Figure 3-3 and Figure 3-4.

The studies were carried out using 10% by weight of the epoxy in stearic acid and PEG-400 in order to simulate the actual extrusion process. As can be seen from the curves of the runs with stearic acid, no discernible exothermic peak was observed in the 150 – 200°C range, which is typically the temperature range in which the reaction occurs. This is attributed to the fact that there is most likely a very low concentration of the epoxy in the reaction mixture, especially considering the fact that the sample size for a DSC run is in the order of ~10 mg.

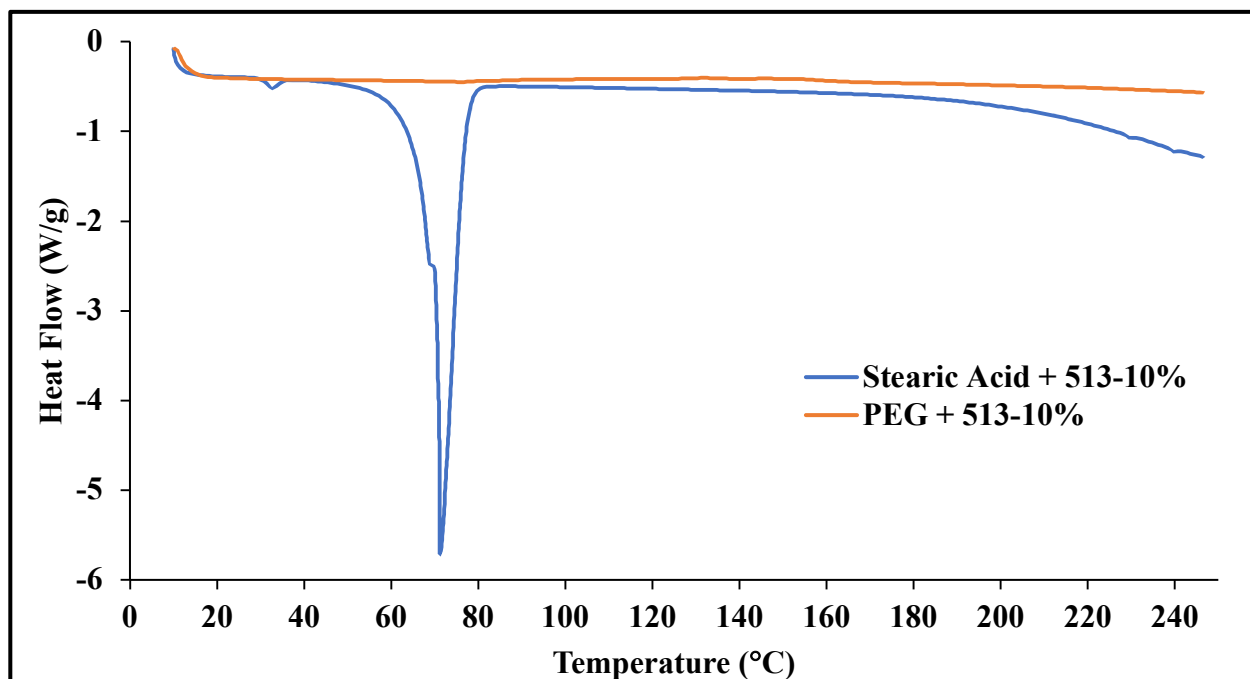


**Figure 3-3:** DSC scans showing the reaction behavior between the UL-513 with stearic acid (blue) and PEG (orange)

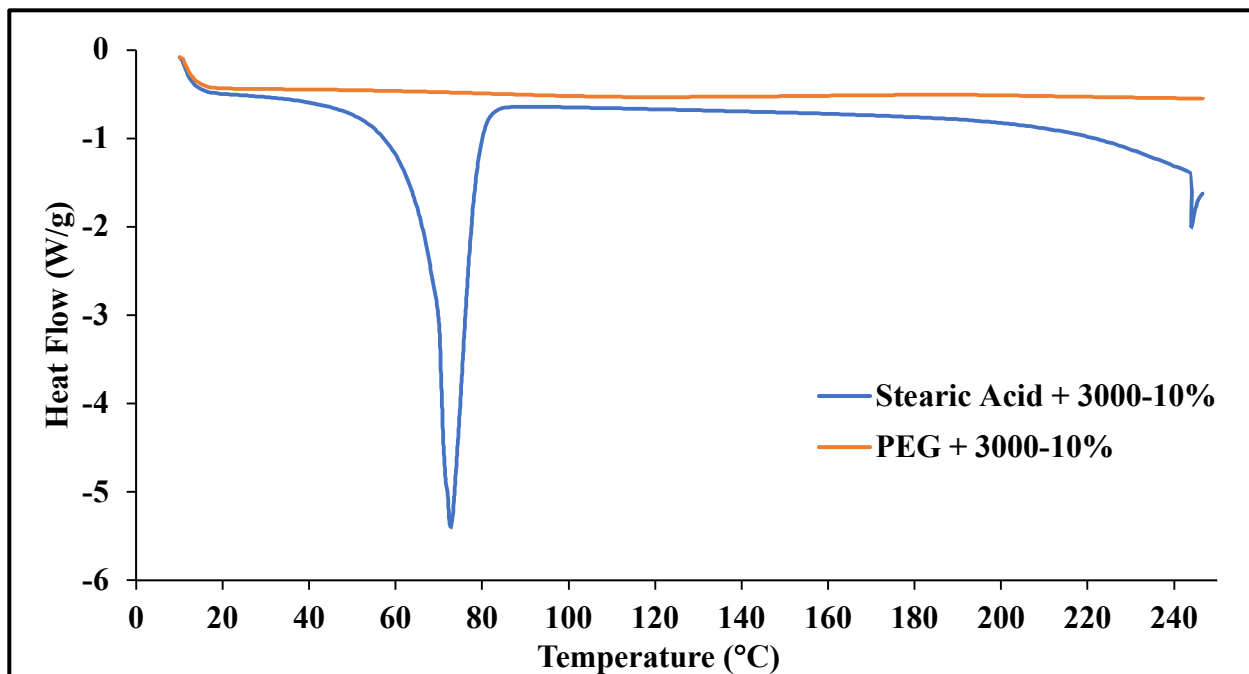


**Figure 3-4:** DSC scans showing the reaction behavior between the NT-3000 with stearic acid (blue) and PEG (orange)

For the runs with the PEG, it is expected that there is likely no reaction within the temperature range used for our extrusion process. Reaction of the epoxy groups with the PEG, if any, occurs at temperatures at above 220°C. Thus, it would be a safe assumption to state that the epoxy groups would just be reacting with the -COOH end groups of the PLA in our case. Despite the model compound not yielding any conclusive results, there is sufficient evidence in literature to establish that the reaction between the -COOH and the epoxy group is thermodynamically feasible within that temperature range [127-130], and gives us proper justification to proceed with the study.

### 3.3.2 Reactive Blending

Reactive extrusion was used as a facile technique to carry out the reactive blending of the epoxies with the PLA. A screw configuration with two kneading blocks was used for the extrusion in order to increase residence time and ensure proper mixing of the reaction mixture. Kneading blocks create additional shear forces and consistently generate new surfaces within the reaction mixture



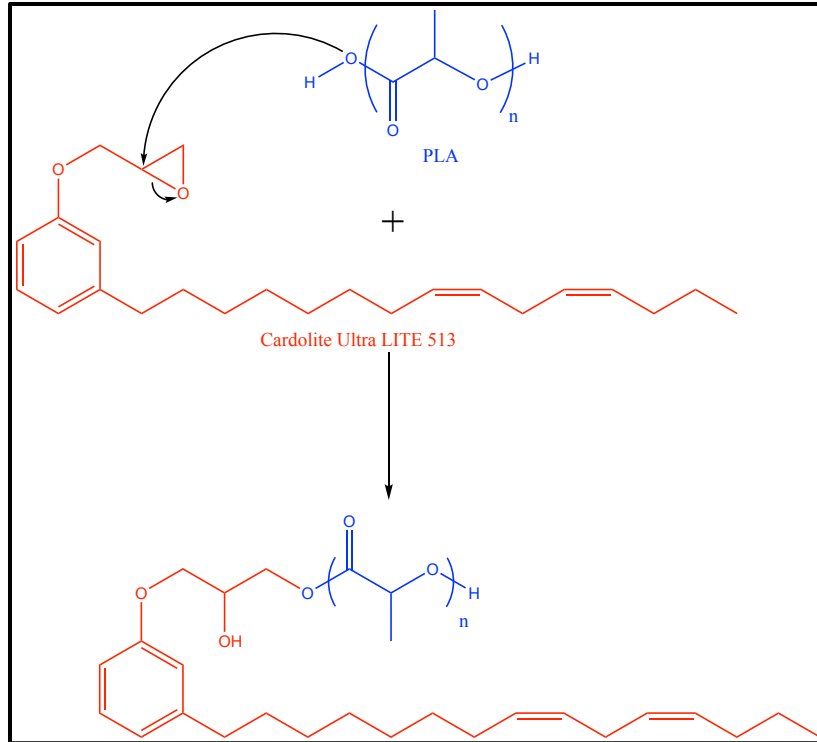


**Figure 3-6:** Schematic of the reaction between PLA and the UL-513

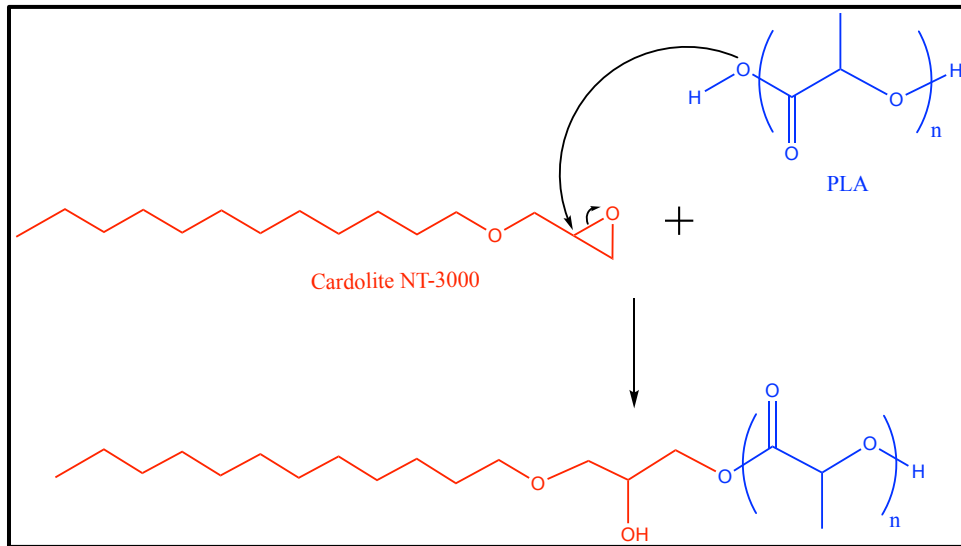


**Figure 3-7:** Schematic of the reaction between PLA and the NT-3000

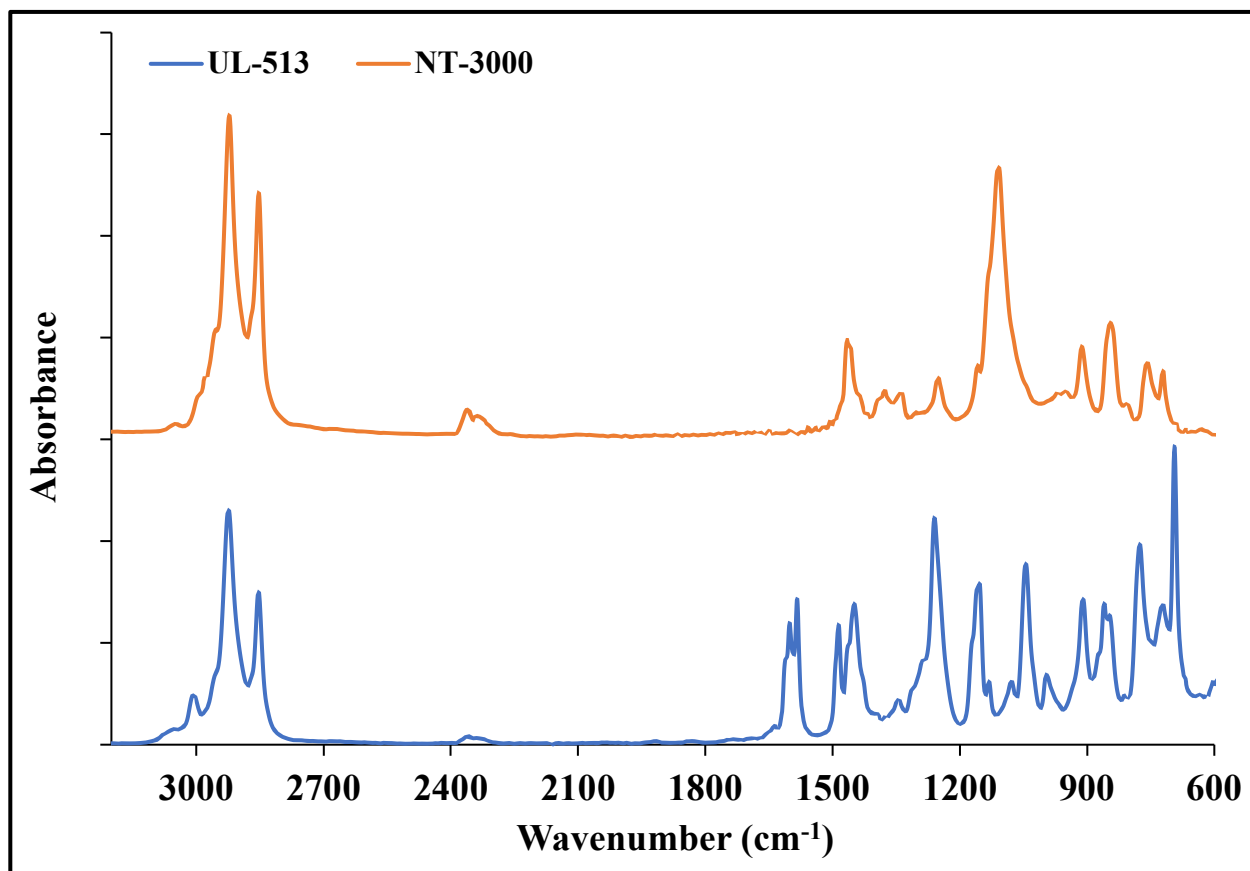
Prior studies have shown that adopting a two-step extrusion procedure for the reaction of PLA with epoxy compounds generates a greater extension of reaction [135, 136]. The two-step process

involves producing a masterbatch of the PLA with a higher loading level of the epoxy compound, followed by a subsequent let down in concentration of the epoxy by extrusion of the masterbatch with neat PLA. This enables the unreacted epoxy groups which are in a molar excess compared to carboxylic groups in the first step to react further when more carboxylic groups become available. In order to achieve that greater extension of reaction and to observe if this contributed to differences in mechanical performance, a similar two-step procedure was adopted for our process. First, a masterbatch with 10% by weight of the monofunctional epoxy compounds was prepared with the PLA. This was then diluted to 1, 2.5, 5 and 7.5% by weight of the epoxy during the injection molding process, where pellets of the 10% masterbatch were added in with pellets of the neat PLA in the appropriate ratio during the single-screw extrusion process prior to the molding. Also, in order to compare properties of the single-step vs. the two-step approach, a direct blend of 5% by weight of epoxy was prepared using the standard extrusion process. The properties of the two 5% by weight epoxy formulations, one obtained through the two-step masterbatch process and the other obtained through the direct blending process were then compared.

### **3.3.3 Characterization of Reactive Blends**

The FT-IR spectra of the epoxy compounds and their purified blends with PLA are shown in Figure 3-8 and Figure 3-9 respectively. Comparing the spectra of the epoxy compounds, several distinct differences can be noted. The peak observed at  $\sim 1600\text{ cm}^{-1}$  in the UL-513 spectrum can be attributed to the aromatic ring stretch of the cardanol molecule. Also, the peak at  $\sim 3000\text{ cm}^{-1}$  corresponds to cis-/trans- C-H stretch observed in alkenes. For the NT-3000, a peak is observed at  $\sim 1370\text{ cm}^{-1}$  that corresponds to the methyl C-H group stretching. In terms of similarity, peaks at  $2850$  and  $2920\text{ cm}^{-1}$  are observed in both the compounds that correspond to methylene C-H stretching [137]. Also, peaks in the range of  $830$  to  $930\text{ cm}^{-1}$  are observed in both that correspond

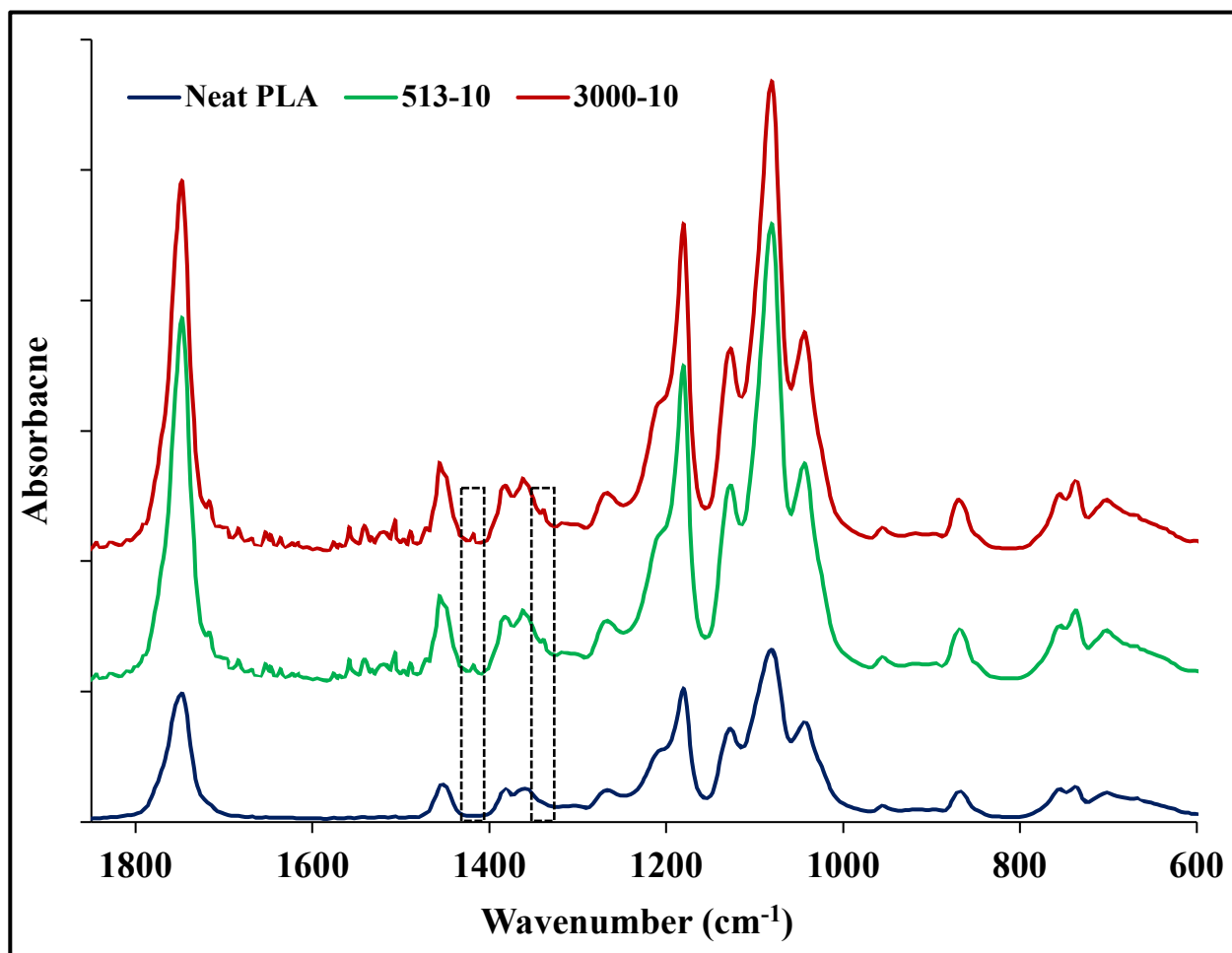
to epoxy (oxirane ring) [138-140].



**Figure 3-8:** FT-IR spectra of the UL-513 and the NT-3000

For the FT-IR spectra of the purified blends of the epoxies with PLA, no major differences were noted, primarily due to the fact that the extent of the reaction was likely low enough not to warrant sufficient grafting of the epoxy on to the PLA chain. Thus, post-purification, most of the epoxy ought to have been removed from the reacted blends. Looking at the spectra for the blends at 10% by weight, only two minor peaks at 1335 cm<sup>-1</sup> and 1415 cm<sup>-1</sup> were marked as key differences when compared with the spectrum for neat PLA. Both of these peaks have been previously attributed to the C-H bending of the methylene group in epoxides and ethers [141, 142]. However, the intensities of these peaks are quite minimal and thus cannot be considered as conclusive evidence of the reaction between the PLA and the epoxy compounds. Near infrared spectroscopy of epoxy

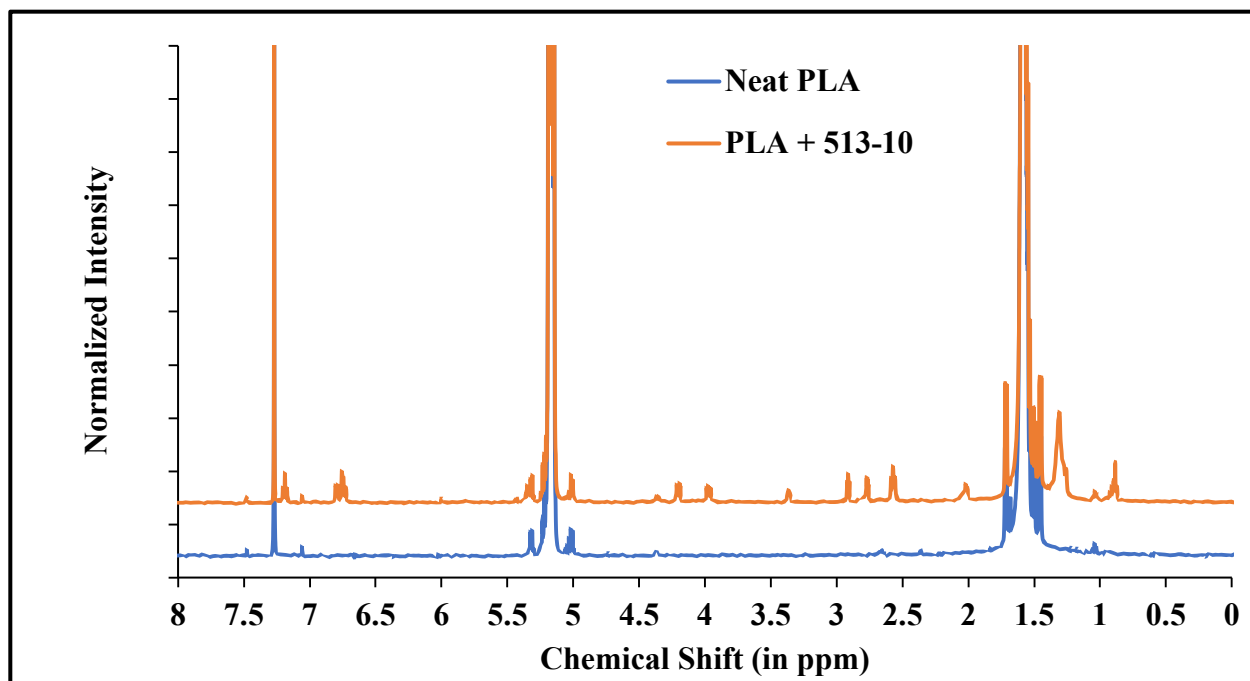
based systems have been found to provide more accurate and could be used as an additional means to study this PLA-epoxy system [143].



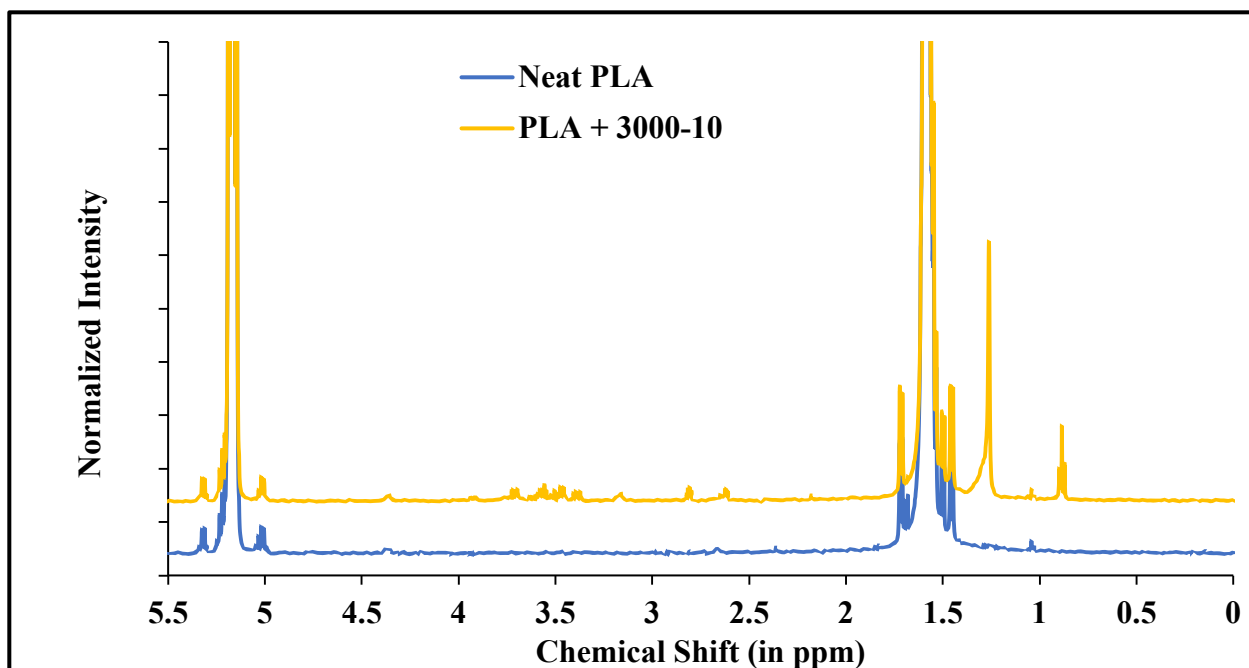
**Figure 3-9:** Comparative FT-IR Spectra of neat PLA and the purified blends of UL-513 and NT-3000 with PLA

Figure 3-10 and Figure 3-11 and show the <sup>1</sup>H NMR spectra of the purified blends of PLA with the UL-513 and the NT-3000 respectively. Each of the spectrums has been overlaid with that of the spectrum for neat PLA to provide clarity for comparison. In both the spectra, the characteristic peaks of PLA at 1.6 ppm and 5.2 ppm corresponding to the methyl and the methine protons on the PLA backbone are distinctly visible. For the purified UL-513 blend, there are noticeable changes with respect to the spectrum for neat PLA. The peaks observed at 7.18 ppm and 6.75 ppm indicates

the presence of the protons from the benzene ring of the UL-513. Similarly, the peaks at 4.19 ppm and 3.96 ppm originate from the methylene protons of the glycidyl group in the UL-513 that connects the phenolic oxygen with the epoxy ring. Similarly, the peaks at 3.36 ppm, and 2.77 and 2.91 ppm, correspond to the methine and methylene protons of the epoxy ring. Multiple peaks corresponding to the methylene protons on the aliphatic chain linked to the benzene ring are observed at 2.02, 1.31 and 1.25 ppm. The signal from the protons of the methyl group at the end of the aliphatic chain is seen at 0.88 ppm [144, 145]. The presence of all of the characteristic peaks from the UL-513 in a sample of the purified reactive blend provides sufficient evidence to conclude that there is indeed reaction between the PLA and the UL-513.



**Figure 3-10:** Comparative NMR Spectra of neat PLA and the purified blend of UL-513

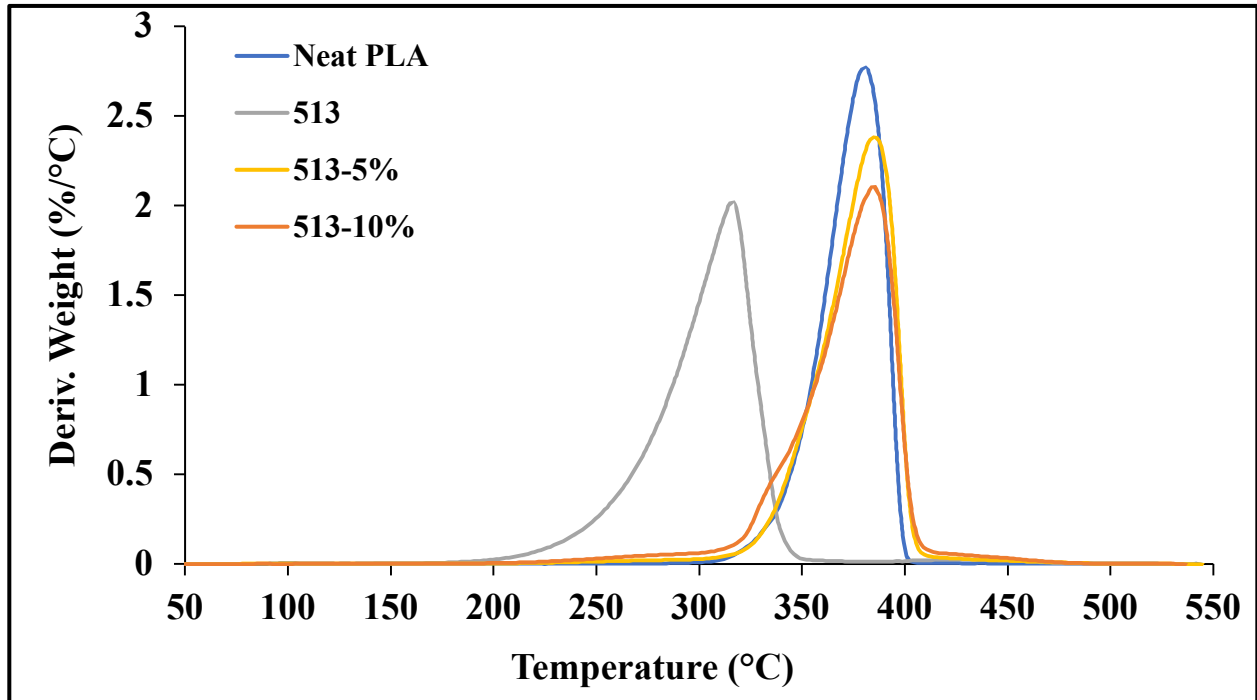


**Figure 3-11:** Comparative NMR Spectra of neat PLA and the purified blend of NT-3000

Similar characteristics were observed with the NT-3000 purified blend. Upon comparison with the spectrum of neat PLA, peaks at 3.65 ppm and 3.55 ppm corresponding to the methylene protons of the glycidyl linkage in the NT-3000 are observed. The peaks at 2.61 ppm and 2.80 ppm correspond to the methine and methylene protons present in the epoxy ring respectively. The broad peak observed at 1.26 ppm corresponds to the methylene protons in the backbone of the NT-3000 whereas the peak at 0.885 ppm corresponds to the methyl group. Again, the spectrum for the purified NT-3000 blend provides sufficient conclusive evidence to claim that the PLA has reacted with the NT-3000. Thus, the NMR approach appears to be more effective at demonstrating the occurrence of reaction between the two components as compared to the previously studied FT-IR results.

The thermal degradation behavior of the epoxy compounds and their blends with PLA was recorded using a TGA analysis in a nitrogen atmosphere. Figure 3-12 and Figure 3-13 show the degradation behavior as a function of temperature. The UL-513 had a peak degradation

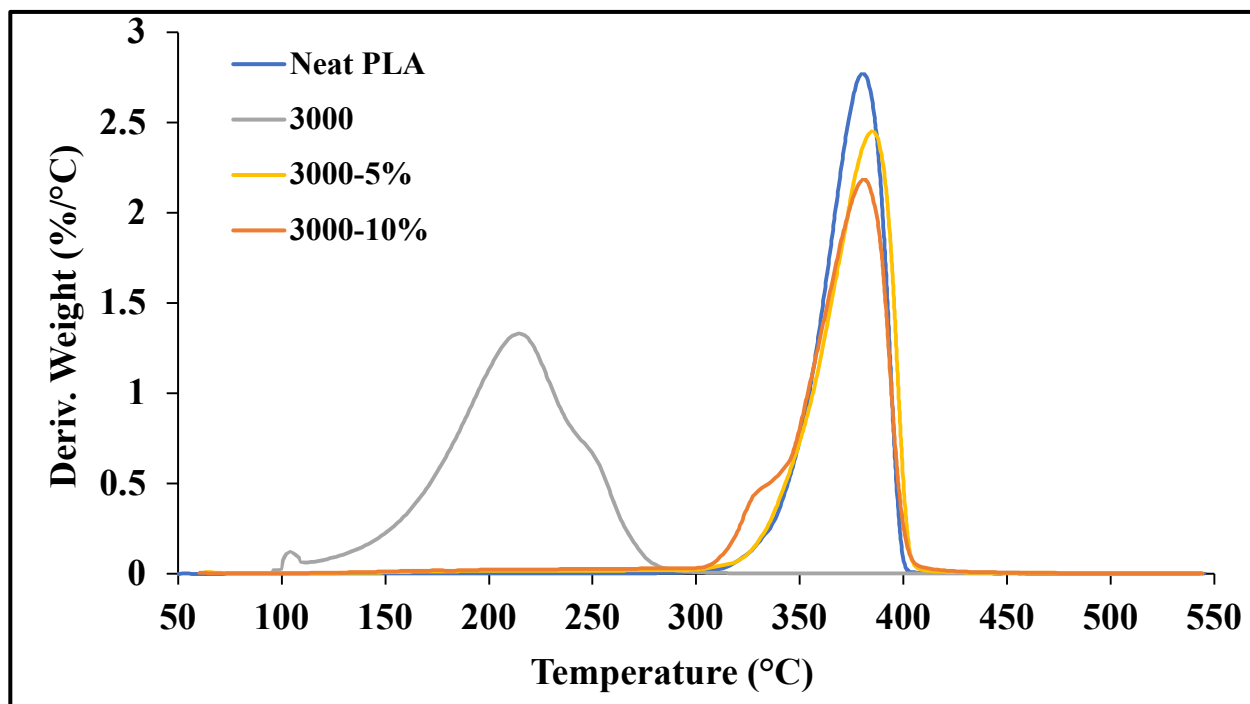
temperature of 318°C whereas the NT-3000 had a peak degradation temperature of 220°C. This follows an expected trend since the UL-513 has a higher molecular weight than the NT-3000 and also possesses an aromatic component that provides additional thermal stability.



**Figure 3-12:** DTG curve comparing thermal degradation behavior of neat PLA and UL-513 with their reacted blends

The thermal degradation behavior for both the UL-513 and NT-3000 blends remained mostly unaffected on comparison with the behavior of neat PLA. For the UL-513 as well as the NT-3000, the blends with 5% of the epoxy compound in PLA showed a single peak that was almost centered on the peak degradation temperature for neat PLA. However, with the incorporation of 10% by weight of the epoxy, a small shoulder was observed in the blends of both the epoxy compounds. This is most likely attributed to the fact that there is a higher percentage of unreacted epoxy in the system which degrades at a lower temperature compared to the reacted blend. Also, comparing the behavior of UL-513 vs. the NT-3000 blends, no significant change was observed, although at a loading level of 10%, the UL-513 blend showed the maximum increase in the peak degradation

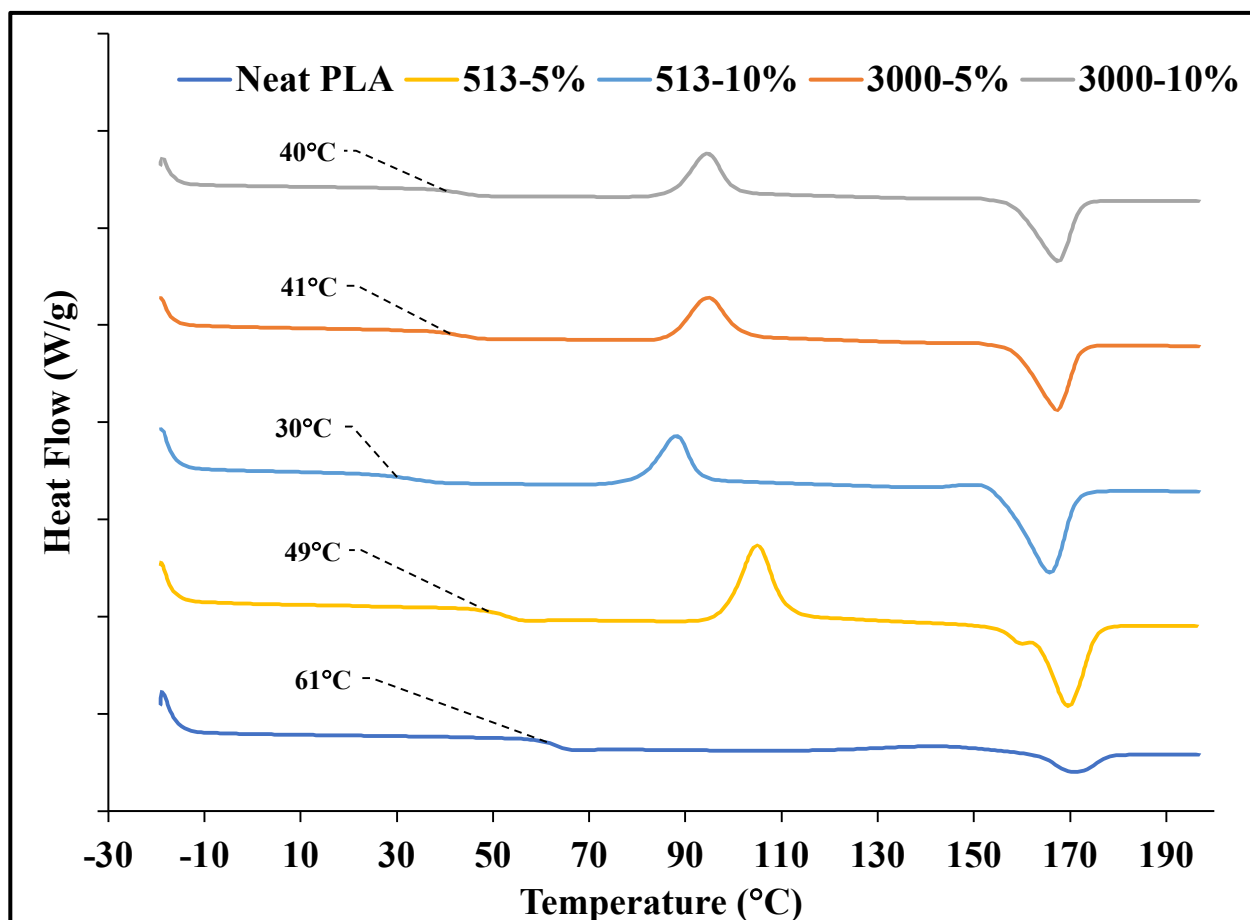
behavior by almost 5°C. A similar behavior was shown at 5% of the NT-3000. This was considered within experimental margin of error and not an actual improvement in the heat stability of the PLA.



**Figure 3-13:** DTG curve comparing thermal degradation behavior of neat PLA and NT-3000 with their reacted blends

The thermal transitions of the blends were studied using standard DSC scans. Figure 3-14 shows the behavior of the UL-513 and NT-3000 blends vs. neat PLA. It can be clearly observed that with the UL-513, the incorporation of 5% by weight in PLA results in a decrease of the  $T_g$  from  $\sim 62^\circ\text{C}$  for neat PLA to  $\sim 50^\circ\text{C}$ . Similarly, the addition of 10% by weight of the UL-513 results in the depression of the  $T_g$  by almost  $30^\circ\text{C}$  (to a final  $T_g$  of  $\sim 30^\circ\text{C}$ ). With the NT-3000 there is a drop in the  $T_g$  of neat PLA by  $\sim 20^\circ\text{C}$  to a final value of  $\sim 40^\circ\text{C}$  at both the 5% and 10% by weight loading levels. This provides clear evidence that both the UL-513 as well as the NT-3000 behave as effective plasticizers for neat PLA. Following the free-volume theory of polymers, the UL-513

and NT-3000 being small molecules, disperse themselves within the PLA chains and successfully increase the free volume available for the motion of the chains, thereby increasing chain mobility and decreasing the overall  $T_g$  of the polymer [116, 146-148]. Since, the  $T_g$  of the PLA was successfully reduced using this approach, using these formulations would result in PLA based materials with higher flexibility and ductility. Subsequent mechanical characterizations were performed on this basis.



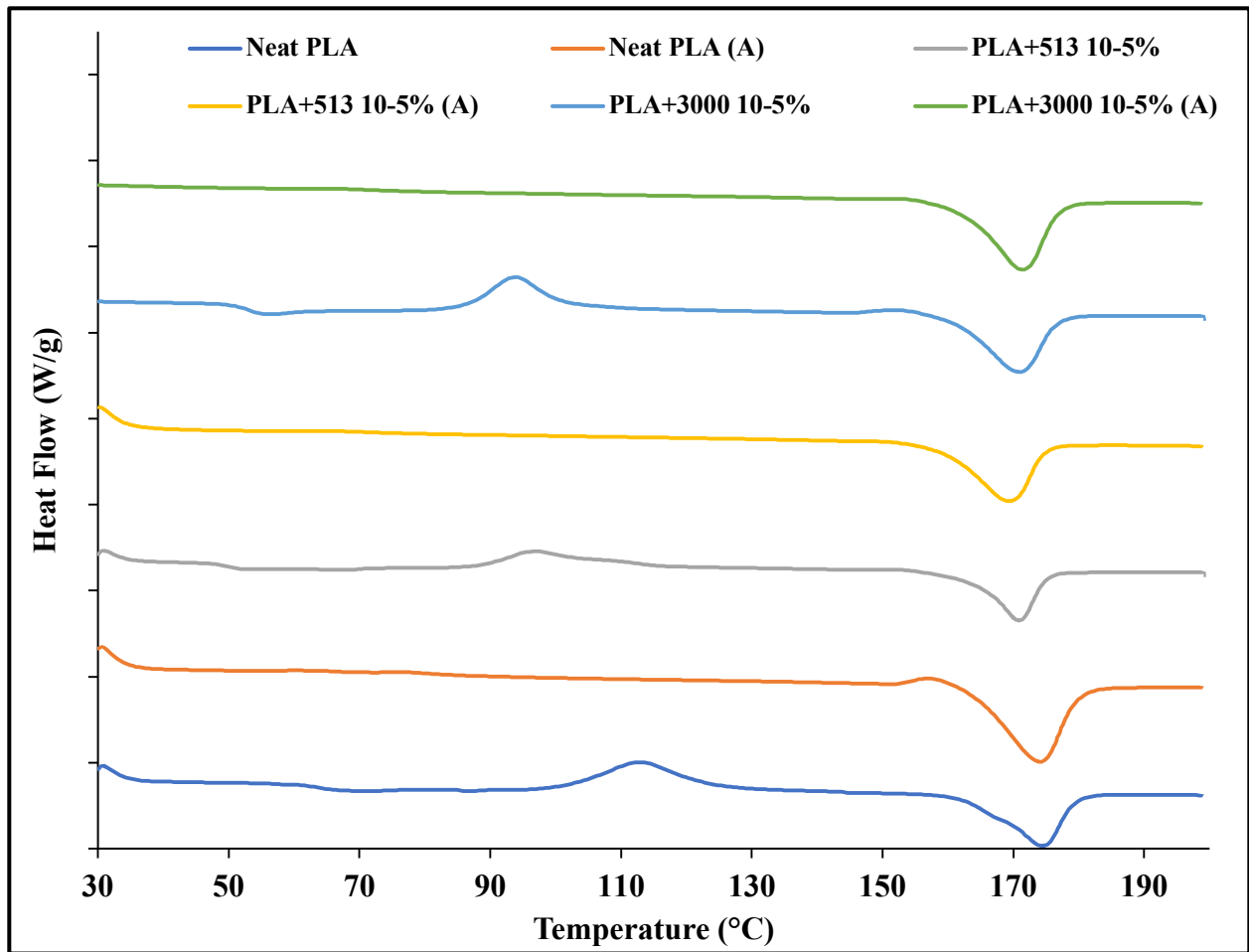
**Figure 3-14:** DSC curves of neat PLA and the reactive blends with UL-513 and NT-3000 (pellets)

Figure 3-15 show the DSC scans of injection molded tensile test specimens of the UL-513 and NT-3000 at 5% prepared from the masterbatch. It gives a comparison of the changes observed due to the annealing process. PLA, being a slow crystallizing polymer, is unable to completely

crystallize during the injection molding process where it goes from melt temperature ( $\sim 190^{\circ}\text{C}$ ) to room temperature in a matter of seconds. This time period is insufficient for it to fully crystallize and thus results in a less crystalline part with poor mechanical properties. The residual domains that are unable to crystallize during the molding process often begin to crystallize when subject to a heating cycle, due to the availability of sufficient thermal energy for the chains to move and arrange themselves forming an ordered arrangement. Thermal annealing is done in order to remove traces of cold-crystallization developed during the injection molding process, thereby leading to a part with higher crystallinity and improved mechanical properties [68, 149-151]. As shown in Figure 3-15 and Table 3-1, the annealing process removes the cold crystallization peak seen at  $\sim 110^{\circ}\text{C}$  for neat PLA and  $\sim 95^{\circ}\text{C}$  for the epoxy modified samples.

**Table 3-1:** Values for thermal transitions points and % crystallinity of the non-annealed and annealed (A) test bars

| Sample             | $T_g$ | $T_{cc}$ | $\Delta H_{cc}$ | $T_m$  | $\Delta H_m$ | % Crystallinity |
|--------------------|-------|----------|-----------------|--------|--------------|-----------------|
| Neat PLA           | 63.65 | 113.09   | 28.1            | 174.47 | 37.36        | 9.94            |
| Neat PLA (A)       | 64.27 | -        | 0               | 169.28 | 42.1         | 45.22           |
| PLA+513 10-5%      | 50.22 | 96.97    | 23.17           | 170.86 | 39.77        | 17.83           |
| PLA+513 10-5% (A)  | 49.19 | -        | 0               | 171.36 | 41.01        | 44.04           |
| PLA+3000 10-5%     | 53.16 | 93.74    | 22.88           | 170.77 | 41.74        | 20.25           |
| PLA+3000 10-5% (A) | 53.66 | -        | 0               | 171.36 | 41.01        | 44.04           |



**Figure 3-15:** DSC curves of neat PLA and the reactive blends with UL-513 and NT-3000 (test bars) - non-annealed and annealed (A)

This effect is seen for all samples regardless of the addition of the epoxy modifier. The major difference with the incorporation of the epoxy modifier is seen in the earlier onset of the cold crystallization peak. Prior studies have associated this effect of faster cold crystallization with the incorporation of either nucleating agents or plasticizers [65, 152-155]. Considering the successful plasticizing effect of the epoxy modifiers in our system, the earlier onset of the  $T_{cc}$  can be attributed to the enhanced mobility of the PLA chains. Having successfully demonstrated the efficacy of the annealing process with respect to achieving maximum percent crystallinity for the injection molded samples, we now proceed to evaluate how the incorporation of the epoxy modifiers

followed by the annealing process affect mechanical properties of the neat PLA.

Figure 3-16 and Figure 3-17 show the storage and loss modulus of the epoxy modified non-annealed and annealed samples as a function of temperature. Looking at the curves for storage modulus for the epoxy modified samples first, it can be observed that with the incorporation of 1% of the epoxy modifiers, there was a slight increase in the storage modulus of the material at room temperature. However, with the addition of 5% of the modifier, the values were similar to that of neat PLA. Also, with increase in the content of the epoxy modifiers, the heat deflection temperature was seen to reduce. This is attributed to the presence of the plasticizing epoxy modifier.

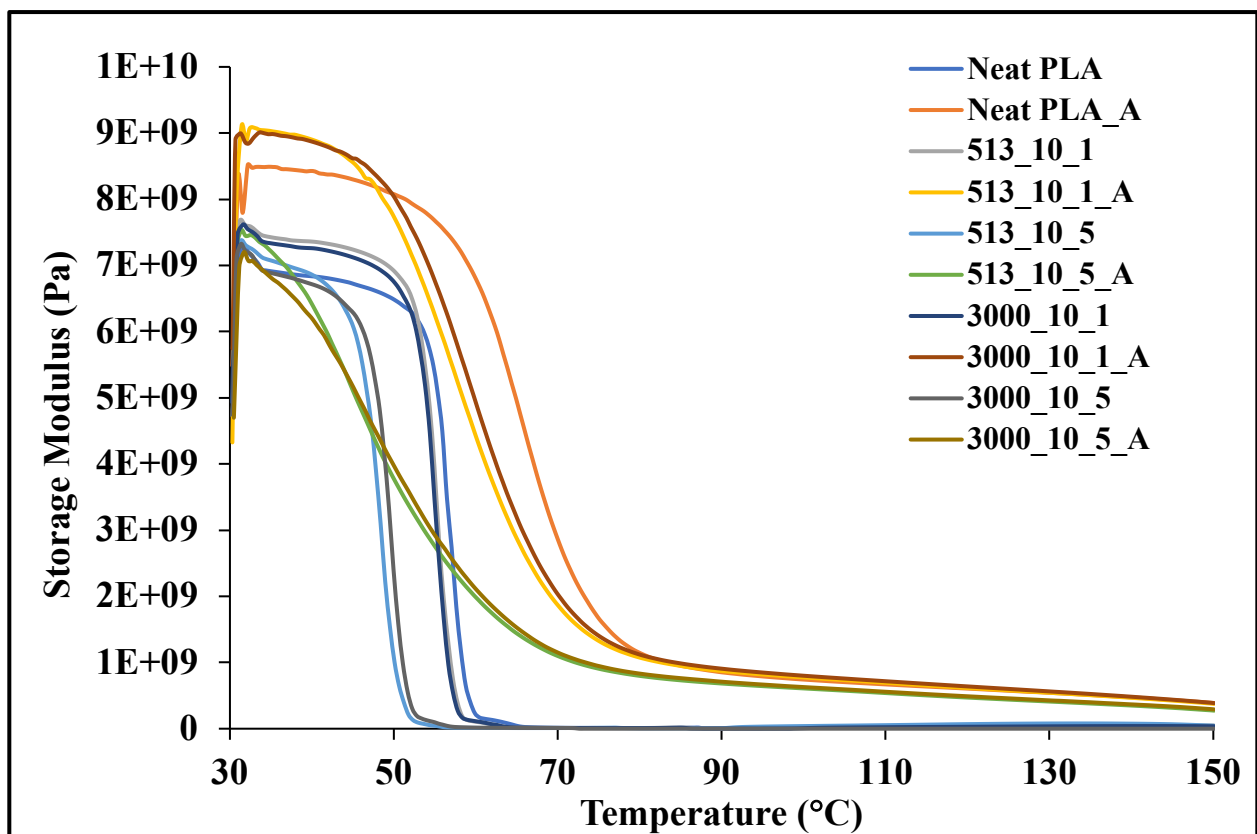
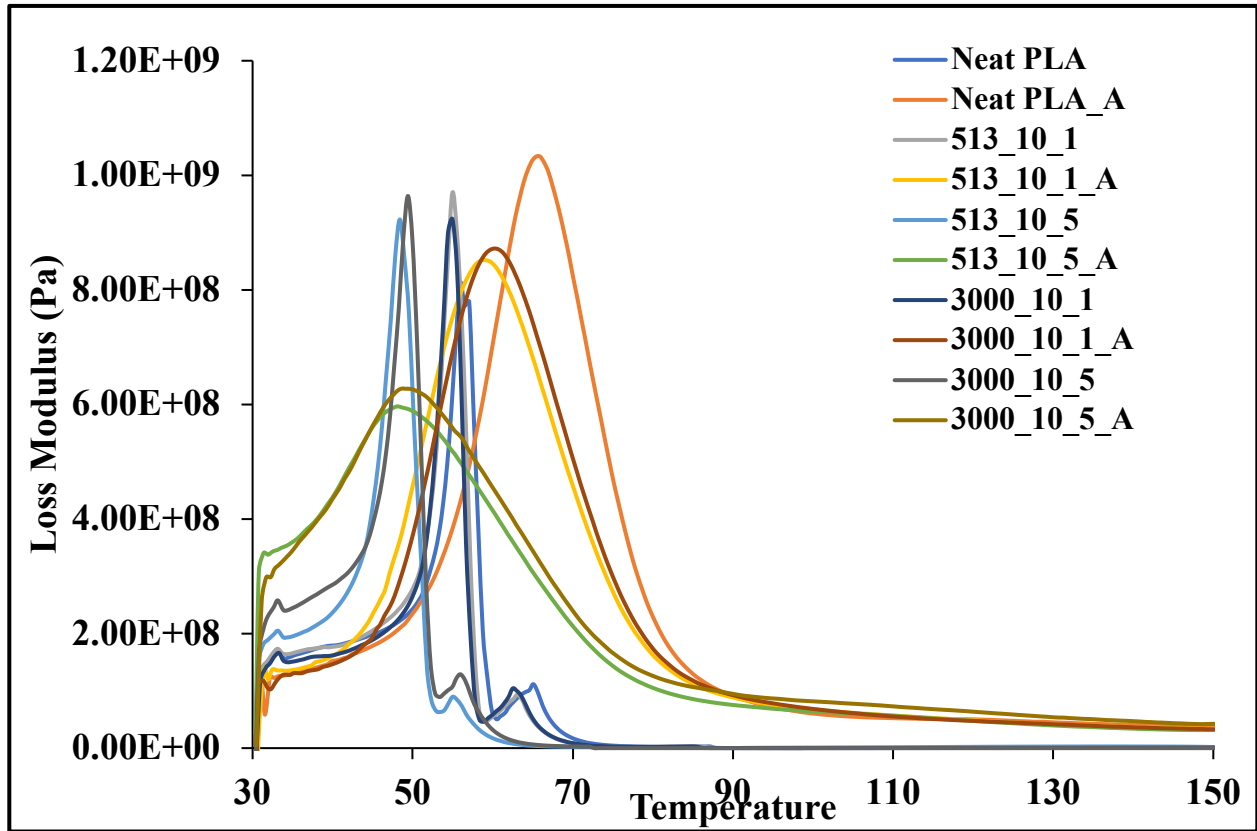


Figure 3-16: DMA analysis of the blends showing storage modulus for the samples (A – annealed)

The annealed samples followed a similar trend amongst themselves, in that, with increase in content of the modifier, the HDT was seen to reduce. Also, the samples with 1% modifier exhibited

a higher storage modulus as compared to the annealed neat PLA [156-158].



**Figure 3-17:** DMA analysis of the blends showing loss modulus for the samples (A – annealed)

The loss modulus of the samples showed similar trends as observed in the storage modulus. The non-annealed samples exhibited two peaks with the smaller peak corresponding to the  $T_g$  obtained from the DSC results. With the increase in content of the epoxy modifier, the  $T_g$  as noted from the second peak was seen to reduce, in agreement with the DSC results. The  $T_g$  dropped by 2~3°C and up to 10°C with the addition of 1% and 5% of the modifiers respectively. The annealed samples showed a single broadened peak with the peak temperature corresponding to the  $T_g$ . The broadening of the peak has been known to indicate the formation a well-ordered crystalline structure [159, 160]. Within the annealed samples, the trend in reduction of  $T_g$  was similar to that of the non-annealed samples, with the most notable difference being the further lowering of the  $T_g$

in the case of the 5% samples. The annealed samples with 5% of the modifier in them were seen to have a further depression in  $T_g$  by around  $\sim 10^\circ\text{C}$  when compared to their non-annealed counterparts. The DMA analysis provides a secondary confirmation of the thermal transitions observed for the samples. It also provides an initial insight on how the mechanical performance of the samples would be affected as a result of change in temperature.

Tensile testing of the samples was done in order to evaluate the effects of increasing modifier loading as well as to monitor the effect of annealing on the samples. Figure 3-18 and Figure 3-19 show the elongation at break values for the UL-513 and the NT-3000 samples respectively. First, considering the non-annealed samples with the UL-513 modifier in them, it was found that the elongation at break was largely unaffected with an increase in the amount of modifier loading. Starting with 1% and going up till 7.5% by weight of the modifier, the elongation at break values were actually observed to be getting marginally lower when compared with that of neat PLA. Also, as discussed earlier, the effect of using a masterbatch to achieve 5% loading level of the modifier as opposed to direct blending at 5% was studied. There appeared to be negligible difference in mechanical properties of samples prepared using either approach. This was contradictory to our initial assumption that using a two-step approach would enhance mechanical performance due to higher extent of reaction. Also, the trend in properties observed for the non-annealed samples seemed to deviate from theoretical assumptions that the incorporation of a plasticizer would lead to a more ductile or flexible material [114, 161-163]. This is most likely due to the fact that despite being a small molecule plasticizer and successfully reducing the  $T_g$  of the material, the UL-513 possesses an aromatic component which has been known to impart stiffness to materials due to the inherent rigidity of the benzene ring [164-167]. Compared to the non-annealed samples, the annealed counterparts were shown to follow an unprecedented trend. Following the annealing of

the samples, with increase in the content of the UL-513, the samples initially did not exhibit any improvements in terms of the elongation at break till up to 2.5% by weight. However, at a loading level of 5% and 7.5% by weight, the annealed samples showed a drastic improvement in performance as opposed to the non-annealed counterparts. The sample prepared by the direct blending of the modifier at 5% was also found to exhibit similar behavior. The elongation at break was found to increase almost by a factor of 5 for the annealed samples at 5% and 7.5% by loading.

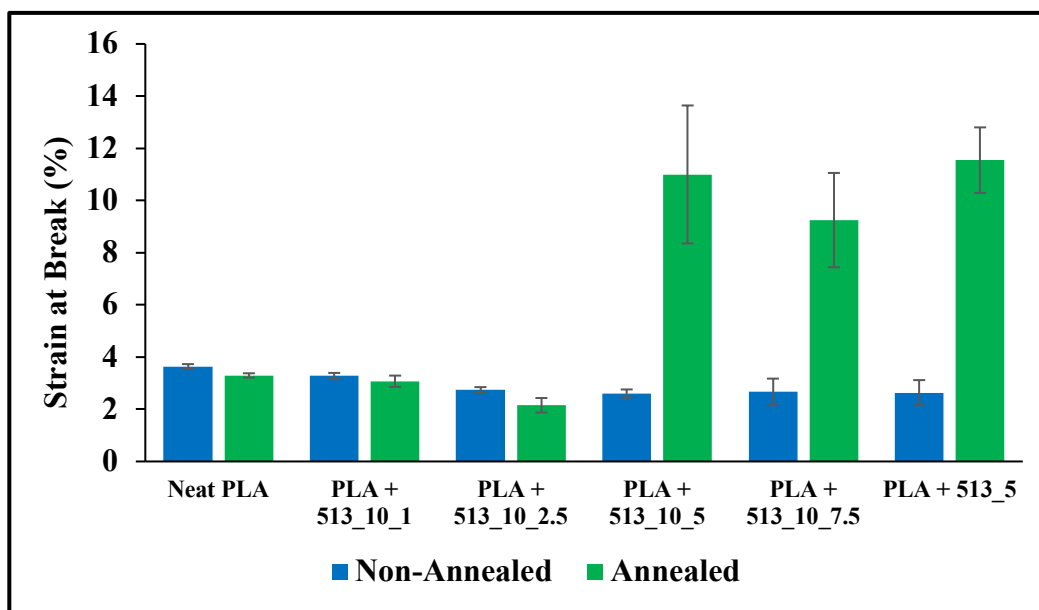


**Figure 3-18:** Comparison of strain at break values for the UL-513 blend samples

A very similar trend was seen in the samples modified with the NT-3000. For the non-annealed samples, there was a marginal drop in the elongation at break values with increasing content of the modifier. However, unlike the non-annealed UL-513 samples, the NT-3000 specimens were shown to have a gradual improvement with increase in modifier content at and above 5% by weight. This is most likely due to the fact that unlike the presence of a stiffness-imparting aromatic component in the UL-513, the NT-3000 happens to be a low molecular weight aliphatic compound, and thus exhibits properties as would be predicted due to the addition of a regular plasticizer [109,

168]. With the annealed samples for the NT-3000 modifier, an almost identical trend in properties was observed, where there was no improvement in performance with annealing at a loading level of up to 1%. However, starting at 2.5% by weight, a significant improvement in elongation at break was observed. This trend continued till 5% by weight, after which with the 7.5% sample, a slight drop in the trend was observed. Again, as with the UL-513, there was almost negligible difference between the 5% sample prepared through the masterbatch route and through direct blending. For both the UL-513 and the NT-3000, the two-step approach of first incorporating the modifier, and then followed by thermal annealing, was shown to generate an unprecedented synergistic improvement in the elongation at break for the samples. An explanation for the behavior will be discussed in the following section.

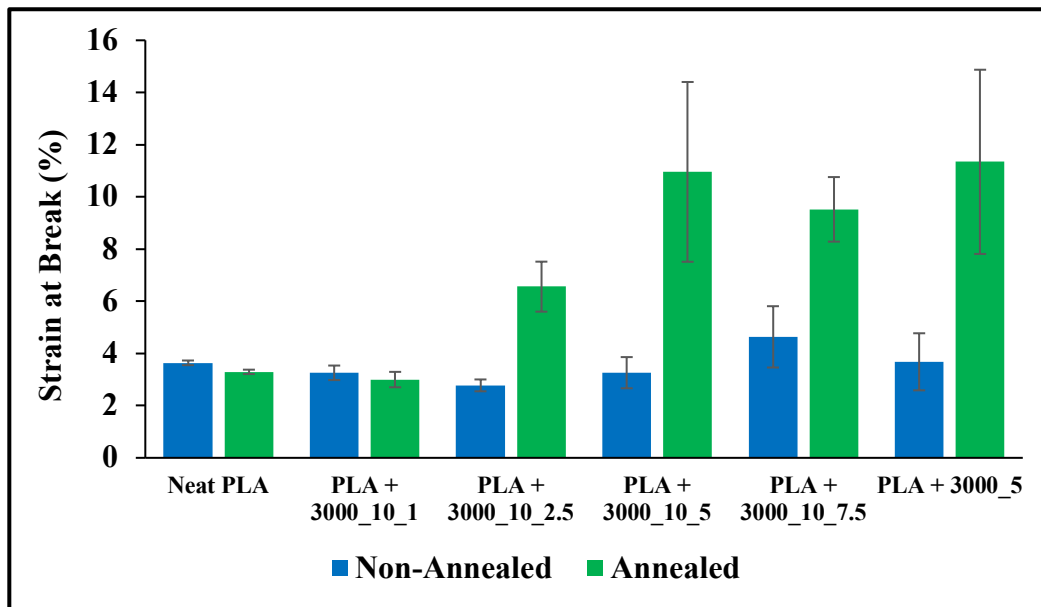


**Figure 3-19:** Comparison of strain at break values for the NT-3000 blend samples

Figure 3-20 and Figure 3-21 show the tensile stress-strain curves for the UL-513 and the NT-3000 samples respectively. Looking at the plots for the UL-513 modifier, it becomes apparent that with an increase in the amount of incorporation of the modifier, the modulus (slope of the stress-strain

curve) and tensile strength of the samples decrease in a constant manner. Although annealing results in an increase in the modulus and tensile strength for the neat PLA, there seems to be no similar effect on samples modified with the UL-513. This behavior follows a predictable trend since incorporation of a plasticizer is typically shown to be accompanied by a simultaneous loss in the stiffness of the specimen [159, 162, 163].

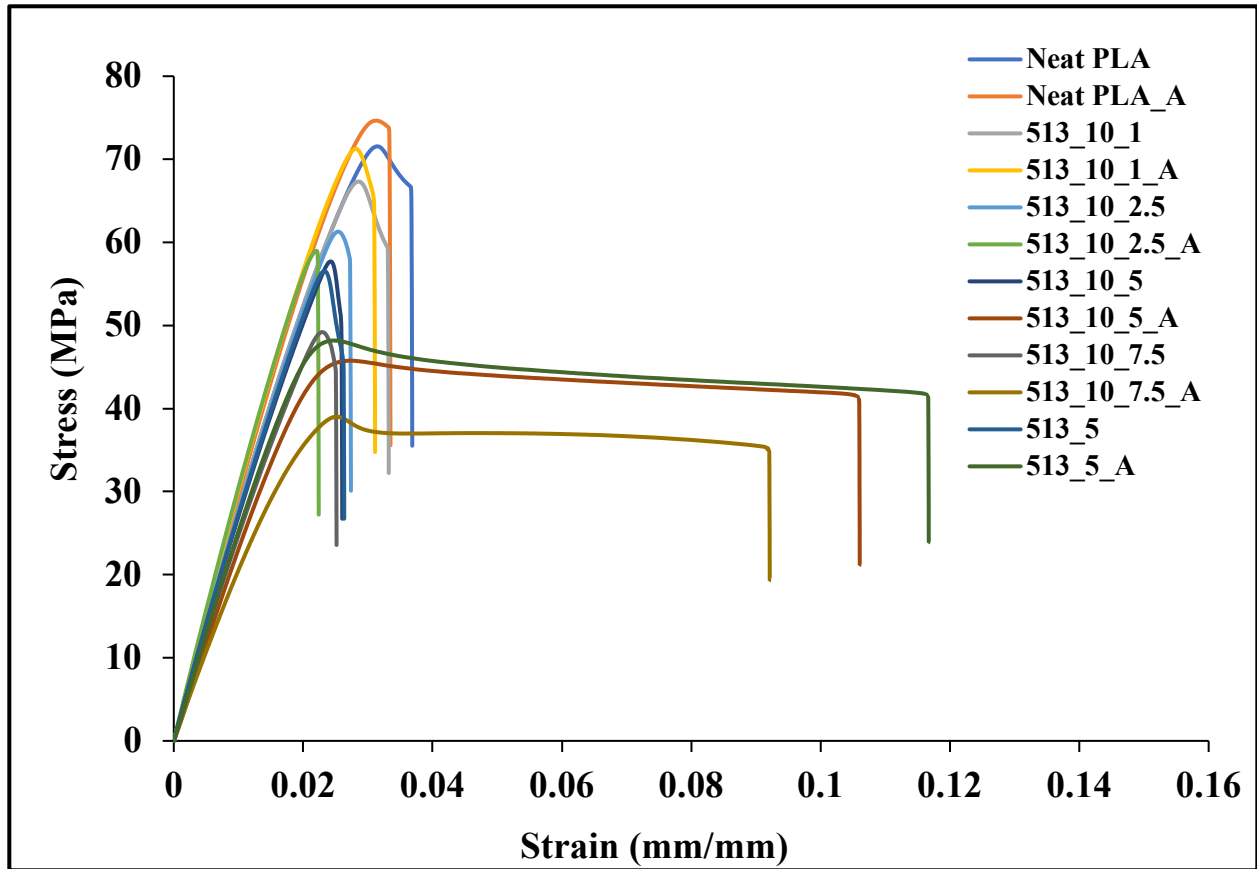


**Figure 3-20:** Stress-strain curves for the UL-513 blends with neat PLA (A - annealed)

For the samples modified with the NT-3000, the stress-strain curves were found to follow an identical trend to that of the samples with the UL-513. With increase in modifier content, the value of modulus and tensile strength were observed to consistently decline. This was in agreement with existing literature where incorporation of a plasticizer is followed by increase in flexibility but reduction in stiffness of the sample [161, 162].

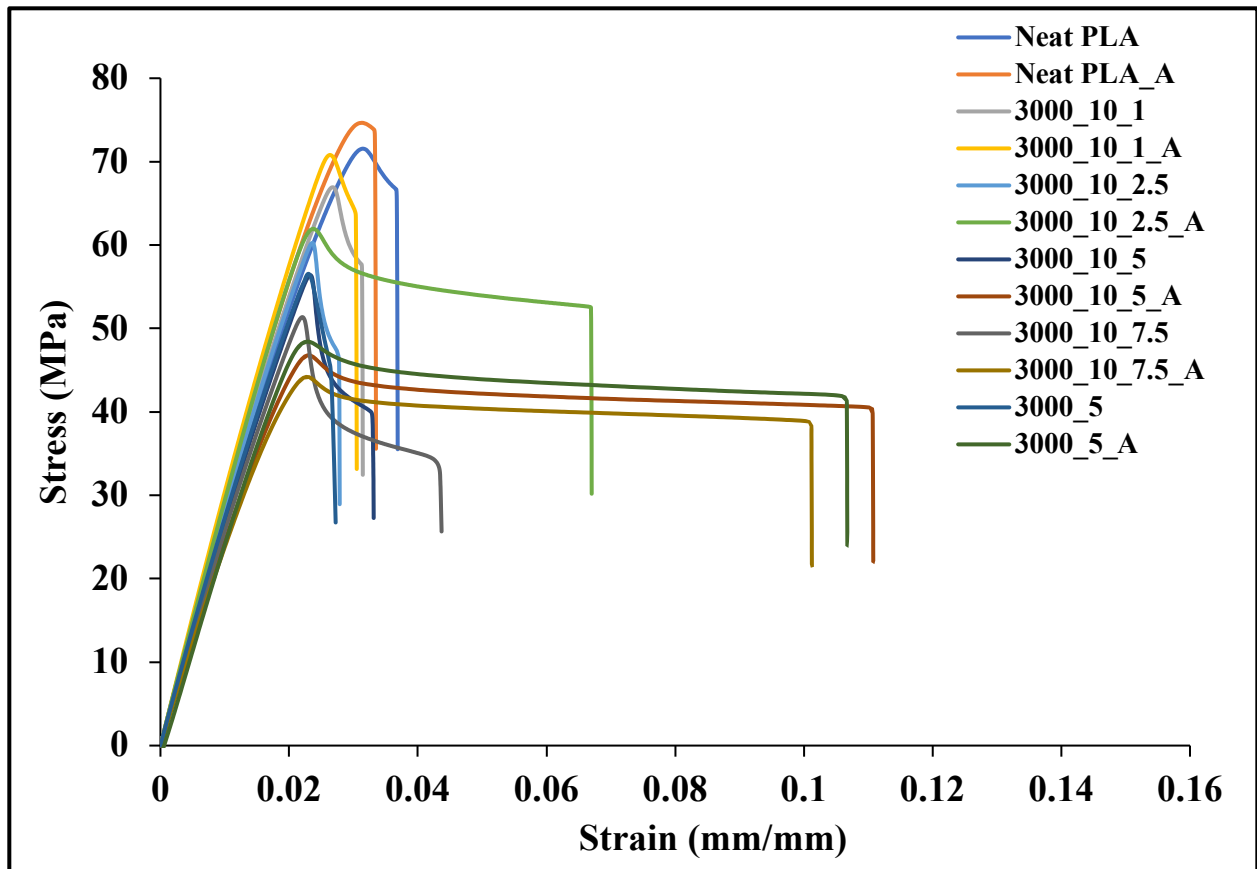


**Figure 3-21:** Stress-strain curves for the NT-3000 blends with neat PLA (A - annealed)

The fracture morphology of the tensile tested specimens with the epoxy modifiers were studied to observe the evolution in the type of fracture with the incorporation of the modifier and the subsequent annealing. Figure 3-22 and Figure 3-23 present the images taken of the fracture surfaces for the UL-513 and the NT-3000 respectively. Identical behavior was observed in samples of both the modifiers. First, comparing the non-annealed samples, the fracture surface of the specimens became progressively “rougher” with an increase in the modifier content. For polymer fracture surfaces, a clean and smooth surface is usually indicative of a brittle fracture whereas a rough or more artefact-ridden surface indicates a ductile fracture [169-172]. Thus, with increasing addition of each modifier, the samples were progressing towards a more ductile behavior as compared to neat PLA. Similarly, looking at the annealed samples, the specimens showed a

progressively rougher surface with increase in the modifier content. Also, comparing annealed specimens with their non-annealed counterparts, the annealed samples were found to have a more uneven surface indicating a transition to a more ductile fracture.

All of the images obtained from the fracture surface morphology were found to be in perfect agreement with the tensile test data studied earlier.

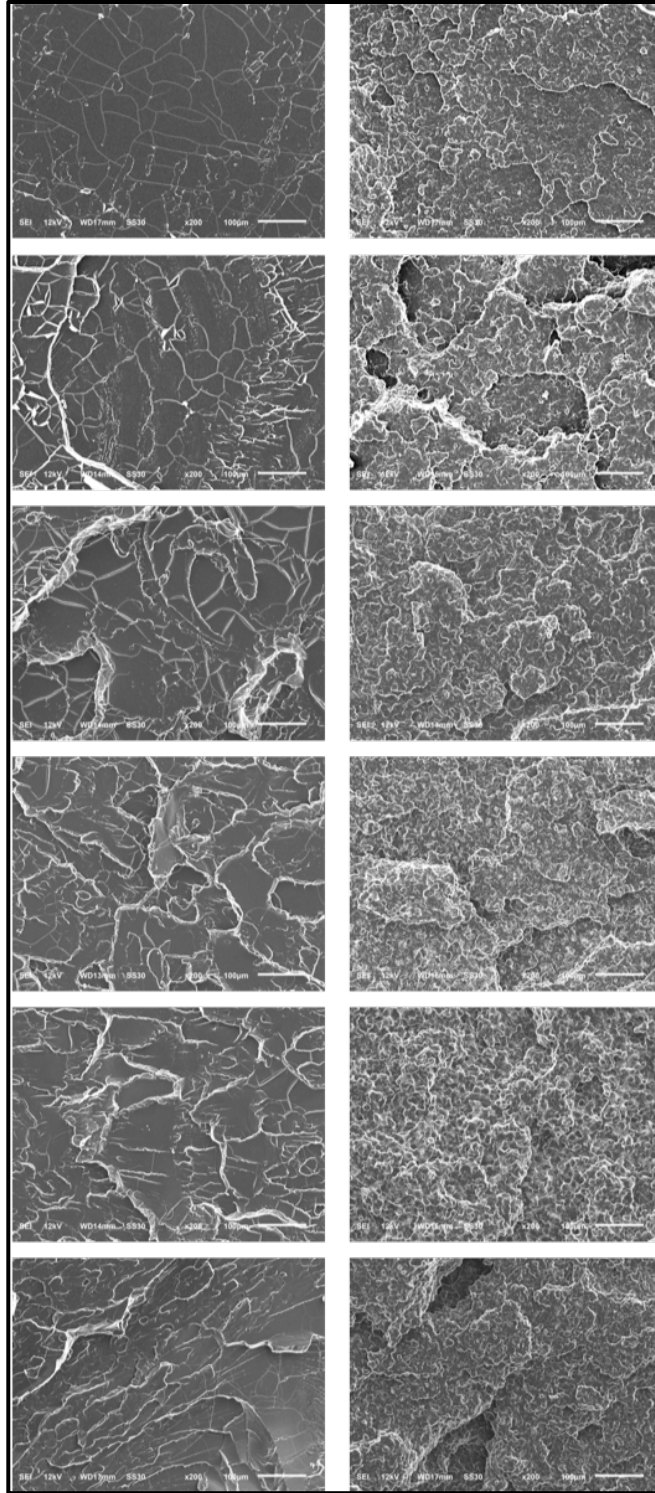


**Figure 3-22:** SEM images of fracture surfaces of tensile tested samples - neat PLA, 10-1, 10-2.5, 10-5, 10-7.5, and 5% UL-513 blend samples (from top to bottom), non-annealed on left and annealed on right

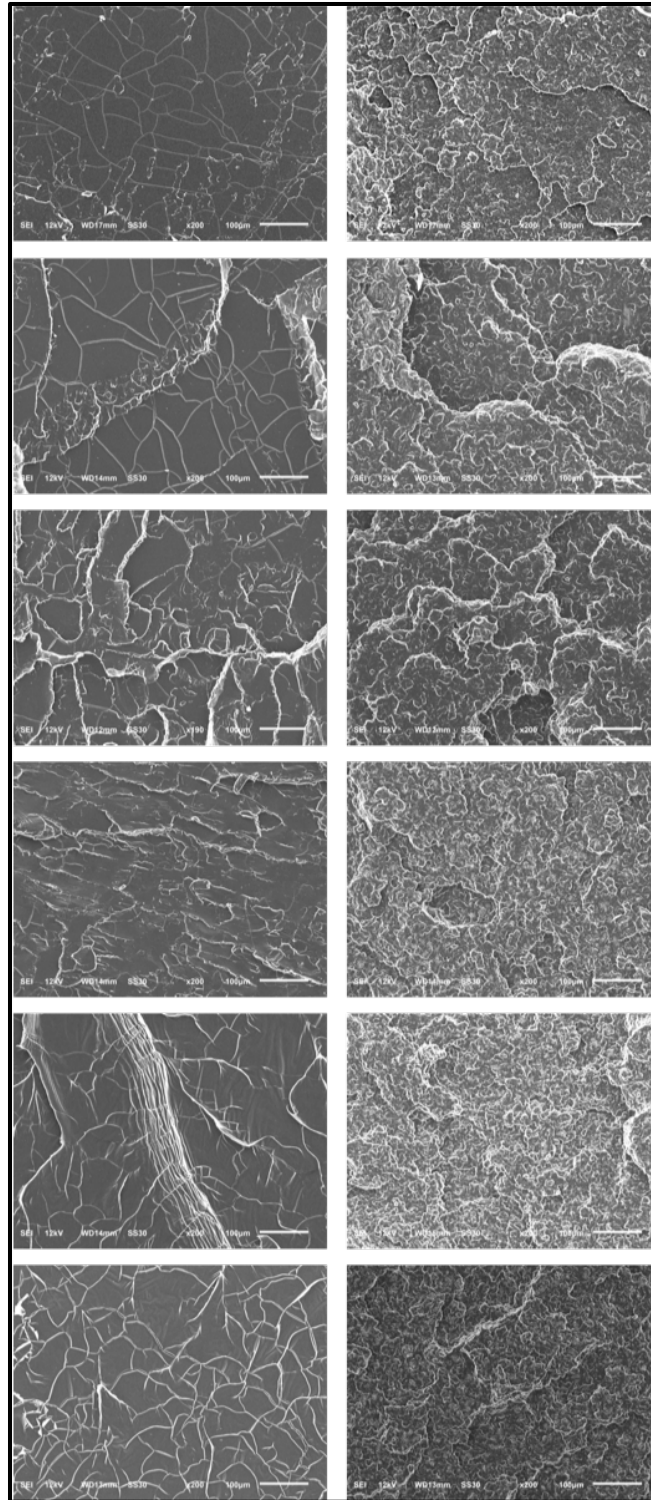


**Figure 3-23:** SEM images of fracture surfaces of tensile tested samples - neat PLA, 10-1, 10-2.5, 10-5, 10-7.5, and 5% NT-3000 blend samples (from top to bottom), non-annealed on left and annealed on right

Notched Izod impact properties of the epoxy modified samples were studied in order to investigate the effect of the plasticizers on the impact properties of neat PLA. The results are as shown in Figure 3-24 and Figure 3-25. Impact performance or the resistance to the propagation of fracture when subject to a directional load is typically found to improve with the incorporation of a plasticizer [173-177]. Considering the non-annealed specimens with the UL-513 modifier first, it can be observed that the impact strength was found to gradually increase with the increase in modifier content from 1 through 5%, however, there was a drop in the value at 7.5%. This follows an expected trend as seen typically with the addition of a plasticizer. Now looking at the annealed samples, a similar trend was observed where the impact strength gradually increased with modifier content but the suffered a decline at the 7.5% level. Also, the values for the annealed samples were found to be consistently higher compared to the non-annealed samples. This increase in value for the annealed vs. the non-annealed samples remained almost identical throughout all samples, including that of neat PLA.

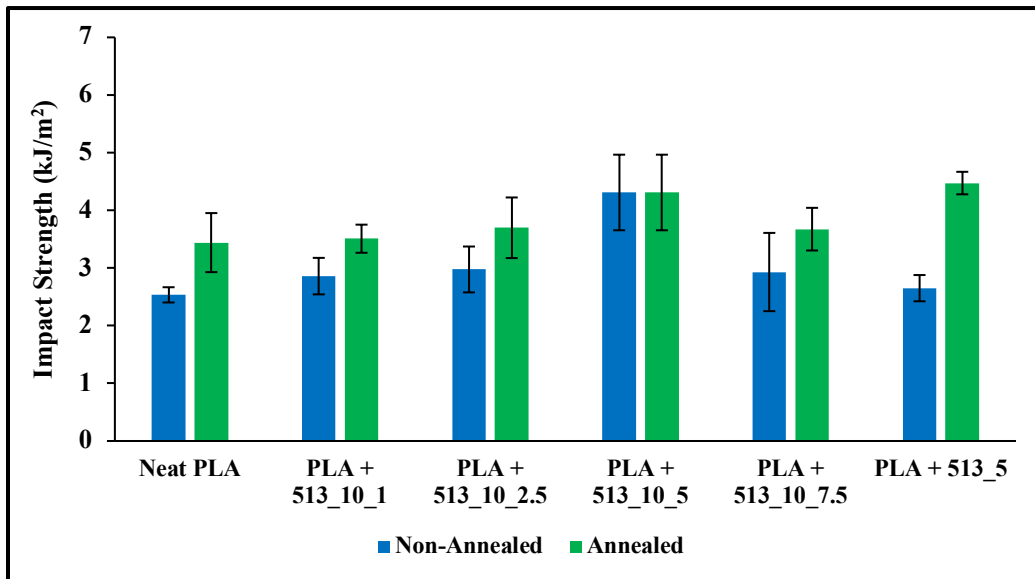


**Figure 3-24:** Comparison of the notched Izod impact strength for the UL-513 blend samples

Also, the non-annealed sample with 5% of the epoxy modifier produced by the masterbatch route

was found to exhibit a higher value, almost up to 1.5 times as much of the sample prepared via the direct blending approach. It would appear that the greater extent of reaction most likely generated in the improvement. However, upon annealing the sample with 5% of the modifier, it had identical values with either of the production routes.

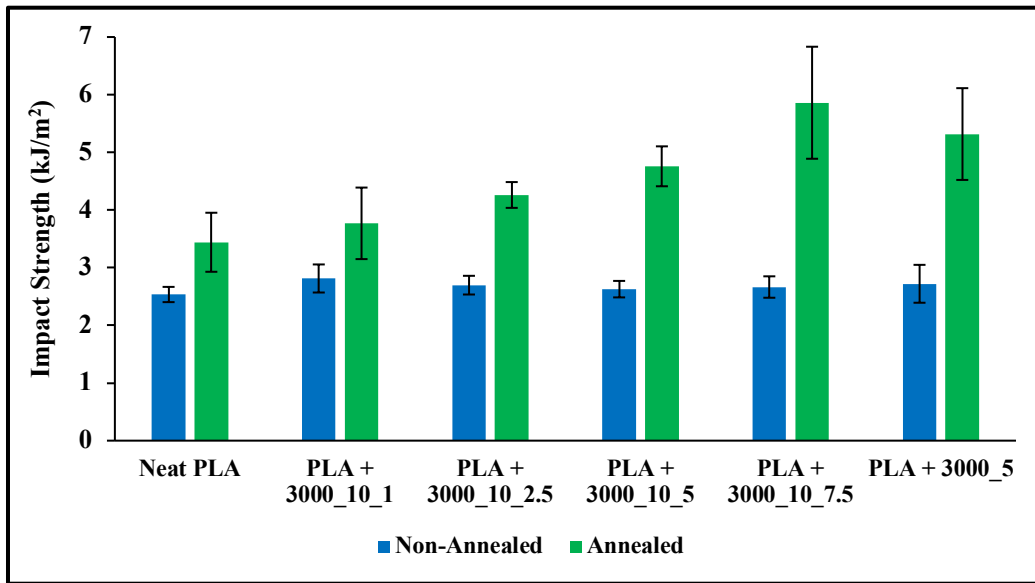


**Figure 3-25:** Comparison of the notched Izod impact strength for the NT-3000 blend samples

Considering the NT-3000 samples, the trend observed differed from that seen with the UL-513 samples. With the non-annealed samples of the NT-3000, the increase in the modifier content had almost a negligible effect in the values for the impact strength. However, a drastic change was observed with all the annealed samples for the NT-3000. It was noted that with the addition of the modifier followed by thermal annealing, a synergistic effect similar to the one observed with the tensile test specimens was seen. Although annealing of the neat PLA sample results in an increase in the impact strength, the increase found in the annealed specimens with the modifier in them was more pronounced and significant. Again, the non-annealed sample with 5% loading had almost identical properties, regardless of the route of production used. The annealed values however were seen to be slightly higher for the direct blending process as opposed to using the masterbatch.

Overall the trends observed for the UL-513 samples appeared to be tending towards a more predictable behavior as compared to the NT-3000.

### **3.3.4 “Crystallization Induced Phase Segregation” Model**

Considering all the mechanical characterization performed so far, a striking similarity can be observed with the PLA-PDMS copolymer system that was discussed in Chapter 1. The synergistic effect of the incorporation of a modifier, followed by thermal annealing resulting in improvements in tensile and impact properties was precisely the summary for the PLA-PDMS system. Looking at how identical these systems are in terms of mechanical behavior, a closer study of the similarities and dissimilarities between the two systems needs to be done in order to arrive at a holistic model that would have an accurate explanation for the behavior of these two systems.

First, in terms of similarities, the two systems had PLA being covalently reacted with a modifier, followed by the preparation of injection molded test specimens, which were then subjected to thermal annealing in order to completely crystallize the PLA domains in the sample. This two-step approach resulted in a trend of mechanical properties where the non-annealed samples showed little or no improvement with just the incorporation of the modifier, however, showed significant improvements in properties once the annealing step was carried out.

Next, let us consider the dissimilarities in the system. First, the PDMS used in the PLA-PDMS system had a considerably higher molecular weight as compared to that of the UL-513 and the NT-3000. The PDMS had a molecular weight of 30,000 g/mol as opposed to 370 g/mol and 270 g/mol of the UL-513 and NT-3000 respectively. Further, no catalyst was used in the synthesis of the epoxy modified resins, whereas a transesterification catalyst was used in the production of the PDMS copolymer. The other major difference was the final amount of modifier loading in the samples. For the PLA-PDMS system, the PLA-PDMS copolymer had a 5% by weight of the

PDMS in the PLA. A minimum of 10% and a maximum of 30% by weight of the copolymer was used during the injection molding with neat PLA. This would essentially translate to a final loading level of 0.5% at minimum and 1.5% at maximum by weight of the PDMS in PLA. For the epoxy modified resins, a minimum of 1% and a maximum of 7.5% by weight of the epoxy modifiers were used in PLA.

Having considered the similarities and dissimilarities in properties of the PLA-PDMS system with that of the PLA-epoxy modified resins, we can arrive at a final model incorporating the conclusions derived from each of the systems. First, we start by slightly modifying the schematic for our proposed model from Chapter 1. Figure 3-26 shows an updated schematic of the same.

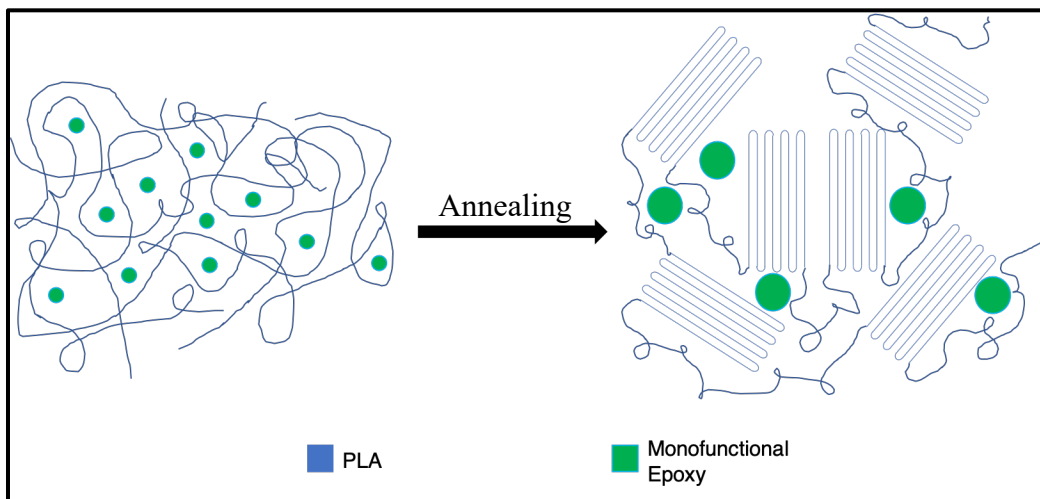


**Figure 3-26:** Schematic demonstrating the "Crystallization Induced Phase Segregation" phenomena in the PLA-epoxy blend samples

Now, looking at the mechanical properties of both systems, it can be seen that the “crystallization -induced phase segregation” theory could offer a comprehensive explanation to properties observed in both systems. The crystallization-induced phase segregation theory is based on the fact that provided there are two phases in a system, one being a semi-crystalline polymer which possesses the ability to crystallize in the presence of sufficient thermal energy, and the other phase

has sufficient mobility to move within the bulk of a polymeric system, the semi-crystalline polymer would start forming highly ordered crystalline domains when subject to a heat treatment step, and in the process would cause the mobile phase to initiate coalescence to form a larger particle size [87-90]. This particle size, which has been established as a primary criterion for polymer toughening, needs to be within a certain range of value for each polymer system in order to demonstrate the optimum improvement in properties [91-93, 178]. Considering a certain fixed range of values for the toughening to be effective, the amount of modifier needed would be dependent on the molecular weight since a higher molecular weight modifier would achieve the minimum threshold of the particle size with a lower quantity of material as opposed to a lower molecular weight modifier. Keeping this theory in mind, the theoretical prediction would be that even at lower loading levels of the PDMS, the minimum particle size in order to achieve toughening would be met. However, to achieve the same particle size, a much higher loading level of the UL-513 and the NT-3000 would be required. The experimental data lines up in agreement with this prediction. It can be seen from the data that significant improvements are observed with the PDMS system even at 0.5% by weight, however with the UL-513 system, improvements are observed only at a loading level of 5%, whereas in the case of the NT-3000, the improvements were observed even at 2.5%.

Furthermore, despite the UL-513 having a higher molecular weight as compared to the NT-3000, the onset of improvements in properties occurred at 2.5% whereas in the UL-513 it was at 5% by weight. As per our proposed model, this is very likely attributed to the relative mobility of the modifier molecule. In this case, the UL-513 with an aromatic group is less mobile compared to the aliphatic NT-3000, thus resulting in a system where the NT-3000 is able to coalesce faster even at lower loading levels to achieve improvements in the properties.

Another distinct difference between the two systems is the fact that the toughness improvements over neat PLA, including both tensile toughness as well as impact properties, recorded with the PLA-PDMS system significantly outweighs the values observed with the epoxy modified resins. This is attributed primarily due to the fact that the PDMS not only has a higher molecular weight but also possesses a -Si-O-Si- backbone which is extremely flexible (rotational energy around the bond is close to 0 kJ/mol) [54]. Also, it is a well-established concept that there tends to be a significant improvement in the toughness of a material once its molecular weight goes beyond its entanglement molecular weight ( $M_e$ ) [179-186]. In existing studies, PDMS has been reported to have an entanglement molecular weight of 24,500 g/mol [187-190]. Since the PDMS that is used for our study to synthesize the PLA-PDMS copolymer has a molecular weight of 30,000 g/mol, it clearly is above its entanglement molecular weight and is expected to exhibit superior tensile toughness as well as enhanced resistance to fracture. In the case of the epoxy modifiers, the molecules tend to have low molecular weight molecules and thus despite undergoing a phase segregation effect and having an increased particle size, the mechanical properties are not as greatly improved as with the PDMS based system. This clearly demonstrates the efficacy of the phase segregation model in accounting for the improvements in toughness observed for both systems.

Another point of difference is that with the PLA-PDMS system, even after the incorporation of the PDMS phase followed by annealing, there was virtually no loss, in fact there was a marginal gain in the modulus and peak load of the material. This was not something that was observed with the epoxy modified PLA, which actually showed a gradual decrease in the moduli and peak load with an increase in the modifier content. Again, the crystallization-induced phase segregation theory can be used to account for this behavior. This behavior can be attributed to the fact that the semi-

crystalline PLA which is the stiffness-imparting part in the all the blends is present at a higher loading level in the PLA-PDMS blends as opposed to the PLA-epoxy blends. Especially after the annealing step during which PLA attains a more crystalline form, the greater the amount of PLA present, the higher should be the modulus and peak load of the specimen. This is another instance where theoretical prediction is validated by the experimental data obtained.

Considering all of the above points where clear validation with experimental data is shown, the “crystallization-induced phase segregation” model is hereby proposed as a holistic model to account for mechanical performance behavior in any similarly designed polymeric system with two components having a semi-crystalline polymeric phase and a mobile phase. Extrapolating to multi-component polymeric blends would require further validation of the model with additional experimental data.

### **3.4 Conclusions and future work**

In summary, novel epoxy-based plasticizers were incorporated into neat PLA to observe their effect on the  $T_g$  of the PLA, as well as to investigate their effect on the mechanical properties. A biobased epoxy derived from cashew nut-shell liquid (CNSL) and a fossil-fuel based epoxy were used for the study. Epoxy based plasticizers were chosen in order to covalently link them with the PLA chain through a reaction between the epoxy ring with the carboxylic end group of the PLA resulting in the formation an ether linkage. This method was adopted since the most common issue with plasticizers is that they tend to leach out of the polymeric matrix due to their low molecular weight. The covalent linkage would ideally prevent the leaching. The reaction between the PLA and the epoxy modifiers were carried out using the reactive extrusion process. The reactive blends were then purified, and characterization was performed to study the occurrence of the reaction, as well as to evaluate mechanical performance of the epoxy modified resins. The epoxy modified

resins were injection molded into test specimens, and thermal annealing was done in order to study its effects on the mechanical behavior.

FT-IR results proved inconclusive, however  $^1\text{H}$  NMR spectra were used to conclusively determine the reaction between the epoxy group and the carboxylic group. Further, thermal degradation behavior was found to be unaffected with respect to neat PLA upon addition of the epoxy modifier. Thermal transitions were recorded using standard DSC scans. The  $T_g$  of the PLA was seen to drop by  $\sim 10^\circ\text{C}$  and  $\sim 20^\circ\text{C}$  with addition of 5 and 10% by weight of the epoxy modifiers, respectively. This clearly demonstrated the plasticizing behavior of the epoxy compounds. Also, the  $T_m$  was found to be unaffected by the addition of the epoxy, however, the  $T_{cc}$  was seen to have an earlier onset indicating an increase in free volume of the sample. Thermal annealing resulted in samples with a higher percent crystallinity overall by eliminating traces of cold crystallization formed during the molding process.

DMA studies of the epoxy modified PLA samples revealed similar trends in thermal properties as observed from the DSC scans. The storage modulus and HDT were found to decrease with the addition of the modifier, however the annealing process resulted in samples with higher storage modulus and elevated HDT. The epoxy modification seemed to have little or no effect on the tensile elongation at break for the samples. However, post-annealing, the elongation at break values were seen to rise steadily after attaining a certain threshold loading level. Notched Izod impact studies revealed similar trends as well. Surface morphology of the tensile tested injection molded samples were found to be in agreement with the trends exhibited during the tensile tests. In order to account for the behavior demonstrated by the epoxy modified PLA samples, a crystallization-induced phase segregation theory was proposed which provides a satisfactory explanation for the improvements seen in the mechanical performance of the samples. However,

a suitable imaging technique such as TEM is still required to physically observe the phenomenon described by this model.

In terms of future work, the effect of incorporating even higher amounts of the plasticizers into neat PLA needs to be studied. Typical applications of plasticizers involve a loading level of up to 30% by weight which results in significant reduction of the  $T_g$  of the material and subsequently a more flexible material. This would involve the use of a liquid injection pump in order to feed the plasticizers during the reactive extrusion process since they are low viscosity fluids and above 10% by weight tend to leak out through the feeder. Thus, further process optimization needs to be performed in order to incorporate higher loading levels of the plasticizer.

## **4 REACTIVE BLENDING OF MULTIFUNCTIONAL EPOXY MODIFIERS FOR RHEOLOGICAL ENHANCEMENT OF POLYLACTIDE**

### **4.1 Introduction**

Plastic based packaging materials continue to be one of the largest consumers of commercially produced plastics, with more than a third of the amount of plastics produced going towards the development of packaging [191]. Packaging also happens to be the single biggest contributor towards plastic waste mostly due to the fact that most packaging solutions are intended for single-use [192]. Growing consumer awareness and enactment of legislature have been significant drivers in developing more sustainable packaging materials with a viable end-of life option [193-197].

PLA, being both biobased and biodegradable under suitable conditions, has long been explored as a sustainable alternative to existing packaging plastics such as LDPE [198-201]. Despite significant research efforts, a cost-effective solution towards PLA-based packaging materials is still lacking. Most packaging materials are produced using processing techniques such as film blowing, blow molding etc., where sufficient melt strength of the polymeric material becomes a critical requirement. Since PLA has an inherently poor melt strength owing to its linear aliphatic structure, its usage in such processing techniques is greatly hindered. A conventional approach towards improving melt strength of a polymer involves the use of suitable modifiers to induce branching of the polymeric chains resulting in a polymer that can withstand the shear forces encountered during the above processing techniques [202]. Specifically, epoxy-based modifiers have previously been used to similar effect in various thermoplastic polyester materials [129, 203]. A similar approach is adopted in the current study to improve the rheological performance of the PLA for its increased adoption as a material of choice for packaging applications. Two different

epoxy compounds will be used as the modifiers for the study. First, Joncryl-4368-C, a multifunctional epoxy-based modifier commercially available from BASF, and second, NC-547, a biobased multifunctional epoxy modifier available from the Cardolite Corporation, will be used for the study. The NC-547 is derived from cardanol which in turn is derived from cashew nut shell liquid (CNSL). Thus, the NC-547 is considered a more sustainable choice of modifier between the two. It is hypothesized that the carboxyl end group of the PLA would react with the epoxy groups of the modifiers leading to the formation of a branched structure. The chemical structures of the Joncryl and the NC-547 are as shown in Figure 4-1 and Figure 4-2 respectively.

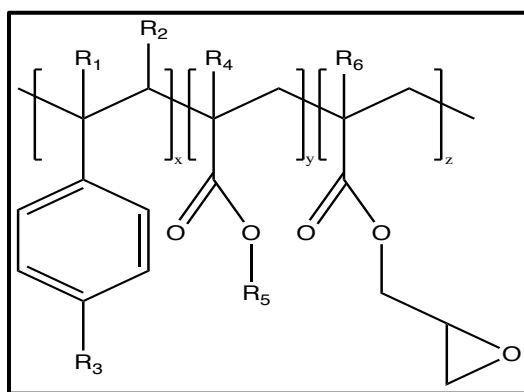


**Figure 4-1:** Chemical structure of the BASF Joncryl-4368-C

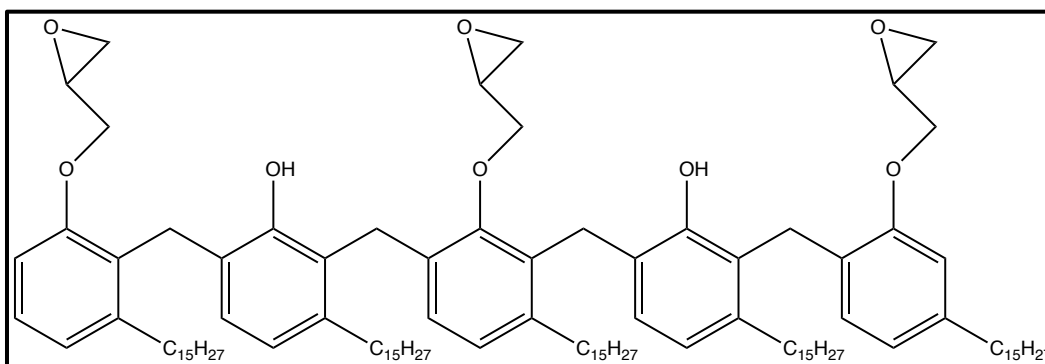


**Figure 4-2:** Chemical structure of the Cardolite NC-547

The reactivity of the epoxy groups with the end-groups of the PLA will be first confirmed through a model compound study. This will be followed by the preparation of the reactive blends of the

epoxy modifiers with PLA in a twin-screw extruder. FT-IR and  $^1\text{H}$  NMR analysis of the samples will be performed in order to prove the occurrence of reaction between the PLA and the epoxy modifiers. Molecular weight distributions and melt flow properties will be studied and recorded, followed by rheological characterization.

Similar studies involving the use of epoxy modifiers to induce branching in PLA have been reported [204-208]. However, none of these studies have looked into the effect of varying molar ratios of the reactants on the final properties of the PLA, which can be critical while commercially scaling up a formulation. Thus, a major objective for the current study was to observe the effects of using different molar ratios of the epoxy modifiers to PLA in the final rheological properties of the samples. Also, the effect of using a two-step reactive blending procedure as opposed to a single-step will be studied. No prior study has looked into using biobased epoxy modifiers derived from sustainable resources as an alternative to the fossil-fuel based modifiers typically used. Hence, this study will provide a unique insight into the use of biobased epoxy modifiers for PLA modification.

## **4.2 Experimental**

### **4.2.1 Materials**

A commercially available semi-crystalline grade of PLA, 3001D, was sourced from NatureWorks LLC (Minnesota, USA) for this study. The 3001D grade of PLA has a weight average molecular weight of  $\sim 150,000$  g/mol and a meso-lactide content of around  $\sim 2\%$ . A multifunctional epoxy compound, Joncryl ADR-4368-C was obtained from BASF (Michigan, USA). It has a molecular weight of 6800 g/mol and is available in the form of solid flakes. It has an epoxy equivalent weight (E.E.W) of 285 g/mol and contains an average of  $\sim 9$  epoxy groups per Joncryl molecule [209]. A biobased multifunctional epoxy compound, NC-547, was obtained from the Cardolite Corporation (Pennsylvania, USA). The NC-547 has a molecular weight of 1715 g/mol and exists in the form

of a highly viscous fluid, with viscosity at 25°C being 20,000-50,000 cPs. It has an E.E.W of 550-850 g/mol and contains ~3 epoxy groups per molecule. All other reagents were obtained through Sigma-Aldrich (Wisconsin, USA) or Fisher Scientific (New Hampshire, USA) and were used as received. The solvents used for NMR were procured from Cambridge Isotope Laboratories (Massachusetts, USA).

#### **4.2.2 Model Compound Study**

A model compound study was performed to evaluate the reactivity of the epoxy compounds with the end-groups of the PLA chain. For the study, stearic acid with two terminal carboxylic acid groups was used to evaluate reactivity of the -COOH termination of the PLA with the epoxy, whereas, polyethylene glycol (PEG-400) with two terminal hydroxyl groups was used to evaluate reactivity of the -OH termination of the PLA with the epoxy group. The stearic acid, PEG-400 and the epoxy compounds were thoroughly mixed in appropriate ratios using a mortar and pestle. A small sample (~10-15 mg) of the reaction mixture was then placed in a DSC hermetic pan and then sealed. The pan was then introduced into the DSC oven. The oven was equilibrated to 10°C before placing the pan inside. The sample was then heated to 250°C at 10°C/min and the heat flow vs. temperature data was recorded. A DSC Q20 (TA Instruments, USA) setup was used to carry out the experiments.

#### **4.2.3 Reactive Blending**

The reactive blends of the two multifunctional epoxy compounds with PLA were carried out using reactive extrusion. Identical processing conditions were used for both the epoxy modifiers to maintain uniformity during comparison of properties. The PLA pellets were dried overnight in a convection oven at 60°C prior to the extrusion process. This was done in order to remove residual moisture in the PLA which might accelerate its degradation under shear in the extruder. The epoxy

modifiers were premixed in the appropriate ratio with the PLA pellets before being fed into the hopper. A Century ZSK-30 co-rotating twin-screw extruder with a screw diameter of 30 mm and a L/D ratio of 42 was used for the reactive blending. The temperature profile used for this process was as follows: 140/150/160/170/180/185/185/185/180/175°C. The screw speed was set at 100 rpm, and the throughput of the runs for both of the epoxy compounds were set at ~100-110 gm/min. The extrudate in the form of a strand was quenched by passing through an ice-cooled water bath and subsequently pelletized. The pellets were then dried overnight in a convection oven at 60°C to remove excess moisture prior to characterization. Two different masterbatches of each of the Joncryl and the NC-547 were prepared. The Joncryl masterbatches had a loading level of 5 and 10% by weight, whereas the NC-547 masterbatches contained 1.5 and 3.5% of the epoxy modifier by weight.

#### **4.2.4 Characterization**

Two different sample purification methods were tested to remove the unreacted epoxy modifiers from the extrudate. First, a Soxhlet extractor was used with toluene as the solvent. Approximately 2.5 gm of the extrudate was placed inside a cellulosic thimble, which was then introduced into the extractor setup. The toluene was heated to its boiling point and an attached condenser was used to condense the toluene vapors back into the extractor. The extraction was carried out over a period of 24 hours. In this manner, the extrudate sample passed through several solvent washing cycles to remove traces of the unreacted epoxy compound. In the second technique, a certain amount of the extrudate was dissolved in DCM, which would dissolve the PLA, the unreacted epoxy, and the reacted PLA-epoxy blend. Once the sample was completely dissolved, an excess of methanol was added to the solution which would leave behind the unreacted epoxy in solution and would precipitate out the PLA and the PLA-epoxy reacted blend [210]. This purification process was

repeated for at least three times to remove all traces of the unreacted epoxy. The purified and solvent washed extrudate was then used for FT-IR and  $^1\text{H}$  NMR analysis.

FT-IR spectra of neat PLA and the purified extrudate in the form of a film were recorded using the ATR mode of a Shimadzu IRAffinity-1 spectrometer (Shimadzu Co., Japan) equipped with a single reflection MIRacle ATR attachment (PIKE Technologies, USA). The spectra were obtained in the absorption mode within the spectral range of  $4000\text{-}600\text{ cm}^{-1}$ . The film samples were prepared by the solvent-casting method, wherein the samples were dissolved in DCM and were cast on to petri dishes. The solvent was then allowed to evaporate at  $40^\circ\text{C}$  in a convection oven.

$^1\text{H}$  NMR analysis of the samples were performed by first dissolving the purified extrudate in a deuterated chloroform ( $\text{CDCl}_3$ ) solvent. The spectra were then recorded on a 500 MHz Varian Unity Plus NMR spectrometer (California, USA) at room temperature. Spectra of the purified extrudate were compared with that of neat PLA to observe for peak shifts post-reaction.

The thermal degradation properties were evaluated using a thermogravimetric analyzer, TGA Q50 (TA Instruments, USA), by heating the sample from room temperature to  $550^\circ\text{C}$  at a rate of  $10^\circ\text{C}/\text{min}$  under a nitrogen atmosphere. The thermal transitions of the samples were obtained by using a differential scanning calorimeter, DSC Q20 (TA Instruments, USA). The samples were first heated up to  $200^\circ\text{C}$  starting at room temperature at a rate of  $10^\circ\text{C}/\text{min}$  under a nitrogen atmosphere to erase any thermal history associated with processing. They were then heated back up to  $200^\circ\text{C}$  at  $10^\circ\text{C}/\text{min}$ . The heat flow vs. temperature data was then recorded and plotted.

Gel swell analysis was performed on the samples in order to observe if there was any formation of cross-linking. The analysis was performed in accordance with the ASTM D2765 standard test method for determination of gel content and swell ratio [61].  $\sim 2.5$  gm of each of the samples in the form of pellets were secured by pouches made using a fine wire mesh. Each of the pouches

was then placed inside a jar containing dichloromethane for 24 hours, after which they were removed and completely dried. The dry sample weights were measured before and after placing them in the solvent.

Molecular weight distributions of the modified PLA resins were obtained by using the gel permeation chromatography (GPC) technique. A Waters GPC (Massachusetts, USA) equipped with a Waters 1515 isocratic HPLC pump, a Waters 717+ autosampler, Waters Styragel columns, and a Waters 2414 refractive index detector were used for the study. Tetrahydrofuran (THF) was used as the mobile phase with a flowrate of 1mL/min. The detector and columns were maintained at 35°C throughout the runs. The samples were dissolved in tetrahydrofuran (THF) at a concentration of 2mg/mL at room temperature. The solution was then filtered using a PTFE syringe filter into vials which were then loaded on to the autosampler plate. A runtime of 50 minutes was used for each sample. Each sample was run in triplicate to establish repeatability of the data. Polystyrene calibration standards were used as references for the final molecular weight calculations.

#### **4.2.5 Rheological Characterization**

Melt flow index (MFI) of the modified PLA resins were measured using a TMI XNR-400 setup (TMI, New York, USA) in accordance with the ASTM D1238-13 standard test method for melt flow rate of thermoplastics by extrusion plastometer [211]. The samples were tested at 190°C with a load of 2.16 kg as per the standard. The material being extruded within a 30 or 60 second time interval was collected and weighed and then extrapolated to a time period of 10 minutes as per the equation below:

$$MFI \text{ (in g/10 min)} = \frac{m \times t_{ref}}{t} \quad (\text{Equation 1})$$

where, m = mass of sample collected in the cut-off time interval,  $t_{ref}$  = reference time of 10 min

(600 s) and,  $t$  = cut-off time interval in seconds (either 30 or 60 s depending on the sample).

Complex viscosity of the samples was measured using a TA Discovery-HR2 rheometer (TA Instruments, USA) with a parallel-plate geometry and a plate separation of 0.9 mm. Injection molded disks of appropriate dimensions were prepared for the experiments. A dynamic frequency sweep was performed in the range of 1 – 100 rad/s. The samples were tested at two different temperatures, 180 and 200°C, and the complex viscosity was recorded over the frequency range as a function of shear rate.

Extensional viscosity of the epoxy modified PLA samples was measured using an extensional viscosity fixture (EVF) on an ARES-G2 rheometer (TA Instruments, USA). Test specimens with dimensions of 18 X 10 X 1 mm were prepared using compression molding prior to the testing. The tests were conducted at a temperature of 180°C and using three different strain rates of 0.5, 1.0 and 5.0 rad/s. The following equation was used to calculate the extensional viscosity of the PLA at a steady strain rate:

$$\eta_E^+ = \frac{T}{2 \times R \times \varepsilon_H \times A_0 \times \left(\frac{\rho_s}{\rho_m}\right)^{2/3} \times \exp(-\varepsilon_H(t))} \quad (\text{Equation 2})$$

where,  $\eta_E^+$  is the value of the tensile stress growth,  $\varepsilon_H$  is the applied Hencky strain rate,  $T$  is the torque measured by the instrument,  $R$  is the radius of the drum of the EVF,  $A_0$  is the initial area of the sample in its solid state, and  $t$  is the time in seconds.  $\rho_s$  and  $\rho_m$ , corresponding to the density of the PLA in its solid state and melt state at 180°C respectively are assumed to be 1.25 g/cm<sup>3</sup> and 1.115 g/cm<sup>3</sup> based on values reported in previous literature [212, 213].

## 4.3 Results and Discussion

### 4.3.1 Model Compound Study

In order to establish the feasibility of reaction between the PLA and the multifunctional epoxy

modifiers, a set of model compound studies were performed. Similar model compound studies have been reported with PLA-based systems previously, however, these were carried out in significant excess of both the reacting groups and did not provide an accurate representation of the molar ratios of the reactants used during the actual synthesis process [62, 135]. It is critical that these studies be carried out in terms of actual molar ratios used during synthesis since the final properties of the epoxy modified materials have been reported to be strongly dependent on these ratios. Thus, each of the model compound studies was carried out at three different molar ratios of the reactants: 1:1, 1:2 and 2:1. The actual modification of the PLA with the epoxy compounds were later performed based on these values. For the model compound studies, stearic acid with two terminal carboxyl groups and poly(ethylene glycol) (PEG-400) with two terminal hydroxyl groups were used to simulate the carboxyl and hydroxyl end-groups of the PLA respectively. It is predicted based on prior literature that the epoxy would preferentially react with the carboxyl groups over hydroxyl groups within the temperature range studied [127-130]. The reaction should be indicated by an exothermic peak in the DSC scan which should increase in intensity with a higher content of carboxyl groups, owing to an increase in the extent of reaction due to greater availability of reaction sites. This is because even at a 1:2 molar ratio of the epoxy to the model compound, the number of epoxy groups still remain in excess. The results obtained from these studies are described as follows.

Figure 4-3 shows the data obtained from DSC scans of the reaction between Joncryl and stearic acid at 1:1, 1:2 and 2:1 molar ratio. The presence of an exothermic peak centered at  $\sim 165^{\circ}\text{C}$  is observed for the samples at all the three ratios. Further, it is clearly observed that the intensity of this peak increases with the increase in content of the carboxyl group containing reactant. This provides sufficient evidence to support the claim that not only is the reaction between the carboxyl

and epoxy groups of the Joncryl feasible, but also that the extent of reaction would increase with a higher molar ratio of the carboxyl groups.

Given a PLA chain and a multifunctional epoxy modifier, if both the carboxyl and hydroxyl end-groups of the chain were each to react with an epoxy group, a cross-linked network would eventually develop due to extensive branching. This is highly undesirable for the production of blown films since the formation of these gels lead to defects and failure in the blown film [214]. Thus, it is essential to ensure that the hydroxyl group of the PLA does not react with an epoxy group within the range of processing temperatures. Figure 4-4 shows the model compound study between the PEG-400 and the Joncryl at the three different molar ratios. It can be clearly observed that there is an absence of any exothermic peak up to 200°C. Since the highest temperature attained during processing is 185°C, it can be safely assumed that there is no likelihood of reaction between the hydroxyl group of the PLA with the Joncryl. A minor elevation in the curves is observed ~220°C, however, this is mostly attributed to an irregular baseline and not an indication of a reaction.

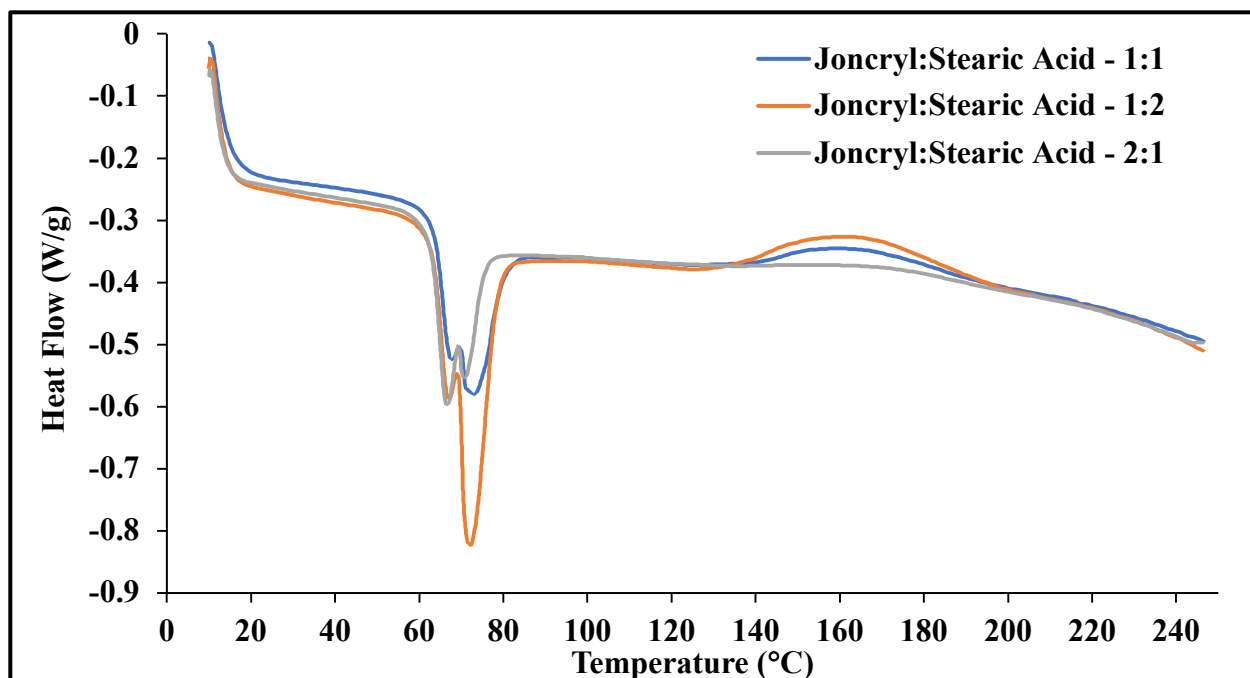


**Figure 4-3:** Model compound study showing the reaction between Joncryl and stearic acid using a DSC scan

Similar model compound studies were performed with the NC-547. Looking at the DSC curves generated for the reaction between the stearic acid with the NC-547 in Figure 4-5, an exothermic peak can be observed at  $\sim 190^{\circ}\text{C}$ , thus confirming the occurrence of a reaction between the carboxyl groups and the epoxy group of the NC-547. The effect of varying molar ratios however was not as apparent as the stearic acid-Joncryl mixture, mostly due to the fact that the NC-547 being a very highly viscous fluid, prevented the formation of a well-mixed system with the solid powder form of the stearic acid. Considering the small sample size used for DSC experiments, samples that are not completely well-mixed would not provide a good quantification of the enthalpy of reaction.

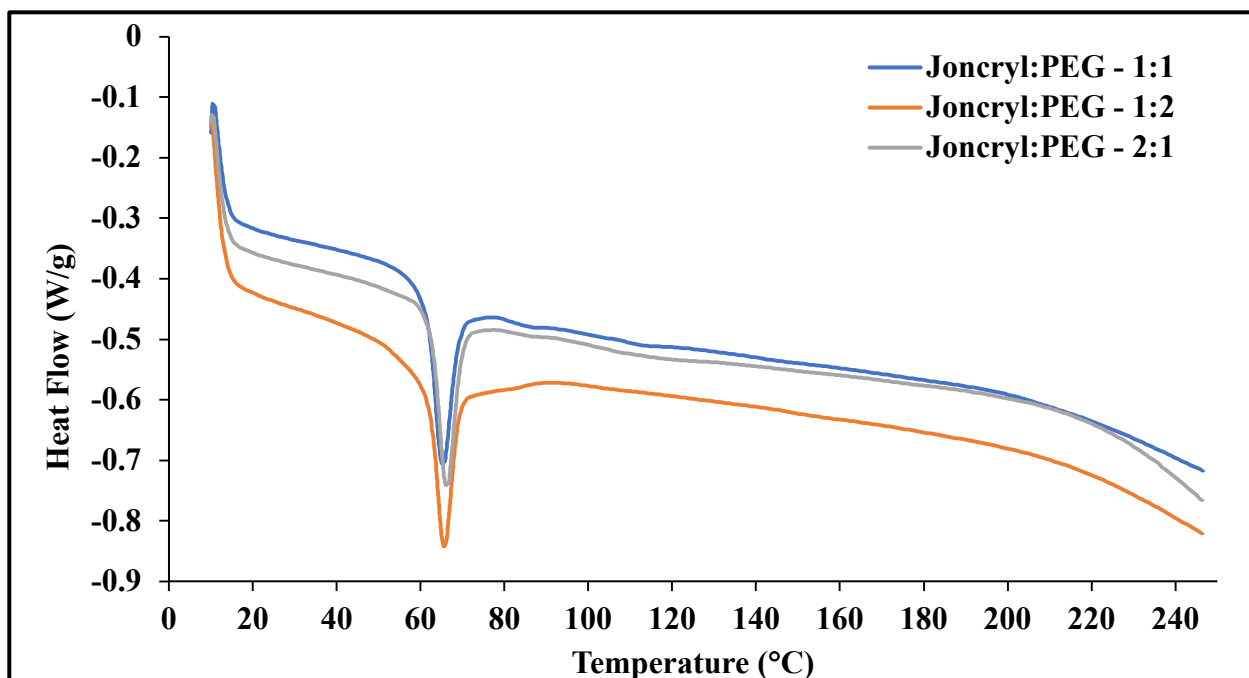


Figure 4-4: Model compound study showing the reaction between Joncryl and PEG using a DSC scan

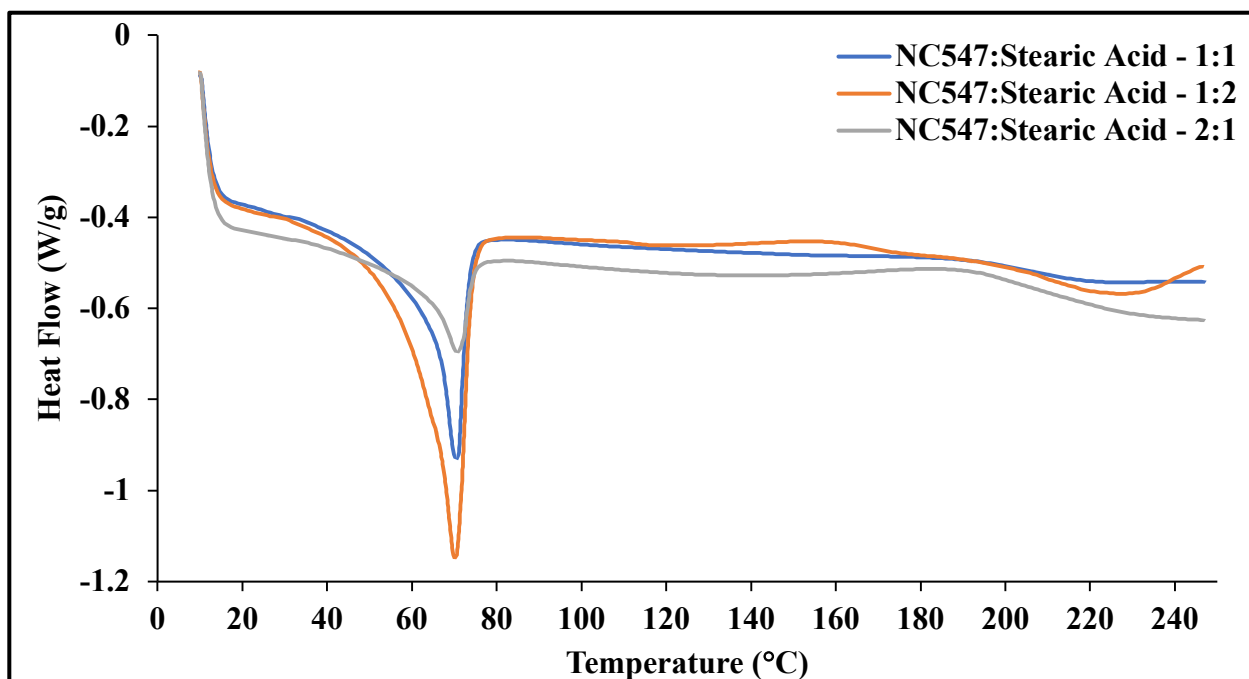
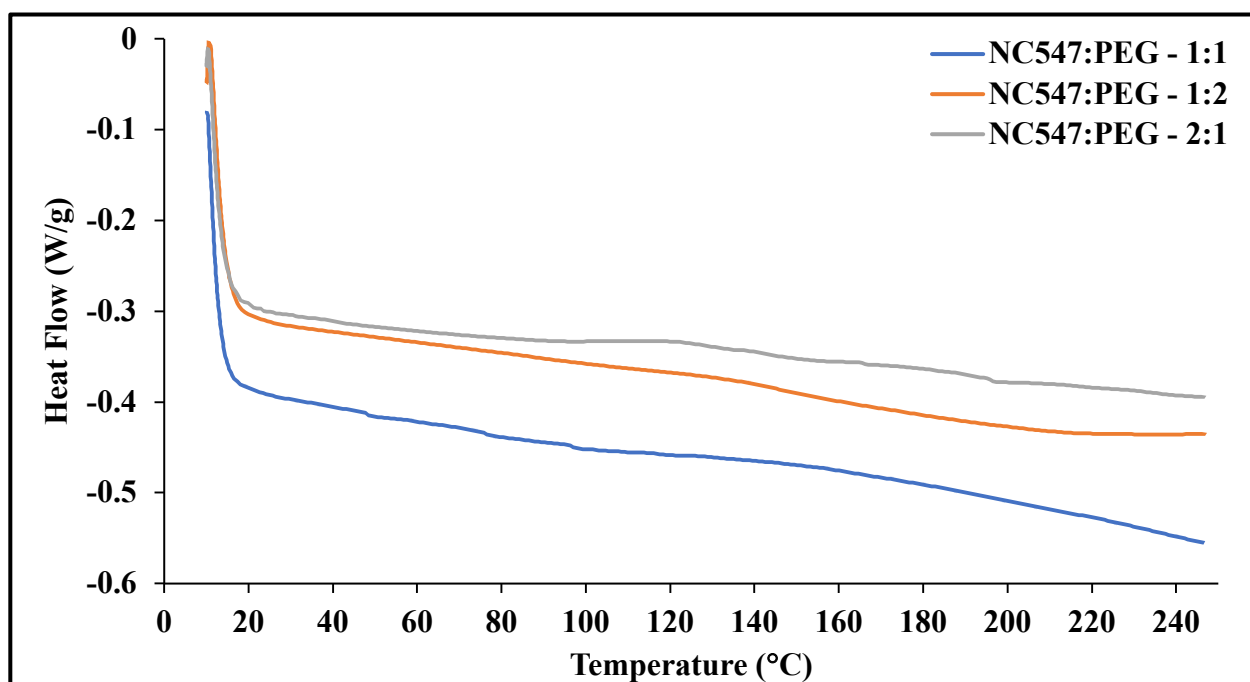


Figure 4-5: Model compound study showing the reaction between NC-547 and stearic acid using a DSC scan

For the study of the NC-547 with the PEG-400 as shown in Figure 4-6, no discernible exothermic peak was observed for the entire range of the testing till up to 250°C, at all molar ratios used. Thus, it could be safely assumed that there would be no reaction between the hydroxyl group of the PLA with the epoxy groups of NC-547.



**Figure 4-6:** Model compound study showing the reaction between NC-547 and PEG using a DSC scan

#### 4.3.2 Reactive Blending

Having successfully established the preferential reactivity of the epoxy groups with the carboxyl group, the reactive blends of the epoxy modifiers with PLA were prepared using reactive extrusion. It has been previously claimed that using a molar excess of the Joncryl results in a linear chain extension behavior whereas using an excess of PLA results in a long-chain branching effect as shown in Figure 4-7 [135]. This is due to the fact that with an excess of Joncryl molecules, there is a greater probability of each PLA chain reacting with a new Joncryl molecule, than with a molecule where an epoxy group has already reacted. However, with an excess of PLA, multiple

PLA chains would react with multiple epoxy groups on a single Joncryl molecule, leading to a branching effect. This hypothesis needed further validation, and the subsequent experimental plan involved reacting the PLA with the epoxy modifiers at fixed molar ratios.

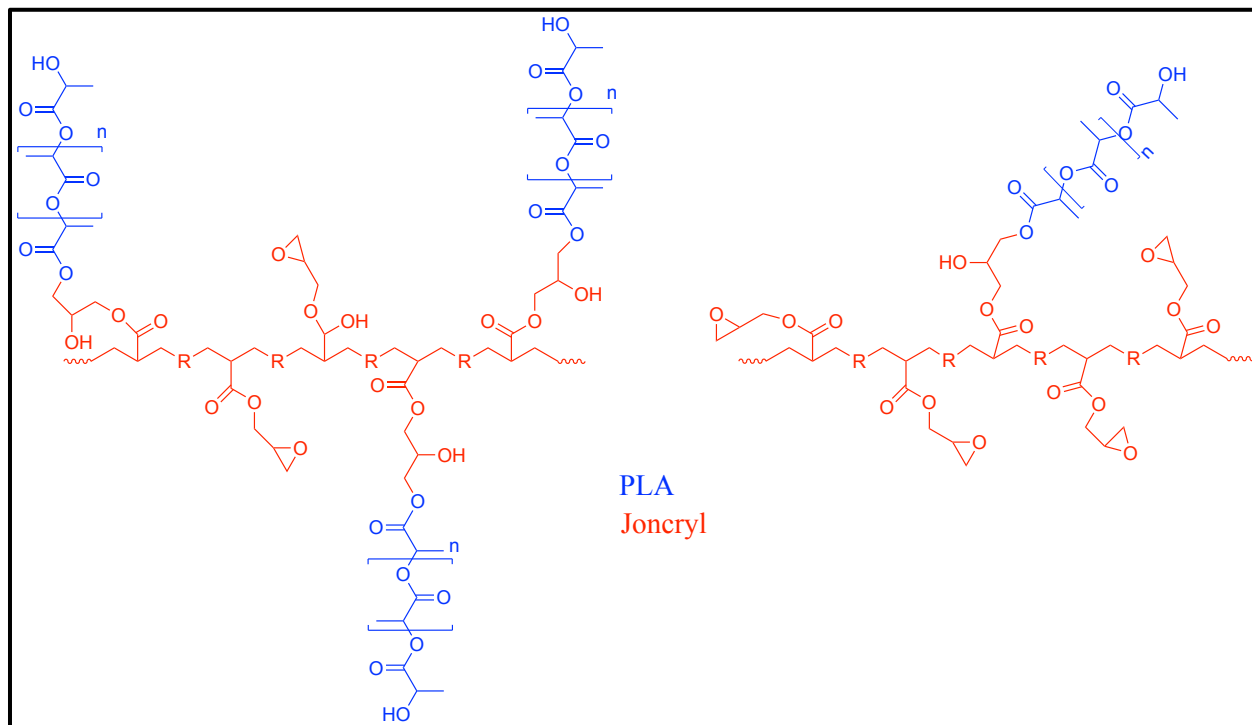
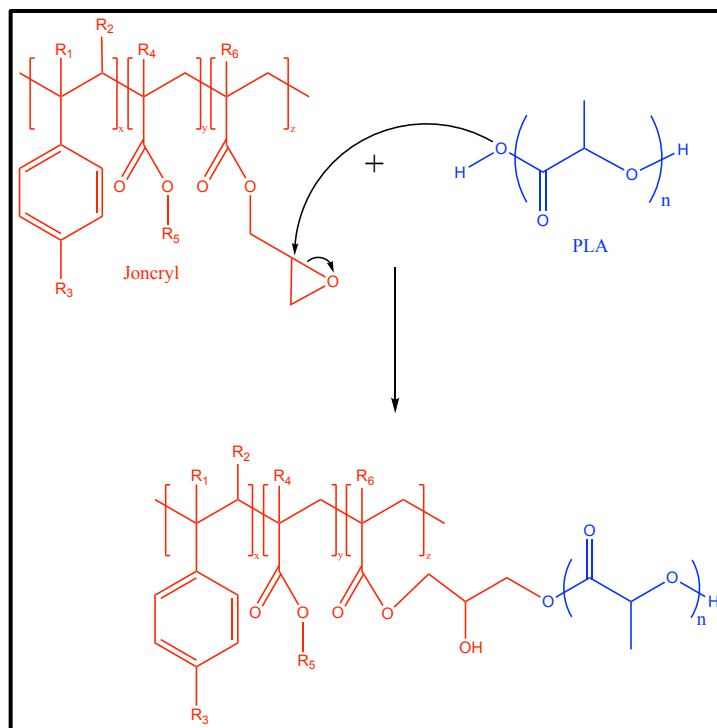


**Figure 4-7:** Predicted structures formed due to the reaction between the PLA and Joncryl at less than 1 molar ratio of Joncryl to PLA (left), and at a greater than 1 molar ratio for Joncryl to PLA (right)

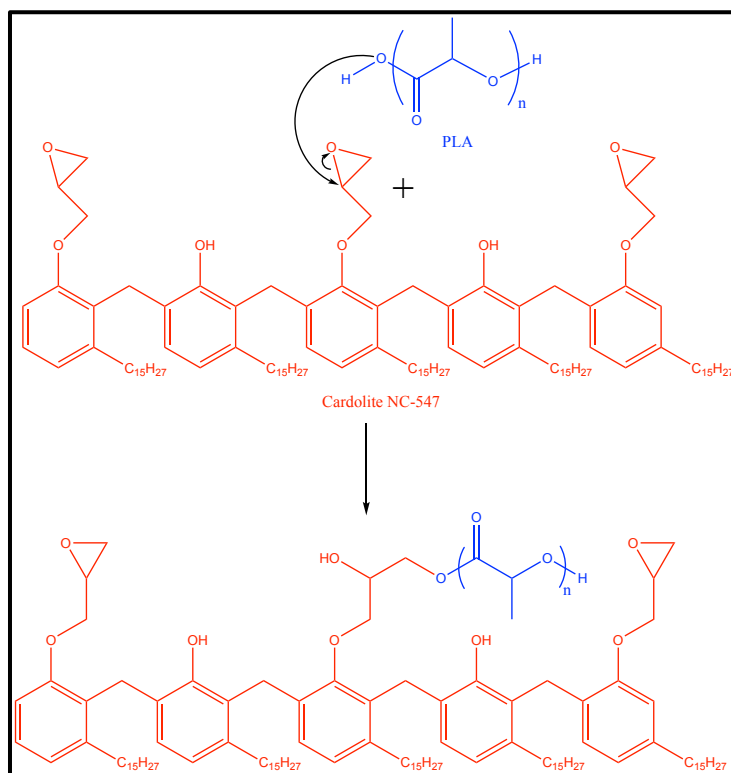
Two blends each of the Joncryl and the NC-547 were prepared, with one at  $<1$  and the other at  $>1$  molar ratio of the epoxy modifiers to PLA. This was done to study the effect of using different molar ratios on the final properties of the material. For the PLA-Joncryl blends, 5% and 10% by weight of the Joncryl was used, which represented a  $<1$  and  $>1$  molar ratio respectively of the epoxy to PLA. Similarly, for the PLA-NC-547 blends, 1.5% and 3.5% by weight of the NC-547 was used, which represented a  $<1$  and  $>1$  molar ratio respectively.

Further, it has been shown that using a two-step process for the reactive blending of the epoxy modifiers with PLA, first involving the synthesis of a high loading level masterbatch, followed by





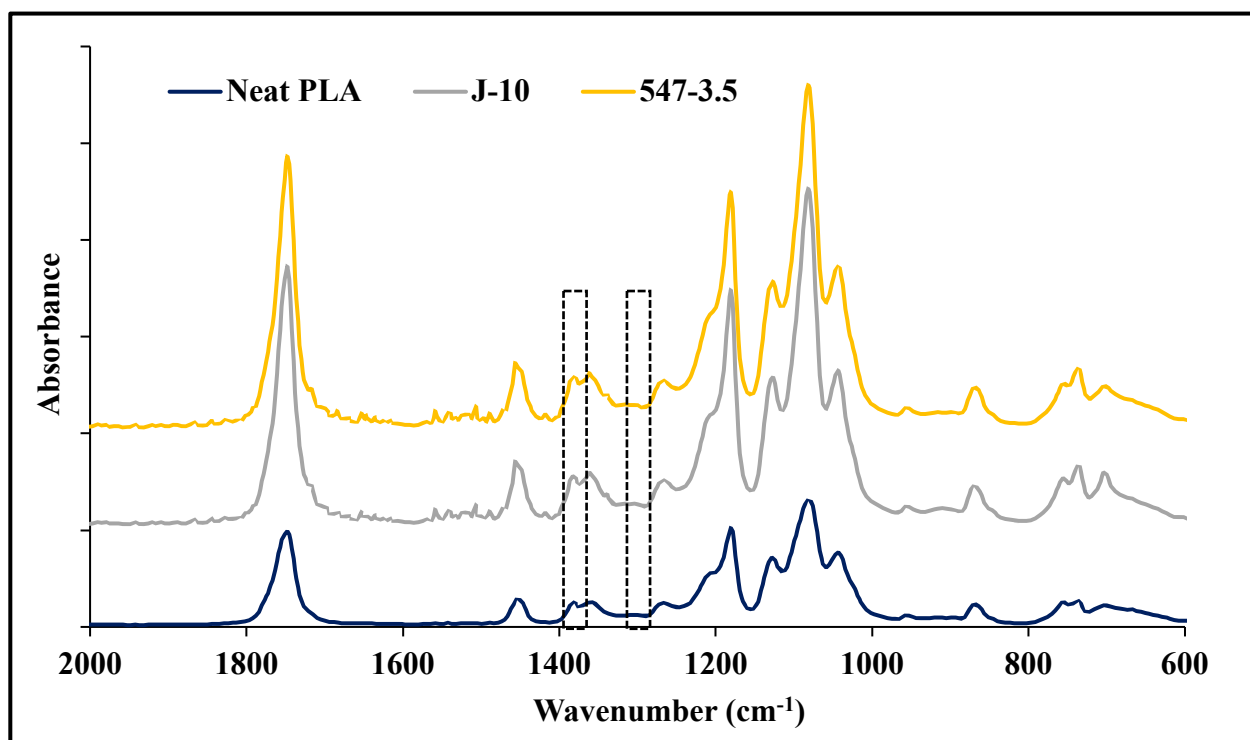
**Figure 4-9:** Schematic of reaction between PLA and Joncryl



**Figure 4-10:** Schematic of reaction between PLA and NC-547

### 4.3.3 Characterization

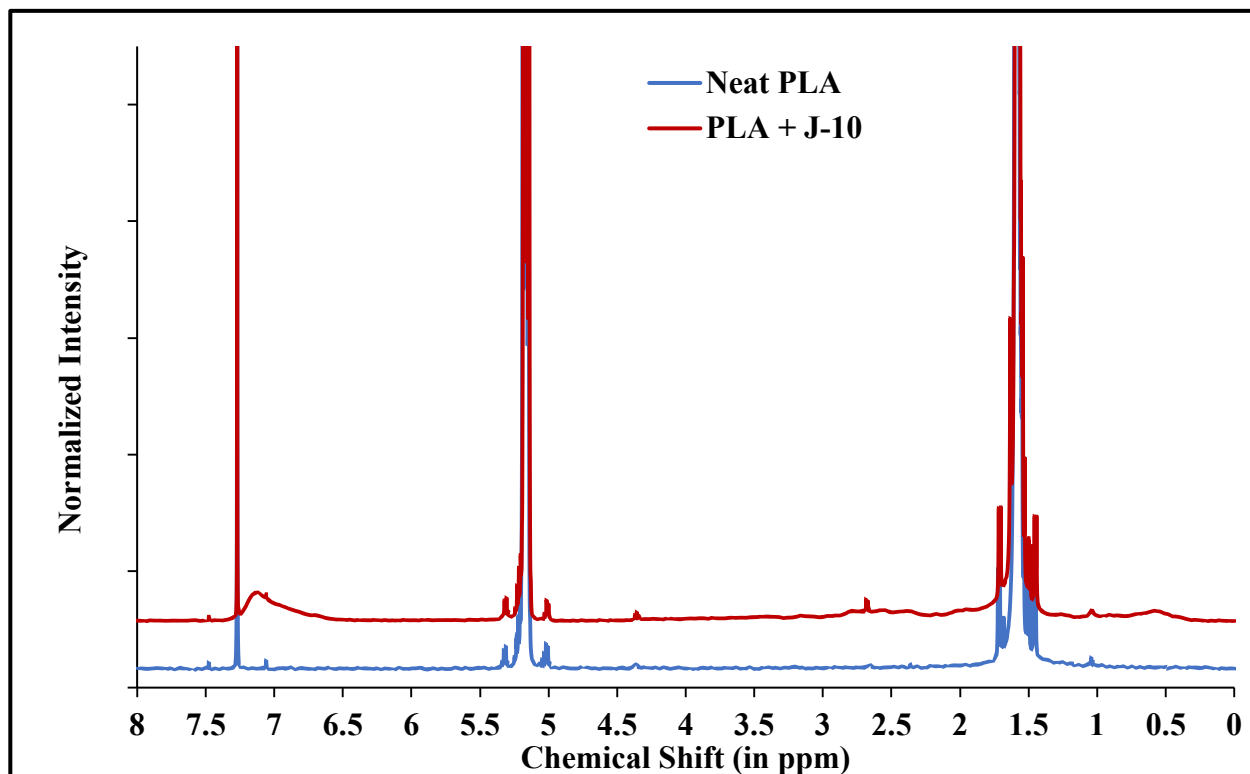
Following the extrusion process, the extrudates underwent a sample purification step where traces of the unreacted epoxy modifiers were removed using techniques described earlier in the chapter.



**Figure 4-11:** Comparative FT-IR Spectra of neat PLA and the blends with Joncryl and NC-547. FT-IR spectra of the purified samples were then recorded and then compared against the spectrum for neat PLA as shown in Figure 4-11 to observe for any changes brought about by the reaction. No major differences were noted between the spectra. Also, since post-purification, most of the epoxy ought to have been removed from the reacted blends, there were no peaks from the epoxy groups. Looking at the spectra for the blends, only two minor peaks at  $1335\text{ cm}^{-1}$  and  $1415\text{ cm}^{-1}$  were marked as key differences when compared with the spectrum for neat PLA. Both of these peaks have been previously attributed to the C-H bending of the methylene group in epoxides and

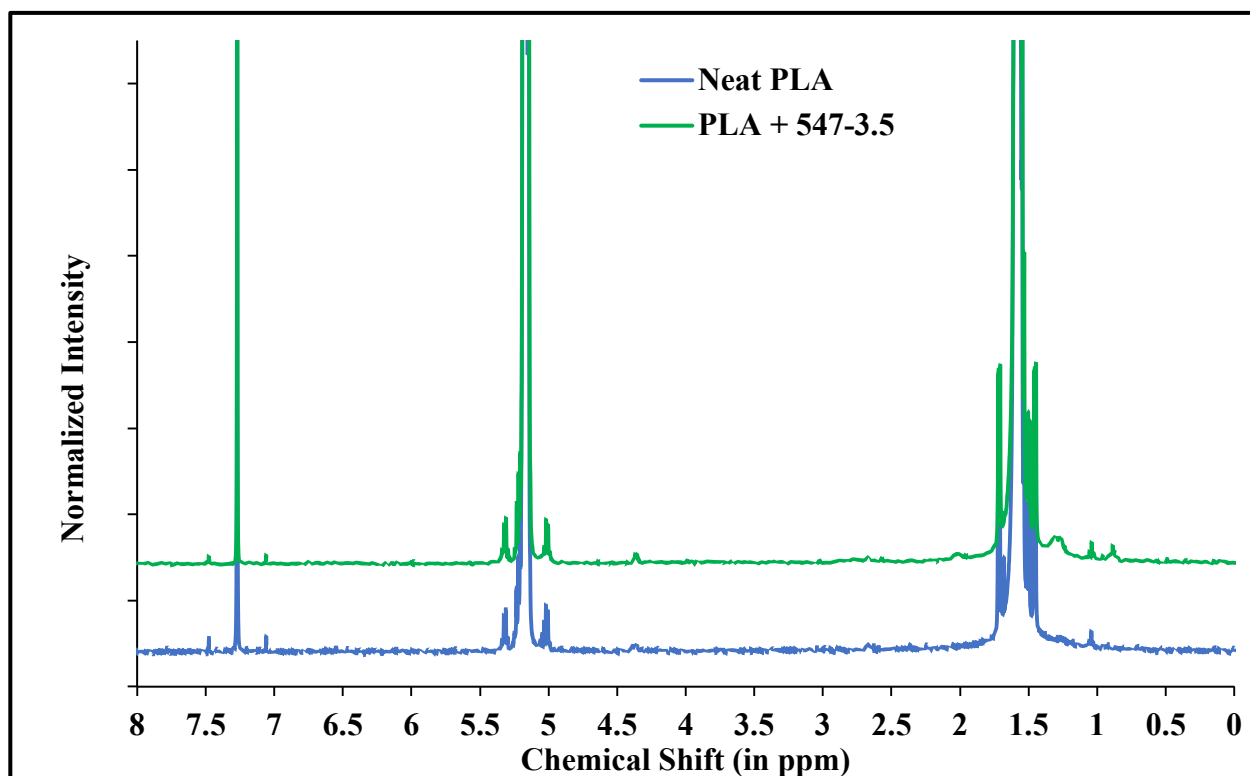
ethers [141, 142]. However, the intensities of these peaks are quite minimal and thus cannot be considered as conclusive evidence of the reaction between the PLA and the epoxy compounds.

Figure 4-12 and Figure 4-13 show the  $^1\text{H}$  NMR spectra of the purified blends of PLA with the Joncryl and the NC-547 respectively. Each of the spectrums has been overlaid with that of the spectrum for neat PLA to provide clarity for comparison. In both the spectra, the characteristic peaks of PLA at 1.6 ppm and 5.2 ppm corresponding to the methyl and the methine protons on the PLA backbone are distinctly visible. For the purified Joncryl blend, there is a noticeable change with respect to the spectrum for neat PLA. A broad peak centered at around 7.1 ppm can be clearly observed. This has been previously attributed to the protons in the aromatic rings of the Joncryl [134]. The presence of a characteristic aromatic peak from the Joncryl in a sample of the purified reactive blend provides conclusive evidence that there is reaction between the PLA and the Joncryl.



**Figure 4-12:** Comparative  $^1\text{H}$  NMR spectra of neat PLA and the reactive blend with Joncryl at 10 % by weight

Looking at the  $^1\text{H}$  NMR spectrum for the purified NC-547 sample, 2 distinct peaks can be observed that are absent in the spectrum for the neat PLA. These two peaks centered at 1.25 and 0.88 ppm correspond to the methylene protons on the aliphatic chain linked to the benzene ring, and the methyl group at the end of the aliphatic chain [144, 145]. The presence of these two peaks from the NC-547 in a sample of the purified reactive blend provides sufficient evidence to conclude that there is reaction between the PLA and the NC-547.



**Figure 4-13:** Comparative  $^1\text{H}$  NMR Spectra of neat PLA and the reactive blend with NC-547 at 3.5 % by weight

Thermal degradation behavior of the epoxy modifiers by themselves, and those of the modified samples were studied and compared with that of neat PLA and are shown in Figure 4-14 and Figure 4-15. An interesting trend was observed in the case of both the Joncryl and the NC-547. It was seen that for the samples with lower concentration of the modifier, i.e., at 5% for the Joncryl and 1.5% for the NC-547, the peak temperature for thermal degradation was found to remain

unaffected by the addition of the modifier. However, at a higher content of 10% for the Joncryl and 3.5% for the NC-547, the peak degradation temperature was found to reduce by ~40 and 30°C respectively. This was an unexpected observation since the peak degradation for both the epoxy modifiers by themselves were higher than the neat PLA itself. There was no particularly satisfactory explanation for this trend. It is predicted to be mostly due to the presence of elevated levels of oligomers and unreacted epoxy molecules in the system.

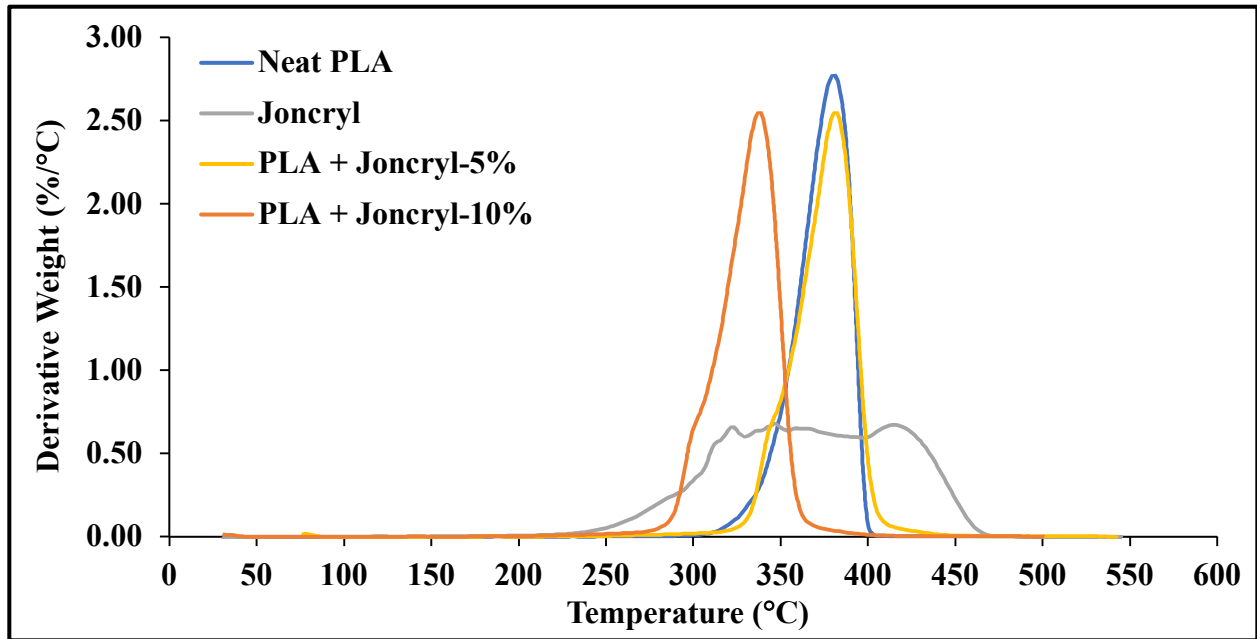


**Figure 4-14:** DTG curves comparing neat PLA and Joncryl with their blends

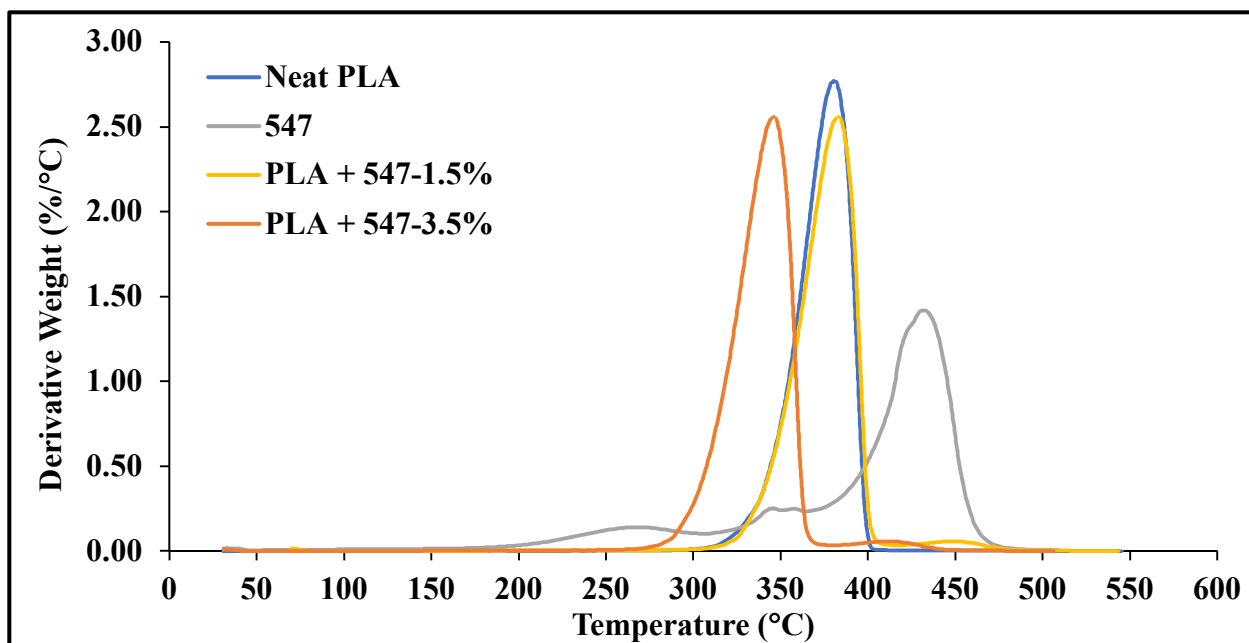


**Figure 4-15:** DTG curves comparing neat PLA and NC-547 with their blends

The thermal transitions of the epoxy modified PLA compounds were studied using the heat flow vs. temperature data from the second heating cycle of the DSC scans and are as shown in Figure 4-16. The reaction with the epoxy compounds did not bring about any noticeable change in the  $T_g$  and  $T_m$  of the PLA. However, the most apparent difference was the shifting of the cold crystallization peak of the PLA to higher values with the addition of the epoxy modifier. This was found to be in complete contradiction with existing literature, where branching and chain extension of PLA has been found to have a faster onset of the cold crystallization peak [65, 215-218]. However, there exists a simple rationale for the behavior shown in our system. The delay in the onset of cold crystallization in the Joncryl and NC-547 modified PLA could be attributed to the presence of a significant amount of bulky aromatic groups in the compound which hinders chain mobility of the PLA thereby delaying the crystallization process.

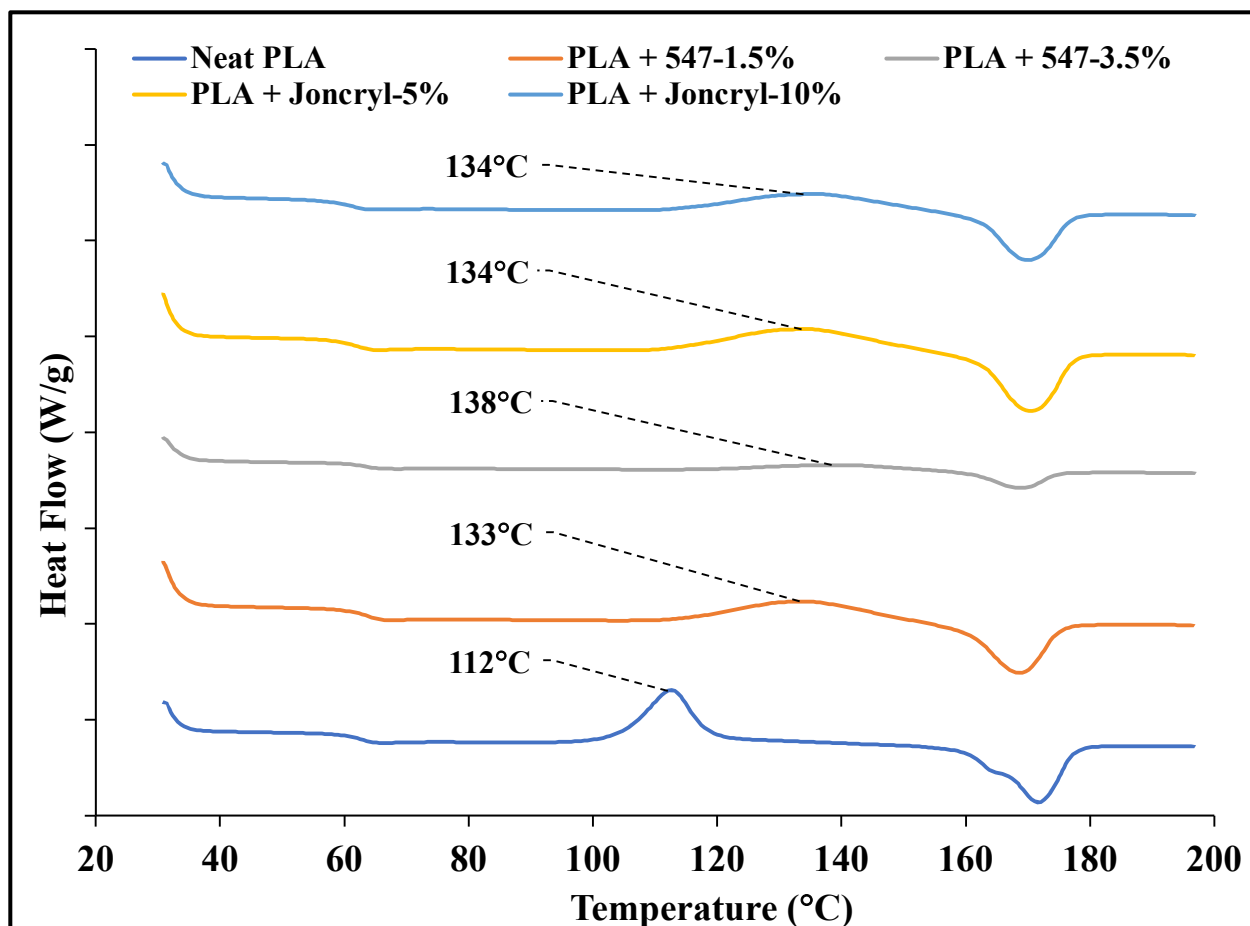


**Figure 4-16:** DSC curves of neat PLA and the blends with Joncryl and NC-547

Gel swell measurements were performed as a precautionary measure to ensure that there was no formation of crosslinking in the samples leading to the formation of gels. The tests following the procedure described earlier, clearly showed that all of the epoxy modified samples were completely soluble in the solvent, thus proving that there were no crosslinking in the samples.

The molecular weight distributions of the samples as shown in Table 4-1 provided a preliminary insight into the effects of using the multifunctional epoxy modifiers as chain extenders or branching agents for the PLA. Comparing the neat PLA with PLA extruded under similar processing conditions used for the synthesis of the epoxy modified samples, it can be seen that there is a loss of molecular weight in the PLA due to chain scission in the presence of elevated

temperature and shear within the extruder. Looking at the Joncryl modified PLA, it can be seen that the sample with 5% by weight had a higher molecular weight (by almost ~30,000 g/mol) as compared to the 10% sample. This provides initial confirmation of the fact that using a molar ratio of <1 of the epoxy to PLA results in a more branched structure. However, upon dilution of the 5 and 10% of the Joncryl samples to 0.5 and 1.0% each, there was only a marginal increase observed in the molecular weight for the 5% vs. the 10%. Thus, despite the initial difference in the branching mechanism, there did not seem to be much effect of using the different molar ratios after the final concentration of the samples had been achieved. However, at all loading levels of the Joncryl, the molecular weights were found to be higher than that of the extruded PLA, thus indicating that the loss of molecular weight during processing had been successfully recovered. The 5 and 10% samples and their respective dilutions to 1% were found to have a higher molecular weight distribution than the neat PLA, thus suggesting successful chain extension.

For the NC-547 samples however, there was no observed increase in the molecular weights when compared to even the extruded PLA. This was attributed to the fact that the NC-547 had a significantly lower number of epoxy groups per molecule as compared to the Joncryl (3 vs. ~9). Also, considering the fact that since the NC-547 was used at lower loading levels in order to be consistent with the molar ratios used, and partly due to processing issues, it would explain why there was no major change observed with the molecular weights of the NC-547 modified samples. Even the diluted samples of the NC-547 which would ideally have a greater extent of reaction with the PLA showed no improvement.

**Table 4-1:** Molecular weight distributions of neat and extruded PLA, and the blends of PLA with Joncryl and NC-547

| Sample            | $M_n$ (g/mol)  | $M_w$ (g/mol)  | PDI         |
|-------------------|----------------|----------------|-------------|
| Neat PLA          | 97956 ± 2519   | 151552 ± 3997  | 1.55 ± 0.01 |
| Extruded PLA      | 83835 ± 707    | 139457 ± 2406  | 1.66 ± 0.03 |
| PLA-J5            | 130188 ± 10297 | 229473 ± 27844 | 1.76 ± 0.07 |
| PLA-J5-0.5        | 92840 ± 5424   | 167684 ± 21278 | 1.81 ± 0.13 |
| PLA-J5-1.0        | 107361 ± 4076  | 220821 ± 2644  | 2.06 ± 0.05 |
| PLA-J10           | 114309 ± 8899  | 194498 ± 21903 | 1.7 ± 0.07  |
| PLA-J10-0.5       | 88575 ± 2547   | 171744 ± 4933  | 1.94 ± 0.04 |
| PLA-J10-1.0       | 105595 ± 4463  | 217044 ± 11538 | 2.06 ± 0.02 |
| PLA-NC547-1.5     | 81603 ± 1198   | 132970 ± 1290  | 1.63 ± 0.03 |
| PLA-NC547-1.5-0.5 | 81346 ± 1078   | 131827 ± 754   | 1.62 ± 0.02 |
| PLA-NC547-3.5     | 82935 ± 2415   | 133259 ± 3205  | 1.61 ± 0.07 |
| PLA-NC547-3.5-1.0 | 76369 ± 1813   | 131835 ± 860   | 1.73 ± 0.04 |

#### 4.3.4 Rheological Characterization

The melt flow index (MFI) or melt flow rate (MFR) of a sample provides a rudimentary understanding of its rheological behavior by measuring its ability to flow in the melt condition when subject to an applied load. An increase in molecular weight or viscosity of a polymeric sample due to linear chain extension or branching typically results in a decrease in MFR of the sample due to an increased resistance to flow [219-223]. Figure 4-17 presents the MFR values obtained for all of the Joncryl and NC-547 samples. It is observed that extruded PLA has a greater value compared to the neat PLA, ~29 g/10 min as opposed to ~27 g/10 min, due to a lower molecular weight. Further, the Joncryl sample at 5% had a lower value (~1.5 g/10 min) than the sample at 10% (~2.7 g/10 min). This again suggests that using the molar ratio at <1 resulted in a more branched structure. The Joncryl samples diluted to 1% using either the 5 or 10% formulations showed negligible difference. However, with the dilutions to 0.5%, the sample made using the 5% masterbatch had a slightly lower value (~4.2 g/10 min) as opposed to the one made with the 10%

masterbatch (~5.9 g/10 min). This showed that using the molar ratio of the epoxy to PLA at <1 might be marginally more beneficial at higher dilutions (0.5%) but did not make a major difference at lower dilutions (1%). For the NC-547 samples at 1.5 and 3.5%, the MFR values were actually found to be lower than that of extruded PLA and almost equal to that of neat PLA, thus suggesting that they could potentially be used as a processing aid to improve melt viscosity during processing. With the diluted samples of the NC-547 at 0.5 and 1.0%, the MFR values were observed to drop even further resulting in values considerably lower than that of neat PLA (18-19 g/10 min vs. 27 g/10 min). These observations provided conclusive proof that there was indeed an occurrence of chain extension of the PLA, however nominal, due to reaction with the epoxy groups of the NC-547. Overall, the MFR data for the Joncryl samples was found to be in perfect agreement with the molecular weight distribution results obtained earlier, however, the NC-547 results seemed to vary in trend. This could be attributed to a more accurate representation of the behavior of the samples using the MFR since the properties are measured using a greater sample size. Also, GPC measurements have not been established to be the most accurate when it comes to distinguishing linear and branched PLA samples [218]. A common observation for both the Joncryl and the NC-547 samples was that a lower MFR was recorded for the samples produced using the two-step processing method thus confirming the fact that residual epoxy groups from the first processing cycle react with more PLA chains during the second processing cycle.

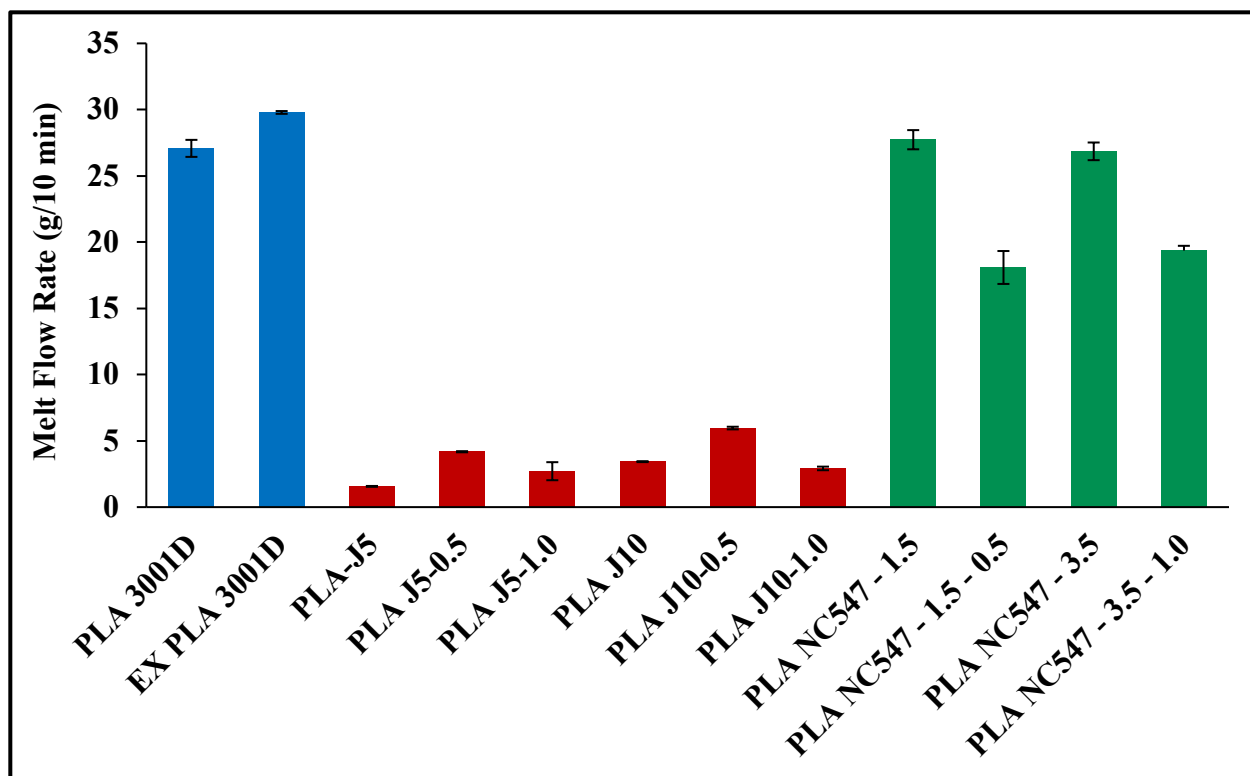


**Figure 4-17:** Melt flow rates of the samples, tested at 190°C with a load of 2.16 kg

Having successfully proven that the reaction between the epoxy modifiers and PLA was leading to a chain extension effect, the complex viscosity of the epoxy modified samples was studied as a function of shear rate in order to establish a better understanding of the type of chain extension being developed. Long chain branching in thermoplastics, specifically PLA, has been shown to produce a non-Newtonian effect by demonstrating significant shear thinning behavior, whereas regular linear chain extension produces a more Newtonian flow where the viscosity is mostly independent of shear rate [130, 224-227]. Long chain branching is essential to processing techniques such as blown films since it allows for greater blow-up ratios enabling the production of films with lower thickness. Hence, it becomes necessary to establish the type of chain extension developed during the reactive extrusion process. The complex viscosity as a function of varying

shear rate between 1 to 100 rad/s was studied for each of the samples. The curves for the Joncryl and the NC-547 are presented on separate plots for better visual clarity.

Figure 4-18 and Figure 4-19 present the results of the complex viscosity of the Joncryl samples as a function of shear rate at 180 and 200°C respectively. It can be clearly observed that neat and extruded PLA demonstrate a Newtonian plateau which is typical of linear polymers. Also, as expected, the extruded PLA is found to have a lower viscosity as compared to the neat PLA. Upon the addition of Joncryl, an immediate transition to a more shear thinning behavior was clearly observed. The values of the viscosities as well as the shear thinning behavior was found to be more pronounced at 5% of Joncryl than at 10%, thus, clearly establishing the formation of a structure predicted earlier in Figure 4-7 with the use of the epoxy modifier at a molar ratio of  $<1$ . However, at the final dilution levels of 0.5 and 1.0%, there seemed to be no effect of using either of the masterbatches, with the curves for the 0.5% samples and 1.0% samples almost resulting in an overlap on one another. Thus, this implies that once all residual epoxy groups are reacted through the second processing step, there is no difference in the type of branching developed, regardless of the type of branching present in the previous processing step. Considering the fact that in industrial applications, a masterbatch is usually prepared first with only 0.5~1.0% of the modifier being required in the final formulation, the loading level of the initial masterbatch is not a critical factor in the final rheological properties of a given formulation. Typically, since masterbatches with higher loading levels are preferable at the commercial scale due to ease of processing and cost-effectiveness, a masterbatch at 10% of Joncryl can be prepared and used for subsequent dilution without fear of loss in rheological performance. The trends in the complex viscosities observed at 200°C for the Joncryl samples were found to be exactly similar to that observed at 180°C, however, with a shift to lower values due to the higher testing temperature. Both the diluted

samples at 0.5% and 1.0% were found to be slightly more dependent on the masterbatch from which they were derived, with the ones derived from the 10% masterbatch showing slightly more enhanced properties. However, this improvement was negligible. Overall, these results clearly establish the presence of a long chain branching structure in the Joncryl samples.

The complex viscosities of the NC-547 modified PLA samples at 180°C and 200°C are presented in Figure 4-20 and Figure 4-21. The curves for all the NC-547 modified samples were found to lie within the curves for extruded and neat PLA, thus indicating that there was a low degree of chain extension during processing leading to an improvement over extruded PLA. However, there was no improvement in properties when compared to the neat PLA. Also, the behavior shown was more in the form of a Newtonian plateau than any actual shear thinning, thus confirming that there was no long chain branching being developed. Within the samples, the NC547 masterbatch at 3.5% was found to have consistently higher values of viscosity as compared to the rest of the samples. This is most likely attributed to the fact that it is the formulation with maximum content of epoxy groups thus resulting in the greatest extent of reaction. Thus, the NC547 samples did not provide any evidence of long-chain branching, showing just a maximum likelihood of linear chain extension.

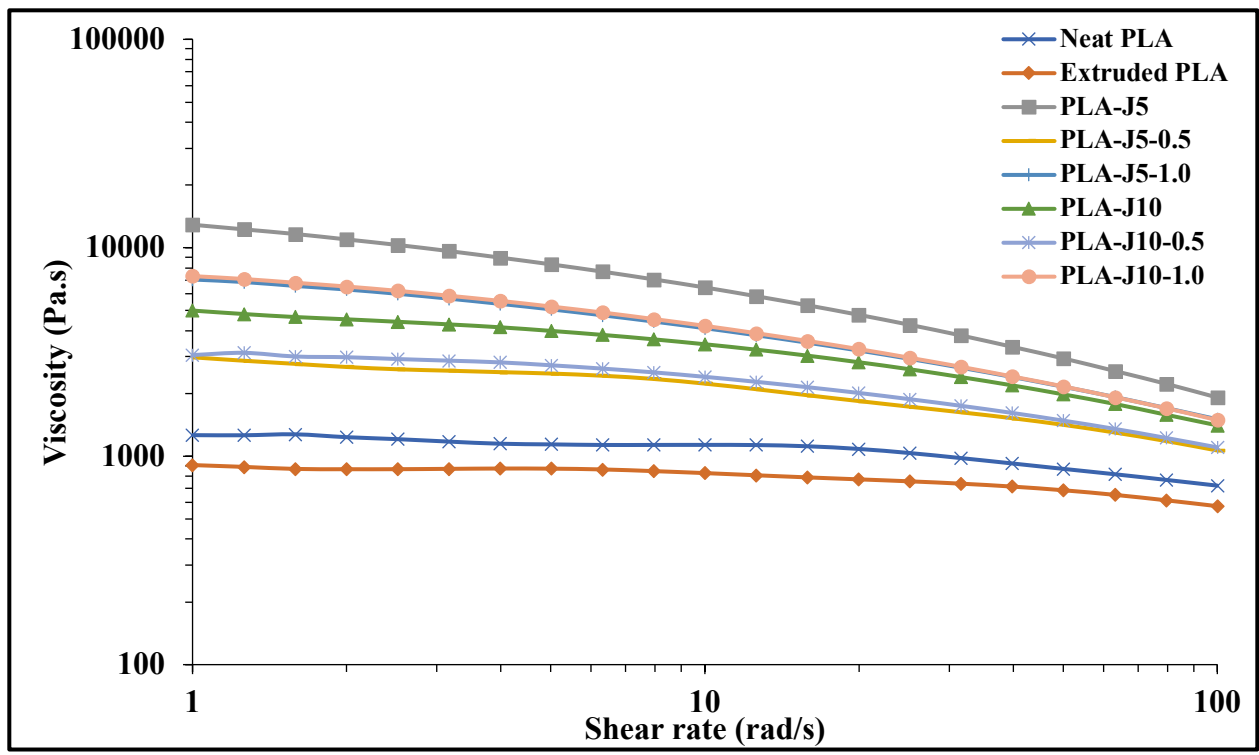


Figure 4-18: Comparison of complex viscosity at varying shear rates for Joncryn blends (180°C)

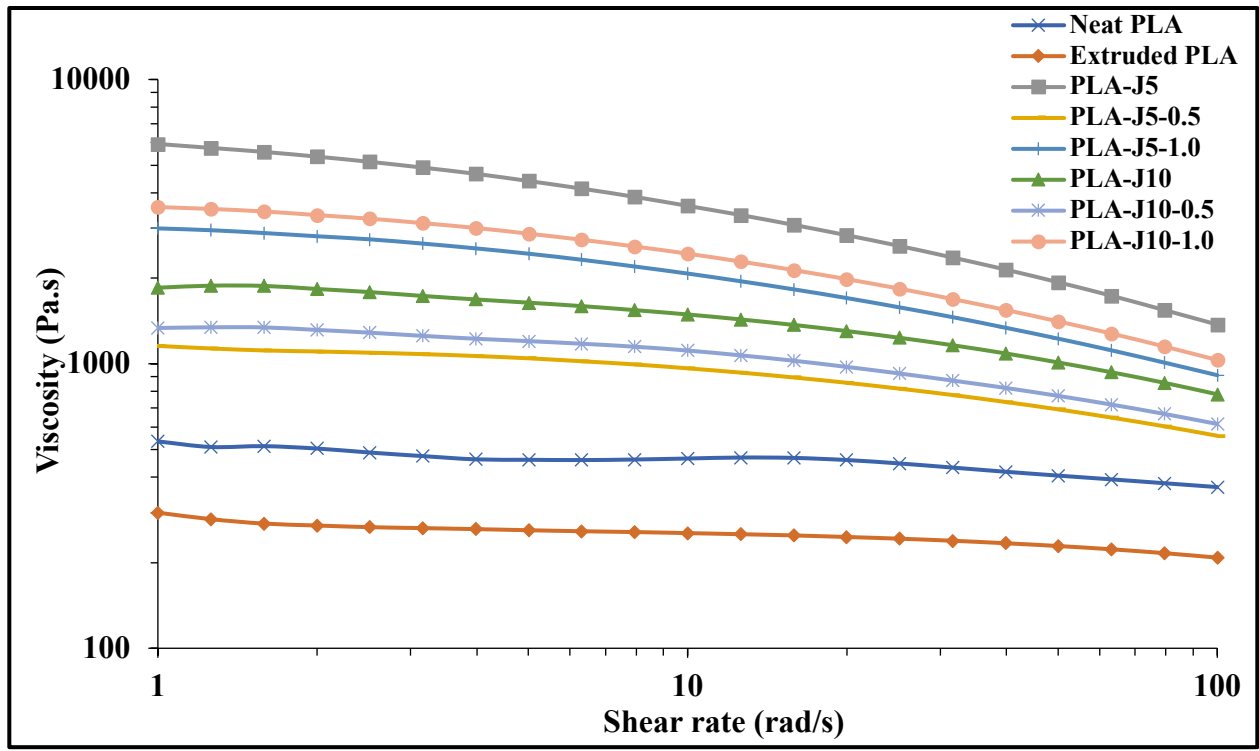


Figure 4-19: Comparison of complex viscosity at varying shear rates for Joncryn blends (200°C)

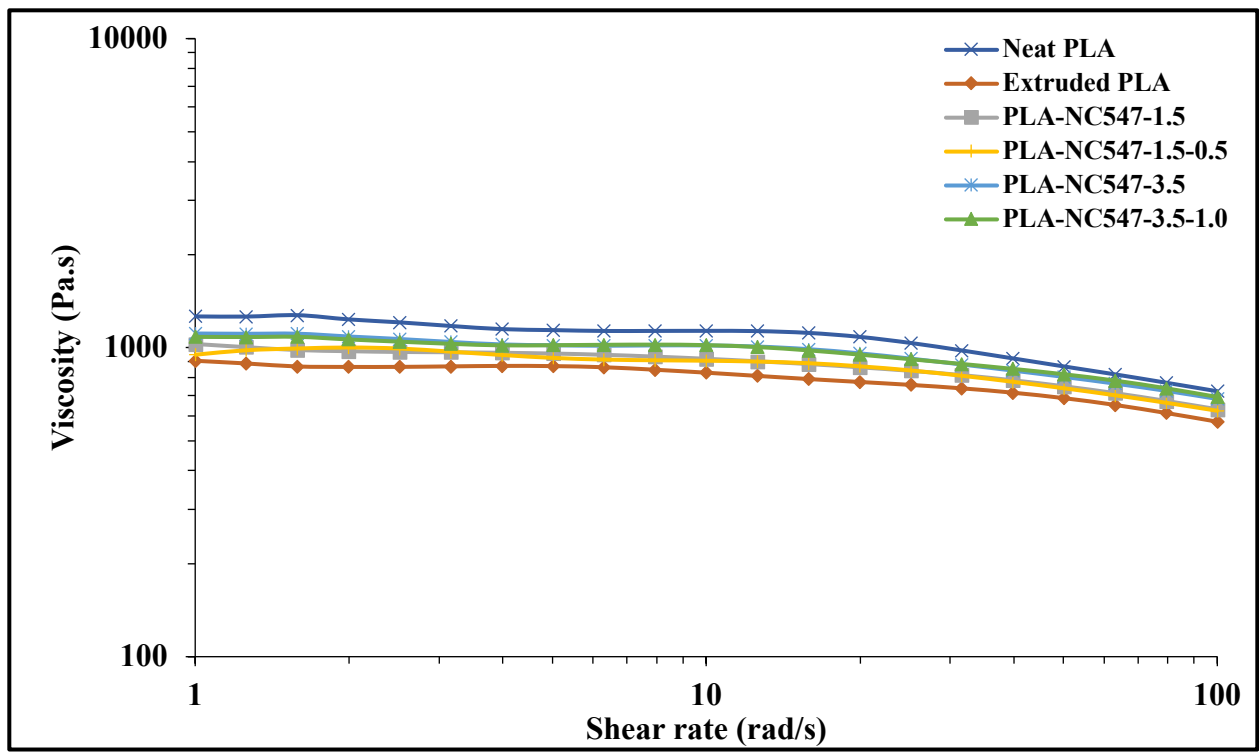


Figure 4-20: Comparison of complex viscosity at varying shear rates for NC547 blends (180°C)

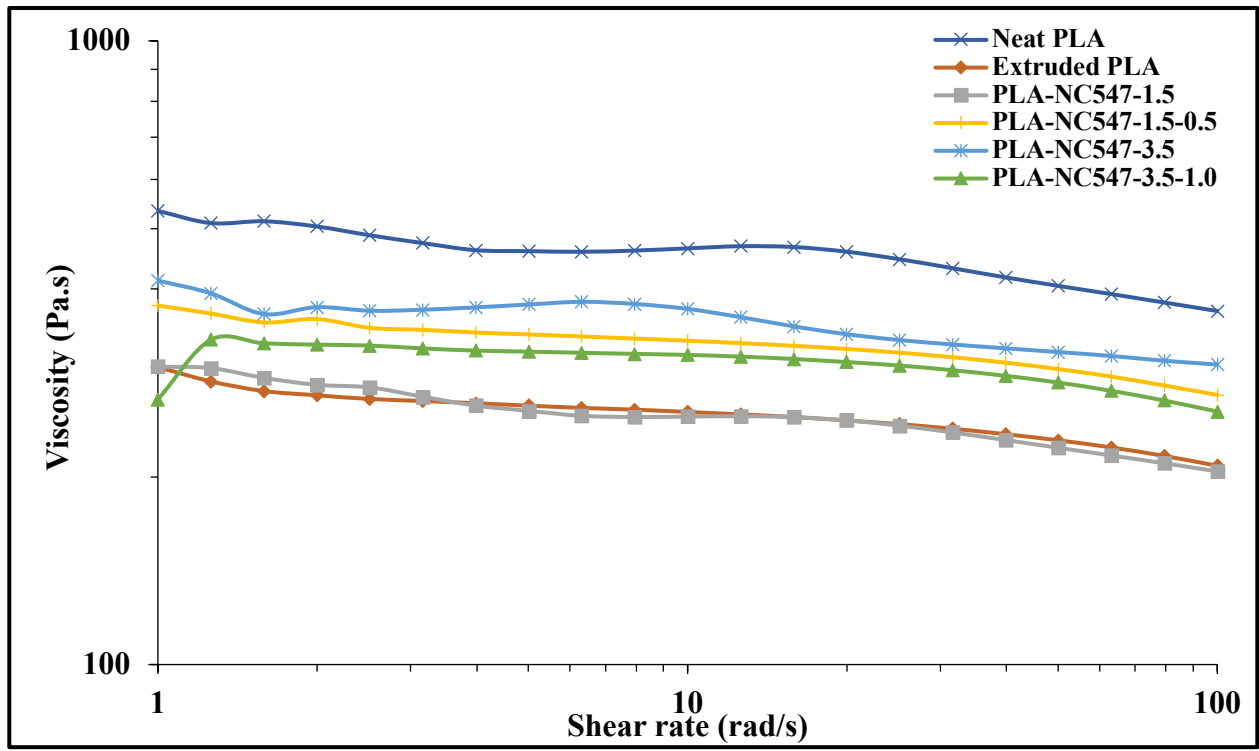


Figure 4-21: Comparison of complex viscosity at varying shear rates for NC547 blends (200°C)

Extensional viscosity ( $\eta_E^+$ ) of a polymer in its melt state is critical for its processability in techniques such as blown films, blow molding etc. Extensional viscosity is strongly dependent on the presence of branching and entanglements within the polymeric sample with long chain branching being primarily responsible for an increase in the properties [202, 228-230]. The  $\eta_E^+$  for all the epoxy modified samples were studied at 180°C at three different strain rates (0.5, 1.0 and 5.0 s<sup>-1</sup>). The data obtained from the studies are presented as follows. Figure 4-22, Figure 4-23, and Figure 4-24 show the uniaxial extensional viscosity behavior for the Joncryl samples under different conditions of strain rate.

For the Joncryl samples, a near identical behavior was observed at all three strain rates. For the Joncryl masterbatch samples, the sample at 5% was found to have a higher  $\eta_E^+$  and better strain hardening as compared to the 10% at all three strain rates. Similarly, for the diluted samples, the formulations at 1% had a higher value of  $\eta_E^+$  and displayed marginal strain hardening behavior as compared to the 0.5% formulations. Also, as observed earlier with the complex viscosity studies, the effect of using different molar ratios for the masterbatches had no discernible effect on the uniaxial extensional behavior of the final diluted formulations. The strain hardening behavior for all samples were seen to be more pronounced at higher strain rates of testing. Overall, the values for the Joncryl modified PLA samples were found to be considerably higher than that of neat and extruded PLA, showing the efficacy of Joncryl in producing a branched structure. The results were found to be in good agreement with all the characterization done so far.

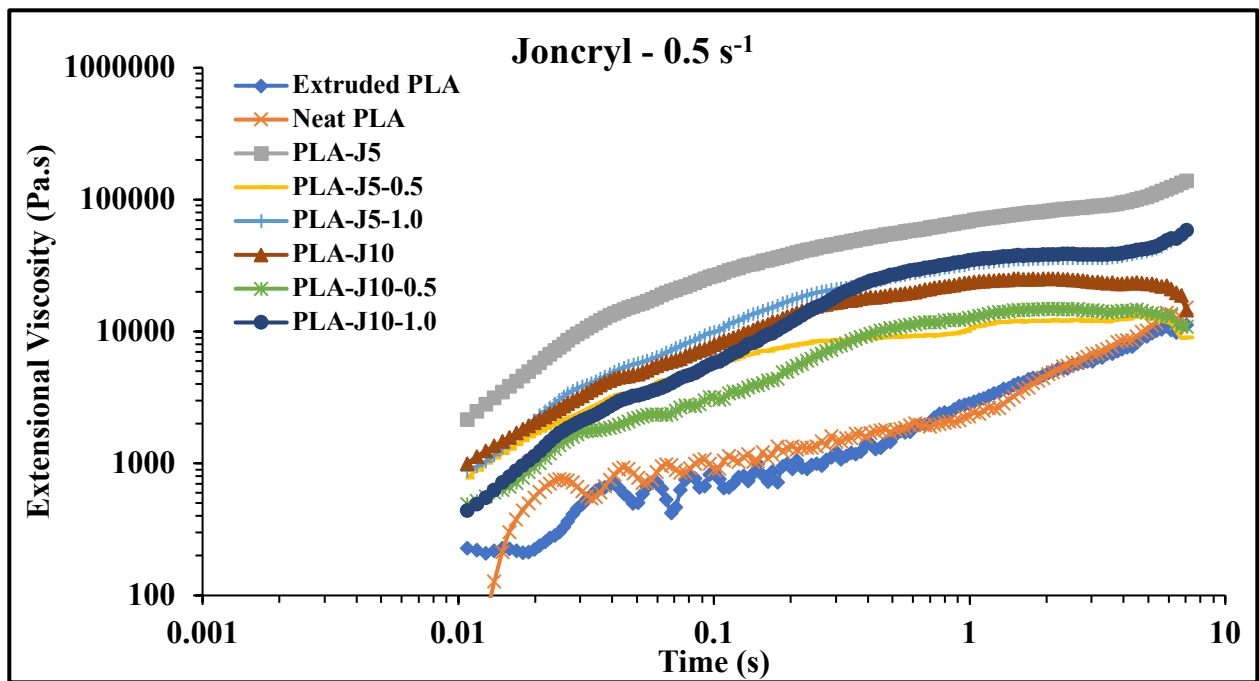


Figure 4-22: Comparison of extensional viscosity at a strain rate of  $0.5 \text{ s}^{-1}$  for Joncryl blends at  $180^\circ\text{C}$

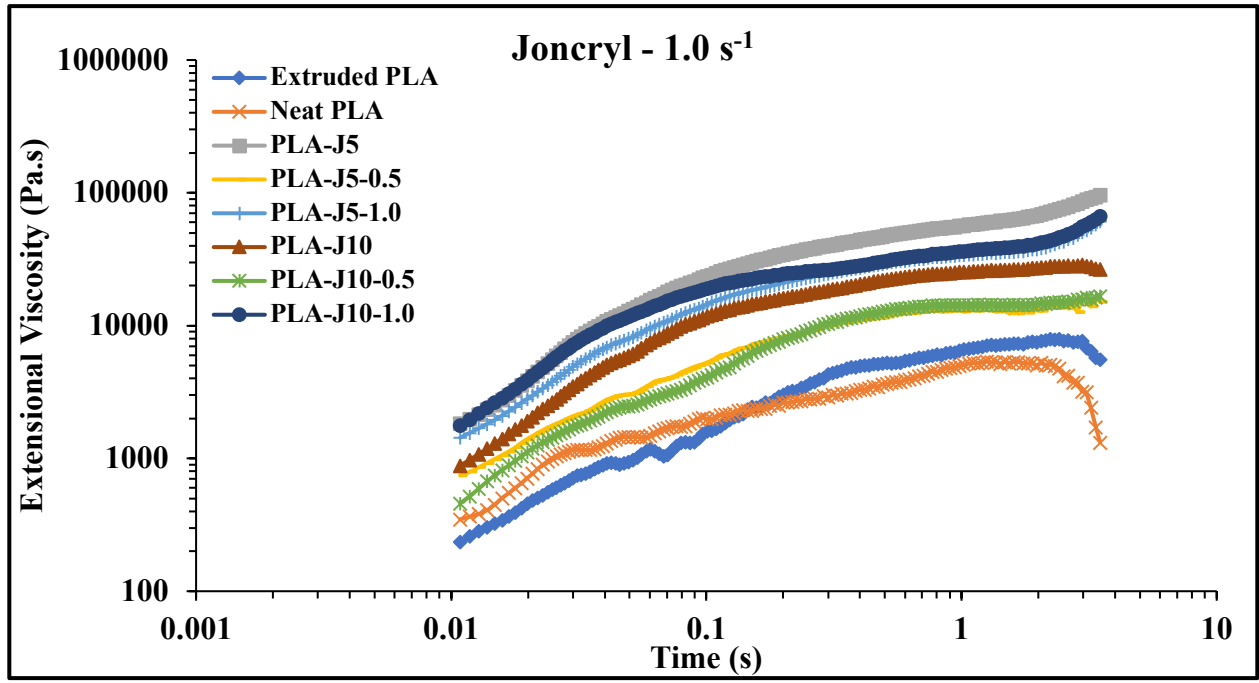
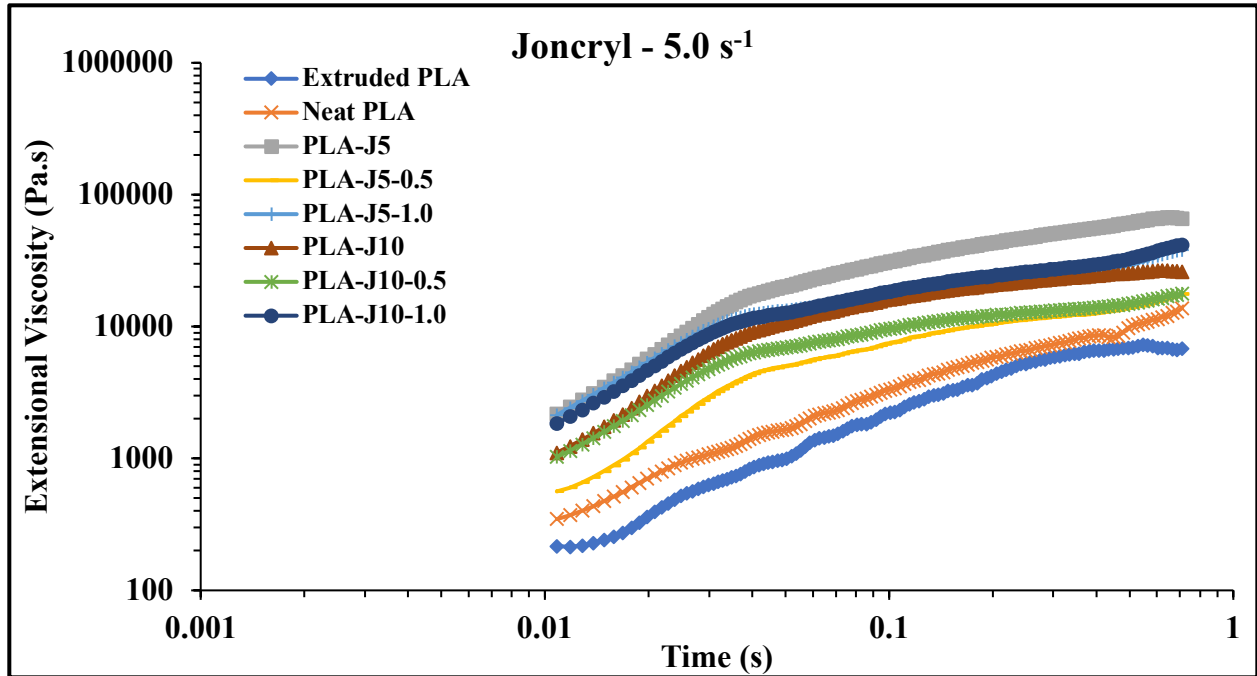
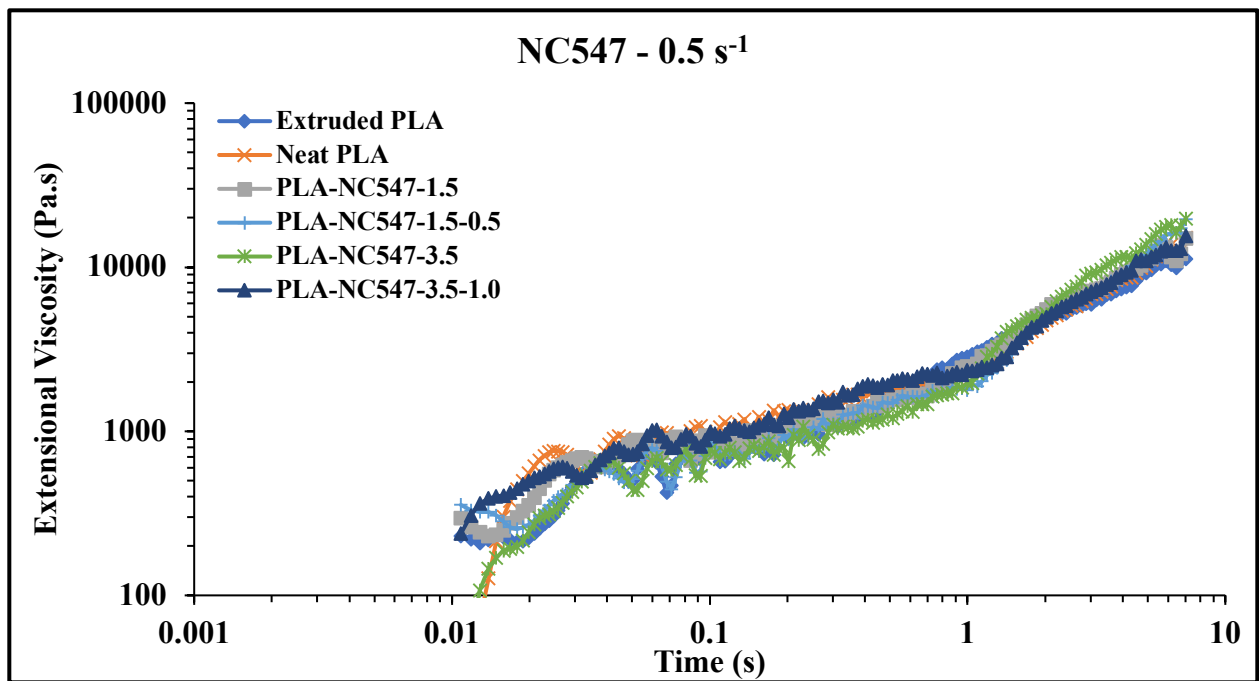


Figure 4-23: Comparison of extensional viscosity at a strain rate of  $1.0 \text{ s}^{-1}$  for Joncryl blends at  $180^\circ\text{C}$



**Figure 4-24:** Comparison of extensional viscosity at a strain rate of  $5.0 \text{ s}^{-1}$  for Joncryl blends at  $180^\circ\text{C}$

The  $\eta_E^+$  data for the NC-547 modified PLA samples are presented in Figure 4-25, Figure 4-26, and Figure 4-27. There was negligible effect of the addition of the NC-547 modifier to the PLA regardless of the amount added and the method of processing used. This behavior was found to be consistent at all the three strain rates of testing. This coupled with the observations from the complex viscosity experiments, clearly shows that there is negligible presence of branching in the PLA samples modified with the NC-547.



**Figure 4-25:** Comparison of extensional viscosity at a strain rate of 0.5 s<sup>-1</sup> for NC-547 blends at 180°C

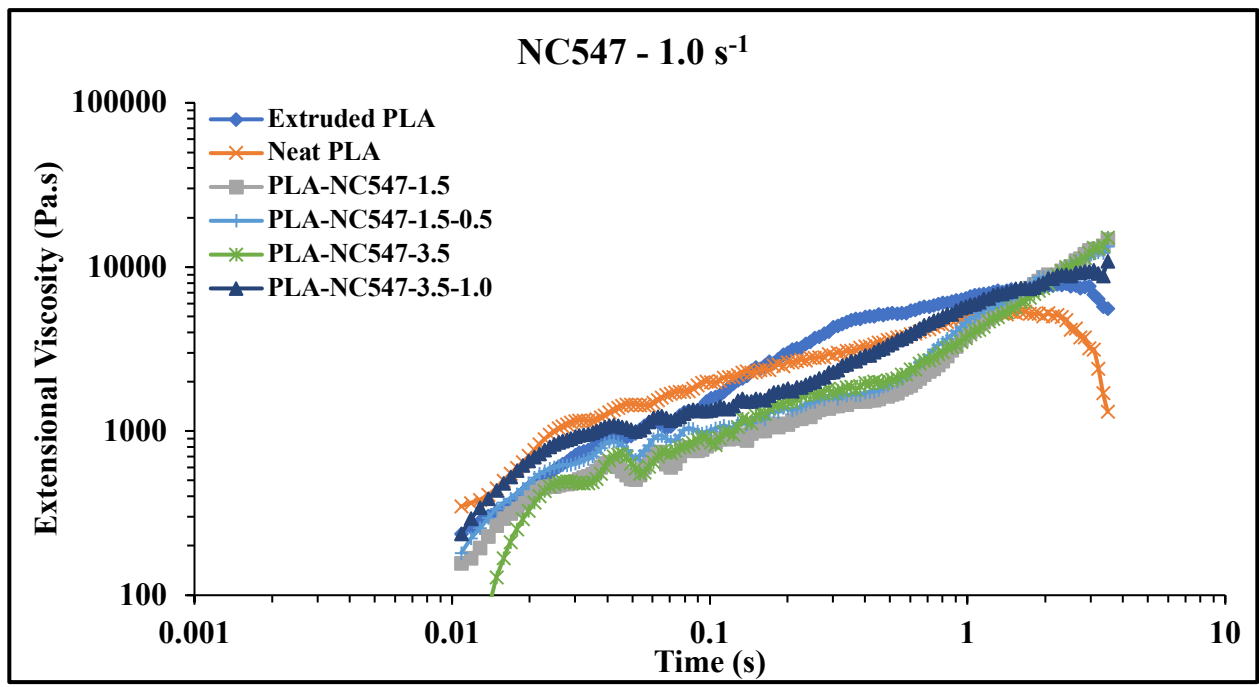


**Figure 4-26:** Comparison of extensional viscosity at a strain rate of 1.0 s<sup>-1</sup> for NC-547 blends at 180°C

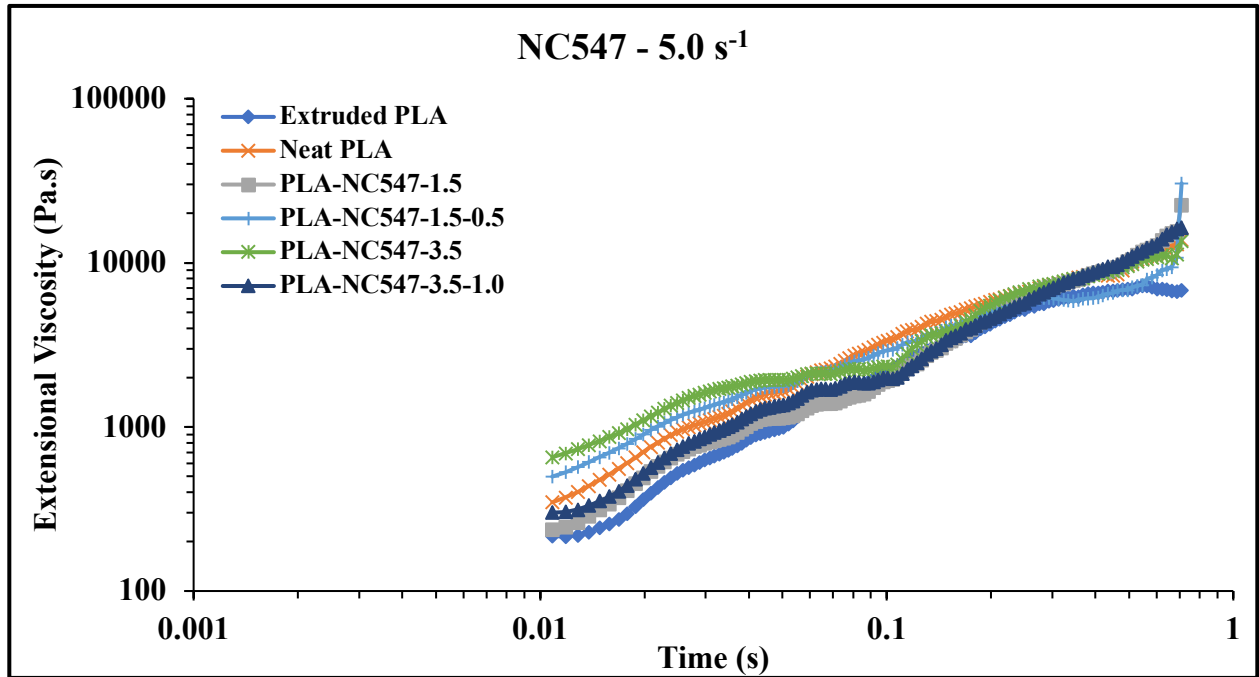


**Figure 4-27:** Comparison of extensional viscosity at a strain rate of  $5.0 \text{ s}^{-1}$  for NC-547 blends at  $180^\circ\text{C}$

Figure 4-28 shows the  $\eta_E^+$  for each sample tested at the strain rates of 0.5, 1.0 and  $5.0 \text{ s}^{-1}$ . The strain hardening behavior for a sample, if any, was observed at the higher strain rates.

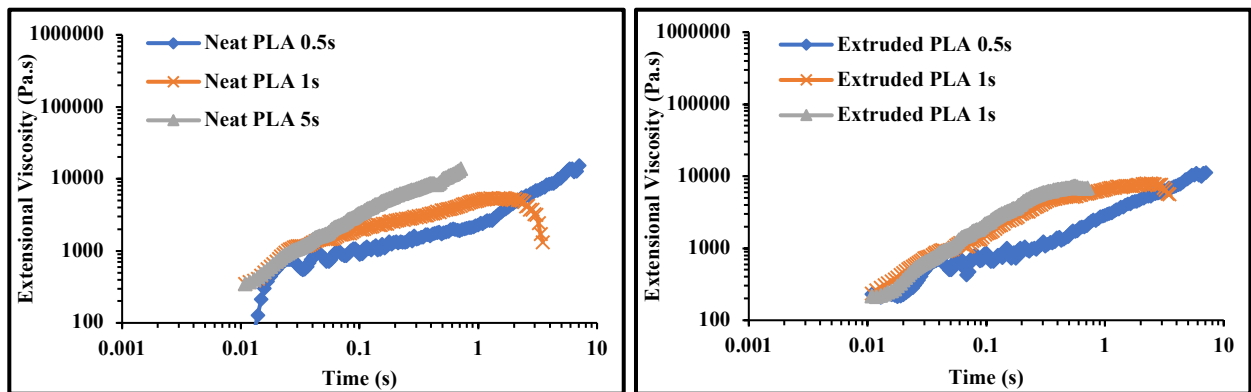


**Figure 4-28:** Extensional viscosity of each sample at 0.5, 1.0 and  $5.0 \text{ s}^{-1}$  at  $180^\circ\text{C}$

Figure 4-28 (cont'd)

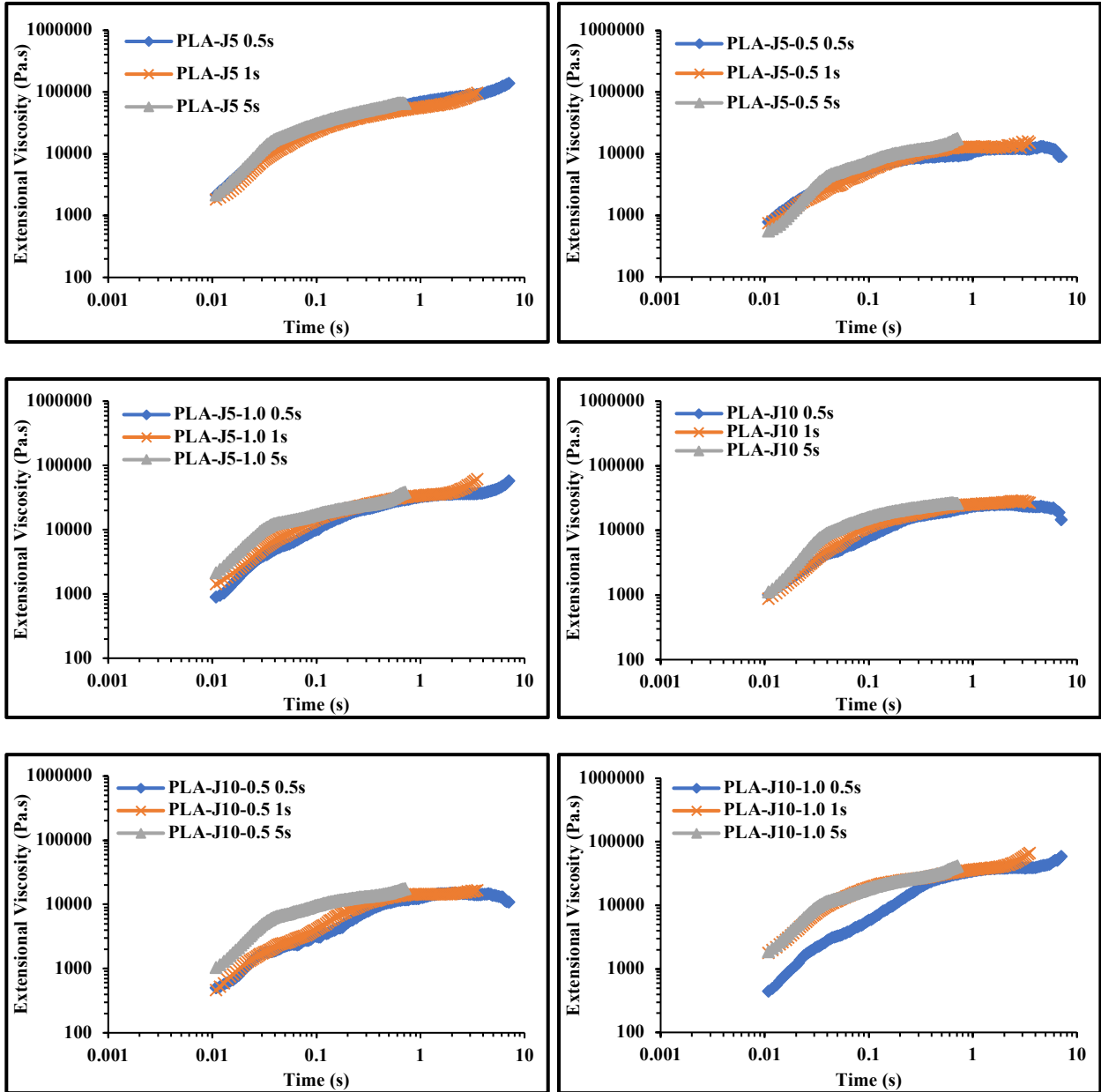
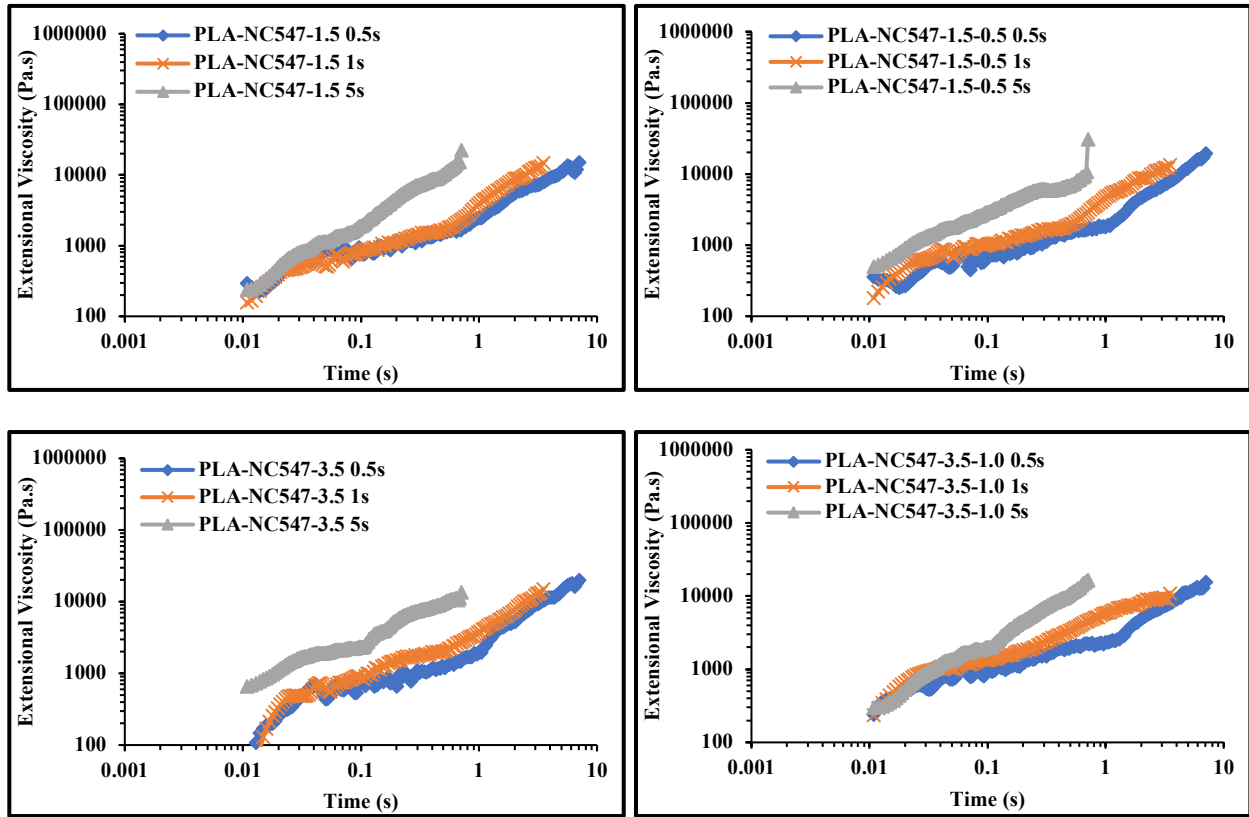


Figure 4-28 (cont'd)



The study of the  $\eta_E^+$  data for the epoxy modified PLA samples established that the reaction with Joncryl could lead to a branched structure of the PLA, and thus Joncryl could be used as a modifier for PLA in applications such as blown films, foams, etc. However, the NC-547 showed no indication of branching and thus, would be a poor substitute for Joncryl in such applications. The primary reason behind these observations is the low potential for branching sites on a given NC-547 molecule since each molecule possesses only 3 epoxy groups whereas Joncryl contains  $\sim 9$  epoxy groups per molecule. Also, a maximum of only 3.5% by weight of the NC-547 was used for the study since this was already at a molar ratio of 2:1 of epoxy modifier to PLA, which was set as an upper limit for the interest of our study. The other limitation was that NC-547 being a highly viscous fluid presented a processing issue in terms of feeding and proved difficult to process

at loading levels of above ~3.5% by weight. However, optimizing process conditions to increase the loading level of the NC-547 needs to be performed to investigate any additional improvements.

#### **4.4 Conclusions and Future Work**

In conclusion, two different multifunctional epoxy compounds were used to modify the rheological properties of PLA. BASF Joncryl-4368-C, a fossil-fuel based chain extender, and a chemically similar bio-based alternative Cardolite NC-547 were the two epoxy modifiers used. First, the reactivity of the two modifiers with PLA was investigated by using stearic acid and poly(ethylene glycol) as model compounds to mimic the carboxyl and hydroxyl end-groups of the PLA. Once reactivity of the epoxy group with the carboxyl end group was successfully established, the reactive blends of the epoxy modifiers with PLA were carried out using a twin-screw extruder. A major objective of the study was to investigate the difference in rheological properties caused due to using different molar ratios of the modifier to the PLA during the reactive blending process. Molar ratios of greater than and less than 1 of the epoxy modifiers to PLA were used to prepare the initial masterbatch for each modifier. The masterbatches were then diluted with neat PLA to final formulations containing 0.5% and 1.0% by weight of the modifiers. The extrudate of the reactive blends were purified and then characterized using FT-IR and <sup>1</sup>H NMR to prove the occurrence of reaction between the PLA and the modifiers. Thermal degradation and thermal transitions of the samples were studied. The  $T_{cc}$  of the samples were found to have a delayed onset with the addition of the modifier. This was attributed to the presence of bulky aromatic groups in the modifiers which hinder the PLA chain mobility. Gel swell analysis of the samples were performed in order to ensure that there was no formation of crosslinking in the system.

Molecular weight distributions for the samples revealed a significant increase in molecular weights of the Joncryl modified PLA samples. At a molar ratio of less than 1 (5% by weight) of epoxy to

PLA, a higher molecular weight was observed. This suggested the formation of a more branched structure as opposed to the sample at a molar ratio of greater than 1 (10% by weight). However, there was negligible difference in molecular weights between using the 5% or 10% masterbatch when the samples were diluted to 0.5% and 1.0% by weight. The NC-547 modified samples, including the final diluted formulations, had a lower molecular weight compared to even extruded PLA. MFI studies showed a similar trend with drastic reduction in the melt flow rates for the Joncryl samples. Again the 5% masterbatch was found to have the lowest MFI, however, again upon dilution, there was no difference in properties of the diluted samples based on the masterbatch used. The NC-547 diluted samples showed lower values of melt flow rate as compared to their masterbatches, proving greater extent of reaction due to the two-step processing method.

Complex viscosity of the samples was studied as a function of shear rate to study the type of chain extension mechanism present in the system. The Joncryl sample at 5% showed the most pronounced shear thinning behavior, confirming the presence of long chain branching. The NC-547 samples however displayed a more Newtonian behavior with viscosity being nearly independent of the shear rate, thus implying that there might only be regular chain extension but no branching. Uniaxial extensional viscosity of the samples confirmed that the Joncryl modified PLA samples developed long chain branching. In both the complex and extensional viscosity studies, the masterbatch with molar ratio at less than 1 for epoxy to PLA was found to have superior rheological performance compared to the sample at a molar ratio of greater than 1. However, upon dilution to final loading levels there was negligible difference in the type of masterbatch used.

Overall the study established that Joncryl is highly effective at creating long chain branched structures with PLA, and can be successfully used as a rheological modifier in applications such as blown films, blow molding, foams etc. On the other hand, the NC-547 could at best be used as

a processing aid for PLA to build back molecular weight lost during processing. However, this was attributed to current loading levels of the NC-547 used. Using appropriate feeding techniques for high viscosity fluids, a higher content of the NC-547 could be used to investigate if there would be any further improvements. This would form the basis for future investigations relating to this study. Further, blown films using the epoxy modified masterbatches are going to be produced to observe for improvements in performance properties of the films due to the epoxy modification.

## **5 POLYLACTIDE BASED DIRECT-LONG FIBER THERMOPLASTICS (D-LFTs) FOR AUTOMOTIVE INTERIOR APPLICATIONS**

### **5.1 Introduction**

Despite its commercial acceptance in low-end single-use plastic applications, PLA has not been considered a viable material-of-choice for applications requiring durability and high structural strength. This is primarily due to its poor impact strength and high sensitivity to thermal and moisture conditions [11, 98, 231, 232]. The sensitivity to heat and moisture is strongly dependent on the crystallinity of the PLA part, and has been successfully addressed in a cost-effective manner by adopting processing techniques such as thermal annealing and addition of nucleating agents during the molding process [233-235]. Improving impact strength and modulus of the PLA for structural applications, however, remains a key issue. A conventional approach to improving these two key performance parameters involves the addition of fiber reinforcements to the polymeric matrix [236-238]. PLA based fiber reinforced composites have been previously developed, however, with the primary intention of producing biodegradable natural fiber composites [239-242]. Hence producing more durable and structurally superior composite materials using PLA is a primary focal point for this study.

One of the most critical factors governing the mechanical performance of a given composite material is the aspect ratio of the reinforcing fiber in the matrix [243-245]. Aspect ratio is defined as the ratio of the length of the fiber to its diameter ( $l/d$ ), thus indicating that a higher aspect ratio results in a greater surface area of the fiber being exposed at the fiber-matrix interface. Since, reinforcing fibers are the primary load-bearing components within the polymeric matrix, a higher aspect ratio of the fiber would indicate a greater surface area available at the fiber -matrix interface thus enabling a more efficient transfer of the applied load [246, 247]. This phenomenon has been

well-studied with several fiber reinforced polymer composites with consistent conclusions that a higher aspect ratio resulted in a greater improvement in mechanical performance as opposed to lower aspect ratio [238, 248]. Thus, an attempt was made in this study to obtain higher aspect ratios of the fiber in the PLA by using continuous rovings of the fibers as opposed to using chopped fiber. This was achieved by adopting a processing technique referred to as Direct-Long Fiber Thermoplastics (LFTs) wherein continuous fiber reinforcements are directly incorporated into the melted polymeric matrix in an extruder. The D-LFT process is a fairly recent development in the composite fabrication industry and has been consistently shown to produce composite materials with high aspect ratios of the reinforcing fibers [249-251]. The D-LFT process also offers the distinct advantage of being a continuous process, thus enabling cost-effective scale-up for commercial production. The D-LFT technique has been successfully adopted for the production of various thermoplastic-based composite materials, however, only one prior study exists where it has been used to produce a PLA-jute composite [252]. Although this study provided promising results, the equipment used was highly specialized requiring a significant capital investment, also, the study does not elaborate on processing conditions and the process optimization required to produce these composites. Further, there have only been a few reports of producing D-LFTs at a lab or pilot scale without using a specialized setup [253-256]. These studies utilized extremely poor techniques for feeding of the fiber and did not investigate the effects of processing parameters on the composites produced. Thus, the focus of our study was not only to develop the first ever reported PLA-based D-LFT, but also to design a highly optimized and cost-effective pilot scale D-LFT production technique that could be easily scaled to produce D-LFTs for other thermoplastic materials with any given reinforcing fiber.

Basalt fiber is derived from the basalt rock, which is a type of igneous rock formed due to the rapid

cooling of volcanic lava. Since it is found in abundance in the Earth’s crust and is relatively easily converted into the form of a fiber by melt spinning (Figure 5-1), it is a sustainable choice for use as a reinforcing fiber. It has a modulus and tensile strength higher than that of glass fiber (Table 5-1), and reportedly has an excellent thermal and chemical resistance, thus making it a superior choice over glass fiber as a reinforcement for PLA [257]. Basalt fiber has gained traction as a reinforcing fiber only recently over the past decade with several studies reported in literature [258-261]. Also, there have only been a handful of reports where basalt fiber has been used as a reinforcement for PLA with promising results [262-264], however all of these studies used chopped fiber resulting in a low aspect ratio. Thus, our study constitutes the first-ever reported instance of a long-fiber reinforced PLA-basalt composite produced using the D-LFT approach.

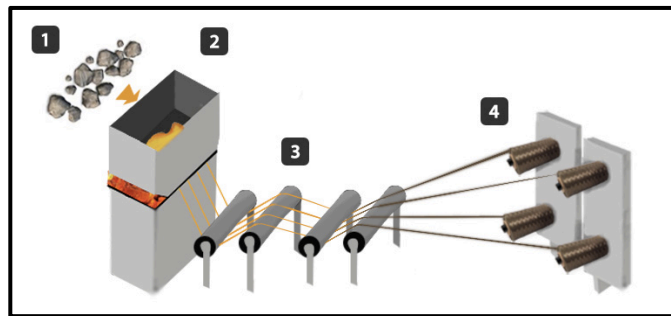


**Figure 5-1:** Schematic showing the production of basalt fiber from basalt rock by melt spinning (Image sourced from [www.basaltlft.com](http://www.basaltlft.com))

**Table 5-1:** Comparison of properties of basalt fiber against glass and carbon fiber [260]

|                                   | E-Glass Fiber | <b>Basalt Fiber</b> | Carbon Fiber |
|-----------------------------------|---------------|---------------------|--------------|
| <b>Tensile Strength [MPa]</b>     | 2700~3000     | <b>3100</b>         | 3800~4400+   |
| <b>Elastic Modulus [GPa]</b>      | 72~76         | <b>88~92</b>        | 230+         |
| <b>Elongation at break [%]</b>    | 4.8           | <b>3.5</b>          | 0.5~1.5      |
| <b>Density [g/cm<sup>3</sup>]</b> | ~2.6          | <b>~2.6</b>         | ~1.8         |

In our study, we will adopt the D-LFT technique to use basalt fiber as a reinforcement to enhance

the mechanical performance of the PLA matrix. E-glass fiber will also be used as a reinforcement to serve as a comparison to the basalt-fiber properties. For both of these long fibers, their chopped short fiber counterparts will also be used to investigate the difference in properties observed. The D-LFT technique will also be studied in-detail and optimization of process parameters will be performed as required.

## **5.2 Experimental**

### **5.2.1 Materials**

A commercially available semi-crystalline injection-molding grade of PLA, 3001D, was used for this study. The PLA was sourced from NatureWorks LLC (Minnesota, USA). The 3001D grade of PLA has a weight average molecular weight of  $\sim 150,000$  g/mol and a meso-lactide content of around  $\sim 2\%$ . Four different types of fibers were used for the study. Continuous (direct) rovings and chopped strands of basalt fiber were kindly provided by Mafic (Meath, Ireland). Both the rovings as well as the chopped fiber had a filament diameter of  $13\ \mu\text{m}$  and a proprietary silane-based sizing for polyester resins. The direct rovings had a linear density of 300 tex, and the chopped fibers had a cut-length of 6 mm. Continuous rovings of glass fibers (corrosion resistant E-glass) were kindly provided by Owens Corning (Ohio, USA). These rovings had a filament diameter of  $13\ \mu\text{m}$ , a linear density of 1100 tex, and also had a proprietary sizing for polyester resins. Chopped strands of glass fibers (E-glass) with a filament diameter of  $13\ \mu\text{m}$  and a cut-length of 6 mm were purchased from Fibre Glast Developments Corporation (Ohio, USA). The chopped strands were sized with a proprietary silane-based agent. Other reagents used were purchased from Sigma-Aldrich (Wisconsin, USA).

### 5.2.2 D-LFT Extrusion Process

The synthesis of the PLA-based composite materials was carried out using a twin-screw extruder. Identical processing conditions were used for each set of fiber samples to maintain uniformity during comparison of properties. The PLA pellets were dried overnight in a convection oven at 60°C prior to the extrusion process. This was done in order to remove residual moisture in the PLA which might accelerate its degradation under shear in the extruder. For both the chopped fiber samples, the fibers were premixed with the PLA pellets prior to being fed in the hopper. In the case of the continuous fiber rovings, a purposefully designed setup as shown in Figure 5-2, was prepared to hold the roving in place at a fixed height above the barrel of the extruder as the fiber was being fed in. A Century ZSK-30 co-rotating twin-screw extruder with a screw diameter of 30 mm and a L/D ratio of 42 was used for the processing. The temperature profile used for this process was as follows: 170/175/180/180/180/185/185/185/180/175°C. The screw speed was set at 200 rpm, and the throughput for the basalt fiber samples and the glass fiber samples were set at 100 and 160 gm/min respectively. The extrudate in the form of a strand was quenched by passing through an ice-cooled water bath and subsequently pelletized. The pellets were then dried overnight in a convection oven at 50°C to remove excess moisture prior to characterization.

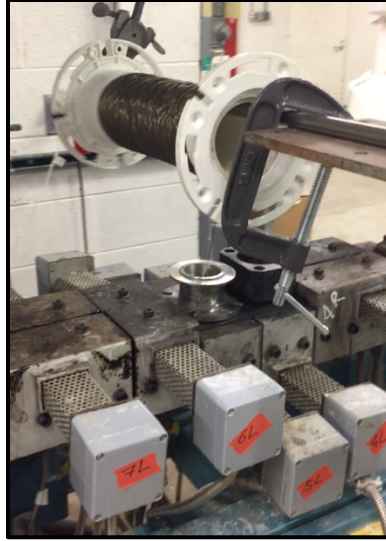


**Figure 5-2:** Setup showing the fiber feeding mechanism for the D-LFT preparation

### 5.2.3 Characterization

Fiber loading levels were measured by using a resin burn-off method or ash-test. A known amount of the extruded pellets was placed in ceramic crucibles which were then placed into a muffle furnace. The temperature in the furnace was then ramped up to 600°C at 40°C/min to burn off the PLA matrix. The residual weight of the crucible was measured and the weight of the fibers present in each sample was calculated using the following gravimetric formula:

$$\text{Fiber content (\% by weight)} = \frac{W_{c,after} - W_{c,before}}{\text{Weight of sample used}} \quad (\text{Equation 1})$$

where,  $W_{c,after}$  is the weight of the crucible containing residual matter after the burn-off test, and  $W_{c,before}$  is the weight of the dried empty crucible before the test.

Fiber length distributions were obtained by cutting a long strand (~3 m) of the extrudate of each sample prior to pelletization. This ~3 m long strand was then cut to pieces of 15 cm in length and placed in ceramic dishes. This was done in order to ensure that pelletization would not contribute to reduction in fiber length distributions. A resin burn-off procedure as described earlier was performed to remove the PLA matrix leaving behind only the reinforcing fibers. These fibers were

then placed in a vial containing acetone to separate them out. The mixture was poured out on to a glass petri dish which was then placed in an oven at  $\sim 60^{\circ}\text{C}$  to remove the acetone. The fibers collected on the petri dish were then studied under a Keyence VHX-6000 digital light microscope equipped with a Keyence VHX software which was used to measure the fiber lengths. A minimum of 250 fibers were used for the calculation of the fiber length distribution for each sample.

The tensile test specimens for the composite samples were prepared using an 85-ton Cincinnati Milacron (Ohio, USA) injection molding machine. The barrel and nozzle temperatures were set at 380/350/350 $^{\circ}\text{F}$  and 375 $^{\circ}\text{F}$  respectively. The mold was held at room temperature. The screw speed was set to 100 rpm and the injection pressure used was 800 psi. The total cycle time was set at around  $\sim 90\text{s}$ .

The thermal transitions of the samples were observed using a differential scanning calorimeter, DSC Q20 (TA Instruments, USA). The samples were first heated up to  $200^{\circ}\text{C}$  starting at room temperature at a rate of  $10^{\circ}\text{C}/\text{min}$  under a nitrogen atmosphere to erase any thermal history associated with processing before being cooled down to  $20^{\circ}\text{C}$ . They were then heated back up to  $200^{\circ}\text{C}$  at  $10^{\circ}\text{C}/\text{min}$ . The heat flow vs. temperature data was then recorded and plotted.

Tensile testing was carried out on an Instron model 5565-P6021 (Massachusetts, USA) mechanical testing fixture setup with a 5 kN load cell. The testing was carried out in accordance with the ASTM D638-14 (Type I sample size) standard test method for tensile properties of plastics [126]. The rate of grip separation was set at 5 mm/min which was as per the ASTM D638 specifications. A minimum of six replicates were used to ensure repeatability of the test data.

The notched Izod impact properties were studied using a Ray-Ran RR-IMT (Warwickshire, UK) pendulum impact tester equipped with a Techni-Test test software. The testing was carried out in accordance with the ASTM D256 standard test method for determining the Izod pendulum impact

resistance of plastics [32]. The samples were notched using a Tinius Olsen Model 22-05-03 Motorized Specimen Notcher (Pennsylvania, USA). The test specimens had dimensions of 63.5 mm X 12.7 mm and the notch marked was 2.54 mm deep. A minimum of six replicates were used to ensure repeatability of the test data.

Dynamic mechanical analysis (DMA) was performed on the samples using an RSA-G2 Solids Analyzer (TA Instruments, USA) to evaluate the storage and loss modulus, as well as the tan delta phase lag factor as a function of temperature. The gage section of the tensile test specimens was cut out into segments of length 50 mm using a bandsaw for the testing. The tests were carried out using the three-point bending mode, within a range of 30°C – 150°C at a heating rate of 3°C/min and a frequency of 1 Hz.

A JEOL 6610LV scanning electron microscope (SEM) was used to obtain the surface morphology images for the fracture surfaces of the tensile and impact test specimens. The fractured surfaces were mounted vertically using a two-part epoxy, and a carbon coating was applied for conductivity. The mounted samples were then imaged under a high vacuum.

## **5.3 Results and Discussion**

### **5.3.1 D-LFT Extrusion Process**

The primary objective of the study was to produce long fiber reinforced PLA-based composites with a higher aspect ratio of the reinforcing fibers. In order to achieve this, continuous rovings of the fibers were used instead of chopped fibers. The rovings of the fibers were directly fed into an exposed port of the extruder where the fibers were drawn in through the conveying motion of the screws. This posed a significant challenge in terms of processing since optimization of the processing conditions involved a greater number of process variables as opposed to using chopped fibers. The process variables were dependent on optimizing two primary criteria: *fiber breakage*

and *fiber dispersion*. These are two contradictory principles yet are vital to the fabrication and performance of composite materials [265-268]. An optimum amount of fiber breakage is essential in order to ensure uniform dispersion of the fiber in the matrix leading to better properties. Excessive fiber breakage results in a reduction in the aspect ratio of the fiber, thus defeating the purpose of using a long fiber reinforcement. On the other hand, not having enough breakage of the fiber results in the formation of “clumps” of fiber which prevents impregnation of the matrix leading to failure of the part. In order to optimize fiber breakage and subsequent dispersion, the two most critical process variables were the *screw configuration of the extruder* and the *point of entry for the fiber feed*. Initially, the fiber was fed in at Zone 8 as shown in Figure 5-3 (top). This setup was used in order to introduce the fiber downstream thus minimizing excessive fiber breakage as opposed to feeding it further upstream. A kneading block similar to the one shown in Figure 5-4 was used at the point of introduction of the fiber at Zone 8 in order to have optimum fiber breakage. However, this setup was found to be ineffective since there was less than optimal fiber breakage resulting in clumping of the fibers. In order to alleviate this, the setup was changed to the one shown in Figure 5-3 (bottom). In this case, the fiber was introduced upstream at Zone 4. To ensure proper impregnation of the fiber by the resin, the PLA needs to be completely melted before the introduction of the fiber. Hence, the temperatures for Zones 1-4 were set to 180°C. Also, a kneading block was used at Zones 2-4 to create additional shear along with the elevated temperatures to achieve complete melting. The screw configuration for this setup also had a kneading block at Zone 8 to ensure proper dispersion of the fiber. Further, it was studied and found that conveying elements were more efficient than kneading elements at maintaining the uptake of the fiber at its feeding point. This setup provided the most optimal conditions for the continuous fiber to be processed and was used for the synthesis of all the composite samples prepared for this

study. The samples with short fibers were also processed using the same screw configuration to compare the effects of processing on the fiber breakage.

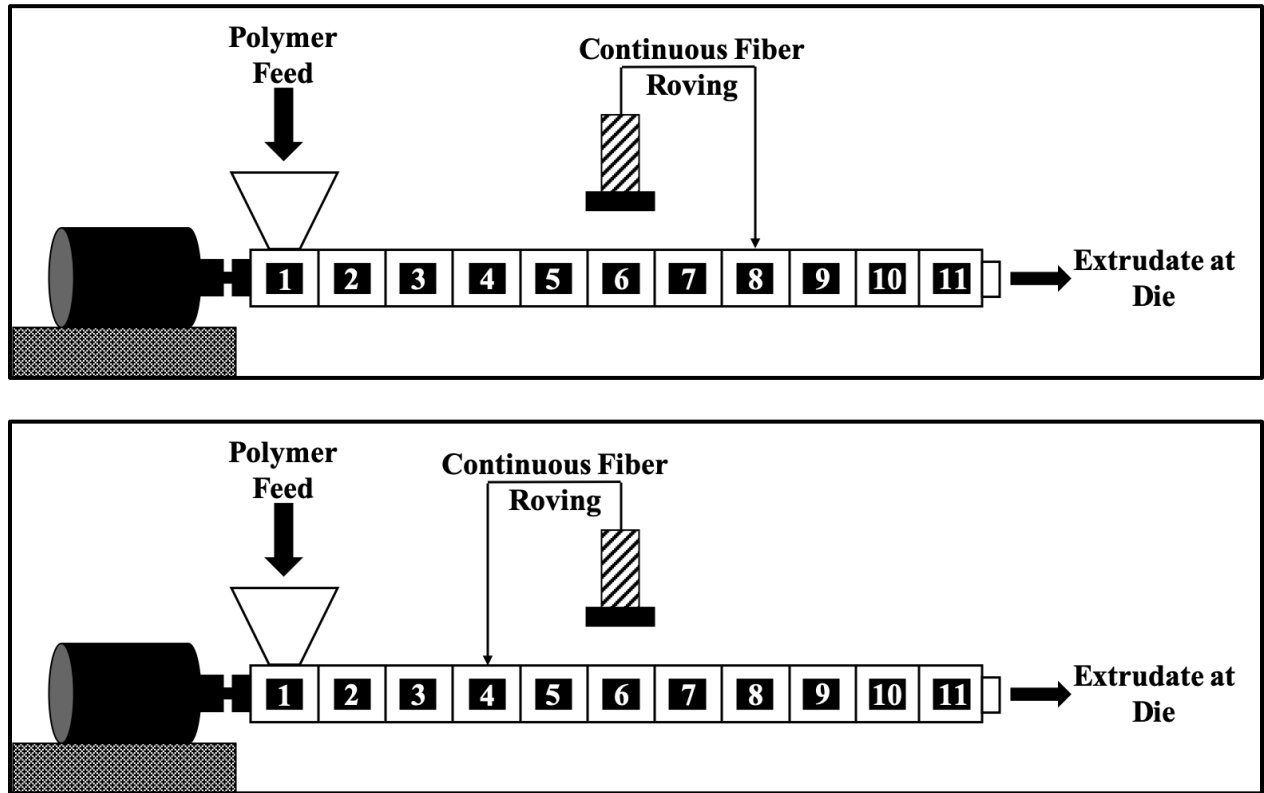


**Figure 5-3:** Schematic showing the extrusion setup used for the D-LFT preparation. Fiber feed point at Zone 8 was used initially (top) and later optimized to feed at Zone 4 (bottom)

Since the fibers were fed into the extruder due to the conveying motion of the screws, the amount and rate of fiber being fed was dependent on the *screw speed* and the *feed rate of the polymer*, thus resulting in two additional process parameters that were required to be optimized. A higher screw speed causes faster drawing of the fiber resulting in a higher loading level of fiber. However, an upper bound for the screw speed is set at around ~200 rpm due to a reduction in residence time above that limit resulting in incomplete melting of the PLA. An increase in feed rate of the polymer also contributed to an increase in the feed rate of the fiber since the conveying motion was enhanced with a greater amount of material flow. However, its effect on the feed rate of the fiber

was not as pronounced as the screw speed. For all processing conditions tested, a screw speed of 200 rpm was found to be most optimal in terms of fiber feeding and was used for the synthesis of all the samples prepared, including the ones with short fiber.

The amount of fiber being fed in was monitored using two different methods: first, using a simple gravimetric approach, the fiber roving was directly weighed before and after each run to measure the quantity of fiber that had been used. The second technique involved measuring the amount of polymer being fed at the hopper and then the actual throughput at the pelletizer. The difference between the two values per unit time would provide the rate at which the fiber was being fed.



**Figure 5-4:** Two kneading blocks as shown above were used to effectively melt PLA before fiber feed and break down fiber after fiber feed

Five different samples were prepared in total. For the short fiber processing, first the amount of fiber loading achieved in their long fiber counterpart was measured. An equal amount of short fiber was fed along with the PLA in order to closely simulate the effects of similar processing on the short fibers. The continuous glass fiber used had a higher linear density than the continuous basalt, thus resulting in higher loading levels of the glass fiber under similar processing conditions. In order to attain a higher loading level of the basalt, two different rovings were fed in simultaneously. This sample is referred to as “Long Basalt X2” for the rest of the study.

### 5.3.2 Characterization

Ash testing of the samples provided an accurate representation of the loading levels in terms of weight % achieved during the processing. Figure 5-5 shows the setup used for the testing. The results obtained are provided in Table 5-2. Volume fractions of the fiber are derived from the weight fractions obtained experimentally using the given formula:

$$f = \frac{f_w}{f_w + (1-f_w)\frac{\rho_f}{\rho_m}} \quad (\text{Equation 2})$$

Where,  $f$  is the fiber volume fraction,  $f_w$  is the fiber weight fraction, and  $\rho_f$  and  $\rho_m$  are the densities of the fiber and matrix respectively. A value of  $1.25 \text{ g/cm}^3$  was used for PLA, whereas both glass and basalt fibers had a density of  $2.6 \text{ g/cm}^3$ . It can be observed that starting with the same amount of fiber during feeding, a lower amount of fiber loading is found in the samples with short fiber. This is attributed to the fact that a small amount of fiber is lost during processing due to adhesion to screws etc. This effect is seen to be amplified with the short fiber samples due to more breakage of the fiber as compared to the long fiber. Also, with the D-LFT processing method, the loading levels for glass fiber were found to be higher than that of the basalt fiber under similar processing conditions. This was due to the fact that the glass fiber roving had a linear density of almost 3 times that of the basalt fiber roving (1100 tex vs. 300 tex) leading to a lower amount of fiber being fed.

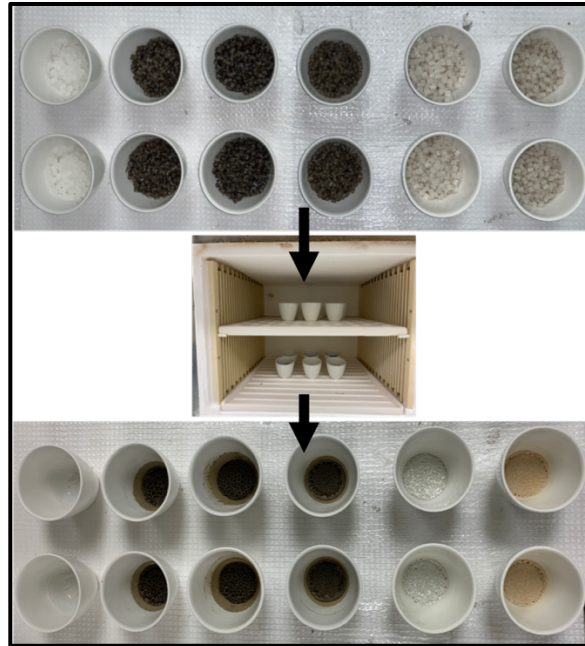


**Figure 5-5:** Ash testing of the samples to measure fiber loading content (before, during and after test)

**Table 5-2:** Fiber weight fractions as obtained from ash test. Fiber volume fractions as calculated using Equation 2

| <b>Sample</b>        | <b>Fiber Content<br/>(in % by weight)</b> | <b>Fiber Content<br/>(in % by volume)</b> |
|----------------------|---|---|
| Neat PLA             | —   | —   |
| PLA + Short Basalt   | 3.47                                      | 1.68                                      |
| PLA + Long Basalt    | 4.62                                      | 2.25                                      |
| PLA + Long Basalt X2 | 8.05                                      | 3.99                                      |
| PLA + Short Glass    | 8.85                                      | 4.38                                      |
| PLA + Long Glass     | 10.18                                     | 5.07                                      |

Fiber length distributions of the samples are presented in Figure 5-6. The aspect ratio (length of fiber/fiber diameter) for each sample was calculated by using the mean length obtained from the distribution divided by the fiber diameter, which was 13  $\mu\text{m}$  for all samples. It can be clearly observed that there was an increase in aspect ratio by using the continuous fiber method as opposed to using chopped fibers. The increase was more pronounced in the case of the basalt fiber than the

glass fiber, mostly due to the fact that the glass fibers are more brittle and are more prone to suffer from excessive fiber breakage compared to the basalt fiber.

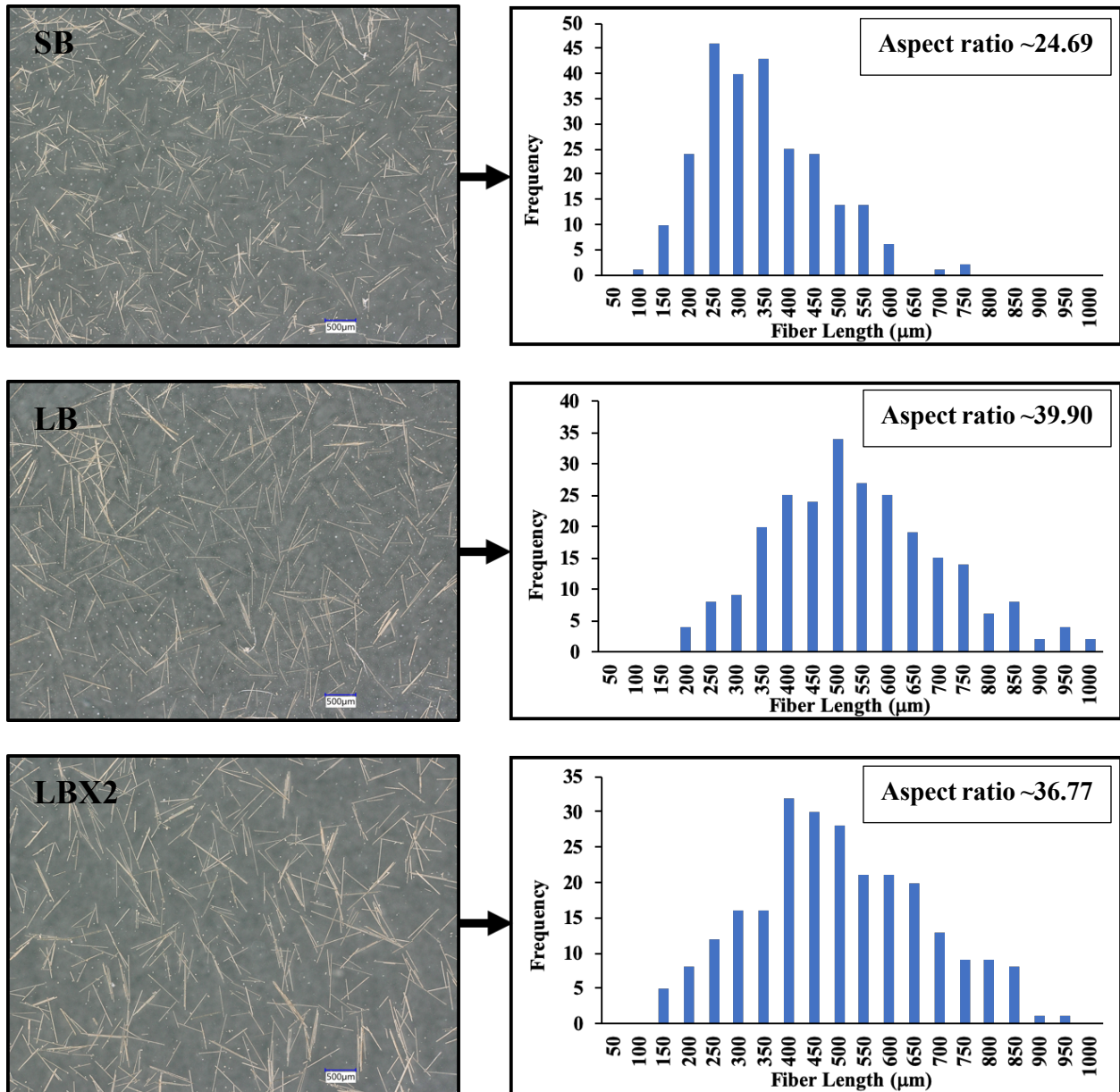
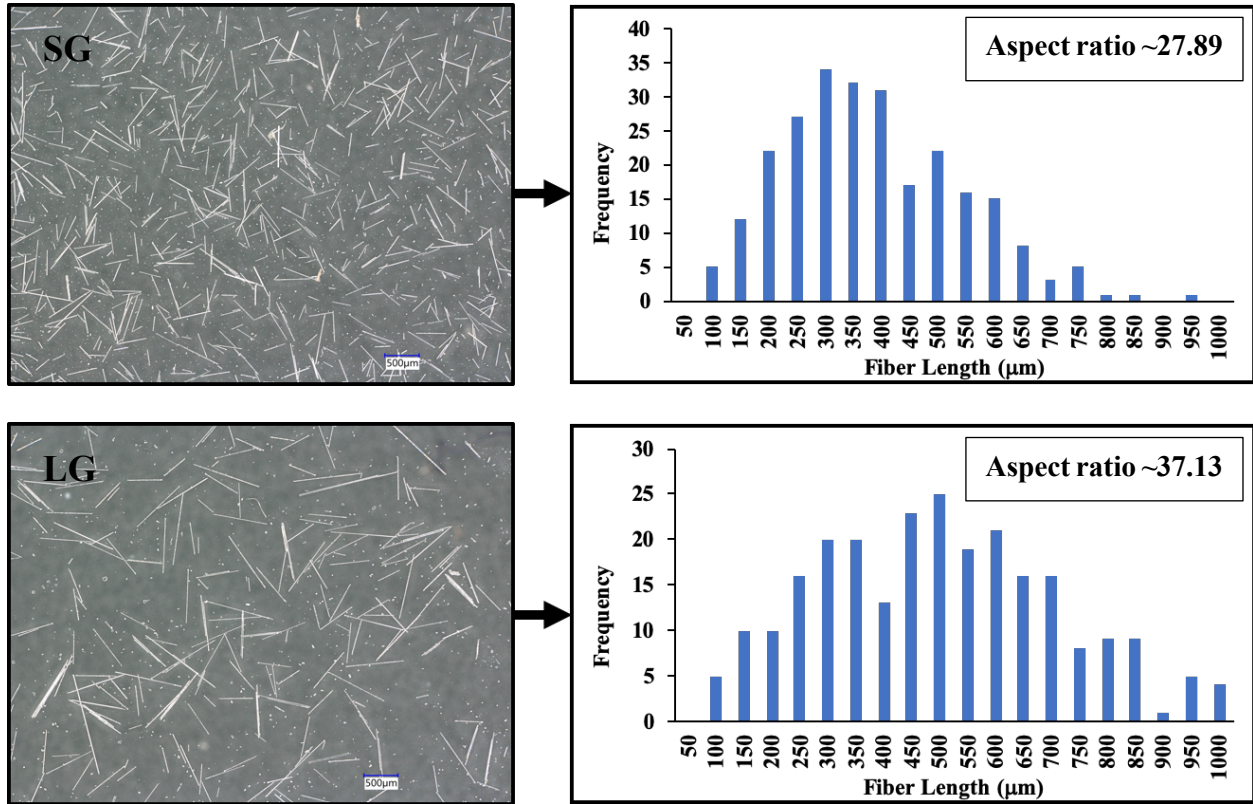


**Figure 5-6:** Optical micrographs of fiber specimens used for measuring fiber length distribution (left) with the corresponding distribution (right)

Figure 5-6 (cont'd)



The thermal transitions of the composite samples, as shown in Figure 5-7, revealed no major changes when compared to those of neat PLA apart from a delayed onset of cold crystallization with incorporation of the fiber. This was in direct contradiction with results obtained from previous studies [241, 269, 270]. This observation could be attributed to the presence of longer fiber segments which hinder the chain mobility of the PLA, thus delaying the onset of the cold crystallization. Melting and glass transition values were however found to be unchanged with the addition of the fiber.

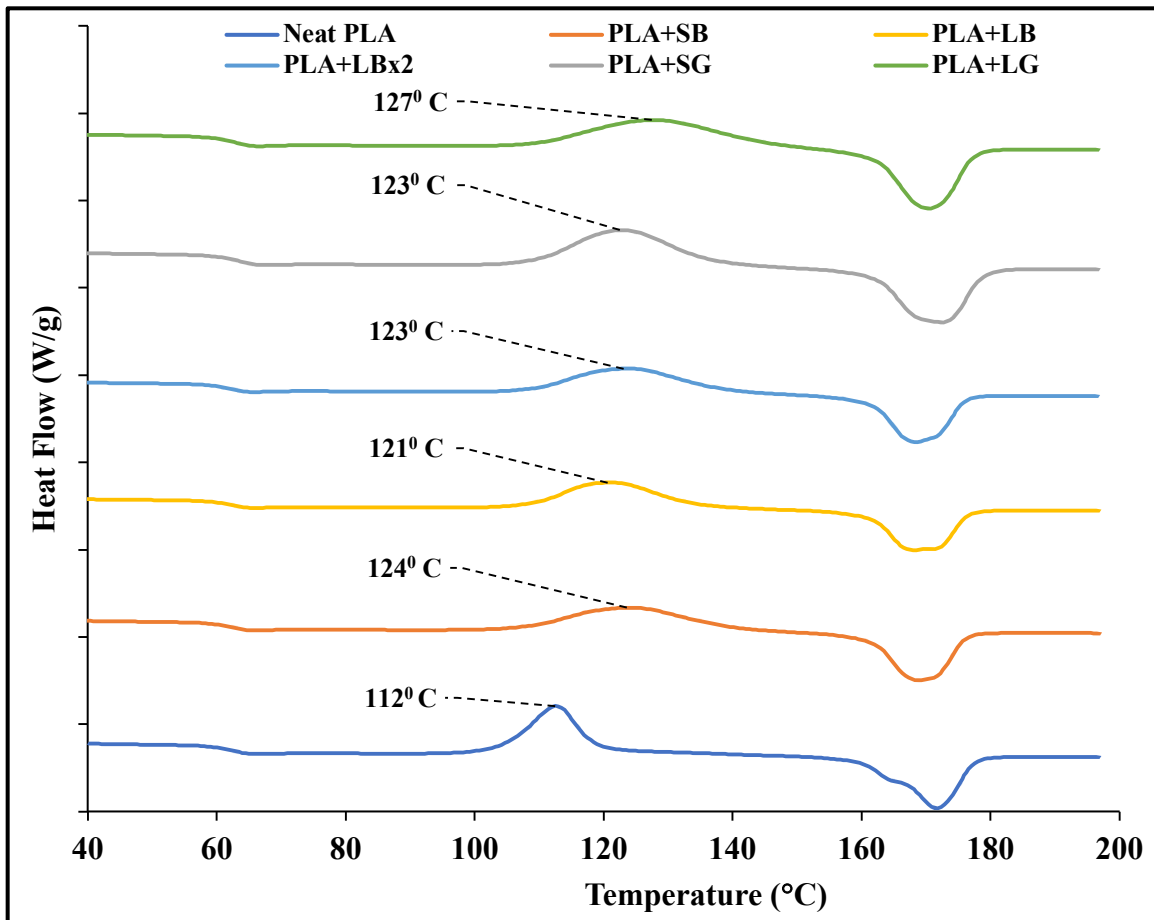


**Figure 5-7:** DSC scans of the composite samples showing thermal transitions

Tensile test data provided the first confirmation of the improvement in properties caused due to the use of the long fiber processing method resulting in a greater aspect ratio. The modulus and tensile strength as seen from the stress-strain curves in Figure 5-8 were found to significantly improve upon using the long fiber. This was mostly due to the increase in the aspect ratio of the fibers, and partially due to a marginally higher loading level of the long fibers as compared to that of the short fibers. However, the effect of the aspect ratio is seen to be more predominant on the mechanical performance of the composite material. The maximum difference in properties between the use of long and short fibers was observed for the glass fiber reinforced samples. The sample reinforced with the short glass fiber had a tensile strength of ~72 MPa, whereas, the sample

with the long glass fiber had a tensile strength of ~86 MPa. This clearly demonstrated the efficacy of the long fiber processing technique at obtaining composite samples with significantly improved mechanical performance.

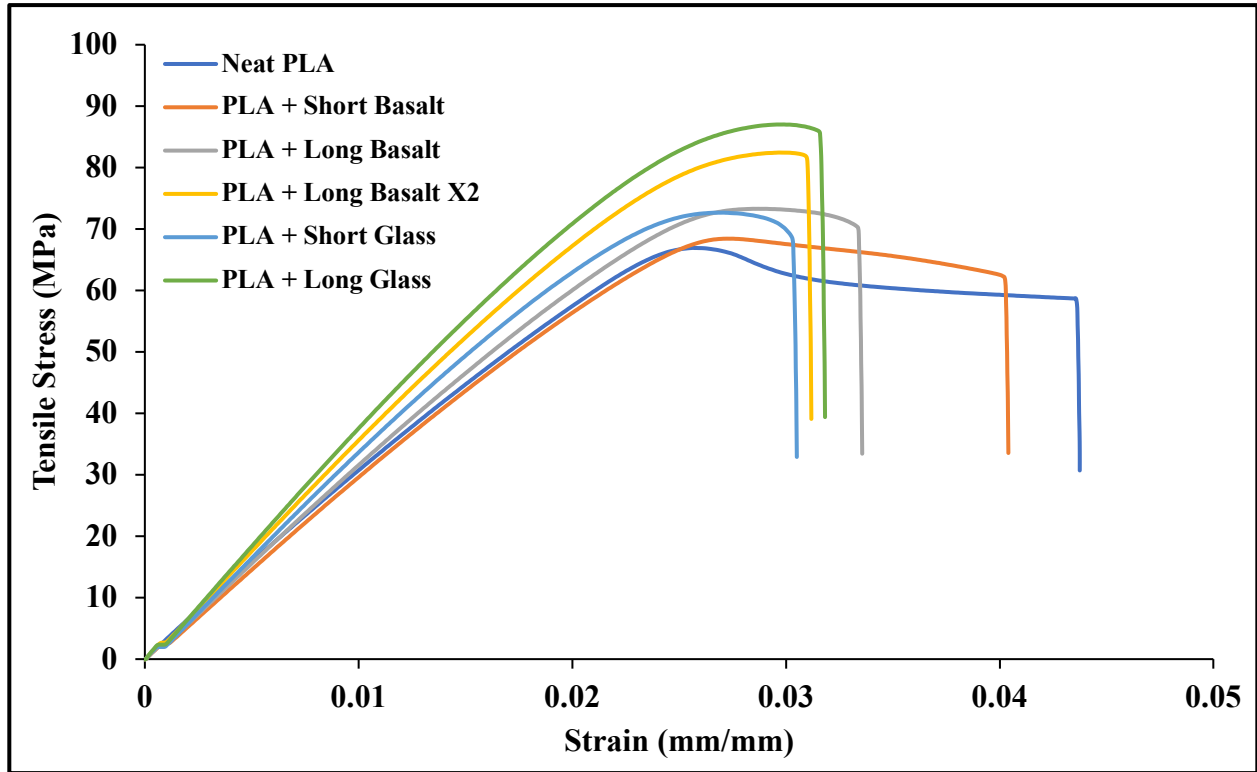


**Figure 5-8:** Comparative stress-strain curves of the composite samples

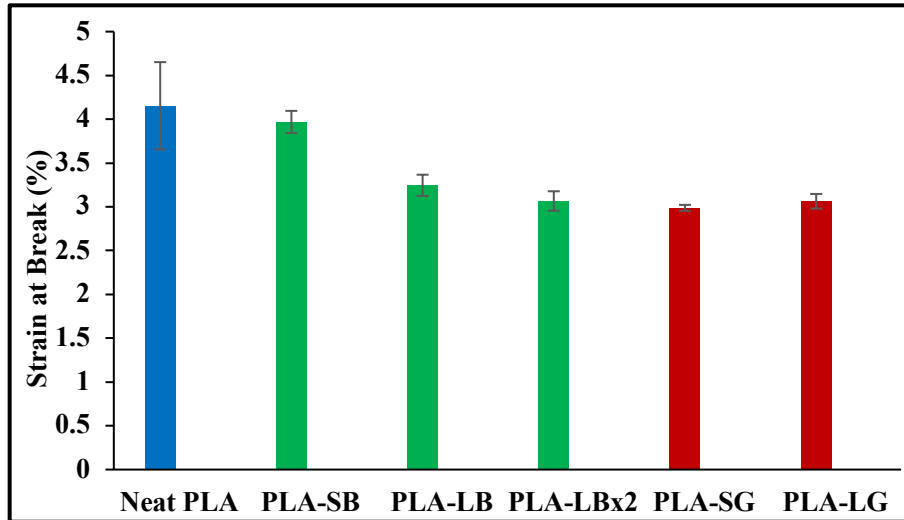


**Figure 5-9:** Strain at break values for the composite samples

The elongation at break, as presented in Figure 5-9, was seen to drop in value with addition of the fiber. This trend was expected since the fibers by themselves have elongation at break values lower than that of neat PLA, and thus would reduce the overall property of the composite.

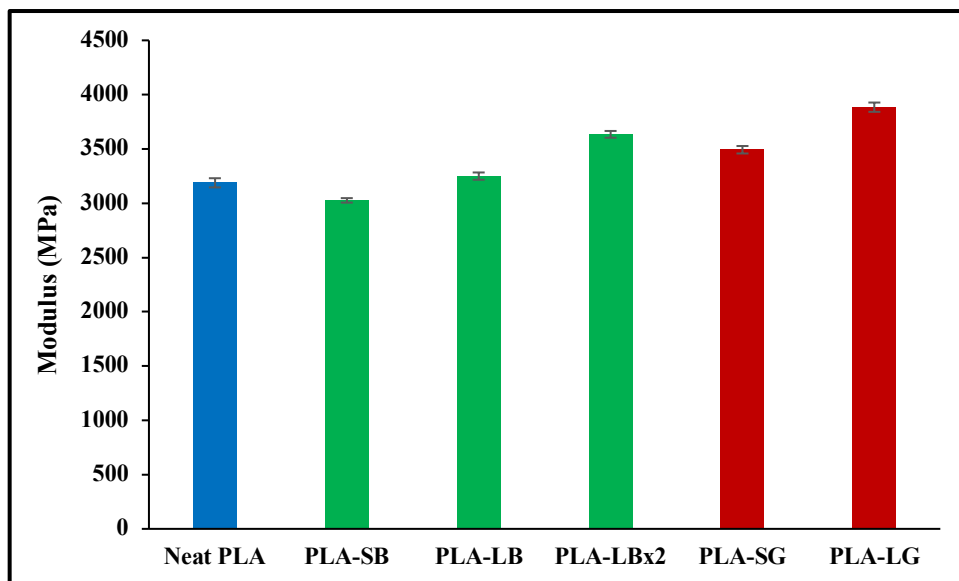


**Figure 5-10:** Tensile moduli of the composite samples

Tensile modulus as shown in Figure 5-10, was found to be dependent on the aspect ratio and the amount of fiber. Comparing the short fiber with their long fiber equivalents, it can be seen that

there is a distinct increase in the modulus of the material. This effect was more pronounced in the glass fiber samples due to higher loading levels.

Three empirical relations were used to predict the tensile modulus of the PLA composite samples. The data from the theoretical predictions were then compared to that obtained experimentally to get additional insight into the type of fiber geometry that exists in a given sample. First, the Halpin-Tsai model for aligned continuous fiber was studied using the following equation [271-273]:

$$E_{HT-ACF} = V_f E_f + (1 - V_f) E_m \quad (\text{Equation 3})$$

where,  $V_f$  is the fiber loading fraction by volume, and  $E_f$  and  $E_m$  are the moduli of the fiber and matrix respectively. The value of  $E_f$  and  $E_m$  used were 88 GPa for basalt, 72 GPa for glass, and 3.18 GPa for the PLA.

Next an inverse-rule-of-mixtures (IROM) model was used via the formula below [237]:

$$E_{IROM} = \left( \frac{V_f}{E_f} + \frac{1-V_f}{E_m} \right)^{-1} \quad (\text{Equation 4})$$

where, the variables indicate the same values as described in the previous step.

Lastly, the Halpin-Tsai model for a randomly oriented short fiber composite sample was used to predict the behavior. The equations for the model are as follows [274]:

$$E = \frac{3}{8} E_L + \frac{5}{8} E_T \quad (\text{Equation 5})$$

$$E_L = E_m \left[ \frac{1 + \left(\frac{2l}{d}\right) \eta_L V_f}{1 - \eta_L V_f} \right] \quad (\text{Equation 6})$$

$$E_T = E_m \left[ \frac{1 + 2\eta_T V_f}{1 - \eta_T V_f} \right] \quad (\text{Equation 7})$$

$$\eta_L = \frac{\left(\frac{E_f}{E_m}\right)^{-1}}{\left(\frac{E_f}{E_m}\right)^{-1} + \left(\frac{2l}{d}\right)} \quad (\text{Equation 8})$$

$$\eta_T = \frac{\left(\frac{E_f}{E_m}\right)^{-1}}{\left(\frac{E_f}{E_m}\right)^{-1} + 2} \quad (\text{Equation 9})$$

Where,  $E_L$  and  $E_T$  represent the longitudinal and transverse moduli,  $\eta_L$  and  $\eta_T$  are constants and  $l/d$  is the aspect ratio of the fiber in the composite sample.

The data obtained from the theoretical predictions were plotted against the experimental data and the behavior was compared. The results are presented in Figure 5-11. It was observed that the closest fit to the experimental data was obtained using the inverse-rule-of-mixtures (IROM) model. The IROM model often indicates the transverse loading of the fiber, thus implying that the fibers were not uniaxially oriented within the final molded part. This remains to be addressed by varying process conditions to obtain samples with even higher aspect ratio which would retain alignment during processing.

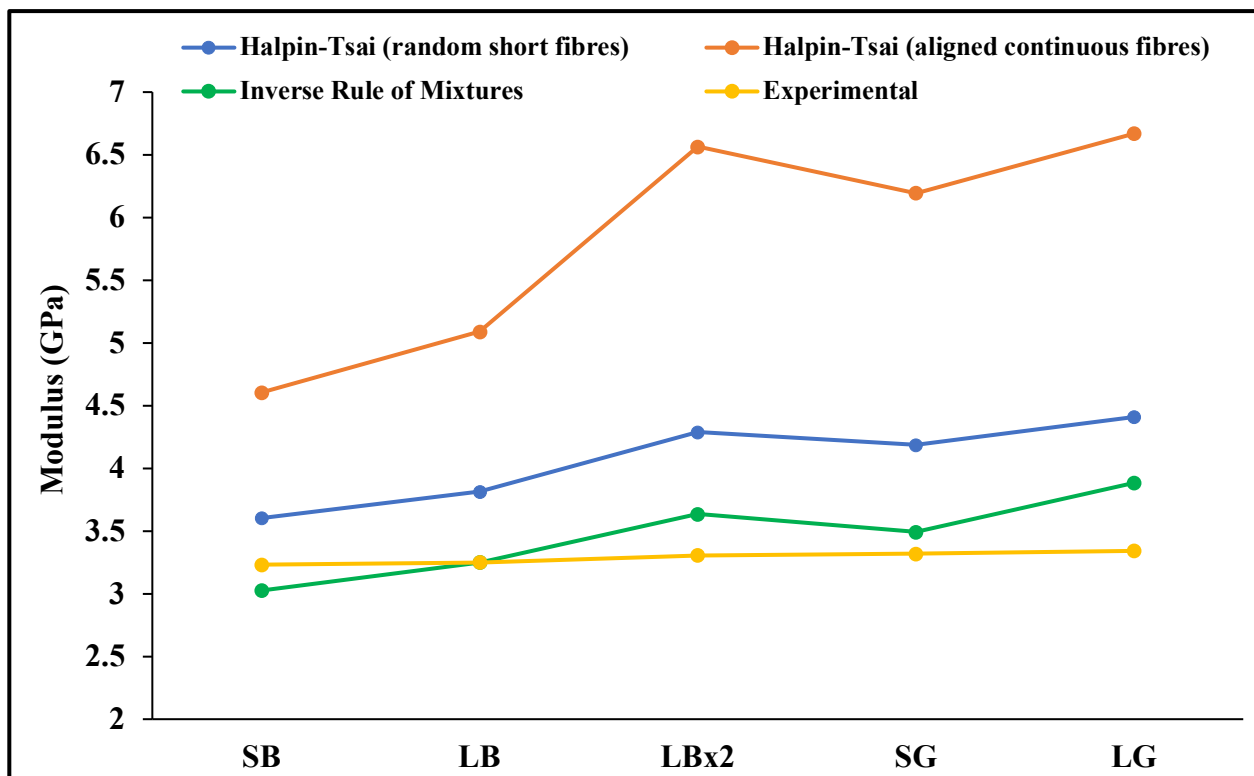


**Figure 5-11:** Comparison of the experimental moduli data with the theoretical predictions using semi-empirical models available in existing literature

The notched Izod impact properties of the samples, shown in Figure 5-12, followed a similar trend to the tensile modulus of the samples, where increase in aspect ratio resulted in an improvement

in the impact strength of the sample. The only exception was the long fiber of the basalt which showed a slight drop. This is mostly attributed to the lower loading level of the fiber in the sample. Again, the long glass fiber sample showed the maximum improvement in the impact properties.

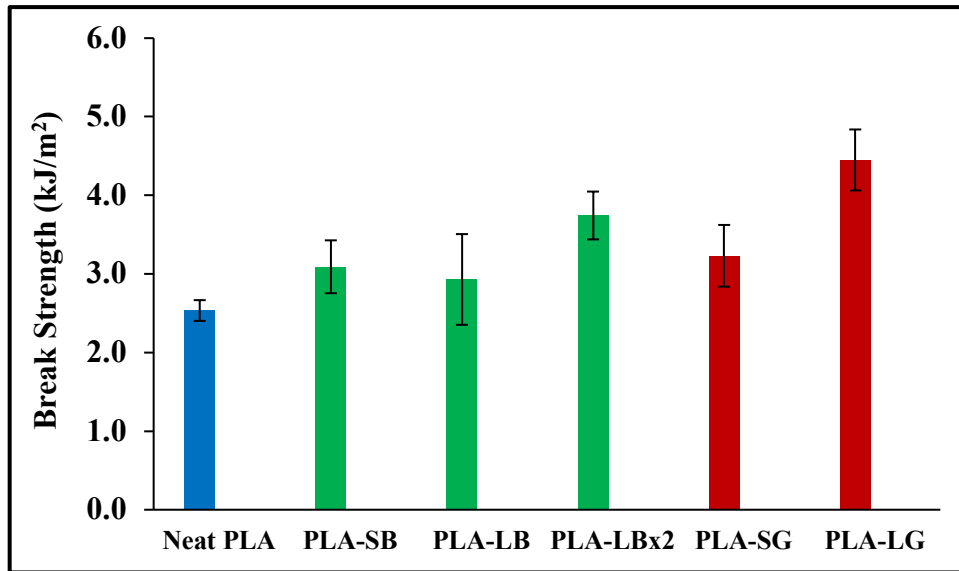


**Figure 5-12:** Impact strength of the composites samples as obtained from notched Izod test

The dynamic mechanical properties of the composite samples were studied as a function of temperature and are presented in Figure 5-13 and Figure 5-14. The trends shown in the tensile and impact studies were mirrored in the dynamic mechanical properties as well. The storage modulus of the samples at room temperature was seen to consistently increase with the increase in aspect ratio of the fibers as well as the amount of fiber loading. There was a sharp drop in the storage modulus values at the heat deflection temperature of PLA at around  $\sim 60^{\circ}\text{C}$ , irrespective of the addition of the fiber.

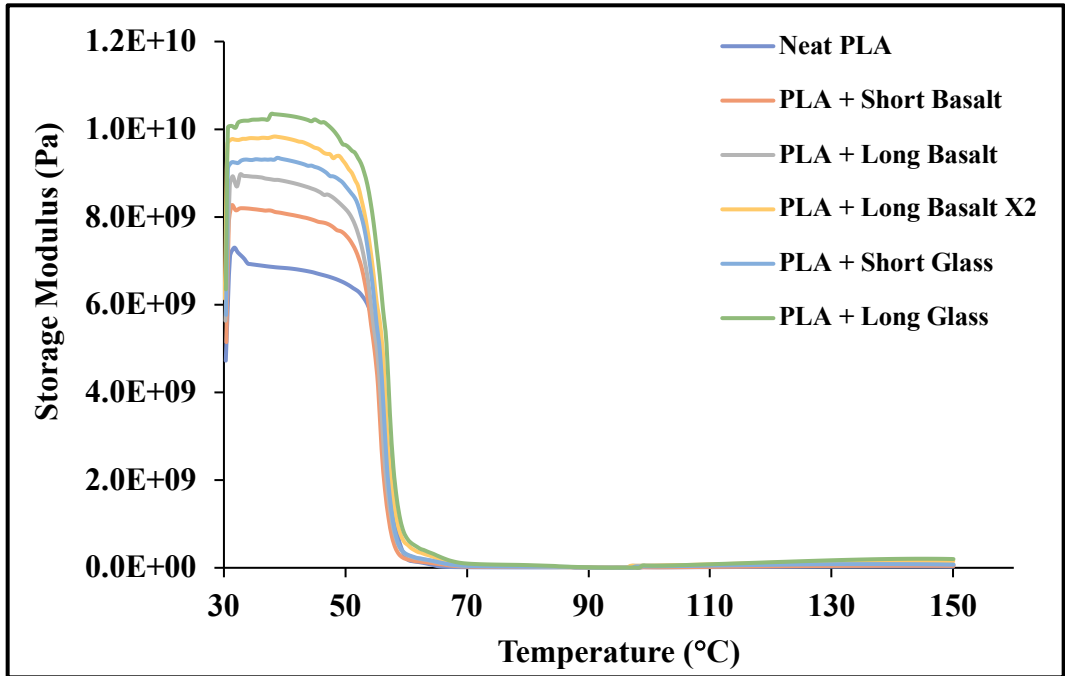


Figure 5-13: Storage moduli for the composite samples as a function of temperature

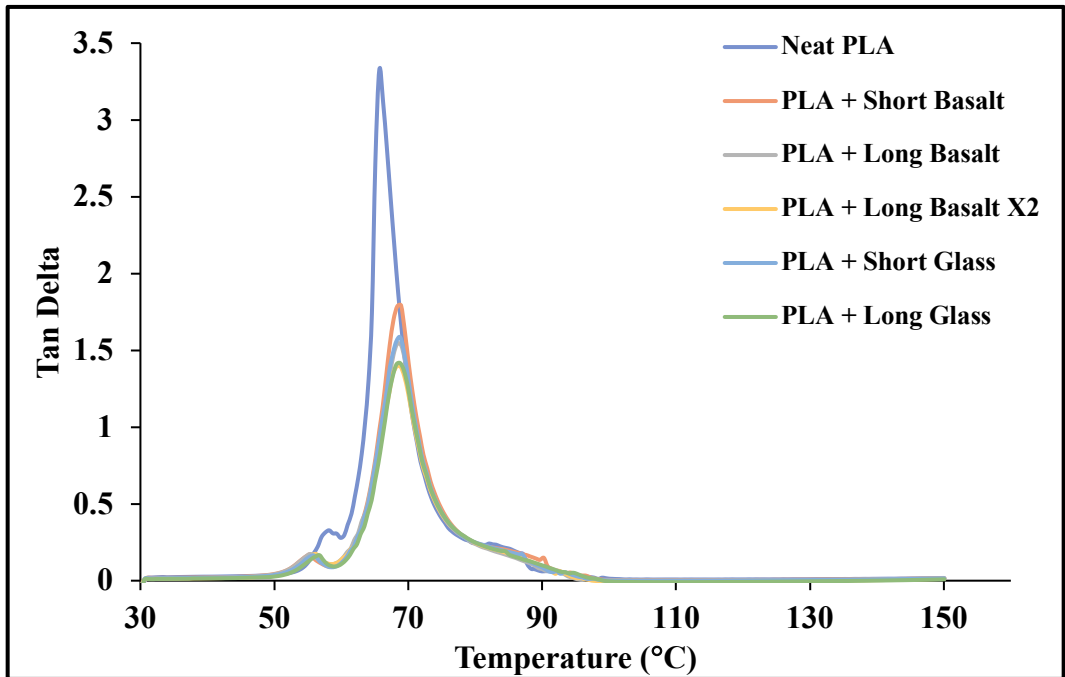
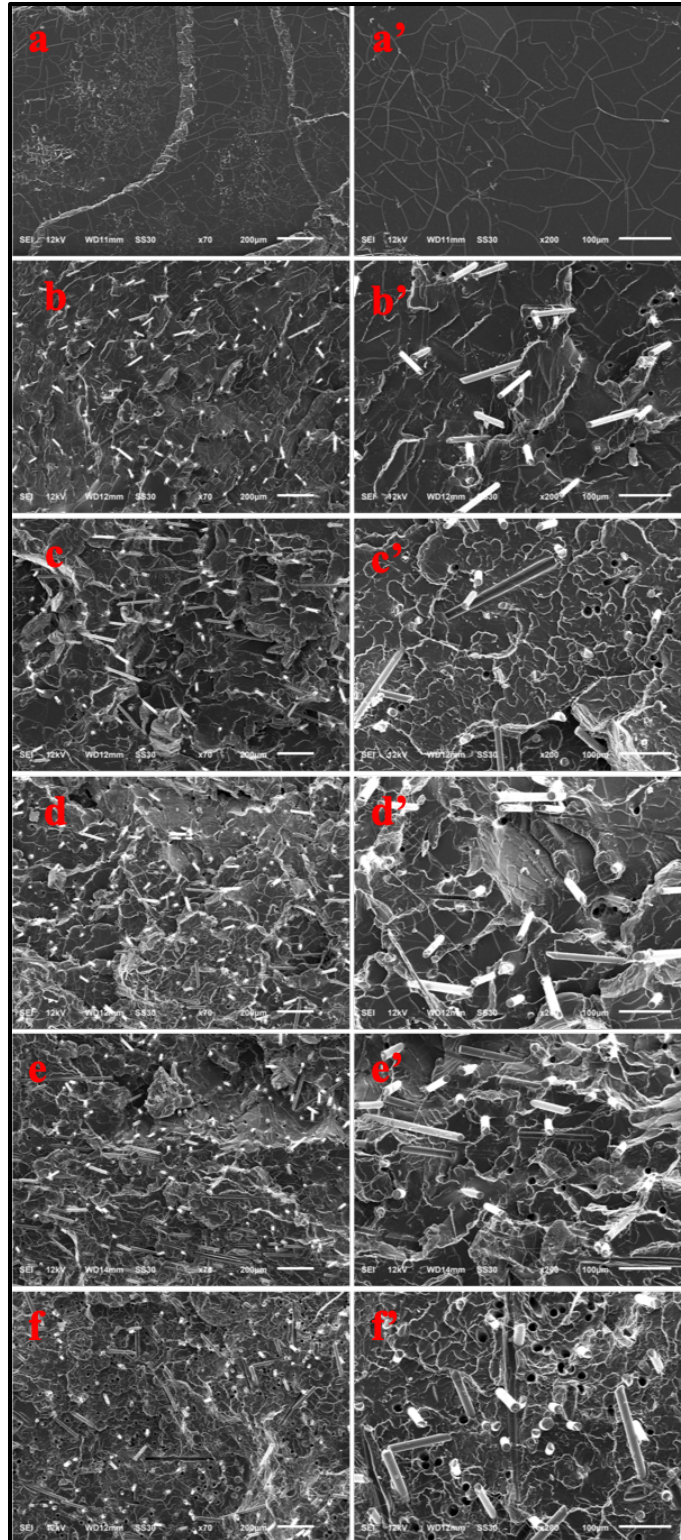


Figure 5-14: Tan Delta for the composite samples as a function of temperature

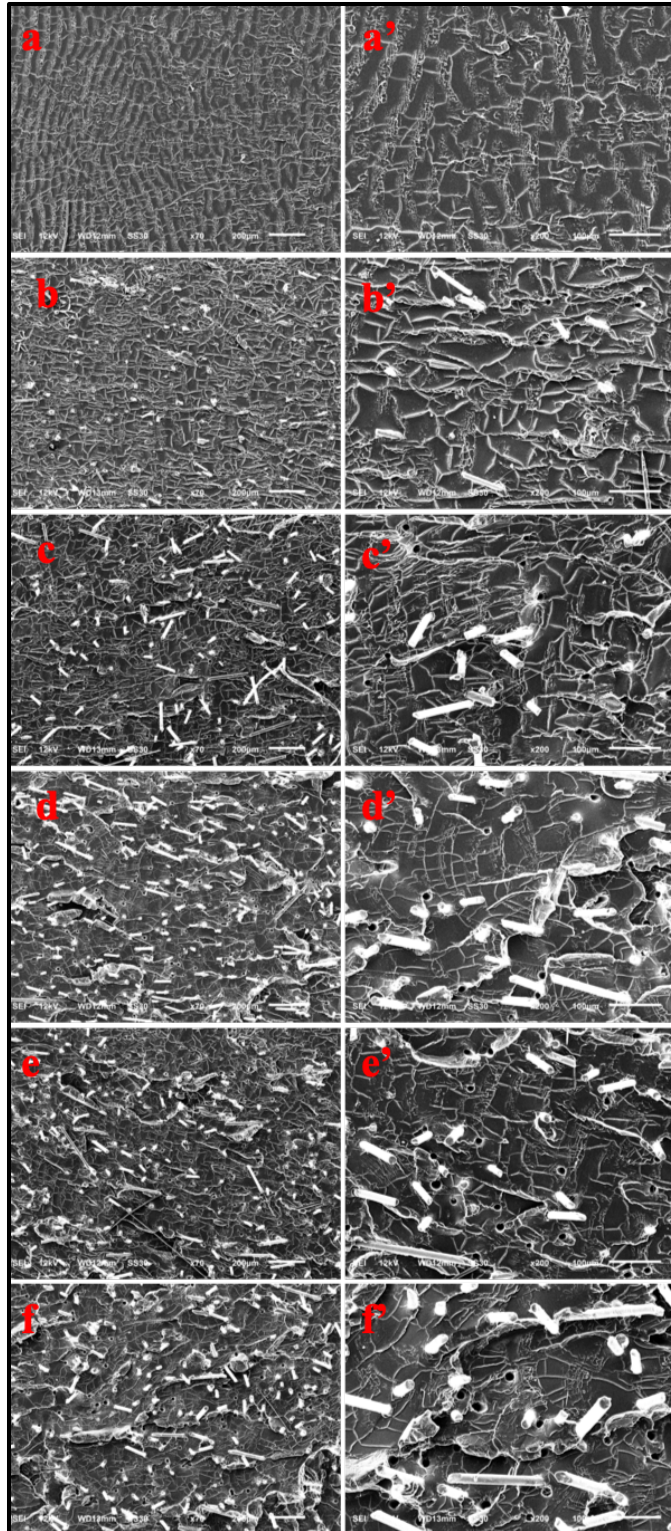
The tan delta plots revealed a marginal increase of about  $\sim 5^{\circ}\text{C}$  in the  $T_g$  of the fiber reinforced PLA samples over neat PLA. The area under the peak for the fiber reinforced samples was found to be significantly lower than that of neat PLA. This is attributed to the fact that chain mobility of the PLA is greatly restricted with the addition of the fiber samples and also signifies less dampening or more elastic behavior, which is in perfect agreement with the tensile and thermal testing performed so far [239, 275-277].

Figure 5-15 and Figure 5-16 show the fracture surface morphologies of the tensile and Izod impact tested samples respectively. For the tensile test specimens, an evolution of a “rougher” surface is observed with the incorporation of the reinforcing fiber indicating a transition to a more ductile fracture. Fiber separation and pullout from the PLA matrix can also be distinctly observed. The separation or pullout is a typical cause for the failure of composite materials [269]. An early separation also indicates poor compatibility between the matrix and fiber that can be improved by using appropriate surface treatments such as chemical sizing on the fibers.

For the notched Izod impact tested samples, significant fibril formation was observed in the direction of propagation of the failure. The fibril formation was increasingly pronounced with increase in fiber content. Similar to the tensile test specimens, fiber pullout and separation from the matrix was observed which was attributed to poor adhesion between the matrix and the fiber.



**Figure 5-15:** SEM images of fracture surfaces of tensile tested samples – (a) neat PLA, (b) SB, (c) LB, (d) LBx2, (e) SG and (f) LG. The images on the left are at a magnification of x70 and the ones on the right are at x200



**Figure 5-16:** SEM images of fracture surfaces of Izod impact tested (impact direction ←) samples – (a) neat PLA, (b) SB, (c) LB, (d) LBx2, (e) SG and (f) LG. The images on the left are at a magnification of x70 and the ones on the right are at x200

## 5.4 Conclusions and Future Work

In conclusion, this study was undertaken with an objective of developing basalt and glass fiber reinforced PLA-based D-LFT composite materials, which was successfully achieved. Optimization of process parameters including screw configuration, point of entry for feeding of the fiber, screw speed and the feed rate of the resin, was performed prior to the synthesis of the PLA composite materials. Along with continuous rovings of the fibers, chopped fibers were also used to serve as a point of comparison in terms of mechanical properties.

Ash testing of the composite samples was performed in order to measure the amount of fiber incorporated during the extrusion processing. With the D-LFT processing samples, loading levels of glass fiber were significantly higher than those for basalt fiber due to a higher linear density of glass fiber roving being used. Fiber length distributions revealed that the aspect ratio was nearly doubled in the case of basalt fibers with the use of the D-LFT technique. Similar improvements were observed for the glass fiber samples; however, the effect was not as pronounced. Thermal properties were largely unchanged due to the incorporation of the fibers apart from a slightly delayed onset of cold crystallization. Mechanical performance characterized by tensile and impact studies revealed a significant improvement in the modulus, tensile strength and impact energy of the D-LFT processed samples due to an increase in aspect ratio over their short fiber counterparts. DMA analyses were found to be in agreement with tensile and DSC data with a steady increase in storage modulus with incorporation of fibers with higher aspect ratios and loading levels.

This work shows great promise in terms of offering a novel, cost-effective method for the fabrication of thermoplastic based fiber reinforced composites with a high aspect ratio. Despite the work done in this study, we feel that we have barely scratched the surface in terms of utilizing the full potential of the D-LFT process. Significantly higher loading levels need to be achieved for the

maximum improvement in properties. This can be done through a combined approach of using a fiber roving with an even higher linear density coupled with appropriate optimization of processing conditions. Specialized screw elements such as the Zahn-Mische element can also be used to improve uptake of the fiber during the feeding [278]. Also, a very critical factor that needs to be evaluated is the role of using a sizing agent best suited for PLA based matrices in order to improve fiber dispersion and adhesion at the fiber-matrix interface.

## 6 SUMMARY AND FUTURE WORK

The work done as a part of this thesis has been solely motivated by the need for development of unique, cost-effective strategies to successfully expand the portfolio of commercial applications of PLA. Four different approaches were used throughout the work in order to achieve that purpose – synthesis of a novel silicone-based modifier to improve toughness, use of a unique biobased plasticizer to impart flexibility, use of epoxy modifiers to enhance melt strength, and last, use of long fiber reinforcements to increase the strength and modulus. Each section of the work was carried out in collaboration with an industrial partner in order to have a viable path towards commercialization.

Chapter 1 focuses on the development of a PLA-PDMS copolymer synthesized via a transesterification chemistry using reactive extrusion as a facile technique. The copolymer was added to neat PLA during the injection molding as an impact modifier. Thermal annealing of the injection molded part resulted in an increase in the percent crystallinity and by extension the heat deflection temperature of the molded part. The addition of the copolymer followed by the subsequent annealing was observed to have an unprecedented synergistic effect on both the tensile and impact toughness of the PLA, which were improved by up to 200 and 500% respectively at a loading level of only 1.5% by weight of the PDMS. This far exceeded the performance requirements for typical applications of injection-molded PLA articles such as single-use cutlery etc. In terms of cost, it had a projected savings of up to 5 cents per pound due to the low amount of modifier needed, which considering economics of scale was quite significant. Further, a model was proposed to explain the unique behavior shown by the annealed PLA-PDMS system. In order to provide a viable route towards commercialization, optimization of molding and annealing

conditions were performed and the use of nucleating agents was explored to convert the two-step process of molding followed by annealing to a one-step process with in-mold annealing.

In Chapter 2, we discuss the use of a biobased mono-functional epoxy modifier derived from cardanol, which in turn is sourced from cashew nut shell liquid (CNSL), thus making the modifier a “green” plasticizer. Reactive extrusion was used for the reaction between the epoxy modifier and PLA resulting in a reduction in the glass transition temperature of the PLA which was reflected in enhanced flexibility of the injection molded PLA specimens. Thermal annealing of these specimens was found to improve heat deflection temperature by  $\sim 20^{\circ}\text{C}$  and the percent crystallinity by  $\sim 100\%$ . The tensile and impact properties of the annealed samples were observed to closely mimic the unique synergistic trend shown by the PLA-PDMS system. The model that was developed in Chapter 1 for the PLA-PDMS system was suitably modified to take into account the behavior of the PLA-epoxy plasticized system. This inexpensive biobased plasticizer showed great promise for replacing conventionally used fossil-fuel based plasticizers such as PEG.

For Chapter 3, multifunctional epoxy-based chain extenders were reactively blended with PLA via twin-screw extrusion to improve the melt strength of PLA for applications in blown films. A petroleum-based epoxy modifier and a biobased substitute derived from cardanol were used for the study. The effects of varying molar ratios of the modifiers to PLA were first evaluated using model compounds to simulate PLA and then validated by reactions with PLA. Two processing techniques – first, by producing a high loading level masterbatch subsequently diluted to the required concentration, and second, producing a direct blend, were studied to observe their impact on final performance properties. Melt strength as characterized using dynamic oscillatory shear and uniaxial extensional viscosity measurements, showed that the fossil-fuel based modifier was highly effective at inducing long-chain branching in the PLA samples, whereas the biobased

modifier was successful at developing linear chain extension in PLA, and thus could be used as a processing aid to recover molecular weight lost during processing.

Lastly, with Chapter 4, the work involved the use of basalt and glass fibers to reinforce the PLA matrix by adopting the Direct-Long Fiber Thermoplastic (D-LFT) approach, wherein continuous rovings of the fibers were directly fed into a twin-screw extruder. The D-LFT technique allowed for a higher aspect ratio of the fiber in the matrix leading to improved load transfer at the fiber-matrix interface. Optimization of the process parameters, including screw configuration, was performed to ensure desired level of fiber breakage and dispersion, and to maximize the fiber content in the final composite material. PLA-based short fiber composites were prepared under similar processing conditions to serve as a comparison to their long fiber counterparts. Fiber length distributions revealed that a higher aspect ratio of fibers was obtained using the D-LFT technique. The implication of this observation was shown to be quite apparent with the mechanical characterization of the fiber reinforced samples which showed that the tensile strength, modulus and impact strength were found to increase significantly with an increase in aspect ratio of the fibers in samples. It was also observed that with equal amounts of fiber being fed, the short fiber samples had a lower level of fiber loading in the final composite material as opposed to the long fibers. This study was the first ever report on producing D-LFT composites in the most cost-effective and scalable manner.

In terms of future work, this thesis serves as a primary guide for the commercial scale-up of each technology developed. In terms of fundamental understanding of polymeric and composite materials, the work offers novelty in two key areas – first, in the development of a model to describe the behavior of two-phase polymeric systems when subjected to thermal annealing, and second, in the design of a unique processing method for incorporating high-aspect ratio reinforcing

fibers in any given thermoplastic matrix. Both of these concepts have never been directly addressed in existing literature thus adding more value to the current work.

The “crystallization induced phase separation” model as initially described in Chapter 1 and then modified in Chapter 3 offers key insights into the behavior of a two-phase polymeric system where one component can undergo crystallization upon heat treatment, whereas the second component possesses sufficient chain mobility to coalesce into a bigger particle size as the first component undergoes crystallization. This phenomenon was observed to have a drastic influence on mechanical properties of the resultant polymer material, resulting in multifold improvements over the properties of the original polymer. Using this model, a number of two-phase polymer systems can be investigated to achieve significant improvements in mechanical performance. Through the use of controlled heating and cooling cycles, the crystallinity of the semi-crystalline polymer domains can be finely tuned to give materials with well-defined microstructures and thus, completely tunable properties depending upon application.

In terms of processing, the D-LFT process described in Chapter 4 can be scaled and optimized for any given combination of fiber and thermoplastic matrix, without the need for specialized equipment of any kind thus eliminating significant capital costs associated with the production of composites. Apart from the general advantages associated with this processing technique, two key areas have been identified which can add significantly more value to the process. First, the existing process can be very easily scaled to produce hybrid composites by using continuous rovings of two different fibers. Hybrid composites are the new frontier in composite materials with applications ranging from automotive parts to aerospace materials [279-283]. These composite materials tend to have superior properties over conventional composites since they use more than one reinforcing fiber to attain synergistic improvements in properties. Our current process has

already been scaled to run two different rovings of fiber with relative ease thus serving as a proof-of-concept for future studies into the development of hybrid composites using this process. The second key area where this processing technique holds promise is the production of in-situ polymer composites, where the fiber is reinforced into the matrix as it undergoes polymerization. There have only been scattered reports of such a processing technique, however, they were prepared in a very small scale using batch reactors and used particulate reinforcements [284, 285]. Using our D-LFT processing technique, a suitable monomeric feed can be introduced upstream in the extruder. Once sufficient polymerization to have a threshold molecular weight has occurred, continuous fiber reinforcements can be introduced, resulting in impregnation of the fiber by the just-polymerized sample. This would of course pose a significant challenge in terms of process optimization, however, through a careful study, this can definitely be achieved making it a pioneering technique to produce continuous fiber reinforced polymers starting with a monomer as feedstock.

As a concluding remark, it would suffice to say that with the completion of this work, a few milestones have been achieved, yet a lot remains to be explored and studied.

## **BIBLIOGRAPHY**

## BIBLIOGRAPHY

1. Neufeld, L., et al. *The new plastics economy: rethinking the future of plastics*. in *World Economic Forum*. 2016.
2. Lebreton, L. and A. Andrady, *Future scenarios of global plastic waste generation and disposal*. Palgrave Communications, 2019. **5**(1): p. 6.
3. Zalasiewicz, J., S. Gabbott, and C.N. Waters. *Plastic Waste: How Plastics Have Become Part of the Earth's Geological Cycle*. in *Waste*. 2019. Elsevier.
4. Jambeck, J.R., et al., *Plastic waste inputs from land into the ocean*. *Science*, 2015. **347**(6223): p. 768-771.
5. Thompson, R.C., et al., *Lost at sea: where is all the plastic?* *Science*, 2004. **304**(5672): p. 838-838.
6. Bergmann, M., M.B. Tekman, and L. Gutow, *Marine litter: Sea change for plastic pollution*. *Nature*, 2017. **544**(7650): p. 297.
7. Ostle, C., et al., *The rise in ocean plastics evidenced from a 60-year time series*. *Nature communications*, 2019. **10**(1): p. 1622.
8. Rillig, M.C., *Microplastic in terrestrial ecosystems and the soil?* 2012, ACS Publications.
9. Vert, M., et al., *Terminology for biorelated polymers and applications (IUPAC Recommendations 2012)*. *Pure and Applied Chemistry*, 2012. **84**(2): p. 377-410.
10. Song, J., et al., *Biodegradable and compostable alternatives to conventional plastics*. *Philosophical transactions of the royal society B: Biological sciences*, 2009. **364**(1526): p. 2127-2139.
11. Gupta, A. and V. Kumar, *New emerging trends in synthetic biodegradable polymers—Polylactide: A critique*. *European polymer journal*, 2007. **43**(10): p. 4053-4074.
12. Drumright, R.E., P.R. Gruber, and D.E. Henton, *Poly(lactic acid) technology*. *Advanced materials*, 2000. **12**(23): p. 1841-1846.
13. Jamshidian, M., et al., *Poly-Lactic Acid: production, applications, nanocomposites, and release studies*. *Comprehensive Reviews in Food Science and Food Safety*, 2010. **9**(5): p. 552-571.
14. Rasal, R.M., A.V. Janorkar, and D.E. Hirt, *Poly (lactic acid) modifications*. *Progress in polymer science*, 2010. **35**(3): p. 338-356.

15. Lim, L.-T., R. Auras, and M. Rubino, *Processing technologies for poly (lactic acid)*. Progress in polymer science, 2008. **33**(8): p. 820-852.
16. Gerald, S., *Green polymers*. Polymer Degradation and Stability, 2000. **68**(1): p. 1-7.
17. Sudesh, K. and T. Iwata, *Sustainability of biobased and biodegradable plastics*. CLEAN–Soil, Air, Water, 2008. **36**(5-6): p. 433-442.
18. Kabasci, S., *Bio-Based Plastics*. 2013: Wiley Online Library.
19. Iwata, T., *Biodegradable and bio-based polymers: future prospects of eco-friendly plastics*. Angewandte Chemie International Edition, 2015. **54**(11): p. 3210-3215.
20. Wool, R. and X.S. Sun, *Bio-based polymers and composites*. 2011: Elsevier.
21. Mülhaupt, R., *Green polymer chemistry and bio-based plastics: dreams and reality*. Macromolecular Chemistry and Physics, 2013. **214**(2): p. 159-174.
22. Hillmyer, M.A., *The promise of plastics from plants*. Science, 2017. **358**(6365): p. 868-870.
23. Garlotta, D., *A literature review of poly (lactic acid)*. Journal of Polymers and the Environment, 2001. **9**(2): p. 63-84.
24. Lunt, J., *Large-scale production, properties and commercial applications of polylactic acid polymers*. Polymer degradation and stability, 1998. **59**(1-3): p. 145-152.
25. Gruber, P.R., et al., *Continuous process for manufacture of lactide polymers with controlled optical purity*. 1992, Google Patents.
26. Kashima, T., et al., *Aliphatic polyester and preparation process thereof*. 1995, Google Patents.
27. Auras, R., *Poly (lactic acid)*. Encyclopedia Of Polymer Science and Technology, 2002.
28. Auras, R.A., et al., *Mechanical, physical, and barrier properties of poly (lactide) films*. Journal of plastic film & sheeting, 2003. **19**(2): p. 123-135.
29. Conn, R., et al., *Safety assessment of polylactide (PLA) for use as a food-contact polymer*. Food and Chemical Toxicology, 1995. **33**(4): p. 273-283.
30. Tokiwa, Y. and B.P. Calabia, *Biodegradability and biodegradation of poly (lactide)*. Applied microbiology and biotechnology, 2006. **72**(2): p. 244-251.
31. Kfoury, G., et al., *Recent advances in high performance poly (lactide): from “green” plasticization to super-tough materials via (reactive) compounding*. Frontiers in chemistry, 2013. **1**: p. 32.

32. Anderson, K.S., K.M. Schreck, and M.A. Hillmyer, *Toughening polylactide*. Polymer Reviews, 2008. **48**(1): p. 85-108.
33. Liu, H. and J. Zhang, *Research progress in toughening modification of poly (lactic acid)*. Journal of polymer science part B: Polymer Physics, 2011. **49**(15): p. 1051-1083.
34. Nampoothiri, K.M., N.R. Nair, and R.P. John, *An overview of the recent developments in polylactide (PLA) research*. Bioresource technology, 2010. **101**(22): p. 8493-8501.
35. Callister, W.D. and D.G. Rethwisch, *Materials science and engineering: an introduction*. Vol. 7. 2007: John Wiley & Sons New York.
36. Perego, G., G.D. Cella, and C. Bastioli, *Effect of molecular weight and crystallinity on poly (lactic acid) mechanical properties*. Journal of Applied Polymer Science, 1996. **59**(1): p. 37-43.
37. Vainio, M.H., T. Karjalainen, and J. Seppala, *Biodegradable lactone copolymers. I. Characterization and mechanical behavior of epsilon-caprolactone and lactide copolymers*. J. Appl. Polym. Sci, 1996. **59**(1281): p. e1288.
38. Haynes, D., et al., *In situ copolyesters containing poly (L-lactide) and poly (hydroxyalkanoate) units*. Biomacromolecules, 2007. **8**(4): p. 1131-1137.
39. Luo, W., et al., *Synthesis and characterization of poly (L-lactide)-poly (ethylene glycol) multiblock copolymers*. Journal of Applied Polymer Science, 2002. **84**(9): p. 1729-1736.
40. Broz, M., D.L. VanderHart, and N. Washburn, *Structure and mechanical properties of poly (D, L-lactic acid)/poly (ε-caprolactone) blends*. Biomaterials, 2003. **24**(23): p. 4181-4190.
41. Noda, I., et al., *Polymer alloys of Nodax copolymers and poly (lactic acid)*. Macromolecular bioscience, 2004. **4**(3): p. 269-275.
42. Harada, M., et al., *Increased impact strength of biodegradable poly (lactic acid)/poly (butylene succinate) blend composites by using isocyanate as a reactive processing agent*. Journal of Applied Polymer Science, 2007. **106**(3): p. 1813-1820.
43. Anderson, K.S., S.H. Lim, and M.A. Hillmyer, *Toughening of polylactide by melt blending with linear low-density polyethylene*. Journal of Applied Polymer Science, 2003. **89**(14): p. 3757-3768.
44. Raquez, J.M., R. Narayan, and P. Dubois, *Recent advances in reactive extrusion processing of biodegradable polymer-based compositions*. Macromolecular Materials and Engineering, 2008. **293**(6): p. 447-470.
45. Xanthos, M., *Reactive extrusion: principles and practice*. Hanser Publishers(Germany), 1992, 1992: p. 304.

46. Dubois, P. and R. Narayan. *Biodegradable compositions by reactive processing of aliphatic polyester/polysaccharide blends*. in *Macromolecular Symposia*. 2003. Wiley Online Library.
47. Tzoganakis, C., *Reactive extrusion of polymers: a review*. Advances in Polymer Technology: Journal of the Polymer Processing Institute, 1989. **9**(4): p. 321-330.
48. Crawford, D.E., *Extrusion—back to the future: Using an established technique to reform automated chemical synthesis*. Beilstein journal of organic chemistry, 2017. **13**(1): p. 65-75.
49. Raquez, J.-M., et al., *Biodegradable materials by reactive extrusion: from catalyzed polymerization to functionalization and blend compatibilization*. Comptes Rendus Chimie, 2006. **9**(11-12): p. 1370-1379.
50. Formela, K., et al., *Reactive extrusion of bio-based polymer blends and composites-Current trends and future developments*. Express Polymer Letters, 2018. **12**(1).
51. Kfoury, G., et al., *Recent advances in high performance poly (lactide): from “green” plasticization to super-tough materials via (reactive) compounding*. Frontiers in chemistry, 2013. **1**.
52. Nagarajan, V., A.K. Mohanty, and M. Misra, *Perspective on polylactic acid (PLA) based sustainable materials for durable applications: Focus on toughness and heat resistance*. ACS Sustainable Chemistry & Engineering, 2016. **4**(6): p. 2899-2916.
53. Colas, A., *Silicones: Preparation, properties and performance*. Dow Corning, Life Sciences, 2005.
54. Owen, M., *Why silicones behave funny*. Chimie nouvelle, 2004(85): p. 27-33.
55. Rodwogin, M.D., et al., *Polylactide– poly (dimethylsiloxane)– polylactide triblock copolymers as multifunctional materials for nanolithographic applications*. ACS nano, 2010. **4**(2): p. 725-732.
56. Tzoganakis, C., *Reactive extrusion of polymers: a review*. Advances in Polymer Technology, 1989. **9**(4): p. 321-330.
57. Turng, L.-S. and Y. Srithep, *Annealing conditions for injection-molded poly (lactic acid)*. Soc. Plast. Eng. Plast. Res., 2014: p. 4.
58. Shi, X., *Design and Engineering of Biobased Materials--Process Engineering & Thermal Recycling of Poly (lactic Acid), and Studies in Functional Silane and Siloxanes*. 2014.
59. Hazer, B., et al., *Synthesis of polylactide-b-poly (dimethyl siloxane) block copolymers and their blends with pure polylactide*. Journal of Polymers and the Environment, 2012. **20**(2): p. 477-484.

60. Khan, M.S., et al., *Physical and tribological properties of PTFE micropowder-filled EPDM rubber*. Tribology International, 2009. **42**(6): p. 890-896.
61. ASTM, D. 2765-01: *Standard Test Methods for Determination of Gel Content and Swell Ratio of Crosslinked Ethylene Plastics*. in *American Society for testing and materials*. 2001.
62. Schneider, J.S., *Design of biobased and biodegradable-compostable engineered plastics based on poly (lactide)*. 2016: Michigan State University.
63. Pretsch, E., et al., *Structure determination of organic compounds*. 2000: Springer.
64. Boehm, P., M. Mondeshki, and H. Frey, *Polysiloxane-Backbone Block Copolymers in a One-Pot Synthesis: A Silicone Platform for Facile Functionalization*. Macromolecular rapid communications, 2012. **33**(21): p. 1861-1867.
65. Nofar, M., et al., *Crystallization kinetics of linear and long-chain-branched polylactide*. Industrial & engineering chemistry research, 2011. **50**(24): p. 13789-13798.
66. Yang, G., et al., *Toughening of poly (L-lactic acid) by annealing: the effect of crystal morphologies and modifications*. Journal of Macromolecular Science, Part B, 2012. **51**(1): p. 184-196.
67. Gamez-Perez, J., et al., *Influence of crystallinity on the fracture toughness of poly (lactic acid)/montmorillonite nanocomposites prepared by twin-screw extrusion*. Journal of applied polymer science, 2011. **120**(2): p. 896-905.
68. Harris, A.M. and E.C. Lee, *Improving mechanical performance of injection molded PLA by controlling crystallinity*. Journal of applied polymer science, 2008. **107**(4): p. 2246-2255.
69. Park, S.-D., M. Todo, and K. Arakawa, *Effect of annealing on the fracture toughness of poly (lactic acid)*. Journal of materials Science, 2004. **39**(3): p. 1113-1116.
70. Bai, H., et al., *Toughening of poly (L-lactide) with poly ( $\epsilon$ -caprolactone): Combined effects of matrix crystallization and impact modifier particle size*. Polymer, 2013. **54**(19): p. 5257-5266.
71. Ge, F., X. Wang, and X. Ran, *Effect of annealing on the properties of polylactide/poly (butylene carbonate) blend*. Advances in Polymer Technology, 2016.
72. Takayama, T., M. Todo, and H. Tsuji, *Effect of annealing on the mechanical properties of PLA/PCL and PLA/PCL/LTI polymer blends*. Journal of the mechanical behavior of biomedical materials, 2011. **4**(3): p. 255-260.
73. Chou, P., et al., *Changes in the crystallinity and mechanical properties of poly (l-lactic acid)/poly (butylene succinate-co-l-lactate) blend with annealing process*. Polymer bulletin, 2011. **67**(5): p. 815-830.

74. Wang, S., et al., *Isothermal Cold Crystallization, Heat Resistance, and Tensile Performance of Polylactide/Thermoplastic Polyester Elastomer (PLA/TPEE) Blends: Effects of Annealing and Reactive Compatibilizer*. *Polymers*, 2016. **8**(12): p. 417.
75. Lin, L., et al., *Super toughened and high heat-resistant poly (lactic acid)(PLA)-based blends by enhancing interfacial bonding and PLA phase crystallization*. *Industrial & Engineering Chemistry Research*, 2015. **54**(21): p. 5643-5655.
76. Oyama, H.T., *Super-tough poly (lactic acid) materials: Reactive blending with ethylene copolymer*. *Polymer*, 2009. **50**(3): p. 747-751.
77. Bai, H., et al., *Tailoring impact toughness of poly (L-lactide)/poly ( $\epsilon$ -caprolactone)(PLLA/PCL) blends by controlling crystallization of PLLA matrix*. *ACS applied materials & interfaces*, 2012. **4**(2): p. 897-905.
78. Zhang, J., et al., *Crystal modifications and thermal behavior of poly (L-lactic acid) revealed by infrared spectroscopy*. *Macromolecules*, 2005. **38**(19): p. 8012-8021.
79. Pothan, L.A., Z. Oommen, and S. Thomas, *Dynamic mechanical analysis of banana fiber reinforced polyester composites*. *Composites Science and Technology*, 2003. **63**(2): p. 283-293.
80. Li, Y. and H. Shimizu, *Toughening of polylactide by melt blending with a biodegradable poly (ether) urethane elastomer*. *Macromolecular bioscience*, 2007. **7**(7): p. 921-928.
81. Feng, F. and L. Ye, *Morphologies and mechanical properties of polylactide/thermoplastic polyurethane elastomer blends*. *Journal of Applied Polymer Science*, 2011. **119**(5): p. 2778-2783.
82. Todo, M., et al., *Fracture micromechanisms of bioabsorbable PLLA/PCL polymer blends*. *Engineering Fracture Mechanics*, 2007. **74**(12): p. 1872-1883.
83. Haafiz, M.M., et al., *Properties of polylactic acid composites reinforced with oil palm biomass microcrystalline cellulose*. *Carbohydrate polymers*, 2013. **98**(1): p. 139-145.
84. Harnisch, K. and H. Muschik, *Determination of the Avrami exponent of partially crystallized polymers by DSC-(DTA-) analyses*. *Colloid and Polymer Science*, 1983. **261**(11): p. 908-913.
85. Schmidt, S.C. and M.A. Hillmyer, *Polylactide stereocomplex crystallites as nucleating agents for isotactic polylactide*. *Journal of Polymer Science Part B: Polymer Physics*, 2001. **39**(3): p. 300-313.
86. Chang, L. and E.M. Woo, *Crystallization of poly (3-hydroxybutyrate) with stereocomplexed polylactide as biodegradable nucleation agent*. *Polymer Engineering & Science*, 2012. **52**(7): p. 1413-1419.

87. Huang, Y.-Y., et al., *Crystallization-induced microdomain coalescence in sphere-forming crystalline– amorphous diblock copolymer systems: neat diblock versus the corresponding blends*. *Macromolecules*, 2004. **37**(2): p. 486-493.
88. Shabana, H., et al., *Phase separation induced by crystallization in blends of polycaprolactone and polystyrene: an investigation by etching and electron microscopy*. *Polymer*, 2000. **41**(14): p. 5513-5523.
89. Sharma, M., G. Madras, and S. Bose, *Unique nanoporous antibacterial membranes derived through crystallization induced phase separation in PVDF/PMMA blends*. *Journal of Materials Chemistry A*, 2015. **3**(11): p. 5991-6003.
90. Zhao, K., et al., *Crystallization-Induced Phase Segregation Based on Double-Crystalline Blends of Poly (3-hexylthiophene) and Poly (ethylene glycol) s*. *Macromolecular rapid communications*, 2010. **31**(6): p. 532-538.
91. Wu, S., *A generalized criterion for rubber toughening: the critical matrix ligament thickness*. *Journal of Applied Polymer Science*, 1988. **35**(2): p. 549-561.
92. Grijpma, D., et al., *Rubber toughening of poly (lactide) by blending and block copolymerization*. *Polymer Engineering & Science*, 1994. **34**(22): p. 1674-1684.
93. Wu, S., *Phase structure and adhesion in polymer blends: a criterion for rubber toughening*. *Polymer*, 1985. **26**(12): p. 1855-1863.
94. Karan, H., et al., *Green bioplastics as part of a circular bioeconomy*. *Trends in plant science*, 2019.
95. Sangeetha, V., et al., *State of the art and future prospectives of poly (lactic acid) based blends and composites*. *Polymer composites*, 2018. **39**(1): p. 81-101.
96. Di Lorenzo, M.L. and R. Androsch, *Industrial Applications of Poly (lactic acid)*. Vol. 282. 2018: Springer.
97. Wang, M., et al., *Progress in toughening poly (lactic acid) with renewable polymers*. *Polymer Reviews*, 2017. **57**(4): p. 557-593.
98. Bhardwaj, R. and A.K. Mohanty, *Advances in the properties of polylactides based materials: a review*. *Journal of Biobased Materials and Bioenergy*, 2007. **1**(2): p. 191-209.
99. Williams, C.K. and M.A. Hillmyer, *Polymers from renewable resources: a perspective for a special issue of polymer reviews*. *Polymer reviews*, 2008. **48**(1): p. 1-10.
100. Immergut, E.H. and H.F. Mark, *Principles of Plasticization, in <bold>Plasticization</bold> and Plasticizer Processes*. 1965, AMERICAN CHEMICAL SOCIETY. p. 1-26.

101. Reinecke, H., R. Navarro, and M. Pérez, *Plasticizers*. Encyclopedia of Polymer Science and Technology, 2002.
102. Frith, E.M. and R. Tuckett, *Polymer-Plasticizer Interaction*. Nature, 1945. **155**(3928): p. 164.
103. Santos, E.F., et al., *Sunflower-oil biodiesel-oligoesters/poly lactide blends: Plasticizing effect and ageing*. Polymer Testing, 2014. **39**: p. 23-29.
104. Ljungberg, N., T. Andersson, and B. Wesslén, *Film extrusion and film weldability of poly (lactic acid) plasticized with triacetine and tributyl citrate*. Journal of Applied Polymer Science, 2003. **88**(14): p. 3239-3247.
105. Ljungberg, N. and B. Wesslen, *The effects of plasticizers on the dynamic mechanical and thermal properties of poly (lactic acid)*. Journal of Applied Polymer Science, 2002. **86**(5): p. 1227-1234.
106. Murariu, M., et al., *Poly lactide (PLA) designed with desired end-use properties: 1. PLA compositions with low molecular weight ester-like plasticizers and related performances*. Polymers for Advanced Technologies, 2008. **19**(6): p. 636-646.
107. Höglund, A., M. Hakkarainen, and A.-C. Albertsson, *Migration and hydrolysis of hydrophobic poly lactide plasticizer*. Biomacromolecules, 2009. **11**(1): p. 277-283.
108. Azwar, E., B. Yin, and M. Hakkarainen, *Liquefied biomass derived plasticizer for poly lactide*. Journal of Chemical Technology & Biotechnology, 2013. **88**(5): p. 897-903.
109. Arias, V., et al., *Poly lactides with "green" plasticizers: Influence of isomer composition*. Journal of Applied Polymer Science, 2013. **130**(4): p. 2962-2970.
110. Jia, Z., et al., *Poly (ethylene glycol-co-propylene glycol) as a macromolecular plasticizing agent for poly lactide: Thermomechanical properties and aging*. Journal of applied polymer science, 2009. **114**(2): p. 1105-1117.
111. Kowalczyk, M., et al., *Plasticization of poly lactide with block copolymers of ethylene glycol and propylene glycol*. Journal of Applied Polymer Science, 2012. **125**(6): p. 4292-4301.
112. Ruellan, A., et al., *Solubility factors as screening tools of biodegradable toughening agents of poly lactide*. Journal of Applied Polymer Science, 2015. **132**(48).
113. Zhang, H., et al., *Influence of acrylic impact modifier on plasticized poly lactide blown films*. Polymer International, 2014. **63**(6): p. 1076-1084.
114. Shirai, M., et al., *Development of biodegradable flexible films of starch and poly (lactic acid) plasticized with adipate or citrate esters*. Carbohydrate polymers, 2013. **92**(1): p. 19-22.

115. Ljungberg, N. and B. Wesslen, *Tributyl citrate oligomers as plasticizers for poly (lactic acid): thermo-mechanical film properties and aging*. *Polymer*, 2003. **44**(25): p. 7679-7688.
116. Hassouna, F., et al., *New development on plasticized poly (lactide): chemical grafting of citrate on PLA by reactive extrusion*. *European Polymer Journal*, 2012. **48**(2): p. 404-415.
117. Wang, K., et al., *Strain-induced deformation mechanisms of polylactide plasticized with acrylated poly (ethylene glycol) obtained by reactive extrusion*. *Polymer International*, 2015. **64**(11): p. 1544-1554.
118. Hassouna, F., et al., *New approach on the development of plasticized polylactide (PLA): Grafting of poly (ethylene glycol)(PEG) via reactive extrusion*. *European Polymer Journal*, 2011. **47**(11): p. 2134-2144.
119. Caillol, S., *Cardanol: A promising building block for biobased polymers and additives*. *Current opinion in green and sustainable chemistry*, 2018. **14**: p. 26-32.
120. Greco, A. and A. Maffezzoli, *Cardanol derivatives as innovative bio-plasticizers for poly-(lactic acid)*. *Polymer Degradation and Stability*, 2016. **132**: p. 213-219.
121. Greco, A., F. Ferrari, and A. Maffezzoli, *Mechanical properties of poly (lactid acid) plasticized by cardanol derivatives*. *Polymer Degradation and Stability*, 2019. **159**: p. 199-204.
122. Greco, A., F. Ferrari, and A. Maffezzoli, *Thermal analysis of poly (lactic acid) plasticized by cardanol derivatives*. *Journal of Thermal Analysis and Calorimetry*, 2018. **134**(1): p. 559-565.
123. Hassouma, F., et al., *Design of new cardanol derivative: synthesis and application as potential biobased plasticizer for poly (lactide)*. *Macromolecular Materials and Engineering*, 2016. **301**(10): p. 1267-1278.
124. Rigoussen, A., et al., *In-depth investigation on the effect and role of cardanol in the compatibilization of PLA/ABS immiscible blends by reactive extrusion*. *European Polymer Journal*, 2017. **93**: p. 272-283.
125. Siparsky, G.L., K.J. Voorhees, and F. Miao, *Hydrolysis of polylactic acid (PLA) and polycaprolactone (PCL) in aqueous acetonitrile solutions: autocatalysis*. *Journal of environmental polymer degradation*, 1998. **6**(1): p. 31-41.
126. International, A., *ASTM D638-14, Standard Test Method for Tensile Properties of Plastics*. 2015: ASTM International.
127. Haralabakopoulos, A., D. Tsiourvas, and C. Paleos, *Chain extension of poly (ethylene terephthalate) by reactive blending using diepoxides*. *Journal of applied polymer science*, 1999. **71**(13): p. 2121-2127.

128. Nguyen, Q.T., et al., *Molecular characterization and rheological properties of modified poly (ethylene terephthalate) obtained by reactive extrusion*. Polymer Engineering & Science, 2001. **41**(8): p. 1299-1309.
129. Japon, S., et al., *Reactive processing of poly (ethylene terephthalate) modified with multifunctional epoxy-based additives*. Polymer, 2000. **41**(15): p. 5809-5818.
130. Corre, Y.-M., et al., *Melt strengthening of poly (lactic acid) through reactive extrusion with epoxy-functionalized chains*. Rheologica Acta, 2011. **50**(7-8): p. 613-629.
131. Giri, P., C. Tambe, and R. Narayan, *Using Reactive Extrusion To Manufacture Greener Products: From Laboratory Fundamentals to Commercial Scale, in Biomass Extrusion and Reaction Technologies: Principles to Practices and Future Potential*. 2018, American Chemical Society. p. 1-23.
132. Bikiaris, D.N. and G.P. Karayannidis, *Chain extension of polyesters PET and PBT with two new diimidodiepoxides. II*. Journal of Polymer Science Part A: Polymer Chemistry, 1996. **34**(7): p. 1337-1342.
133. Najafi, N., et al., *Control of thermal degradation of polylactide (PLA)-clay nanocomposites using chain extenders*. Polymer Degradation and Stability, 2012. **97**(4): p. 554-565.
134. Meng, Q., M.-C. Heuzey, and P.J. Carreau, *Control of thermal degradation of polylactide/clay nanocomposites during melt processing by chain extension reaction*. Polymer degradation and stability, 2012. **97**(10): p. 2010-2020.
135. Schneider, J., et al., *Epoxy functionalized poly (lactide) reactive modifier for blown film applications*. Journal of Applied Polymer Science, 2015. **132**(28).
136. Schneider, J., S. Manjure, and R. Narayan, *Reactive modification and compatibilization of poly (lactide) and poly (butylene adipate-co-terephthalate) blends with epoxy functionalized-poly (lactide) for blown film applications*. Journal of Applied Polymer Science, 2016. **133**(16).
137. Coates, J., *Interpretation of infrared spectra, a practical approach*. Encyclopedia of analytical chemistry: applications, theory and instrumentation, 2006.
138. Tavassoli-Kafrani, M.H., F.R. van de Voort, and J.M. Curtis, *The use of ATR-FTIR spectroscopy to measure changes in the oxirane content and iodine value of vegetable oils during epoxidation*. European Journal of Lipid Science and Technology, 2017. **119**(7): p. 1600354.
139. Patterson, W., *Infrared Absorption Bands Characteristic of Oxirane Ring*. Analytical Chemistry, 1954. **26**(5): p. 823-835.
140. Ikeda, R., et al., *A new crosslinkable polyphenol from a renewable resource*. Macromolecular Rapid Communications, 2000. **21**(8): p. 496-499.

141. Rocks, J., et al., *The kinetics and mechanism of cure of an amino-glycidyl epoxy resin by a co-anhydride as studied by FT-Raman spectroscopy*. Polymer, 2004. **45**(20): p. 6799-6811.
142. Jalila, E.A., N. EL-Aouni, and A.E. Harf, *SYNTHESIS, STRUCTURAL CHARACTERIZATION BY NMR AND IR AND RHEOLOGICAL STUDY OF EPOXY RESIN OCTAFUNCTIONAL*. Moroccan Journal of Chemistry. **4**(1): p. 4-1 (2016) 14-23.
143. González, M.G., J.C. Cabanelas, and J. Baselga, *Applications of FTIR on epoxy resins-identification, monitoring the curing process, phase separation and water uptake*, in *Infrared Spectroscopy-Materials Science, Engineering and Technology*. 2012, IntechOpen.
144. Kim, Y.H., et al., *Enzymatic epoxidation and polymerization of cardanol obtained from a renewable resource and curing of epoxide-containing polycardanol*. Journal of Molecular Catalysis B: Enzymatic, 2007. **45**(1-2): p. 39-44.
145. Jaillet, F., et al., *New biobased epoxy materials from cardanol*. European Journal of Lipid Science and Technology, 2014. **116**(1): p. 63-73.
146. Byun, Y., Y.T. Kim, and S. Whiteside, *Characterization of an antioxidant polylactic acid (PLA) film prepared with  $\alpha$ -tocopherol, BHT and polyethylene glycol using film cast extruder*. Journal of Food Engineering, 2010. **100**(2): p. 239-244.
147. Pillin, I., N. Montrelay, and Y. Grohens, *Thermo-mechanical characterization of plasticized PLA: Is the miscibility the only significant factor?* Polymer, 2006. **47**(13): p. 4676-4682.
148. Kulinski, b. and E. Piorkowska, *Crystallization, structure and properties of plasticized poly (L-lactide)*. Polymer, 2005. **46**(23): p. 10290-10300.
149. Srithep, Y., P. Nealey, and L.S. Turng, *Effects of annealing time and temperature on the crystallinity and heat resistance behavior of injection-molded poly (lactic acid)*. Polymer Engineering & Science, 2013. **53**(3): p. 580-588.
150. Tang, Z., et al., *The crystallization behavior and mechanical properties of polylactic acid in the presence of a crystal nucleating agent*. Journal of Applied Polymer Science, 2012. **125**(2): p. 1108-1115.
151. Yu, L., et al., *Effect of annealing and orientation on microstructures and mechanical properties of polylactic acid*. Polymer Engineering & Science, 2008. **48**(4): p. 634-641.
152. Asadi, V., et al., *Incorporation of inorganic fullerene-like WS 2 into poly (ethylene succinate) to prepare novel biodegradable nanocomposites: A study on isothermal and dynamic crystallization*. RSC Advances, 2016. **6**(6): p. 4925-4935.
153. Zheng, W., et al., *Poly (lactic acid)/montmorillonite blown films: Crystallization, mechanics, and permeation*. Journal of Applied Polymer Science, 2017. **134**(36): p. 45260.

154. Andjelić, S. and R.C. Scogna, *Polymer crystallization rate challenges: the art of chemistry and processing*. Journal of Applied Polymer Science, 2015. **132**(38).
155. Zhou, C., et al., *Direct investigations on strain-induced cold crystallization behavior and structure evolutions in amorphous poly (lactic acid) with SAXS and WAXS measurements*. Polymer, 2016. **90**: p. 111-121.
156. Silverajah, V., et al., *A comparative study on the mechanical, thermal and morphological characterization of poly (lactic acid)/epoxidized palm oil blend*. International journal of molecular sciences, 2012. **13**(5): p. 5878-5898.
157. Ren, Z., L. Dong, and Y. Yang, *Dynamic mechanical and thermal properties of plasticized poly (lactic acid)*. Journal of Applied Polymer Science, 2006. **101**(3): p. 1583-1590.
158. Kamthai, S. and R. Magaraphan. *Thermal and mechanical properties of polylactic acid (PLA) and bagasse carboxymethyl cellulose (CMCB) composite by adding isosorbide diesters*. in *AIP Conference Proceedings*. 2015. AIP Publishing.
159. Silverajah, V., et al., *Mechanical, thermal and morphological properties of poly (lactic acid)/epoxidized palm olein blend*. Molecules, 2012. **17**(10): p. 11729-11747.
160. Jia, S., et al., *Morphology, Crystallization and Thermal Behaviors of PLA-Based Composites: Wonderful Effects of Hybrid GO/PEG via Dynamic Impregnating*. Polymers, 2017. **9**(10): p. 528.
161. Carbonell-Verdu, A., et al., *PLA films with improved flexibility properties by using maleinized cottonseed oil*. European Polymer Journal, 2017. **91**: p. 248-259.
162. Hughes, J., et al., *Improved flexibility of thermally stable poly-lactic acid (PLA)*. Carbohydrate polymers, 2012. **88**(1): p. 165-172.
163. Arrieta, M.P., et al., *Development of flexible materials based on plasticized electrospun PLA-PHB blends: Structural, thermal, mechanical and disintegration properties*. European Polymer Journal, 2015. **73**: p. 433-446.
164. Frazer, A. and F. Wallenberger, *Aromatic polyhydrazides: a new class of highly bonded, stiff polymers*. Journal of Polymer Science Part A: General Papers, 1964. **2**(3): p. 1147-1156.
165. Dammont, F. and T. Kwei, *Dynamic mechanical properties of aromatic, aliphatic, and partially fluorinated epoxy resins*. Journal of Polymer Science Part A-2: Polymer Physics, 1967. **5**(4): p. 761-769.
166. Wan, J., et al., *A novel biobased epoxy resin with high mechanical stiffness and low flammability: synthesis, characterization and properties*. Journal of Materials Chemistry A, 2015. **3**(43): p. 21907-21921.

167. Cranford, S.W., D.B. Brommer, and M.J. Buehler, *Extended graphynes: simple scaling laws for stiffness, strength and fracture*. *Nanoscale*, 2012. **4**(24): p. 7797-7809.
168. Ljungberg, N. and B. Wesslén, *Preparation and properties of plasticized poly (lactic acid) films*. *Biomacromolecules*, 2005. **6**(3): p. 1789-1796.
169. Chieng, B., et al., *Epoxidized vegetable oils plasticized poly (lactic acid) biocomposites: mechanical, thermal and morphology properties*. *Molecules*, 2014. **19**(10): p. 16024-16038.
170. Arrieta, M.P., et al., *Combined effect of poly (hydroxybutyrate) and plasticizers on polylactic acid properties for film intended for food packaging*. *Journal of Polymers and the Environment*, 2014. **22**(4): p. 460-470.
171. Al-Mulla, E.A.J., et al., *Properties of epoxidized palm oil plasticized poly(lactic acid)*. *Journal of Materials Science*, 2010. **45**(7): p. 1942-1946.
172. Park, K., J.U. Ha, and M. Xanthos, *Ionic liquids as plasticizers/lubricants for polylactic acid*. *Polymer Engineering & Science*, 2010. **50**(6): p. 1105-1110.
173. Kodal, M., H. Sirin, and G. Ozkoc, *Effects of reactive and nonreactive POSS types on the mechanical, thermal, and morphological properties of plasticized poly (lactic acid)*. *Polymer Engineering & Science*, 2014. **54**(2): p. 264-275.
174. Notta-Cuvier, D., et al., *Tailoring Poly(lactide) Properties for Automotive Applications: Effects of Co-Addition of Halloysite Nanotubes and Selected Plasticizer*. *Macromolecular Materials and Engineering*, 2015. **300**(7): p. 684-698.
175. Li, F.J., et al., *Effect of polyethylene glycol on the crystallization and impact properties of polylactide-based blends*. *Polymers for Advanced Technologies*, 2015. **26**(5): p. 465-475.
176. Ge, H., et al., *Thermal, mechanical, and rheological properties of plasticized poly (L-lactic acid)*. *Journal of Applied Polymer Science*, 2013. **127**(4): p. 2832-2839.
177. Murariu, M., et al., *Poly(lactide) (PLA)-CaSO<sub>4</sub> composites toughened with low molecular weight and polymeric ester-like plasticizers and related performances*. *European Polymer Journal*, 2008. **44**(11): p. 3842-3852.
178. Bitinis, N., et al., *Structure and properties of poly(lactide)/natural rubber blends*. *Materials Chemistry and Physics*, 2011. **129**(3): p. 823-831.
179. Mikos, A.G. and N.A. Peppas, *Polymer chain entanglements and brittle fracture*. *The Journal of chemical physics*, 1988. **88**(2): p. 1337-1342.
180. Dobkowski, Z., *Determination of critical molecular weight for entangled macromolecules using the tensile strength data*. *Rheologica acta*, 1995. **34**(6): p. 578-585.

181. Tsukeshiba, H., et al., *Effect of polymer entanglement on the toughening of double network hydrogels*. The Journal of Physical Chemistry B, 2005. **109**(34): p. 16304-16309.
182. Kanai, H., V. Sullivan, and A. Auerbach, *Impact modification of engineering thermoplastics*. Journal of applied polymer science, 1994. **53**(5): p. 527-541.
183. Grijpma, D., J. Penning, and A. Pennings, *Chain entanglement, mechanical properties and drawability of poly (lactide)*. colloid and polymer science, 1994. **272**(9): p. 1068-1081.
184. Brown, H., *A molecular interpretation of the toughness of glassy polymers*. Macromolecules, 1991. **24**(10): p. 2752-2756.
185. Gent, A. and A. Thomas, *Effect of molecular weight on the tensile strength of glassy plastics*. Journal of Polymer Science Part A-2: Polymer Physics, 1972. **10**(3): p. 571-573.
186. Nunes, R.W., J.R. Martin, and J.F. Johnson, *Influence of molecular weight and molecular weight distribution on mechanical properties of polymers*. Polymer Engineering & Science, 1982. **22**(4): p. 205-228.
187. Graessley, W. and S. Edwards, *Entanglement interactions in polymers and the chain contour concentration*. Polymer, 1981. **22**(10): p. 1329-1334.
188. Zang, Y.H. and P.J. Carreau, *A correlation between critical end-to-end distance for entanglements and molecular chain diameter of polymers*. Journal of applied polymer science, 1991. **42**(7): p. 1965-1968.
189. Aharoni, S.M., *Correlations between chain parameters and the plateau modulus of polymers*. Macromolecules, 1986. **19**(2): p. 426-434.
190. Yilgor, I., et al., *Contribution of soft segment entanglement on the tensile properties of silicone-urea copolymers with low hard segment contents*. Polymer, 2009. **50**(19): p. 4432-4437.
191. Geyer, R., J.R. Jambeck, and K.L. Law, *Production, use, and fate of all plastics ever made*. Science advances, 2017. **3**(7): p. e1700782.
192. de la Caba, K., et al., *From seafood waste to active seafood packaging: An emerging opportunity of the circular economy*. Journal of cleaner production, 2018.
193. Steenis, N.D., et al., *Effects of sustainable design strategies on consumer preferences for redesigned packaging*. Journal of Cleaner Production, 2018. **205**: p. 854-865.
194. Guillard, V., et al., *The next generation of sustainable food packaging to preserve our environment in a circular economy context*. Frontiers in nutrition, 2018. **5**: p. 121.
195. Ghoshal, G., *Recent Trends in Active, Smart, and Intelligent Packaging for Food Products*, in *Food Packaging and Preservation*. 2018, Elsevier. p. 343-374.

196. Siracusa, V. and M.D. Rosa, *Sustainable Packaging*, in *Sustainable Food Systems from Agriculture to Industry*. 2018, Elsevier. p. 275-307.
197. Kaur, G., et al., *Recent trends in green and sustainable chemistry & waste valorisation: rethinking plastics in a circular economy*. *Current opinion in green and sustainable chemistry*, 2018. **9**: p. 30-39.
198. Siracusa, V., et al., *Biodegradable polymers for food packaging: a review*. *Trends in Food Science & Technology*, 2008. **19**(12): p. 634-643.
199. Auras, R., B. Harte, and S. Selke, *An overview of polylactides as packaging materials*. *Macromolecular bioscience*, 2004. **4**(9): p. 835-864.
200. Ahmed, J. and S.K. Varshney, *Poly lactides—chemistry, properties and green packaging technology: a review*. *International journal of food properties*, 2011. **14**(1): p. 37-58.
201. Sinclair, R., *The case for polylactic acid as a commodity packaging plastic*. *Journal of Macromolecular Science, Part A: Pure and Applied Chemistry*, 1996. **33**(5): p. 585-597.
202. Mallet, B., K. Lamnawar, and A. Maazouz, *Improvement of blown film extrusion of poly (lactic acid): Structure–processing–properties relationships*. *Polymer Engineering & Science*, 2014. **54**(4): p. 840-857.
203. Dhavalikar, R. and M. Xanthos, *Parameters affecting the chain extension and branching of PET in the melt state by polyepoxides*. *Journal of applied polymer science*, 2003. **87**(4): p. 643-652.
204. Najafi, N., et al., *Rheological and foaming behavior of linear and branched polylactides*. *Rheologica Acta*, 2014. **53**(10-11): p. 779-790.
205. Randall, J.R., K. Cink, and J.C. Smith, *Branching polylactide by reacting OH or COOH polylactide with epoxide acrylate (co) polymer*. 2009, Google Patents.
206. Liu, J., et al., *Preparation and rheological characterization of long chain branching polylactide*. *Polymer*, 2014. **55**(10): p. 2472-2480.
207. Liu, J., et al., *Long chain branching polylactide: Structures and properties*. *Polymer*, 2010. **51**(22): p. 5186-5197.
208. Jaskiewicz, A., et al., *How does a chain-extended polylactide behave?: a comprehensive analysis of the material, structural and mechanical properties*. *Polymer Bulletin*, 2014. **71**(7): p. 1675-1690.
209. Al-Ittry, R., K. Lamnawar, and A. Maazouz, *Improvement of thermal stability, rheological and mechanical properties of PLA, PBAT and their blends by reactive extrusion with functionalized epoxy*. *Polymer Degradation and Stability*, 2012. **97**(10): p. 1898-1914.

210. Tiwary, P. and M. Kontopoulou, *Tuning the rheological, thermal, and solid-state properties of branched PLA by free-radical-mediated reactive extrusion*. ACS Sustainable Chemistry & Engineering, 2018. **6**(2): p. 2197-2206.
211. ASTM, *Standard test method for flow rates of thermoplastics by extrusion plastometer*. 2006.
212. Sato, Y., et al., *Pressure-volume-temperature behavior of polylactide, poly (butylene succinate), and poly (butylene succinate-co-adipate)*. Polymer Engineering & Science, 2000. **40**(12): p. 2602-2609.
213. Mihai, M., M.A. Huneault, and B.D. Favis, *Rheology and extrusion foaming of chain-branched poly (lactic acid)*. Polymer Engineering & Science, 2010. **50**(3): p. 629-642.
214. Spalding, M.A., et al., *Troubleshooting and mitigating gels in polyethylene film products*. Journal of Plastic Film & Sheeting, 2018. **34**(3): p. 300-323.
215. Zuideveld, M., et al., *Miscibility and properties of linear poly (L-lactide)/branched poly (L-lactide) copolyester blends*. Polymer, 2006. **47**(11): p. 3740-3746.
216. Nouri, S., C. Dubois, and P.G. Lafleur, *Synthesis and characterization of polylactides with different branched architectures*. Journal of Polymer Science Part B: Polymer Physics, 2015. **53**(7): p. 522-531.
217. Corre, Y.M., et al., *Influence of the chain extension on the crystallization behavior of polylactide*. Polymer Engineering & Science, 2014. **54**(3): p. 616-625.
218. Dorgan, J.R., H. Lehermeier, and M. Mang, *Thermal and rheological properties of commercial-grade poly (lactic acid) s*. Journal of Polymers and the Environment, 2000. **8**(1): p. 1-9.
219. Singh, G., et al., *Mechanical properties and morphology of polylactide, linear low-density polyethylene, and their blends*. Journal of applied polymer science, 2010. **118**(1): p. 496-502.
220. Baimark, Y. and O. Cheerarot, *Effect of chain extension on thermal stability behaviors of polylactide bioplastics*. Oriental Journal of Chemistry, 2015. **31**(2): p. 635-641.
221. Carlson, D., et al., *Maleation of polylactide (PLA) by reactive extrusion*. Journal of applied polymer science, 1999. **72**(4): p. 477-485.
222. Yang, S.-l., et al., *Thermal and mechanical properties of chemical crosslinked polylactide (PLA)*. Polymer Testing, 2008. **27**(8): p. 957-963.
223. Carlson, D., et al., *Free radical branching of polylactide by reactive extrusion*. Polymer Engineering & Science, 1998. **38**(2): p. 311-321.

224. Gu, L., et al., *Star vs long chain branching of poly (lactic acid) with multifunctional aziridine*. Journal of Rheology, 2017. **61**(4): p. 785-796.
225. Wood-Adams, P.M., *The effect of long chain branches on the shear flow behavior of polyethylene*. Journal of Rheology, 2001. **45**(1): p. 203-210.
226. Jaszkievicz, A., et al., *Investigation of Processability of Chain-Extended Polylactides During Melt Processing–Compounding Conditions and Polymer Molecular Structure*. Macromolecular Materials and Engineering, 2014. **299**(3): p. 307-318.
227. Incarnato, L., et al., *Structure and rheology of recycled PET modified by reactive extrusion*. Polymer, 2000. **41**(18): p. 6825-6831.
228. Laun, H. and H. Schuch, *Transient elongational viscosities and drawability of polymer melts*. Journal of Rheology, 1989. **33**(1): p. 119-175.
229. Nouri, S., C. Dubois, and P.G. Lafleur, *Effect of chemical and physical branching on rheological behavior of polylactide*. Journal of Rheology, 2015. **59**(4): p. 1045-1063.
230. Keshtkar, M., et al., *Extruded PLA/clay nanocomposite foams blown with supercritical CO<sub>2</sub>*. Polymer, 2014. **55**(16): p. 4077-4090.
231. Kricheldorf, H.R., *Syntheses and application of polylactides*. Chemosphere, 2001. **43**(1): p. 49-54.
232. Jin, F.-L., et al., *Recent advances in heat resistance modification of poly (lactic acid): A review*. Composites Part B: Engineering, 2018.
233. Park, S.D., et al., *Effect of crystallinity and loading-rate on mode I fracture behavior of poly (lactic acid)*. Polymer, 2006. **47**(4): p. 1357-1363.
234. Li, S. and S. McCarthy, *Influence of crystallinity and stereochemistry on the enzymatic degradation of poly (lactide) s*. Macromolecules, 1999. **32**(13): p. 4454-4456.
235. Nagarajan, V., et al., *Overcoming the fundamental challenges in improving the impact strength and crystallinity of PLA biocomposites: influence of nucleating agent and mold temperature*. ACS applied materials & interfaces, 2015. **7**(21): p. 11203-11214.
236. Landel, R.F. and L.E. Nielsen, *Mechanical properties of polymers and composites*. 1993: CRC press.
237. Ku, H., et al., *A review on the tensile properties of natural fiber reinforced polymer composites*. Composites Part B: Engineering, 2011. **42**(4): p. 856-873.
238. Saheb, D.N. and J.P. Jog, *Natural fiber polymer composites: a review*. Advances in Polymer Technology: Journal of the Polymer Processing Institute, 1999. **18**(4): p. 351-363.

239. Lee, B.-H., et al., *Bio-composites of kenaf fibers in polylactide: Role of improved interfacial adhesion in the carding process*. *Composites Science and Technology*, 2009. **69**(15-16): p. 2573-2579.
240. Plackett, D., et al., *Biodegradable composites based on L-polylactide and jute fibres*. *Composites science and technology*, 2003. **63**(9): p. 1287-1296.
241. Nyambo, C., A.K. Mohanty, and M. Misra, *Poly lactide-based renewable green composites from agricultural residues and their hybrids*. *Biomacromolecules*, 2010. **11**(6): p. 1654-1660.
242. Wu, C.-S., *Renewable resource-based composites of recycled natural fibers and maleated polylactide bioplastic: Characterization and biodegradability*. *Polymer Degradation and Stability*, 2009. **94**(7): p. 1076-1084.
243. Kwon, H.-J., et al., *Tensile properties of kenaf fiber and corn husk flour reinforced poly (lactic acid) hybrid bio-composites: role of aspect ratio of natural fibers*. *Composites Part B: Engineering*, 2014. **56**: p. 232-237.
244. Takao, Y. and M. Taya, *The effect of variable fiber aspect ratio on the stiffness and thermal expansion coefficients of a short fiber composite*. *Journal of composite materials*, 1987. **21**(2): p. 140-156.
245. Tandon, G.P. and G.J. Weng, *The effect of aspect ratio of inclusions on the elastic properties of unidirectionally aligned composites*. *Polymer composites*, 1984. **5**(4): p. 327-333.
246. Mallick, P.K., *Fiber-reinforced composites: materials, manufacturing, and design*. 2007: CRC press.
247. Agarwal, B.D., L.J. Broutman, and K. Chandrashekhara, *Analysis and performance of fiber composites*. 2017: John Wiley & Sons.
248. Gibson, R.F., *A review of recent research on mechanics of multifunctional composite materials and structures*. *Composite structures*, 2010. **92**(12): p. 2793-2810.
249. Krause, W., et al., *LFT-D—a process technology for large scale production of fiber reinforced thermoplastic components*. *Journal of Thermoplastic Composite Materials*, 2003. **16**(4): p. 289-302.
250. Schemme, M., *LFT—development status and perspectives*. *Plastics, Additives and Compounding*, 2008. **10**(2): p. 38-43.
251. Thattai parthasarathy, K.B., et al., *Process simulation, design and manufacturing of a long fiber thermoplastic composite for mass transit application*. *Composites Part A: Applied Science and Manufacturing*, 2008. **39**(9): p. 1512-1521.

252. Fujiura, T., et al., *Improvement of mechanical properties of long jute fiber reinforced polylactide prepared by injection molding process*. WIT Trans Ecol Environ, 2010. **138**: p. 181-188.
253. Ranganathan, N., et al., *Effect of long fiber thermoplastic extrusion process on fiber dispersion and mechanical properties of viscose fiber/polypropylene composites*. Polymers for Advanced Technologies, 2016. **27**(5): p. 685-692.
254. Ranganathan, N., *Long Fiber Extrusion and Improved Energy Absorption Behaviour of Hybrid Thermoplastic Composite*. 2016.
255. Ranganathan, N., et al., *Impact toughness, viscoelastic behavior, and morphology of polypropylene–jute–viscose hybrid composites*. Journal of Applied Polymer Science, 2016. **133**(7).
256. Ranganathan, N., et al., *Structure property relation of hybrid biocomposites based on jute, viscose and polypropylene: The effect of the fibre content and the length on the fracture toughness and the fatigue properties*. Composites Part A: Applied science and manufacturing, 2016. **83**: p. 169-175.
257. Deák, T. and T. Czigány, *Chemical composition and mechanical properties of basalt and glass fibers: A comparison*. Textile Research Journal, 2009. **79**(7): p. 645-651.
258. Czigány, T. *Basalt fiber reinforced hybrid polymer composites*. in *Materials Science Forum*. 2005. Trans Tech Publ.
259. Sim, J. and C. Park, *Characteristics of basalt fiber as a strengthening material for concrete structures*. Composites Part B: Engineering, 2005. **36**(6-7): p. 504-512.
260. Dhand, V., et al., *A short review on basalt fiber reinforced polymer composites*. Composites Part B: Engineering, 2015. **73**: p. 166-180.
261. Liu, Q., et al., *Investigation of basalt fiber composite mechanical properties for applications in transportation*. Polymer composites, 2006. **27**(1): p. 41-48.
262. Yang, W., et al., *Carbon nanotube reinforced polylactide/basalt fiber composites containing aluminium hypophosphite: thermal degradation, flame retardancy and mechanical properties*. RSC Advances, 2015. **5**(128): p. 105869-105879.
263. Liu, T., et al., *Basalt fiber reinforced and elastomer toughened polylactide composites: mechanical properties, rheology, crystallization, and morphology*. Journal of Applied Polymer Science, 2012. **125**(2): p. 1292-1301.
264. Ying, Z., et al., *Polylactide/basalt fiber composites with tailorable mechanical properties: Effect of surface treatment of fibers and annealing*. Composite Structures, 2017. **176**: p. 1020-1027.

265. Inceoglu, F., et al., *Correlation between processing conditions and fiber breakage during compounding of glass fiber-reinforced polyamide*. *Polymer Composites*, 2011. **32**(11): p. 1842-1850.
266. Le Baillif, M. and K. Oksman, *The effect of processing on fiber dispersion, fiber length, and thermal degradation of bleached sulfite cellulose fiber polypropylene composites*. *Journal of Thermoplastic Composite Materials*, 2009. **22**(2): p. 115-133.
267. Von Turkovich, R. and L. Erwin, *Fiber fracture in reinforced thermoplastic processing*. *Polymer Engineering & Science*, 1983. **23**(13): p. 743-749.
268. Inoue, A., et al., *Effect of screw design on fiber breakage and dispersion in injection-molded long glass-fiber-reinforced polypropylene*. *Journal of Composite Materials*, 2015. **49**(1): p. 75-84.
269. Masirek, R., et al., *Composites of poly (L-lactide) with hemp fibers: Morphology and thermal and mechanical properties*. *Journal of applied polymer science*, 2007. **105**(1): p. 255-268.
270. Suryanegara, L., A.N. Nakagaito, and H. Yano, *The effect of crystallization of PLA on the thermal and mechanical properties of microfibrillated cellulose-reinforced PLA composites*. *Composites Science and Technology*, 2009. **69**(7-8): p. 1187-1192.
271. Fiore, V., et al., *PLA based biocomposites reinforced with Arundo donax fillers*. *Composites Science and Technology*, 2014. **105**: p. 110-117.
272. Jonoobi, M., et al., *Mechanical properties of cellulose nanofiber (CNF) reinforced polylactic acid (PLA) prepared by twin screw extrusion*. *Composites Science and Technology*, 2010. **70**(12): p. 1742-1747.
273. Halpin, J.C. and J. Kardos, *The Halpin-Tsai equations: a review*. *Polymer engineering and science*, 1976. **16**(5): p. 344-352.
274. Pilla, S., et al., *Poly lactide-pine wood flour composites*. *Polymer Engineering & Science*, 2008. **48**(3): p. 578-587.
275. Goriparthi, B.K., K. Suman, and N.M. Rao, *Effect of fiber surface treatments on mechanical and abrasive wear performance of polylactide/jute composites*. *Composites Part A: Applied Science and Manufacturing*, 2012. **43**(10): p. 1800-1808.
276. Pilla, S., et al., *Microcellular and solid polylactide-flax fiber composites*. *Composite Interfaces*, 2009. **16**(7-9): p. 869-890.
277. Pilla, S., et al., *Poly lactide-recycled wood fiber composites*. *Journal of Applied Polymer Science*, 2009. **111**(1): p. 37-47.

278. Benedito, A., et al., *Dispersion and characterization of thermoplastic polyurethane/multiwalled carbon nanotubes by melt mixing*. Journal of Applied Polymer Science, 2011. **122**(6): p. 3744-3750.
279. Sathishkumar, T., J.a. Naveen, and S. Satheeshkumar, *Hybrid fiber reinforced polymer composites—a review*. Journal of Reinforced Plastics and Composites, 2014. **33**(5): p. 454-471.
280. Kretsis, G., *A review of the tensile, compressive, flexural and shear properties of hybrid fibre-reinforced plastics*. Composites, 1987. **18**(1): p. 13-23.
281. Gururaja, M. and A.H. Rao, *A review on recent applications and future prospectus of hybrid composites*. International Journal of Soft Computing and Engineering (IJSCE), 2012. **1**(6): p. 352-355.
282. Sanjay, M., G. Arpitha, and B. Yogesha, *Study on mechanical properties of natural-glass fibre reinforced polymer hybrid composites: A review*. Materials today: proceedings, 2015. **2**(4-5): p. 2959-2967.
283. Jawaid, M. and H.A. Khalil, *Cellulosic/synthetic fibre reinforced polymer hybrid composites: A review*. Carbohydrate polymers, 2011. **86**(1): p. 1-18.
284. Viswanathan, G., et al., *Single-step in situ synthesis of polymer-grafted single-wall nanotube composites*. Journal of the American Chemical Society, 2003. **125**(31): p. 9258-9259.
285. Xu, Z. and C. Gao, *In situ polymerization approach to graphene-reinforced nylon-6 composites*. Macromolecules, 2010. **43**(16): p. 6716-6723.